Development and Biological Characterization of Novel Class I Histone Deacetylases Modulators

DISSERTATION

zur Erlangung des akademischen Grades

Doctor rerum naturalium (Dr. rer. nat.)

der Naturwissenschaftlichen Fakultät I Biowissenschaften

der Martin-Luther-Universität Halle-Wittenberg

vorgelegt von

Herrn M.Sc. Mohamed Adel Mohamed Abdelsalam

Gutachter:

Prof. Dr. Wolfgang Sippl, Halle

Prof. Dr. Mike Schutkowski, Halle

Prof. Dr. Ralph Holl, Hamburg

Verteidigungsdatum: 13.11.2023

Abstract

In recent years, histone deacetylases (HDACs) have gained substantial interest as key epigenetic modulators involved in several physiological processes by regulating chromatin structure and subsequently controlling gene expression in cells. Aberrant expression of HDACs has been associated with various pathological disorders, including cancer. As a result, pharmacological inhibition of HDACs has emerged as a promising therapeutic strategy, especially in the field of oncology. The work presented in this thesis focuses on developing novel modulators of class I HDACs and evaluating their biological role in different types of cancer.

First, a series of thirty novel 2-aminobenzamide derivatives were designed and synthesized as class I selective HDAC inhibitors. Several compounds exhibited improved potency and selectivity for HDAC1, 2, and 3 compared to reported class I HDAC inhibitors. Some of the developed compounds exhibited potent cellular activity against different acute myeloid leukemia (AML) and pancreatic cancer cell lines. The most promising compound in this series strongly induced apoptosis in different AML cell lines, and it was found to be superior to the clinically evaluated HDAC inhibitor entinostat.

The developed inhibitors were further used as a training set to generate binding free-energy calculation models that could help to predict the activity of future planned derivatives and to reduce the time required to prioritize compounds for further studies. A good correlation was found between the in vitro activity and calculated binding free energy values for HDAC 1, 2, and 3 isoforms. Additionally, the reliability and predictive accuracy of the best-performing models were evaluated on an external test set of newly synthesized inhibitors.

Furthermore, a prodrug concept was applied in an attempt to obtain candidates with improved therapeutic indices. A novel series of bioreducible prodrugs were designed by masking the 2-aminobenzamide part of several class I HDAC inhibitors using different nitroarylmethyl motifs so that they could be reduced by the nitroreductase (NTR) enzyme. Cellular assays showed that two prodrugs were activated by the NTR system and exhibited potent activity against AML cells with moderate selectivity windows.

Targeted protein degradation is a novel medicinal chemistry tool that was applied in the current work to design degraders for class I HDACs. Several heterobifunctional molecules were synthesized by combining different HDAC inhibitors and E3 ligase ligands. The

PROTACs were characterized in vitro as well as for their degradation effects in pancreatic cancer cell lines.

The current work discussed also the recent advances in developing inhibitors for schistosome HDACs, with particular focus on *sm*HDAC8 as a novel therapeutic target for schistosomiasis.

The results obtained in the present work could serve as promising starting points for further optimization to obtain novel candidates with potential anticancer activity.

Keywords: Epigenetics, class I HDAC, HDAC inhibitors, Anticancer, Zinc-binding group, 2-Aminobenzamide, Targeted protein degradation, PROTACs, Hydrophobic tagging, Hypoxia, Prodrugs, Nitroreductase, Acute myeloid leukemia, Binding free-energy calculations, Schistosomiasis, *sm*HDAC8.

Kurzfassung

Histondeacetylasen (HDACs) haben in den letzten Jahren als wichtige epigenetische Modulatoren stark an Bedeutung gewonnen. Sie sind an mehreren physiologischen Prozessen beteiligt indem sie die Chromatinstruktur regulieren und anschließend die Genexpression in den Zellen steuern. Eine gestörte Expression von HDACs wird mit verschiedenen pathologischen Störungen, einschließlich Krebs, in Verbindung gebracht. Infolgedessen hat sich die pharmakologische Hemmung von HDACs als vielversprechende therapeutische Strategie erwiesen, insbesondere im Bereich der Onkologie. Die in dieser Arbeit vorgestellten Arbeiten konzentrieren sich auf die Entwicklung neuartiger Modulatoren von HDACs der Klasse I und die Bewertung ihres Potenzials als Krebsmedikamente.

Zunächst wurde eine Reihe von dreißig neuen 2-Aminobenzamid-Derivaten als selektive HDAC-Inhibitoren der Klasse I entwickelt und synthetisiert. Mehrere Verbindungen zeigten eine verbesserte Wirksamkeit und Selektivität für HDAC1, 2 und 3 im Vergleich zu bereits bekannten Klasse-I-HDAC-Inhibitoren. Einige der entwickelten Verbindungen zeigten eine starke zelluläre Aktivität gegen verschiedene Zelllinien von akuter myeloischer Leukämie (AML) und Bauchspeicheldrüsenkrebs. Die vielversprechendste Verbindung dieser Reihe löste bei verschiedenen AML-Zelllinien eine starke Apoptose aus und erwies sich dem klinisch untersuchten HDAC-Inhibitor Entinostat als überlegen.

Die entwickelten Inhibitoren wurden außerdem als Datensatz verwendet, um Berechnungsmodelle für die freie Bindungsenergie zu erstellen, die zur Vorhersage der Aktivität künftig geplanter Derivate beitragen und den Zeitaufwand für die Priorisierung von Verbindungen für weitere Studien verringern könnten. Es wurde eine gute Korrelation zwischen der in-vitro-Aktivität und den berechneten Werten der freien Bindungsenergie für die Isoformen von HDAC 1, 2 und 3 festgestellt. Darüber hinaus wurden die Zuverlässigkeit und die Vorhersagegenauigkeit der besten Modelle anhand einer externen Testgruppe von neu synthetisierten Inhibitoren bewertet.

Außerdem wurde das Prodrug-Konzept angewandt, um Kandidaten mit verbesserten therapeutischen Indizes zu finden. Durch Maskierung des 2-Aminobenzamid-Teils mehrerer HDAC-Inhibitoren der Klasse I mit verschiedenen Nitroarylmethyl-Motiven wurde eine neue Reihe bioreduzierbarer Prodrugs entwickelt, die durch das Enzym Nitroreductase (NTR) reduziert werden können. Zelluläre Assays zeigten, dass zwei Prodrugs durch das NTR-

Prodrug-System aktiviert wurden und eine starke Aktivität gegen AML-Zellen mit moderaten Selektivitätsfenstern aufwiesen.

Der gezielte Proteinabbau ist ein neuartiges Instrument der medizinischen Chemie, das in der aktuellen Arbeit zur Entwicklung von Degradatoren für HDACs der Klasse I eingesetzt wurde. Mehrere heterobifunktionelle Moleküle wurden durch die Kombination verschiedener HDAC-Inhibitoren und E3-Ligase-Liganden synthetisiert. Die PROTACs wurden in vitro an HDACs als auch auf ihre Degradation in Pankreas Krebszelllinien getestet.

In der aktuellen Arbeit wurden auch die jüngsten Fortschritte bei der Entwicklung von Inhibitoren für Schistosomen-HDACs, mit besonderem Augenmerk auf *sm*HDAC8 als neuartiges therapeutisches Ziel für Schistosomiasis.

Die in der vorliegenden Arbeit erzielten Ergebnisse könnten als vielversprechende Ausgangspunkte für weitere Optimierungen dienen, um neue Kandidaten mit potenzieller krebsbekämpfender und antiparasitärer Wirkung zu erhalten.

Schlagwörter: Epigenetik, Klasse I HDAC, HDAC-Inhibitoren, Krebsbekämpfung, Zinkbindende Gruppe, 2-Aminobenzamid, Gezielter Proteinabbau, PROTACs, Hydrophobes Tagging, Hypoxie, Prodrugs, Nitroreduktase, Akute myeloische Leukämie, Berechnungen der freien Energie der Bindung, Schistosomiasis, *sm*HDAC8.

Acknowledgements

Dedication

To my mother, thank you for always loving me and guiding me. Even though you are no longer here with me I can still feel your love guiding me. You are always in my heart. Until we meet again!

To my father, brother and sister, thanks for your prayers, help and support.

List of Contents

List of figures

List of abbreviations

Ac-CoA	Cofactor acetyl coenzyme A
AML	Acute myeloid leukemia
AUTOTACs	AUTOphagy-TArgeting Chimeras
BCL2	B-cell lymphoma 2
BFE	Binding free energy
Boc3-Arg	*tert*-butyl carbamate-protected arginine
CDKN1A	Cyclin-dependent kinase inhibitor 1A
CFDA	China Food and Drug Administration
CHAMP	CHAperone-Mediated Protein degradation
CpG	Cytosine-phosphate guanine
CRBN	Cereblon
CTCL	Cutaneous T-cell lymphoma
DC$_{50}$	Half-maximal degradation concentration
DNA	Deoxyribonucleic acid
DNMTs	DNA methyltransferases
ERα	Estrogen receptor alpha
EZH2	Enhancer of zeste homolog 2
FDA	U.S. Food and Drug Administration
FLT3	FMS-like tyrosine kinase 3
GI$_{50}$	Half-maximal growth inhibitory concentration
HATs	Histone acetyltransferases
HCT116	Human colorectal carcinoma 116
HDACi	HDAC inhibitors
HDACs	Histone deacetylases
HEK293	Human embryonic kidney cells 293
HER3	Human epidermal growth factor receptor 3
HSP70	Heat shock protein 70
HyT	Hydrophobic tags
ITDs	Internal tandem duplications
KATs	Lysine acetyltransferases
KDACs	Lysine deacetylases

KMT	Lysine methyltransferase
LC–MS	Liquid chromatography–mass spectrometry
LSD	Lysine-specific demethylase
LYTACs	Lysosome-targeting chimeras
5mC	5-methylCytosine
MD	Molecular dynamics
NAD$^+$	Nicotinamide adenine dinucleotide
NCoR	Nuclear receptor corepressor
NF-κB	Nuclear factor kappa B
NTR	Nitroreductase
NuRD	Nucleosome remodeling and deacetylases
PDAC	Pancreatic ductal adenocarcinoma
PDB	Protein data bank
***Pf*DHFR**	*Plasmodium falciparum* dihydrofolate reductase
***Pf*HDACs**	*Plasmodium falciparum* HDACs
POI	Protein of interest
PROTACs	Proteolysis targeting chimeras
PSN1	Pancreatic adenocarcinoma
PTCL	Peripheral T-cell lymphomas
PTMs	Post-translational modifications
R^2	Coefficient of determination
REST	Repressor Element-1 Silencing Transcription factor
RMSE	Root-mean-square error
RNA	Ribonucleic acid
RNS	Reactive nitrogen species
ROS	Reactive oxygen species
Rpd3	Reduced potassium dependency 3
SAHA	Suberoylanilide hydroxamic acid
SIAH	Seven in absentia homolog
Sin3A	SWI-independent-3A
Sir2	Silent information regulator 2
SIRT	Sirtuin

SMC3	Structural maintenance of chromosomes protein 3
smHDAC	Schitosoma mansoni HDAC
SMRT	Silencing mediators for retinoid and thyroid hormone receptors
STAT3	Signal transducer and activator of transcription 3
TPD	Targeted protein degradation
TSA	Trichostatin A
VHL	Von Hippel-Lindau
ZBG	zinc-binding group

1. Introduction

1.1. Epigenetic modifications and regulation of gene expression

Generally, epigenetics is defined as the study of heritable alterations in gene expression that do not involve changes in the underlying DNA sequence and accordingly determine whether genes are turned on (expressed) or off (silenced) [1, 2]. DNA methylation and histone post-translational modifications (PTMs) are among the most extensively studied epigenetic control mechanisms that are crucially involved in the regulation of cellular differentiation as well as other physiological processes [1, 3]. DNA methylation is one of the first identified epigenetic mechanisms and is associated with gene repression [4]. This process involves the covalent addition of a methyl group to the C-5 position of cytosine residues, specifically in cytosine-phosphate guanine (CpG) dinucleotides, to form 5-methylcytosine (5mC). DNA methylation is mediated through a family of enzymes called DNA methyltransferases (DNMTs) and controls gene expression by inhibiting the binding of different transcription factors to DNA or by recruiting proteins involved in gene silencing [4]. Histone post-translational modifications are the second major epigenetic regulatory mechanism which play a crucial role in regulating the accessibility of chromatin to RNA polymerase and transcription factors, hence controlling gene expression [5]. While epigenetic alterations are required for normal physiological processes, they can also be associated with some diseases [6]. Aberrations in any of the systems that regulate epigenetic modifications can result in abnormal gene activation or silencing. Such alterations have been well documented in many pathological diseases, especially cancer. Unlike other genetic alterations, most epigenetic modifications are reversible, a property that makes them an attractive target for the development of therapeutics that can combat diseases associated with epigenetic disorders [5, 7]. As histone PTMs are the main focus of the present work, they will be discussed in more detail.

1.2. Modulation of chromatin structure via post-translational modifications

In eukaryotes, the genetic materials are tightly packed into chromosomes, which are made up of a nucleoprotein complex called chromatin (**Figure 1**). The fundamental building unit of chromatin is the nucleosome, which consists of 147 base pairs of DNA wrapped around four pairs of highly conserved core histone proteins, namely H2A, H2B, H3, and H4 [8]. Another subtype of histone proteins is the linker histone protein H1, which binds to nucleosomal cores around DNA entry and exit sites to stabilize both nucleosome and chromatin architectures [8, 9]. Adjacent nucleosomes are connected by the linker DNA, forming a structure that looks like "beads on a string" [9]. Histone proteins contain a flexible *N*-terminal region called the

"histone tail" protruding from the DNA-wrapped core. These histone tails contain a high portion of positively charged lysine residues that interact with the acidic phosphate-sugar backbone of the DNA, leading to a compact chromatin structure [8, 10]. Therefore, as long as the chromatin is condensed into the primary nucleosome structure, DNA becomes less accessible for transcription factors. On the other hand, the loss of this chromatin structure enables the transcription machinery to access the genomic DNA, and transcription is thus promoted [11]. The *N*-terminal tails of histones are decorated by a myriad of covalent post-translational modifications, including but not limited to methylation, acetylation, phosphorylation, and ubiquitination [12, 13]. These modifications have a regulatory mechanism that can control many aspects of cellular functions, including chromosome dynamics, chromatin packaging, gene expression, and DNA replication [13]. In general, most of the PTMs are reversible processes and are dynamically regulated by three groups of specific proteins as follows: epigenetic writers such as lysine methyltransferase (KMT) and lysine acetyltransferases (KATs, also known as histone acetyltransferases or HATs), which place specific marks on histone tails; epigenetic readers like bromodomains that can recognize these marks and interact with them; and finally erasers such as lysine-specific demethylase (LSD) and lysine deacetylases (KDACs, also known as histone deacetylases or HDACs), which catalyze the removal of acetyl as well as other acyl groups including long fatty acid chains [14, 15]. KDAC/HDACs are also acting on numerous non-histone proteins, e.g. HDAC6 acts on alpha-tubulin [16] or HDAC8 acts on the transcription factor (p53) and the structural maintenance of chromosomes 3 (SMC3) [17]. Since histone and protein acetylation is the primary focus of this work, it will be discussed in more detail.
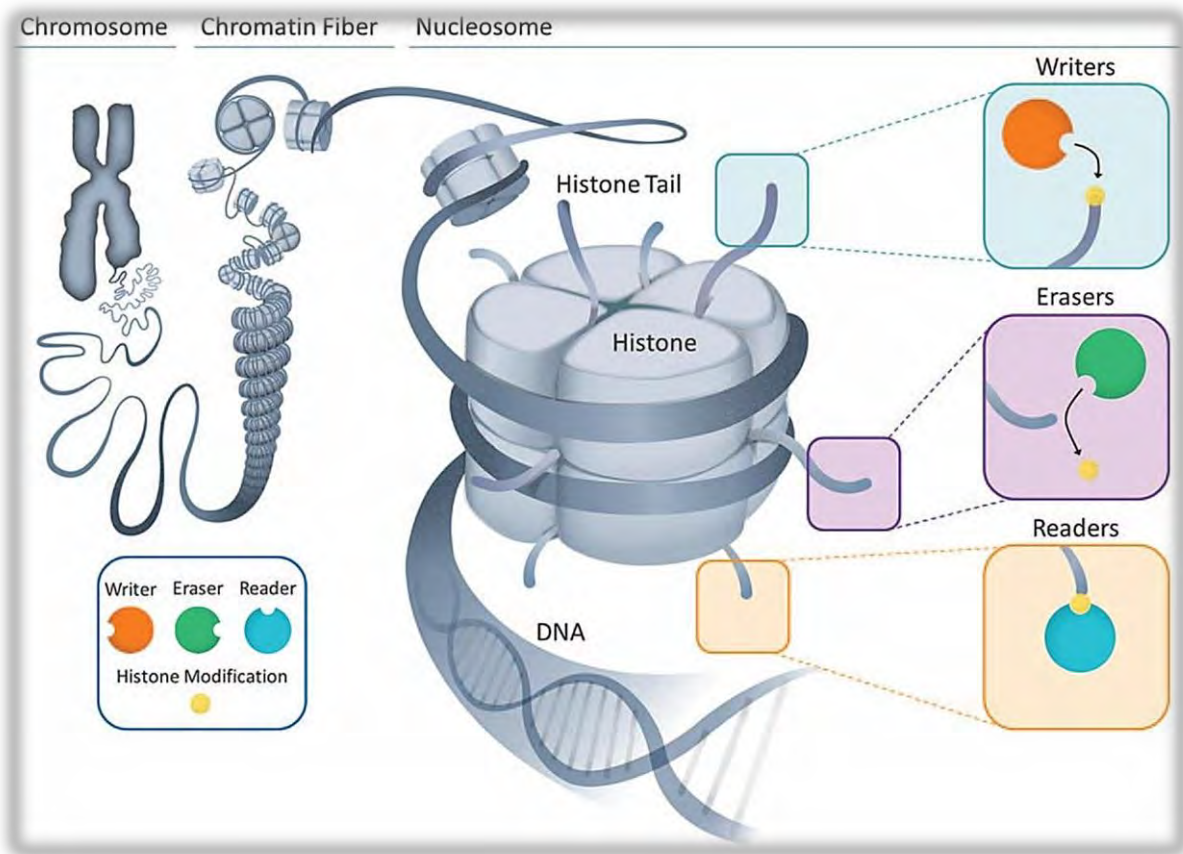
Figure 1: Chromatin structure and histone post-translational modifications (PTMs). The nucleosome is the fundamental building unit of chromatin and consists of DNA wrapped around core histone proteins, creating a compact structure essential for packing and stability of chromosomes. PTMs occur on the histone tails and are carried out by writers (adding), erasers (removing) covalent modifications and recognized by readers. Reproduced with permission from [18].

1.3. Histone acetylation

Reversible histone acylation is one of the well-studied PTMs and is linked to diverse processes such as control of gene expression and transcription, cell cycle progression, and DNA repair [19]. This particular modification is regulated by two enzyme families with opposing activities, namely histone acetyltransferases (KATs or HATs) and histone deacetylases (KDACs or HDACs) (**Figure 2**) [19]. It is worth mentioning that KATs and KDACs can acetylate and deacetylate lysine residues in histone and other non-histone proteins; therefore, these terms are more scientifically accurate [20]. However, as the abbreviations HATs and HDACs become more common, they will be used from now on to

refer to these enzymes. HATs catalyze the transfer of an acyl (mainly acetyl) group from the acetyl coenzyme A (Ac-CoA) to the ε-amino group of lysine residues in histone tails (**Figure 2**) [21]. Such modification results in decreasing the electrostatic affinity between these histones and DNA, and consequently leads to chromatin relaxation that enables the activation of gene transcription. Besides the acetylation of histones, HATs can acetylate other non-histone proteins such as the transcription factors p53, c-MYC, and the cytoskeletal protein α-tubulin [21]. Conversely, histone deacetylases (HDACs) are responsible for the removal of acyl (mainly acetyl) groups from acetylated lysine residues of histones, counteracting the effects of HATs by returning the histones to their initial state with the subsequent suppression of gene expression (**Figure 2**) [22]. HDACs can also remove acetyl marks from non-histone proteins such as p53 and α-tubulin [23]. Of particular interest for this work are HDACs; therefore, they will be discussed in more detail.
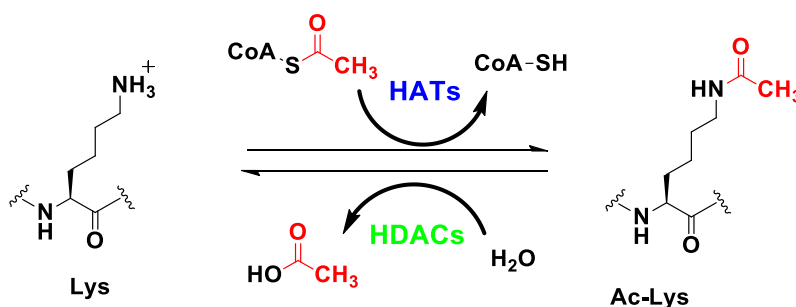
Figure 2: Regulation of histone acetylation dynamics. Histone acetyltransferases (HATs) transfer the acetyl group from acetyl Co-enzyme A to the lysine residue of the histone proteins. In contrast, histone deacetylases (HDACs) remove acetyl groups from the acetylated lysine.

1.4. Histone deacetylases

To date, eighteen different human HDACs have been identified and divided into two main families based on their cofactor dependency: the classical HDACs family and the non-classical HDACs, or sirtuins. The classical HDACs have a zinc ion in their active site, which is responsible for their catalytic activity (**Figure 3**), and they are subdivided based on their sequence similarity to yeast deacetylases into three classes. Class I HDACs (HDAC1-3 and HDAC8) are similar to yeast protein Rpd3, class II HDACs (HDAC4-7, HDAC9, and HDAC10) have sequence similarity to yeast protein Hda1, and class IV (HDAC11) shares sequence similarity to Rpd3 and Hda1 [22, 24]. The non-classical HDACs, or sirtuins (SIRT1-7), belong to class III HDACs and obtained the sirtuins nomenclature as they are

homologous to the yeast silent information regulator 2 (Sir2). Unlike classical HDACs, sirtuins require the cofactor nicotinamide adenine dinucleotide (NAD^+) instead of the zinc ion for their deacetylase activity [22, 24]. Recently, HDACs have gained great interest as promising epigenetic targets due to their essential role in regulating various biological processes, including metabolism, DNA damage response, cell cycle, apoptosis, angiogenesis, and several other physiological functions [25]. Moreover, their overexpression has been associated with many pathological disorders, which are extensively discussed in many papers and reviews [26-29]. Class I HDACs will be discussed in the next part as they are the main focus of this work.
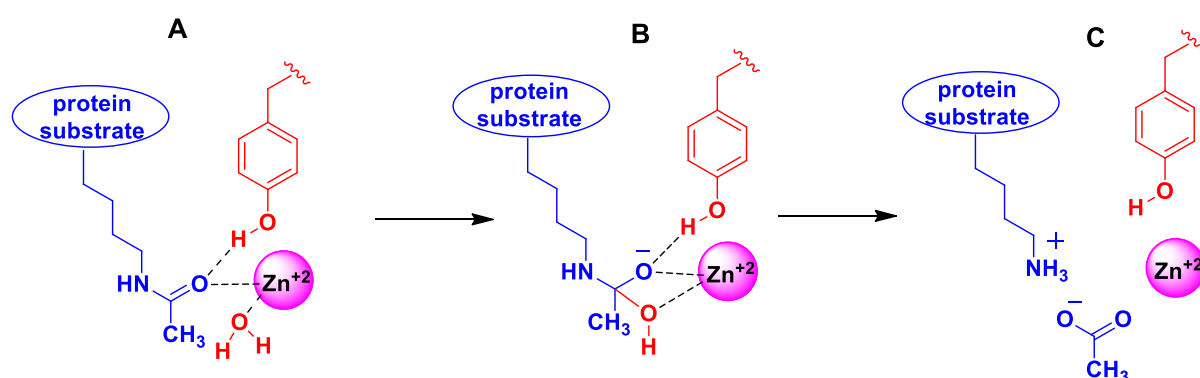
Figure 3: The catalytic mechanism of hydrolysis of acetyllysine by classical HDACs. (**A**) Interactions between the acetyllysine of the protein substrate with the zinc ion and tyrosine residue in the HDAC active site. (**B**) Formation of tetrahedral intermediate through the nucleophilic attack by the zinc-bound water molecule on the carbonyl group. (**C**) Dissociation of the tetrahedral intermediate yields the deacetylated lysine residue and acetate ion [30].

1.5. Class I HDACs structural features and their catalytic activity

Class I HDACs are ubiquitously expressed and share a highly conserved deacetylase domain [31]. HDAC1 and 2 are nuclear enzymes, whereas HDAC3 and 8 can be found in both the cytoplasm and nucleus [32, 33]. Generally, class I HDACs are recruited in large multiprotein complexes with each other or with their co-repressors for maximal catalytic activity, except for HDAC8, which is fully active in isolation and does not require the formation of a multiprotein complex for its deacetylase activity [34]. HDAC1 and 2 are activated through recruitment into several corepressor complexes [35]. For example, both isoforms combine with the LSD1 protein and the corepressor of REST1-3 proteins to generate the CoREST complex [36, 37]. In addition, the nucleosome remodeling and deacetylase nuclear receptor

co-repressor (NuRD) and the SWI-independent-3A (Sin3A) are other known HDAC1/2 corepressor complexes [38]. On the other hand, HDAC3 is exclusively associated with silencing mediators for retinoid and thyroid hormone receptors (SMRT) and nuclear receptor corepressor (NCoR) to form the SMRT/NCoR co-repressor complex [39]. It has been reported that the interaction between the SMRT/NCoR complex and HDAC3 is essential for the stimulation of HDAC3 deacetylase activity [36, 39]. In addition to histones, class I HDAC can deacetylate other non-histone proteins (e.g., p53, STAT3, E2F1, ERα) leading to the regulation of several cellular processes [20]. For example, the tumor suppressor proteins p53 and E2F1 are known substrates of HDAC1 owing to their predominant nuclear localization [40, 41]. HDAC3 was also proposed to deacetylate nuclear factor kappa B (NF-κB) p65, resulting in repression of its transcriptional activity [42].

The active site of class I HDACs is highly conserved with high sequence similarities (**Figure 4**). For instance, HDAC1 and 2 share more than 80% sequence homology, while HDAC3 shares around 50% sequence homology with HDAC1 and 2 [43]. Despite being a member of class I HDACs, HDAC8 shows lower sequence similarity with HDAC1-3 [43]. Generally, the catalytic core of class I HDACs shows the classical HDAC structure, comprising a large catalytic domain, which consists of a central 8-stranded β-sheet surrounded by several α-helices and interconnecting loops. HDAC1-3 additionally show an unstructured C-terminal tail (35–160 residues), which is not found in HDAC8 [43-45]. This C-terminal domain is used to recruit the enzymes to protein complexes that modulate their enzymatic activities. Additionally, the activity of HDAC1-3 is regulated by posttranslational modifications to such a C-terminal tail [44]. A second structural difference distinguishing HDAC8 from other class I HDACs is that HDAC8 has a wider substrate binding pocket and a larger surface opening compared with HDAC1-3 [44]. The active site entrance of class I HDACs is found on the surface of these enzymes, with the catalytic zinc ion deeply buried in a narrow cavity at the bottom of a tube-like channel (also called an acetyllysine binding tunnel) [43]. A 14 Å long internal cavity called the 'foot pocket' (**Figure 4**) lies perpendicular to the end of the former tube-like channel and has been proposed to form an exit route for the acetate by-product after the hydrolysis reaction. This foot pocket is found mainly in class I HDACs. Some studies also reported the presence of a large hydrophobic pocket in HDAC11, which can accommodate long-chain fatty acyl groups [46, 47]. The foot pocket is larger in HDAC1-3 compared with HDAC8, mainly due to the replacement of leucine residue with tryptophan (Trp141) in case of HDAC8 [43, 48]. Moreover, it was reported that HDAC8 has a specific side pocket formed

by the L1, L6 loops and the catalytic tyrosine allowing the binding of L-shaped inhibitors which are not able to bind to the active site of other HDAC isoforms due to the L1-L6 lock [49]. Additionally, Ser113/Ser118 of HDAC1/2 are replaced by a tyrosine residue in HDAC3 hindering inhibitors with bulky groups from accessing the foot pocket [43]. All the above-mentioned specific features can be exploited for the development of selective class I HDAC inhibitors, as will be discussed later.
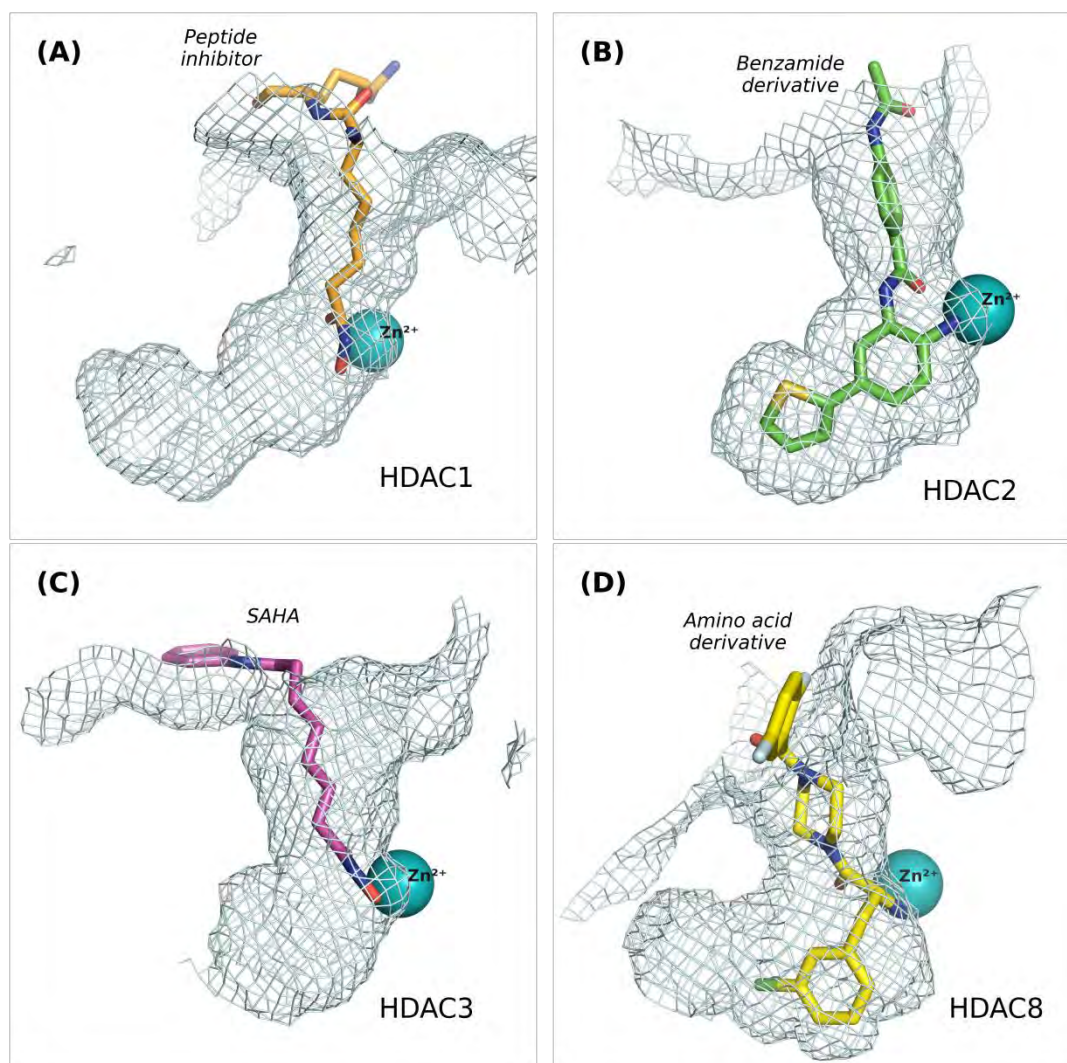
Figure 4: Structural comparison of the binding site and foot pocket of HDAC1-3 and 8. (A) HDAC1 in complex with a peptide inhibitor (PDB ID: 4BKX), (B) HDAC2 in complex with a 2-aminobenzamide derivative (PDB ID: 4LY1), (C) HDAC3 (PDB ID: 4A69) in complex with SAHA (taken from HDAC2 crystal structure; PDB ID: 4LXZ), (D) HDAC8 in complex with an amino acid derivative (PDB ID: 3SFF)

1.6.   Class I HDACs as potential therapeutic targets

As previously mentioned, HDACs can induce several molecular effects through the deacetylation of histone and non-histone substrates. Hence, the dysregulation of HDACs could increase the acetylation level and alter the expression of certain genes which are associated with the initiation and progression of cancers and other diseases [24, 26, 50, 51]. The aberrant expression of class I HDACs is most notably linked with various solid and hematological malignancies and is highly attributed to advanced disease as well as poor patient outcomes [52]. For instance, elevated levels of HDAC1 was reported in several cancers, including colon adenocarcinoma [53], gastric, prostate, and breast cancers [54]. HDAC 2 and 3 overexpression was reported in Hodgkin's lymphoma [55] and colorectal cancers [54]. Furthermore, overexpression of HDAC8 was found to be correlated with neuroblastoma [56]. The aberrant activity of HDACs has also been associated with neurodegenerative diseases [57, 58], inflammatory diseases [59], HIV latency [60], and metabolic disorders [61]. Moreover, several human parasites depend on HDACs for maturation and survival [62, 63]. As a result of the aforementioned findings, HDACs have emerged as promising therapeutic targets for the treatment of cancer and other diseases. Within the primary focus of the current work are HDAC inhibitors as anticancer agents; therefore, they will be discussed in more detail. Additionally, another part of this thesis includes a review article summarizing the recent advances in the design of antischistosomal HDAC inhibitors.

1.6.1   HDAC inhibitors as anticancer agents

Over the last three decades, HDAC inhibitors (HDACi) have gained great interest as potential therapeutic candidates for the treatment of several subtypes of blood malignancies. HDACi can induce cancer cell death via several pathways. Among these pathways is the induction of cell cycle arrest through the increased transcription of genes such as the cyclin-dependent kinase inhibitor p21 (*CDKN1A*) [64]. HDACi can also induce apoptosis via transcriptional induction of pro-apoptotic genes and repression of anti-apoptotic ones, including several members of the *BCL2* family [65]. Other pathways include angiogenesis inhibition [66], autophagy induction [67, 68], and reactive oxygen species accumulation, which results in oxidative stress and cell death [69]. Most HDACi share a common pharmacophore comprising a capping group, a zinc-binding group (ZBG), and a hydrophobic linker connecting both groups (**Figure 5**) [45]. The capping group occupies the entrance region to

the active site of the enzyme. This part of the enzyme is less conserved and consists of variable amino acid residues among different HDAC isozymes. The presence of aromatic substituents in the capping group can induce additional hydrophobic interactions with the rim of the enzyme [70]. The ZBG coordinates the zinc ion in the catalytic active site either in a monodentate or bidentate fashion [71]. HDAC inhibitors are traditionally classified according to the chemical structures of their ZBG into hydroxamic acids [72], 2-aminobenzamides [73], cyclic peptides [74], short-chain fatty acids [75], thiols [76], and ketones [77]. Moreover, other zinc binders have been recently reported such as alkylated acid hydrazides [78, 79] and trifluoromethyloxadiazoles [80]. To date, four HDACi have been granted US Food and Drug Administration (FDA) approval for the treatment of different hematological malignancies (**Figure 5**). The approved inhibitors include vorinostat (SAHA, **I**) [81], panobinostat (LBH589, **II**) [82], and belinostat (PXD101, **III**) [83], which are hydroxamic acid-based pan-HDAC inhibitors and are used for the treatment of patients with cutaneous T-cell lymphoma (CTCL), peripheral T-cell lymphoma (PTCL), and multiple myeloma, respectively. Romidepsin (**IV**, thiol-prodrug/depsipeptide) is a class I selective HDACi and is approved for the treatment of PTCL and CTCL [84]. Finally, the 2-aminobenzamide-based HDACi (tucidinostat, formerly known as chidamide, **V**) was approved by the China Food and Drug Administration (CFDA) to treat patients with PTCL [85].
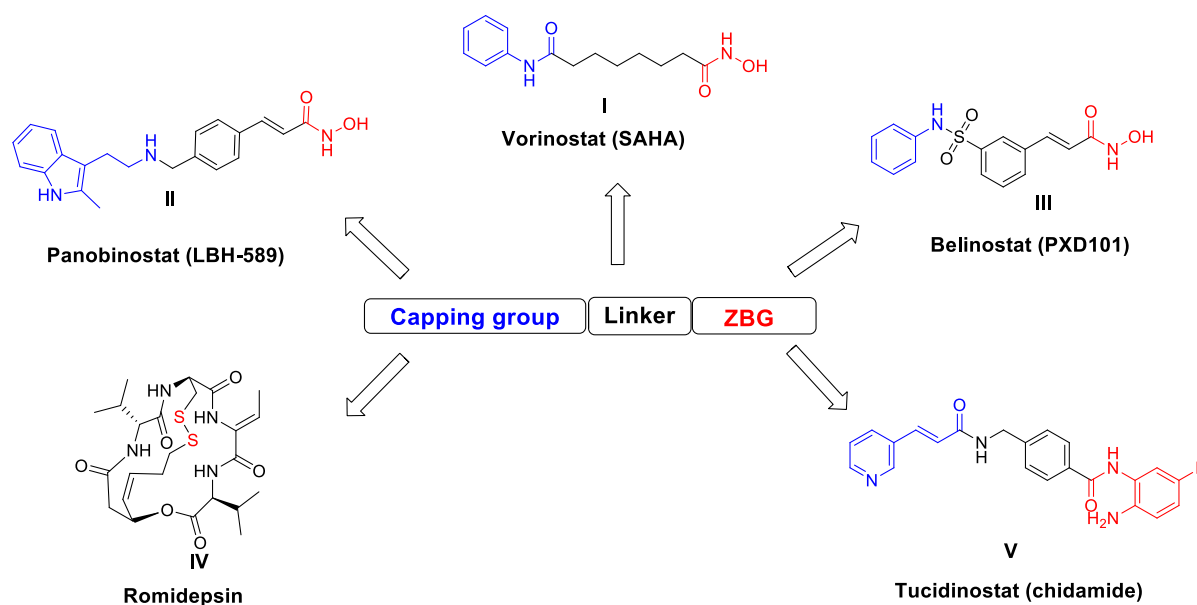
Figure 5: General pharmacophore model of HDAC inhibitors and chemical structures of the approved HDAC inhibitors.

Moreover, many other HDACi are currently in different phases of clinical trials, either as single agents or in combination with other chemotherapeutic agents [86]. However, the majority of HDACi suffer from some limitations, including poor pharmacokinetic properties, low therapeutic indices, and severe adverse effects such as thrombocytopenia, cardiotoxicity, and gastrointestinal disorders [86, 87]. This may be due to the non-selective inhibition of different HDAC isoforms since most of the currently available HDACi are pan-inhibitors or are at best class selective inhibitors. In addition, it was reported that the hydroxamic acid (ZBG) in many HDACi can undergo a Lossen rearrangement to yield the corresponding isocyanate derivative, which is associated with mutagenicity [88]. Furthermore, acquired resistance to HDACi was clinically reported, thus limiting their efficacy [86]. Such problems may be the main reasons to exclude several potent candidates from further drug development processes. Therefore, several strategies have been reported to overcome such drawbacks. These strategies include the design of selective HDAC inhibitors and applying the prodrug concept to the currently available HDAC inhibitors to enhance the tissue selectivity. Moreover, the flexibility in the general pharmacophoric model of HDACi makes them tunable to be merged with other pharmacophore cores for the design of multi-targeted hybrids. The targeted chemical degradation of specific HDAC isoforms is another tool that has been recently applied to specifically degrade different HDAC isoforms, which might provide many advantages over conventional HDAC inhibitors. These different strategies will be discussed in the following part.

1.6.2. Selective class I HDAC inhibitors

The design of isoform-selective HDAC inhibitors has gained increasing attention in recent years as a promising approach to avoid the undesirable side effects associated with pan-HDACi. Among class I HDACs, the HDAC8 isozyme has distinct structural and functional features that can be utilized to design selective HDAC8 inhibitors [49]. On the other hand, other members of class I HDACs have minor structural differences, which render the design of HDAC1, 2, and 3 selective inhibitors challenging [43]. Despite the few structural differences, it is still possible to achieve the required isoform selectivity through the modification of different pharmacophoric elements of classical HDAC inhibitors. The 2-aminobenzamide scaffold is widely used as ZBG for the design of selective class I HDACi (**Figure 6**). Entinostat (MS-275, **VI**) is an example of the 2-aminobenzamide-based HDACi, which is currently in different phases of clinical trials for the treatment of hormone receptor-positive advanced breast cancer and Hodgkin lymphoma [89, 90]. Entinostat showed more

than 55-fold selectivity for HDAC1 over HDAC8. Moreover, within class I, entinostat showed a 12-fold preference for HDAC1 compared to HDAC3. Mocetinostat (MGCD0103, **VII**) [91] and tacedinaline (CI-994, **VIII**) [92] are other aminobenzamide analogs that showed not only class I, but also some isoform selectivity (**Figure 6**).

The foot pocket is a characteristic structural feature that can be exploited to enhance the selectivity among different class I HDAC isoforms. This pocket is close to the catalytic active site and is lined with hydrophobic residues; therefore, the substitution of the 2-aminobenzamide ZBG with bulky aryl groups could favorably enhance isoform selectivity. In this regard, several HDAC inhibitors bearing different aromatic substituents at the C-5 position of the benzamide part showed improved selectivity profiles. For example, analogs of entinostat (**IX** and **X**) with 2-thienyl or phenyl moieties showed a very high preference for HDAC1 over HDAC3 (**Figure 6**) [93]. Interestingly, the presence of the 2-thienyl moiety on the benzamide part of tacedinaline, as in the case of compound (**XI**), resulted in more than 100-fold selectivity for HDAC1 and 2 over HDAC3 [92]. One possible reason for the improved selectivity of substituted benzamides is the presence of serine residues in the foot pocket of both HDAC 1 and 2 isoforms, whereas there is a bulkier tyrosine residue in HDAC3 causing steric hindrance, thus limiting the access of bulky substituents. It was also reported that small substituents, such as the fluoro atom at the C-4 position of the benzamide scaffold, can be well tolerated in the foot pocket of HDAC3, and these derivatives showed improved selectivity over HDAC1 and 2. For example, BRD3308 (**XII**), a derivative of tacedinaline with a fluoro atom, displayed more than 18-fold selectivity for HDAC3 over HDAC1 and 2 (**Figure 6**) [94]. Additionally, RGFP996 (**XIII**) showed higher selectivity for HDAC3 over other isoforms [95]. Therefore, modifications of the substitution pattern on the benzamide scaffold can be utilized as a promising tool to achieve the required individual HDAC1, 2, and 3 isoform selectivity.

VI

Entionstat (MS-275)

IC$_{50}$ (HDAC1) = 0.18 ± 0.07 µM
IC$_{50}$ (HDAC2) = 1.16 ± 0.13 µM
IC$_{50}$ (HDAC3) = 2.31 ± 0.80 µM
IC$_{50}$ (HDAC8) > 10 µM

VII

Mocetinostat (MGCD0103)

IC$_{50}$ (HDAC1) = 0.15 ± 0.02 µM
IC$_{50}$ (HDAC2) = 0.29 ± 0.08 µM
IC$_{50}$ (HDAC3) = 1.66 ± 0.69 µM
IC$_{50}$ (HDAC8) > 10 µM

VIII

Tacedinaline (CI-994)

IC$_{50}$ (HDAC1) = 0.9 µM
IC$_{50}$ (HDAC2) = 0.9 µM
IC$_{50}$ (HDAC3) = 1.2 µM
IC$_{50}$ (HDAC8) > 20 µM

IX

IC$_{50}$ (HDAC1) = 0.006 µM
IC$_{50}$ (HDAC3) > 10 µM

X

IC$_{50}$ (HDAC1) = 0.01 µM
IC$_{50}$ (HDAC3) = 6.18 µM

XI

IC$_{50}$ (HDAC1) = 0.04 µM
IC$_{50}$ (HDAC2) = 0.1 µM
IC$_{50}$ (HDAC3) > 20 µM
IC$_{50}$ (HDAC8) > 20 µM

XII

BRD3308

IC$_{50}$ (HDAC1) = 1.08 ± 0.44 µM
IC$_{50}$ (HDAC2) = 1.15 ± 0.38 µM
IC$_{50}$ (HDAC3) = 0.06 ± 0.02 µM

XIII

RGFP966

IC$_{50}$ (HDAC1) > 15 µM
IC$_{50}$ (HDAC2) > 15 µM
IC$_{50}$ (HDAC3) = 0.08 µM

Figure 6: Examples of reported 2-aminobenzamide selective HDAC1/2/3 inhibitors.

1.6.3. Targeted degradation of class I HDACs

Recently, targeted protein degradation (TPD) has attracted substantial interest as an innovative therapeutic modality [96, 97]. The concept of TPD is to induce the degradation of the protein of interest (POI) through hijacking the endogenous protein degradation machinery. The proteolysis targeting chimeras (PROTACs) tool has emerged as one of the most promising TPD technologies that have recently moved from academia to the pharmaceutical and biotechnology industries [96]. In addition to PROTACs, several TPD strategies, including hydrophobic tags (HyT) [98], molecular glues [99], lysosome-targeting chimeras (LYTACs) [100], autophagy-targeting chimeras (AUTOTACs) [101], and chaperone-mediated protein degradation (CHAMP) [102] have been recently developed. In the following part, PROTACs and HyT technologies will be discussed in more detail.

1.6.3.1. Mechanism of action of PROTACs

A classical PROTAC molecule comprises a POI-targeting warhead, an E3 ubiquitin ligase ligand, and an appropriate linker connecting the two ligands (**Figure 7**). PROTACs induce

13

proximity between the POI and an E3 ligase through the formation of a ternary complex which facilitates the transfer of ubiquitin from the E2 ubiquitin-conjugating enzyme to lysine residues on the surface of the POI, hence marking the protein for its degradation through the 26S proteasome (**Figure 7**) [97]. Compared with conventional inhibitors, PROTACs have potential advantages: (1) PROTACs work in a sub-stoichiometric and catalytic way (i.e. the PROTAC molecule can be recycled to induce target protein degradation at lower doses compared to traditional inhibitors, thereby reducing possible side effects). (2) TPD via PROTACs could minimize drug resistance through suppression of mutations and/or overexpression of POI. (3) In many cases, selective degradation among closely related targets or mutants was successfully achieved through PROTACs [97]. Several PROTACs are currently in different phases of clinical trials for the treatment of different types of cancer [96, 103].
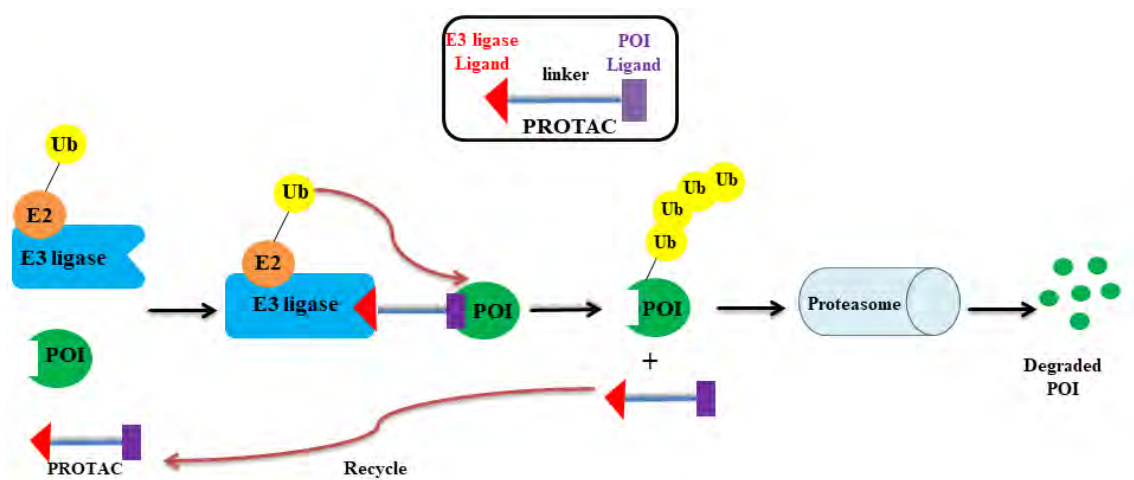
Figure 7: Schematic illustration of the mechanism of action of PROTACs. Typical PROTAC molecule consists of ligand that bind to a protein of interest (POI), an E3 ubiquitin ligase ligand, and a linker connecting both units. The formation of POI-PROTAC-E3 ligase ligand ternary complex leads to the transfer of the ubiquitin to the POI. The proteasome recognizes the polyubiquitinated protein and mediates the degradation of the POI. The PROTAC molecule can be regenerated to repeat the degradation cycle.

1.6.3.2. Selective class I HDAC-PROTACs

During the last five years, many HDAC-PROTACs have been reported to selectively degrade individual HDAC isoforms such as HDAC4, 6, and 8 [104-108]. Additionally, several class I HDAC degraders have been recently reported. PROTACs **XIV-XVI** (**Figure 8**) are examples of class I HDAC-degraders, which were designed by tethering the Von Hippel-Lindau (VHL)

E3 ligase ligand with the class I HDACi (tacedinaline) using different linkers [109, 110]. PROTAC **XIV** induced 50% degradation of HDAC 1, 2, and 3 at a 1 µM concentration in human colorectal carcinoma (HCT116) cells [109]. Modification of the linker composition of PROTAC **XIV** resulted in enhanced degradation potency as in the case of PROTACs **XV** and **XVI**, which induced degradation of HDAC1-3 in HCT116 cells at submicromolar concentrations [110]. PROTACs **XVII** and **XVIII** are another class I HDAC degraders that were also designed based on tacedinaline while replacing the VHL ligand with the cereblon (CRBN) E3 ligase ligand pomalidomide (**Figure 8**) [111]. PROTAC **XVII** induced the degradation of HDAC3 in RAW 264.7 macrophages at a 10 µM concentration. However, degradation of HDAC1 and 2 was observed only at higher concentrations. Substitution of the benzamide scaffold of tacedinaline with a fluoro atom at the C-4 position resulted in enhanced potency and selectivity against HDAC3, as in the case of PROTAC **XVIII** which exhibited selective HDAC3 degradation (DC$_{50}$ of 0.32 µM) [111]. In 2020, Xiao et al. reported the first-in-class selective HDAC3 degrader (PROTAC **XIX**) (**Figure 8**) using the class I HDAC inhibitor (**SR-3558**) as the POI warhead [112]. They have previously identified **SR-3558** as a potent class I HDACi with benzoyl alkylated hydrazide as a novel ZBG [78]. PROTAC **XIX** potently and selectively induced degradation of HDAC3 in MDA-MB-468 cells in a time- and and dose-dependent manner [112].
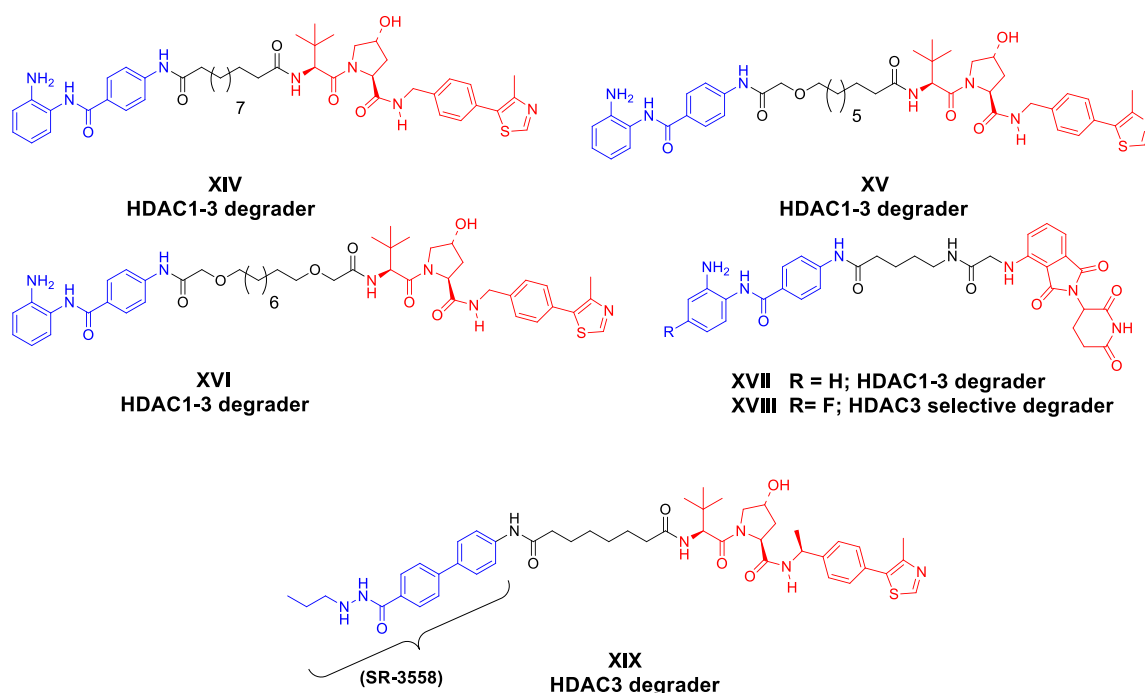
Figure 8: Examples of reported selective HDAC1/2/3 degraders.

1.6.3.3. Mechanism of action of hydrophobic tags (HyT)

Like PROTACs, hydrophobic tags are bifunctional molecules consisting of a POI-targeting ligand connected to a bulky hydrophobic fragment (such as an adamantyl group or *tert*-butyl carbamate-protected arginine (Boc3-Arg) moiety) through an appropriate linker [113-116]. Although the exact mechanism of proteasomal degradation induced by Hyt is still unclear, two proposed mechanisms were reported based on the hydrophobic fragment used for the design of Hyt degraders. The first mechanism of action is associated with the adamantyl-based Hyt, in which the adamantyl group may either induce destabilization of the POI leading to the recruitment of molecular chaperones like the heat shock protein Hsp70 to the misfolded protein, followed by degradation through the proteasome S26 or such adamantyl moiety can be directly recognized by chaperones without prior POI destabilization (**Figure 9**) [117]. In the case of Boc3-Arg-mediated degradation, it is postulated that such hydrophobic mark can bind directly to the proteasome S20 to promote the degradation of POI [115, 117].
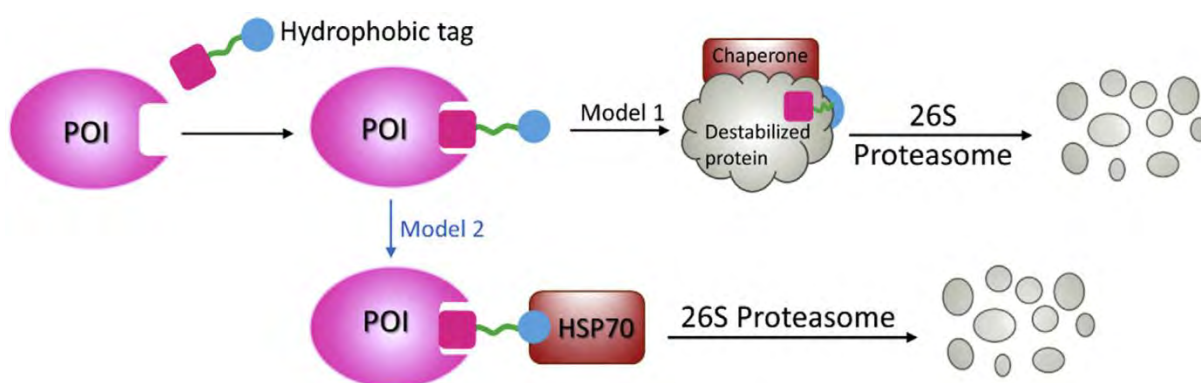
Figure 9: Proposed molecular mechanisms of adamantyl-based HyT. In model 1, the adamantyl moiety induces destabilization of POI, which leads to recruitment of chaperones, followed by proteasomal degradation. In model 2, the adamantyl moiety is directly recognized by chaperones, followed by proteasomal degradation. Reproduced with permission from [117].

To date, no hydrophobic tag-based degrader has been reported to induce the degradation of HDAC isoforms. However, this technique has been successfully applied to degrade other targets. Among the recently developed Hyt-based degraders is TX2-121-1 (**XX**) (**Figure 10**), which was designed as an epidermal growth factor receptor-3 (HER3) degrader by connecting a HER3 ligand to the adamantyl moiety via a short linker [118]. Another example is MS1943 (**XXI**), the first-in-class enhancer of zeste homolog 2 (EZH2) selective degrader [119].
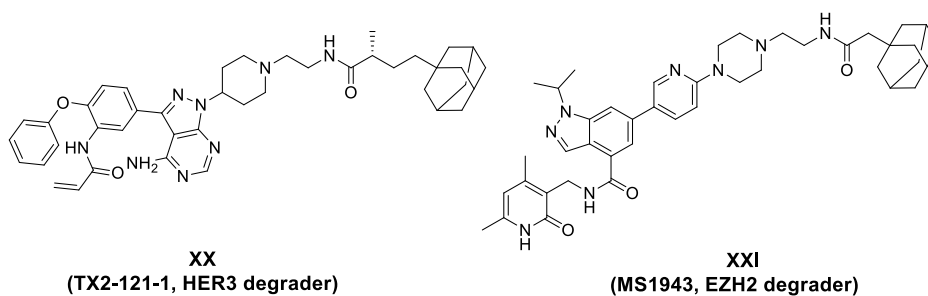
Figure 10: Representative examples of reported adamantyl-based HyT degraders.

1.6.4. HDAC inhibitors-based prodrugs

Prodrugs are inactive forms of drugs that undergo chemical or enzymatic transformations to release the bioactive form of their parent drugs. The prodrug strategy has been widely used in the drug development process for more than 100 years to improve both the pharmacokinetic and pharmacodynamic properties of drugs. In addition, this approach can be utilized in the field of targeted cancer therapy to enhance targeted-tissue specificity and improve drug delivery to selected cell types, thus minimizing off-target side effects. The prodrug concept has already been applied to several reported HDACi to obtain candidates with improved therapeutic properties. Liao et al. developed the SAHA-based prodrug **XXII** by masking the hydroxamate ZBG with an aryl boronic acid scaffold (**Figure 11**) [120]. This aryl boronic acid moiety is sensitive to reactive oxygen species (ROS) and reactive nitrogen species (RNS) and undergoes self-immolation resulting in the intracellular release of the free hydroxamic acid [120]. Compound **XXII** was tested against MV4-11, a type of acute myeloid leukemia cells characterized by high levels of ROS and RNS. In vitro studies showed that the prodrug was successfully activated by the elevated level of such reactive species and exhibited potent anti-leukemic activity [120]. Bhagat et al. designed another SAHA-based prodrug **XXIII** to improve the specificity of SAHA against cancer cells [121]. They used the ROS-sensitive group, 4-hydroxymethylphenylboronic acid pinacol ester, as a masking group which can be specifically activated in the presence of a high level of hydrogen peroxide to release the parent drug (**Figure 11**) [121]. Compound **XXIII** demonstrated selective cytotoxicity against multiple cancer cells over healthy cells.

Hypoxia, a state of deficiency in oxygen supply reaching the cell, is another characteristic feature in malignant cells that can be exploited to design prodrugs that specifically release their parent drugs in tumor cells [122]. This approach was applied to some known HDACi, where a bioreductive masking group was connected to the ZBG thereby producing an inactive

compound that undergoes a chemical reduction in hypoxic tumor cells to release the active drug. Several bioreductive protecting groups were reported including quinones, *N*-oxides, and nitroaryl groups [122]. Recently, different hypoxia-activated prodrugs (**XXIV**-**XXVI**) have been designed using 4-nitrobenzyl or 1-methyl-2-nitroimidazole as masking groups for the hydroxamic acid functionality in different HDACi such as SAHA and panobinostat (**Figure 11**) [123, 124]. In vitro studies showed that these prodrugs underwent reduction under hypoxic conditions followed by fragmentation and release of active drugs.
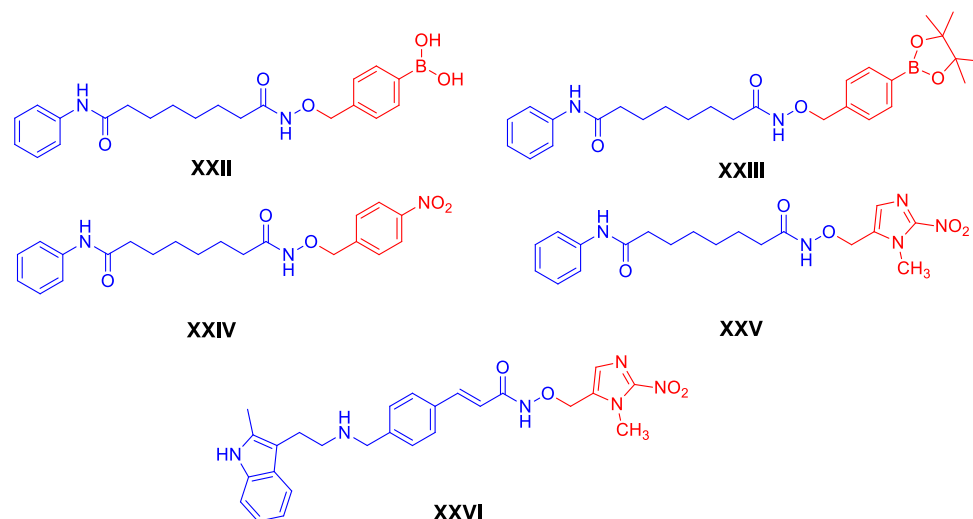
Figure 11: Examples of HDAC inhibitors-based prodrugs.

1.6.5. HDAC inhibitors in anticancer combination therapies

Although HDACi showed great promise in treating various types of blood malignancies, resistance to HDACi remains a major problem that usually results in the maintenance and regeneration of tumor cells [125-127]. Several mechanisms of HDACi-based resistance have been identified, such as drug efflux, epigenetic alterations, autophagy, and anti-apoptotic pathway alterations [126-128]. One strategy that could overcome such a problem is the use of a combination of HDACi with other anticancer agents such as tyrosine kinase inhibitors [129-131], proteasome inhibitors [132-134], immune checkpoint inhibitors [135-137], and topoisomerase inhibitors [138, 139]. Such combination regimens can synergistically increase the sensitivity and efficacy of HDACi and reduce the possibility of resistance development. Acute myeloid leukemia (AML) is a representative example, where combination therapy of HDAC and kinase inhibitors could be utilized to achieve a synergetic effect [140, 141]. AML is an aggressive hematological malignancy characterized by increased proliferation and differentiation of hematopoietic stem cells resulting in bone marrow failure and organs

infiltration [142]. Aberrant expressions of class I HDAC isoforms are linked to AML. Additionally, HDACs are aberrantly recruited to oncogenic fusion proteins which play essential roles in the progress of leukemogenesis [27, 143]. FMS-like tyrosine kinase-3 (FLT3) is a transmembrane receptor protein that plays an essential role in the survival, proliferation, and differentiation of hematopoietic cells [144]. FLT3-ITD mutations (internal tandem duplications) are the most commonly identified genetic mutations of the *FLT3* gene that are found in around 25% of AML patients [144]. In recent years, it has been shown that combined pharmacological inhibition of HDACs and FLT3-ITD can synergistically induce apoptotic cell death in AML cells [145, 146]. HDAC inhibitors induce proteasomal degradation of FLT3-ITD through the transcriptional induction of the E2 ubiquitin conjugase (UBCH8), in addition to the phosphorylation-dependent binding of FLT3-ITD by the UBCH8-associated (SIAH1, SIAH2) E3 ubiquitin ligases [145, 147]. It has been reported that entinostat (MS-275) induced the degradation of FLT3-ITD through suppressing the activity of HSP90 in AML cells [148]. Moreover, a phase I trial of vorinostat (SAHA) in combination with sorafenib (FLT3 inhibitor) showed a clinical response in poor-risk AML patients [140], suggesting that the combination of HDAC and FLT3 inhibitors may be useful for the treatment of AML patients with FLT3 mutations.

1.6.6. HDAC inhibitors as antiparasitic agents

Neglected parasitic diseases are serious health conditions associated with high mortality and/or morbidity rates and affecting more than one billion people, mainly in poor and less developed countries [62]. Despite the incremental progress in pharmaceutical research and industry for targeting global diseases, there are only a few drugs that are used for the treatment of neglected infections. Additionally, the main problem with current antiparasitic therapeutics is drug resistance and consequent treatment failure [62]. Therefore, the discovery of new antiparasitic agents with novel modes of action is crucial to overcome the problem of drug resistance. In this regard, repurposing the drugs that have already been approved for the treatment of other human diseases represents a promising approach to identify new antiparasitic candidates. This approach could accelerate the drug development process due to the reduced time, cost, and risk compared with traditional drug discovery [63]. Owing to the numerous similarities between cancer cells and parasites in terms of metabolic and reproductive properties, anticancer agents are currently under investigation as potential therapeutics for different parasitic infections [63]. Since parasitic epigenetic modulators such as histone deacetylases play essential roles in the regulation of parasite gene expression and

some of them are crucial for the survival and growth of major human parasites, HDACs are currently emerging as potential novel therapeutic targets for various parasitic infections such as schistosomiasis [149], malaria [150-156], trypanosomiasis [157, 158], toxoplasmosis [159, 160], and leishmaniasis [161].

1.6.6.1. HDAC inhibitors as antischistosomal agents

Schistosomiasis is one of the most devastating neglected tropical parasitic diseases that affects more than 200 million people worldwide mostly in Africa, Asia, and South America [162]. The infection is caused by blood flukes (trematode worms) from the genus *Schistosoma*, mainly *S. mansoni*, *S. haematobium*, and *S. japonicum* [163]. Schistosomiasis control and treatment depend mainly on the periodic, large-scale drug administration of praziquantel as preventive and curative chemotherapy [163]. Although praziquantel is active against parasitic flatworms, some studies have demonstrated that reliance on this drug could result in the emergence of drug resistance [164-166]. As a result, identifying new antischistosomal agents with novel mechanisms of action is of high interest. Studies revealed that several orthologs of human histone deacetylases, including *sm*HDAC1, 3, and 8, are expressed in different stages of the parasite life cycle with *sm*HDAC8 being the most abundant isoform [167]. Therefore, several studies have focused on the *sm*HDAC8 isoform as an attractive target for the treatment of schistosomiasis. Some approved HDACi in addition to other *sm*HDAC8 inhibitors were reported to display in vitro inhibition of parasitic enzymatic activity accompanied with phenotypic effects. These studies are thoroughly reviewed in [149], a part of this thesis.

2. Objectives of the work

As previously discussed in the introductory part, histone deacetylases regulate several cellular processes by maintaining the dynamics of lysine acetylation level of histone and non-histone proteins. Consequently, dysregulation of HDACs expression is associated with many pathological disorders. Therefore, pharmacological inhibition of HDACs emerged as a promising approach in medicinal chemistry research, especially in the field of oncology, with five approved HDAC inhibitors for the treatment of various subtypes of blood malignancies in addition to many other inhibitors in clinical trials. However, several HDAC inhibitors suffer from some limitations, including poor pharmacokinetic properties, off-target side effects, mutagenicity, and the emergence of resistance. Following that, the main aim of the present work is to develop novel modulators for class I HDACs with improved therapeutic efficacy and better safety profiles through the application of different drug design approaches. In this regard, the following specific objectives will be applied:

2.1. Development of novel class I HDAC inhibitors

Since aberrant expression of class I HDACs is highly linked to the incidence and progression of many blood and solid tumors, we will focus in the first project on the development of selective class I HDAC inhibitors. The developed compounds will be evaluated for their in vitro activity against different HDAC isoforms to determine their potency and selectivity profiles. Additionally, the most promising compounds will be evaluated for their biological activity against acute myeloid leukemia and pancreatic cancer cell lines.

It is worth mentioning that the high sequence similarity between individual HDAC isoforms renders the design of selective class I HDAC isoforms challenging. Therefore, different computational approaches such as docking studies, molecular dynamics simulations, and binding free energy calculations will also be utilized to predict the selectivity of the developed inhibitors and minimize the time required to prioritize compounds for further biological studies.

2.2. Design of class I HDAC inhibitors-based prodrugs

Hypoxia is one of the characteristic tumor-intrinsic factors that can be utilized to design prodrugs that specifically release their parent drugs in tumor cells. The second project focuses on the development of novel bioreducible prodrugs for class I HDAC inhibitors by exploiting tumor hypoxic conditions to enhance targeted-tissue specificity and overcome the off-target side effects associated with many HDACi. The design of planned prodrugs is based on

masking the zinc-binding group of different HDAC inhibitors using different nitroaryl alcohols. The resulted masked prodrugs should have lower activity on class I HDACs while regaining the inhibitory action of the parent compounds after activation by nitroreductases in hypoxic cells. The synthesized prodrugs as well as their parent HDAC inhibitors will be tested for their in vitro activity against class I HDACs. Additionally, the cytotoxic activity of the developed prodrugs will be evaluated against wild-type and nitroreductase (NTR) transfected-THP1 leukemic cells.

2.3. Development of class I HDAC degraders

As previously mentioned, the targeted protein degradation (TPD) concept serves as a powerful and innovative tool for drug discovery and has potential advantages compared to conventional inhibitors. Following that, the main focus of the third project will be the application of different TPD techniques, including PROTACs and hydrophobic tags to develop selective degraders for class I HDACs. Different reported HDAC inhibitors will be used as protein of interest warheads and will be connected to either different E3 ligase ligands for the design of PROTACs or to the hydrophobic adamantyl scaffold for the design of hydrophobic tag-based degraders. Additionally, various linkers of different lengths and compositions will be used for the design of the planned degraders. The synthesized compounds will be screened for their in vitro activity against different HDAC isoforms. Moreover, the developed compounds will be screened against different cancer lines to determine their cytotoxicity and their ability to degrade the target enzymes.

2.4. HDAC inhibitors as antischistosomal agents

There is growing evidence that therapeutic applications of HDAC inhibitors are not limited to the field of oncology since there are several studies indicating that different HDAC isozymes are dysregulated in several pathological disorders. Human parasitic diseases are representative examples that are currently considered valid drug targets for the application of HDAC inhibitors. Several orthologs of human HDACs are expressed at different stages of the life cycle of Schistosoma species. Additionally, repurposing the approved HDAC inhibitors as well as other inhibitors in clinical trials represents a promising approach for identifying new antiparasitic candidates. In this regard, there will be a brief review discussing the recent advances in developing inhibitors for schistosomal histone deacetylases, with a particular focus on *Sm*HDAC8 as a novel therapeutic target.

3. Results

The results of the work in this dissertation are reported in the following scientific manuscripts. In addition, other unpublished results are presented in **chapter 4.**

3.1. Synthesis, Molecular Docking and Biological Characterization of Pyrazine Linked 2-Aminobenzamides as New Class I Selective Histone Deacetylase (HDAC) Inhibitors with Anti-Leukemic Activity

Hany S Ibrahim, **Mohamed Abdelsalam**, Yanira Zeyn, Matthes Zessin, Al-Hassan M Mustafa, Marten A Fischer, Patrik Zeyen, Ping Sun, Emre F Bülbül, Anita Vecchio, Frank Erdmann, Matthias Schmidt, Dina Robaa, Cyril Barinka, Christophe Romier, Mike Schutkowski, Oliver H Krämer, Wolfgang Sippl

Abstract

Class I histone deacetylases (HDACs) are key regulators of cell proliferation and they are frequently dysregulated in cancer cells. We report here the synthesis of a novel series of class-I selective HDAC inhibitors (HDACi) containing a 2-aminobenzamide moiety as a zinc-binding group connected with a central (piperazin-1-yl)pyrazine or (piperazin-1-yl)pyrimidine moiety. Some of the compounds were additionally substituted with an aromatic capping group. Compounds were tested in vitro against human HDAC1, 2, 3, and 8 enzymes and compared to reference class I HDACi (Entinostat (MS-275), Mocetinostat, CI994 and RGFP-966). The most promising compounds were found to be highly selective against HDAC1, 2 and 3 over the remaining HDAC subtypes from other classes. Molecular docking studies and MD simulations were performed to rationalize the in vitro data and to deduce a complete structure activity relationship (SAR) analysis of this novel series of class-I HDACi. The most potent compounds, including 19f, which blocks HDAC1, HDAC2, and HDAC3, as well as the selective HDAC1/HDAC2 inhibitors 21a and 29b, were selected for further cellular testing against human acute myeloid leukemia (AML) and erythroleukemic cancer (HEL) cells, taking into consideration their low toxicity against human embryonic HEK293 cells. We found that 19f is superior to the clinically tested class-I HDACi Entinostat (MS-275). Thus, 19f is a new and specific HDACi with the potential to eliminate blood cancer cells of various origins.

Article

Synthesis, Molecular Docking and Biological Characterization of Pyrazine Linked 2-Aminobenzamides as New Class I Selective Histone Deacetylase (HDAC) Inhibitors with Anti-Leukemic Activity

Hany S. Ibrahim [1,2,†], Mohamed Abdelsalam [1,3,†], Yanira Zeyn [4], Matthes Zessin [1,5], Al-Hassan M. Mustafa [4,6], Marten A. Fischer [4], Patrik Zeyen [1], Ping Sun [1], Emre F. Bülbül [1], Anita Vecchio [1], Frank Erdmann [1], Matthias Schmidt [1], Dina Robaa [1], Cyril Barinka [7], Christophe Romier [8], Mike Schutkowski [5], Oliver H. Krämer [4,*,‡] and Wolfgang Sippl [1,*,‡]

1 Department of Medicinal Chemistry, Institute of Pharmacy, Martin-Luther-University of Halle-Wittenberg, 06120 Halle (Saale), Germany; hany.ibrahim@pharmazie.uni-halle.de (H.S.I.); mohamed.abdelsalam@pharmazie.uni-halle.de (M.A.); matthes.zessin@googlemail.com (M.Z.); patrik.zeyen@gmail.com (P.Z.); ping.sun@pharmazie.uni-halle.de (P.S.); emre.bulbul@pharmazie.uni-halle.de (E.F.B.); anitavecchio95@gmail.com (A.V.); frank.erdmann@pharmazie.uni-halle.de (F.E.); matthias.schmidt@pharmazie.uni-halle.de (M.S.); dina.robaa@pharmazie.uni-halle.de (D.R.)
2 Department of Pharmaceutical Chemistry, Faculty of Pharmacy, Egyptian Russian University, Badr City, Cairo 11829, Egypt
3 Department of Pharmaceutical Chemistry, Faculty of Pharmacy, Alexandria University, Alexandria 21521, Egypt
4 Department of Toxicology, University Medical Center, 55131 Mainz, Germany; yanira.zeyn@uni-mainz.de (Y.Z.); alabdeen@uni-mainz.de (A.-H.M.M.); mfisch05@students.uni-mainz.de (M.A.F.)
5 Department of Enzymology, Institute of Biochemistry, Martin-Luther-University of Halle-Wittenberg, 06120 Halle (Saale), Germany; mike.schutkowski@biochemtech.uni-halle.de
6 Department of Zoology, Faculty of Science, Aswan University, Aswan 81528, Egypt
7 Institute of Biotechnology of the Czech Academy of Sciences, BIOCEV, Prumyslova 595, 25250 Vestec, Czech Republic; cyril.barinka@ibt.cas.cz
8 Département de Biologie Structurale Intégrative, Institut de Génétique et de Biologie Moléculaire et Cellulaire (IGBMC), CNRS, INSERM, Université de Strasbourg, CEDEX, 67404 Illkirch, France; romier@igbmc.fr
* Correspondence: okraemer@uni-mainz.de (O.H.K.); wolfgang.sippl@pharmazie.uni-halle.de (W.S.)
† These authors contributed equally to the work.
‡ Equal last author contribution.

Abstract: Class I histone deacetylases (HDACs) are key regulators of cell proliferation and they are frequently dysregulated in cancer cells. We report here the synthesis of a novel series of class-I selective HDAC inhibitors (HDACi) containing a 2-aminobenzamide moiety as a zinc-binding group connected with a central (piperazin-1-yl)pyrazine or (piperazin-1-yl)pyrimidine moiety. Some of the compounds were additionally substituted with an aromatic capping group. Compounds were tested in vitro against human HDAC1, 2, 3, and 8 enzymes and compared to reference class I HDACi (Entinostat (MS-275), Mocetinostat, CI994 and RGFP-966). The most promising compounds were found to be highly selective against HDAC1, 2 and 3 over the remaining HDAC subtypes from other classes. Molecular docking studies and MD simulations were performed to rationalize the in vitro data and to deduce a complete structure activity relationship (SAR) analysis of this novel series of class-I HDACi. The most potent compounds, including 19f, which blocks HDAC1, HDAC2, and HDAC3, as well as the selective HDAC1/HDAC2 inhibitors 21a and 29b, were selected for further cellular testing against human acute myeloid leukemia (AML) and erythroleukemic cancer (HEL) cells, taking into consideration their low toxicity against human embryonic HEK293 cells. We found that 19f is superior to the clinically tested class-I HDACi Entinostat (MS-275). Thus, 19f is a new and specific HDACi with the potential to eliminate blood cancer cells of various origins.

1. Introduction

Epigenetic regulation refers to heritable or long-term changes in gene expression that do not rely on an alteration of the DNA sequence [1]. Histone modification is a widely studied epigenetic modification, which involves the covalent alteration of histone tails through acetylation, methylation, phosphorylation, sumoylation, and ubiquitination [2]. Histone acetylation is one of the most well studied post-translational modifications. This process is controlled by the action of two opposing enzyme families. Histone acetyl transferases (HATs) catalyze the addition of the acetyl group on the protonated ε-amino group of lysine residues of histone proteins. This modification results in a loss of the positive charge and reduces the interactions between histone proteins and DNA [3]. The histone deacetylases (HDACs) catalyze the removal of acetyl groups and this can result in the formation of the condensed chromatin (heterochromatin) and a repression of gene transcription [3]. Human HDACs are classified according to their sequence homology and domain organization into four groups. These are the zinc-dependent deacetylases of class I (HDAC1, 2, 3, and 8), class II (HDAC4, 5, 6, 7, 9, and 10), and class IV (HDAC11), and the NAD+-dependent class III (sirtuins SIRT1-7) [4].

Class I (HDACs 1, 2, 3, and 8) are located mainly in the nucleus and have an essential role in cell proliferation, cell cycle progression and the establishment and maintenance of the aberrant phenotype of cancer cells [5]. Hypoacetylation of histone H4 is a common distinctive feature in early stages of human cancer [6]. Given that HDACs are important for tumor development and progression, HDAC inhibitors (HDACi) have been developed and studied as potential anticancer therapeutics over recent years [7]. HDACi have been tested against solid tumors and blood malignancies. Four class I/II/IV HDACi (pan-HDACi) were approved by authorities for the treatment of patients with cutaneous/peripheral T-cell lymphoma and multiple myeloma [8]. HDACi can be classified according to their zinc binding groups (ZBG) into five main groups: hydroxamates, 2-aminobenzamides, cyclic peptides, thiols, short-chain fatty acids, ketones and others [9]. The hydroxamate-based HDACi Vorinostat (SAHA) [10], Belinostat (PXD101), Panobinostat (LBH589), as well as the thiol-prodrug/depsipeptide Romidepsin (FK228) have been approved by the US Food and Drug Administration (FDA) for the treatment of different types of cancer and hematological malignancies [11–13]. Promising clinical results in phase I/II clinical trials were also obtained the pan-HDACi Givinostat in patients with the blood disorder polycythemia vera [14].

Remarkably, the modulation of HDAC1, HDAC2, and HDAC3 presents a specific possibility to interfere with signaling pathways that are hijacked by tumor cells, and class-I HDACs are highly expressed in different cancers, including leukemia [15–19]. Class-I selective inhibitors have already reached clinical studies like MS-275 (I), phase II Hodgkin's lymphoma, or Mocetinostat (II), and phase II in relapsed lymphoma (Figure 1) [20–22]. Notably, normal cells are largely unaffected by HDACi which verifies that HDACs are key for the development and maintenance of the tumor cell phenotype [23]. To fully exploit and achieve clinical expectations on these drugs, more potent and specific HDACi are required [24,25].

Most HDACi have a common pharmacophore consisting of three different fragments as follows: a ZBG, a capping group, and a linker connecting both groups [26]. The ZBG is responsible for chelating Zn^{2+} in the active site of HDACs. Modification of the ZBG often changes the potency of inhibitors significantly [27]. The capping group usually includes hydrophobic/bulky moieties, such as aromatic or heteroaromatic groups, mediating interactions at the rim of the HDAC enzyme. The interactions with the residues at the entrance of the binding pocket were also shown to contribute to HDAC subtype selectivity [28].

Entinostat (MS-275) (I)

IC$_{50}$ (HDAC1) 0.125 μM
IC$_{50}$ (HDAC2) 0.340 μM
IC$_{50}$ (HDAC3) 0.370 μM
IC$_{50}$ (HDAC8) 14   μM

Mocetinostat (II)

IC$_{50}$ (HDAC1) 0.15 μM
IC$_{50}$ (HDAC2) 0.29 μM
IC$_{50}$ (HDAC3) 1.66 μM
IC$_{50}$ (HDAC4-8) > 10 μM

Chidamide (III)

Phase II, HR(+) breast cancer
Approved by China FDA for the treatment of peripheral T-cell lymphoma
IC$_{50}$ (HDAC1) 0.095 μM
IC$_{50}$ (HDAC2) 0.160 μM
IC$_{50}$ (HDAC3) 0.067 μM
IC$_{50}$ (HDAC8) 0.733 μM

Tacedinaline (IV)

Phase II, Advanced non-small cell lung cancer
IC$_{50}$ (HDAC1) 0.9   μM
IC$_{50}$ (HDAC2) 0.9   μM
IC$_{50}$ (HDAC3) 1.2   μM
IC$_{50}$ (HDAC8) > 20 μM

BRD3308 (V)

IC$_{50}$ (HDAC1) 1.08 μM
IC$_{50}$ (HDAC2) 1.15 μM
IC$_{50}$ (HDAC3) 0.064 μM

BG45 (VI)

Inhibit tumor growth in mouse model of multiple myeloma 1
IC$_{50}$ (HDAC1) 2.0   μM
IC$_{50}$ (HDAC2) 2.2   μM
IC$_{50}$ (HDAC3) 0.289 μM

(VII)

IC$_{50}$ (HDAC1) 0.02 μM
IC$_{50}$ (HDAC2) 0.1   μM

(VIII)

IC$_{50}$ (HDAC1) 0.010 μM
IC$_{50}$ (HDAC2) 0.056 μM
IC$_{50}$ (HDAC3) > 10 μM
IC$_{50}$ (HDAC4-8) > 20 μM

(IX)

IC$_{50}$ (HDAC1) 0.048 μM
IC$_{50}$ (HDAC2) 0.90 μM
IC$_{50}$ (HDAC3) 11   μM

Figure 1. Examples of previously reported 2-aminobenzamides and their inhibitory activity towards different HDAC subtypes. The different pharmacophoric groups of the inhibitors are marked in color (ZBG in red, substitutions interacting with the HDAC1/HDAC2 foot pocket in green, linker colored in blue, capping group colored in pink).

Although the hydroxamic acid is an often used and potent ZBG, it was observed that hydroxamic acid-based HDAC inhibitors often lack cellular potency and often show off-target effects [29,30]. Additionally, the progress of cell mutagenicity and genotoxicity by such compounds is still a main factor to exclude many potent candidates from further drug development steps [31].

It has been shown that 2-Aminobenzamides improve HDAC class I selectivity and strongly inhibit the class-I HDACs1, -2, and -3. The 2-aminobenzamide group acts as ZBG instead of the hydroxamate group in other HDACi. This replacement allows them to have selectivity towards the HDAC subtypes HDAC1, HDAC2, and HDAC3. According to the general skeleton of 2-aminobenzamides, such as HDACi, Entinostat (MS-275, I) and Mocetinostat (II) have an unsubstituted 2-aminobenzamide scaffold as ZBG connected through a linker to a pyridine ring acting as a capping group (Figure 1) [32,33]. Chidamide (CS005, III) shows the same general skeleton with an additional fluoro substitution on the 2-aminobenzamide moiety [34,35]. It has been found that 2-Aminobenzamides Tacedinaline (CI-994, IV), BRD3308 (V) and BG45 (VI) are examples of inhibitors without a capping group (Figure 1) [36–38]. The crystal structure of HDAC2 revealed that the 2-aminobenzamide part could access the foot pocket next to the catalytic region [39]. In this regard, another strategy to increase the selectivity towards HDAC1 and HDAC2 subtypes is the addition of an aromatic moiety, like thienyl or phenyl, to the position-5 of the 2-aminobenzamide group. This fills the internal cavity of the foot pocket near to the catalytic region, as in the case of compound VII–IX. These inhibitors are more active and selective against HDAC1/HDAC2 over HDAC3 (Figure 1) [40,41].

The aim of the current study was to develop novel class-I selective HDAC inhibitors with improved in vitro activity as well as stronger anti-leukemic effects compared to known reference inhibitors. Due to the above mentioned problems with hydroxamic acids and the good class-I selectivity of 2-aminobenzamides shown by, e.g., MS-275 [42], we focused on this chemotype. A first idea was to substitute the middle phenyl ring of MS-275 with more polar pyrazine or pyrimidine rings to result in better solubility of the final compounds. At the beginning of the study, we first docked the reference inhibitors shown in Figure 1 to the available crystal structures of HDAC1, HDAC2 and HDAC3 to obtain ideas for structural optimization. For example, attachment of a basic piperazine to a pyrimidine or pyrazine ring mimicking the middle ring of MS-275 showed ionic hydrogen bonding with an aspartate residue conserved in HDAC1, HDAC2 and HDAC3 (D99 in HDAC1, D104 in HDAC2, D93 in HDAC3). The capping groups of reported HDAC inhibitors interact with amino acids at the rim of the binding channel; in the case of MS-275, these are aromatic and hydrophobic interactions with H27/33/22 and P29/34/23 in HDAC1, HDAC2 and HDAC3, respectively (Supplementary Figure S1). Accordingly, we designed compounds with different aromatic rings as capping groups and different linker lengths to analyze the effect of capping groups on class-I HDAC activity. In addition, the 2-aminobenzamide scaffold was substituted at different positions to investigate the effect of increased subtype selectivity toward HDAC1/HDAC2 on the anti-leukemic activity. Mono- or di-substitutions with different small groups at position 4 and/or position 5 were performed to complete the SAR studies. The realized structural changes are summarized in Figure 2.
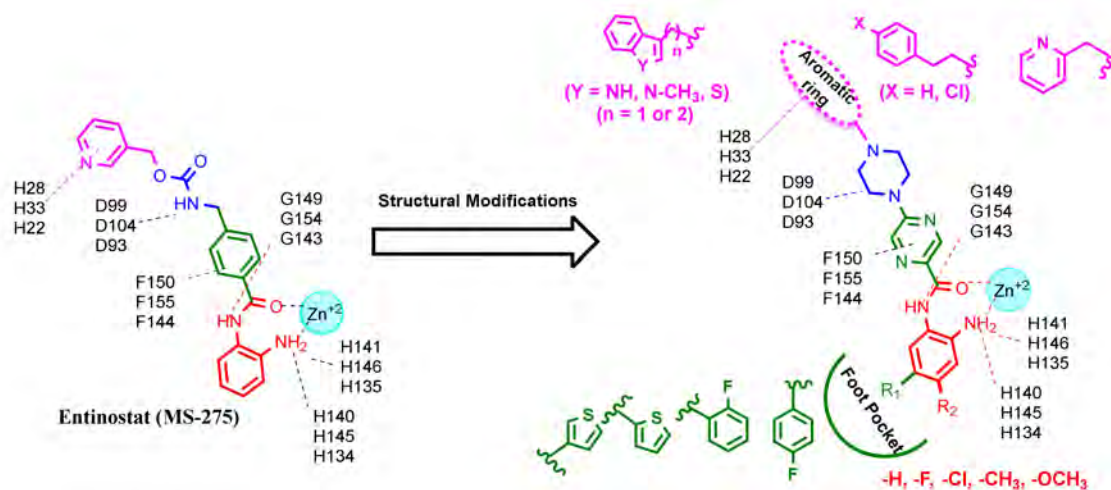
Figure 2. Structural modifications of Entinostat (MS-275) based on its interaction with the active site of HDAC 1 (red amino acid labels), HDAC 2 (blue amino acid labels) and HDAC 3 (green amino acid labels) subtypes to design novel compounds with different substitutions to obtain full SAR studies.

2. Results and Discussion

2.1. Chemistry

To obtain the designed compounds, we planned a three-step synthesis. The first step was the synthesis of carboxylic acid derivatives 4a–c and 7a–j, as illustrated in Scheme 1, (Supplementary Table S1a,b). The second step was the synthesis of different *o*-phenylenediamine derivatives (9a–c, 12a–e and 17a–d) as shown in Scheme 2. Finally, coupling of obtained acid derivatives and *o*-phenylenediamines was carried out, using Boc protection and de-protection, to obtain the final compounds 19a–o, 21a–c, 23a–c, 25a,b, 27a–c and 29a–d.
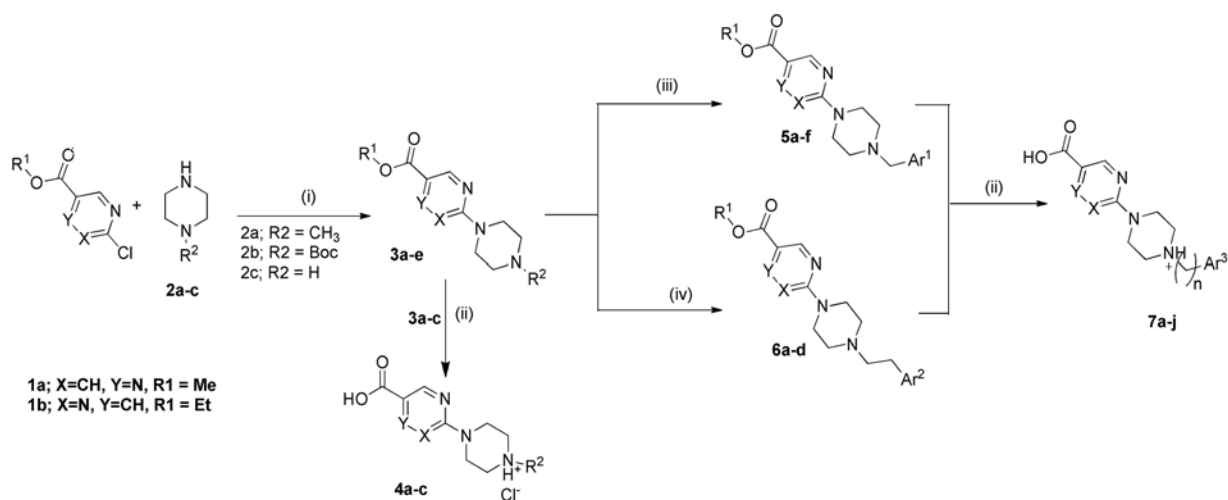
Scheme 1. Synthesis of carboxylic acid intermediates **4a–c** and **7a–j**. Reagents and conditions: (**i**) Toluene, 130 °C, 1 h. (**ii**) Compounds **3a–c**, 2.5 eq 1N NaOH, MeOH, 70 °C, 3 h. (**iii**) Compounds **3d,e**, Ar^1-CHO, Na(OAc)$_3$BH, AcOH, DCM, RT, 5 h. (**iv**) Compound **3d**, BrCH$_2$CH$_2$Ar^2, K$_2$CO$_3$, CH$_3$CN, M.W, 120 °C, 90 min.
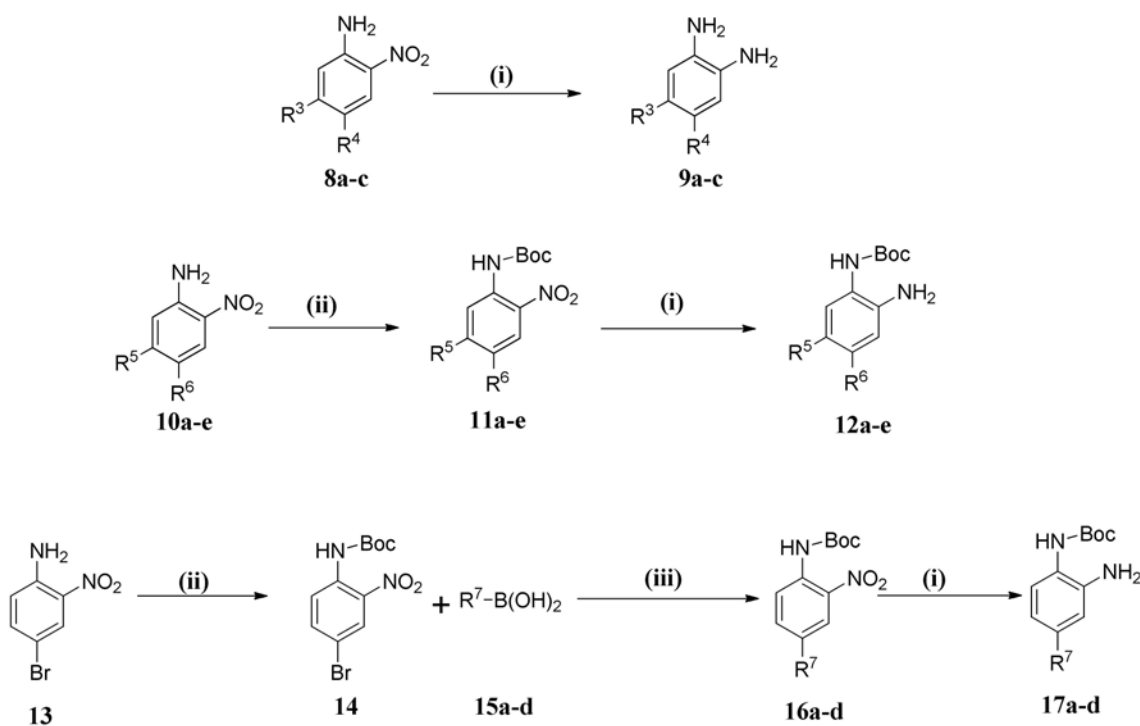
Scheme 2. Synthesis of 1,2-phenylenediamine derivatives **9a–c**, **12a–e** and **17a–d**. Reagents and conditions: (**i**) HCOONH$_4$, Pd/C 10%, MeOH. (**ii**) Boc$_2$O, TEA, DMAP, DCM (**iii**) Tetrakis P(Ph)$_3$Pd, Deg. DME, Na$_2$CO$_3$.

As shown in Scheme 1, esters 3a–e were obtained by direct alkylation of piperazine derivatives 2a–c using methyl 5-chloropyrazine-2-carboxylate (1a) or ethyl 2-chloropyrimidine-5-carboxylate (1b) in refluxing toluene. Esters 3d,e with a free piperazinyl moiety were further extended to the capping groups either by reductive amination or microwave-assisted alkylation, to yield the corresponding N-alkylated derivatives 5a–f and 6a–d. All

synthesized esters in this scheme were converted into acids through alkaline hydrolysis by heating in 2.5 eq. 1N aq. NaOH.

Scheme 2, (Supplementary Table S2) illustrates the synthesis of three different types of 1,2-phenylenediamine derivatives. The first type includes free 1,2-phenylenediamine derivatives (9a–c), which were prepared by catalytic reduction of the corresponding nitro compounds (8a–c) using ammonium formate and Pd/C 10%. The second type (12a–e), which are Boc protected with simple substituents, were synthesized in two steps by protection of the amino group in the corresponding nitroaniline derivatives (10a–e) using Boc_2O in presence of Et_3N and DMAP (N,N-Dimethylpyridin-4-amin) followed by catalytic hydrogenation as previously described to produce the corresponding aniline derivative (12a–e). The third type represents mono Boc protected-1,2-phenylenediamines with aryl substituents (R^7). These compounds were prepared through Suzuki coupling between the Boc protected-4-bromo-2-nitroaniline and the appropriate aromatic boronic acid by refluxing in 1,2-dimethoxyethane using tetrakis (triphenylphosphine)palladium(0) as a catalyst, followed by reduction of the nitro group to the corresponding aniline derivative (17a–d).

The third main step in the synthetic pathway to prepare the 2-aminoanilide compounds was an amide coupling between the carboxylic acid derivatives and 1,2-phenylenediamines using the coupling reagent HATU (O–N, N, N′, N′-tetramethyluronium-hexafluorphosphate) in the presence of DIPEA (N,N-Diisopropylethylamine) as the base. The time of this reaction depends on the reactivity of the amino group of the 1,2-phenylenediamine derivative. The coupling reaction to yield 19a–o, as shown in Scheme 3, (Supplementary Table S3) takes from 1 h to 2 h.
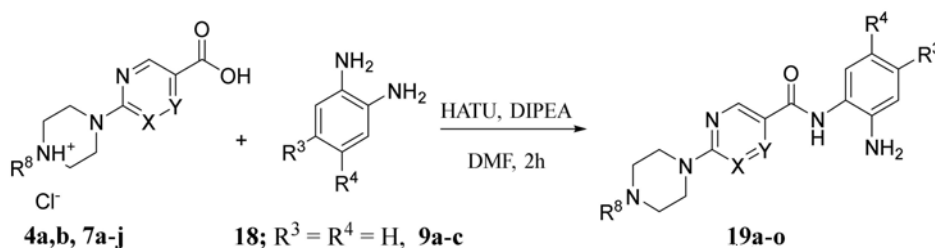
Scheme 3. Synthesis of the final compounds **19a–o**. Reagents and conditions: HATU, DIPEA, DMF, 1–2 h, RT.

Coupling of the *o*-phenylene-diamines in which one of the amino groups is protected by Boc proceeded as previously described using HATU and DIPEA as a catalyst. However, this reaction needed overnight stirring at room temperature due to the low reactivity of the free amino group in compounds 20a–c. This reaction was followed by a deprotection step using trifluoroacetic acid (TFA) to obtain compounds 21a–c (Scheme 4). The deprotection step had an effect on compounds having a Mannich base in the capping group, as in compound 22a. In this case it was removed from the compound due to the acidic effect of TFA to yield compound 23a (Scheme 4). In another trial to make Boc deprotection for compound 22b using 4M HCl in dioxane, the capping group was also unstable. Therefore, we could only obtain the target compound 23b (with capping group) in a very low yield (5%) by preparative HPLC. On the other hand, to avoid the problem of the instability of the Mannich bases toward acidic condition required for Boc deprotection, the methylene carbon connecting the indole capping group and piperazine scaffold was replaced by an ethylene linker. We obtained the target compound 23c after Boc deprotection using TFA without any hydrolysis of the capping group (Scheme 5).
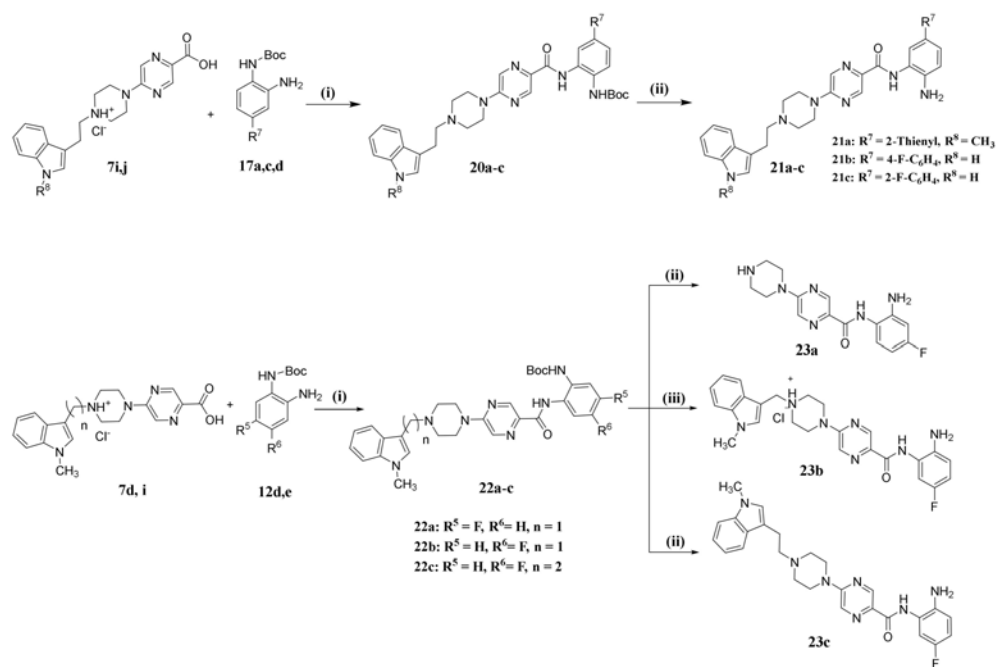
Scheme 4. Synthesis of the final compounds **21a–c** and **23a–c**. Reagents and conditions: (**i**) HATU, DIPEA, Dry DMF, RT, Overnight. (**ii**) TFA, DCM, 0 °C, 30 min. (**iii**) **22b**, 4M HCl, Dioxane, 0 °C, 30 min.
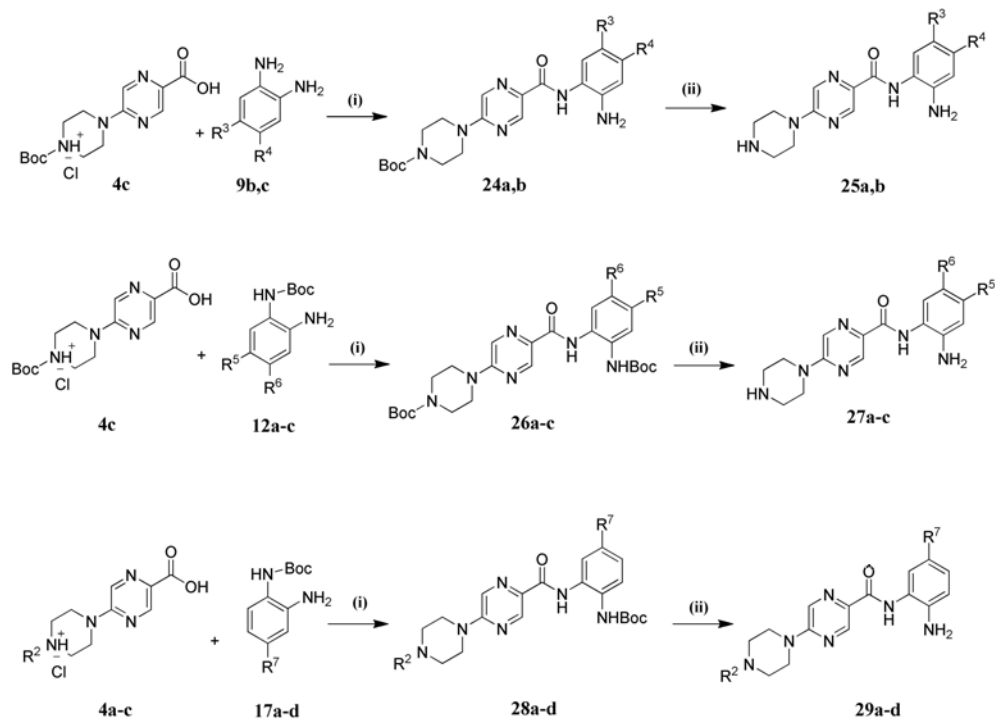
(*) Boc for **28** and H for **29**

Scheme 5. Synthesis of the final compounds **25a,b**, **27a–c** and **29a–d**. Reagents and conditions: (**i**) HATU, DIPEA, Dry DMF, RT. (**ii**) TFA, DCM, 0 °C, 30 min.

The cleavage of the capping group in compound 23a and its promising inhibitory activity against HDAC1, 2 and 3 motivated us to synthesize a series of compounds lacking the capping group as in case of 25a,b, 27a–c and 29b,c. This was achieved using Boc-protected piperazine intermediates 24a,b, 26a–c and 28b,c followed by deprotection using TFA (Scheme 5), (Supplementary Table S4). To extend our SAR studies, we synthesized further N-methyl piperazine derivatives (29a,d) using the previously established procedure, as illustrated in Scheme 5 (Supplementary Table S4).

2.2. Biological Evaluation

In Vitro Testing of HDAC Inhibitory Activity

The synthesized compounds were tested for inhibitory activity against human class I HDACs (HDAC1, -2, -3, and -8) using a fluorogenic peptide derived from p53 (Ac-RHKK(Acetyl)-AMC), as shown in Table 1 [43]. We included several reported inhibitors of HDAC1, HDAC2, and HDAC3 (CI994, MS-275, Mocetinostat and RGFP966) as reference compounds. The most promising inhibitors were also tested against a panel of HDAC subtypes (including HDAC4, -5, -6, -7, -9 and -11) and, as expected, none of these compounds showed strong inhibition of the other HDACs, as shown in Table 2.

Table 1. Inhibitory activity of the synthesized compounds against class I HDACs.

Cpd. No.	X	Y	R^1	R^2	R^3	HDAC1 (IC$_{50}$ μM)	HDAC2 (IC$_{50}$ μM)	HDAC3 (IC$_{50}$ μM)	HDAC8 (% Inhib.)
19a	CH	N		H	H	0.51 ± 0.05	0.80 ± 0.07	1.12 ± 0.07	0% @ 1 μM
19b	CH	N		H	H	25.8% @ 2 μM	30.3% @ 2 μM	65.2% @2 μM	3.4% @ 1 μM
19c	N	CH		H	H	33.9% @ 2 μM	20.1% @ 2 μM	26.8% @2 μM	0% @ 1 μM
19d	CH	N		H	H	0.52 ± 0.07	1.43 ± 0.08	1.06 ± 0.04	0% @ 1 μM
19e	CH	N		H	H	0.21 ± 0.07	0.71 ± 0.04	0.84 ± 0.03	0% @ 1 μM
19f	CH	N		H	H	0.13 ± 0.01	0.28 ± 0.01	0.31 ± 0.01	0% @ 1 μM
19g	CH	N		H	H	0.31 ± 0.03	0.96 ± 0.05	0.49 ± 0.06	0% @ 1 μM
19h	CH	N		F	F	0.81 ± 0.07	0.74 ± 0.03	0.57 ± 0.02	n.d.

Table 1. *Cont.*
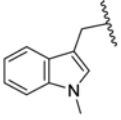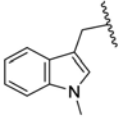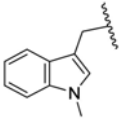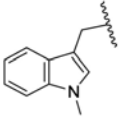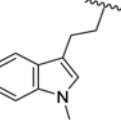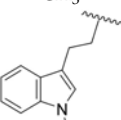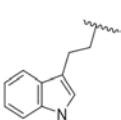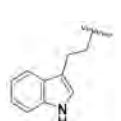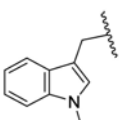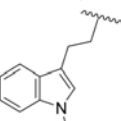
Cpd. No.	X	Y	R¹	R²	R³	HDAC1 (IC$_{50}$ μM)	HDAC2 (IC$_{50}$ μM)	HDAC3 (IC$_{50}$ μM)	HDAC8 (% Inhib.)
19i	CH	N	1-methylindol-3-yl ethyl	Cl	H	3.0 ± 0.2	2.7 ± 0.2	1.9 ± 0.1	n.d.
19j	N	CH	1-methylindol-3-yl ethyl	H	H	0.45 ± 0.06	0.93 ± 0.04	1.75 ± 0.06	0% @ 1 μM
19k	CH	N	1-methylindol-3-yl ethyl	H	H	0.14 ± 0.02	0.56 ± 0.04	0.59 ± 0.03	0% @ 1 μM
19l	CH	N	1-methylindol-3-yl ethyl	F	F	0.29 ± 0.03	0.56 ± 0.02	0.81 ± 0.05	n.d.
19m	CH	N	1-methylindol-3-yl propyl	F	H	0.40 ± 0.06	1.48 ± 0.19	0.40 ± 0.02	n.d.
19n	N	CH	CH$_3$	H	H	5% @ 1 μM	7% @ 1 μM	13% @ 1 μM	n.d.
19o	CH	N	CH$_3$	H	H	27% @ 1 μM	15% @ 1 μM	30% @ 1 μM	n.d.
21a	CH	N	1-methylindol-3-yl ethyl	H	2-Thienyl	0.26 ± 0.01	2.47 ± 0.22	0% @ 1 μM	n.d.
21b	CH	N	1H-indol-3-yl ethyl	H	4-F-C$_6$H$_4$	0.70 ± 0.08	0.77 ± 0.06	0% @ 1 μM	0% @ 1 μM
21c	CH	N	1H-indol-3-yl ethyl	H	2-F-C$_6$H$_4$	0.76 ± 0.07	0.76 ± 0.04	15 ± 1	0% @ 1 μM
23a	CH	N	H	F	H	3.30 ± 0.18	2.20 ± 0.20	0.40 ± 0.01	0% @ 1 μM
23b	CH	N	1-methylindol-3-yl ethyl	H	F	0.27 ± 0.03	0.50 ± 0.03	0.50 ± 0.02	38% @ 1 μM
23c	CH	N	1-methylindol-3-yl propyl	H	F	0.33 ± 0.02	1.37 ± 0.08	0.59 ± 0.04	n.d.
25a	CH	N	H	Cl	H	0% @ 1 μM	0% @ 1 μM	8.7 ± 0.4	n.d.
25b	CH	N	H	F	F	4.3 ± 0.3	4.2 ± 0.10	1.6 ± 0.1	n.d.
27a	CH	N	H	H	CF$_3$	0% @ 1 μM	0% @ 1 μM	0% @ 1 μM	n.d.
27b	CH	N	H	CH$_3$	H	0% @ 1 μM	0% @ 1 μM	0% @ 1 μM	n.d.

Table 1. *Cont.*

Cpd. No.	X	Y	R [1]	R [2]	R [3]	HDAC1 (IC$_{50}$ µM)	HDAC2 (IC$_{50}$ µM)	HDAC3 (IC$_{50}$ µM)	HDAC8 (% Inhib.)
27c	CH	N	H	OCH$_3$	H	20.0 ± 1.0	14.0 ± 2.0	14.0 ± 1.0	n.d.
29a	CH	N	CH$_3$	H	3-Thienyl	0.11 ± 0.01	0.18 ± 0.06	4.4 ± 0.1	n.d.
29b	CH	N	H	H	2-Thienyl	0.07 ± 0.01	0.26 ± 0.01	6.1 ± 0.7	n.d.
29c	CH	N	H	H	4-F-C$_6$H$_4$	0.16 ± 0.03	0.34 ± 0.01	6.7 ± 0.5	n.d.
29d	CH	N	CH$_3$	H	2-F-C$_6$H$_4$	0.18 ± 0.01	0.26 ± 0.07	12.0 ± 1.0	n.d.
CI994	–	–	–	–	–	37% @ 1 µM	36% @ 1 µM	32% @ 1 µM	n.d.
RGFP-966	–	–	–	–	–	16 ± 2	11 ± 1	1.3 ± 0.1	n.d.
MS-275	–	–	–	–	–	0.93 ± 0.1	0.95 ± 0.03	1.8 ± 0.1	n.d.
Mocetinostat	–	–	–	–	–	0.33 ± 0.04	0.34 ± 0.01	0.93 ± 0.05	n.d.

n.d. not determined, – no substituents.

Table 2. Inhibitory activity of compounds 19f and 21a against class II and class IV HDACs.

Cpd. No.	HDAC4 (IC$_{50}$ µM)	HDAC5 (IC$_{50}$ µM)	HDAC6 (IC$_{50}$ µM)	HDAC7 (IC$_{50}$ µM)	HDAC9 (IC$_{50}$ µM)	HDAC11 (IC$_{50}$ µM)
19f	>20	>20	>20	>20	>20	>20
21a	>20	>20	>20	>20	>20	7.5 ± 1

The synthesized compounds can be categorized into four main groups based on the substitution pattern of the 2-aminobenzamide scaffold and presence or absence of capping groups. The first group comprises compounds with capping groups and unsubstituted 2-aminobenzamide scaffolds. The second group includes compounds with capping groups and substituted 2-aminobenzamide scaffolds. The third group contains compounds with unsubstituted 2-aminobenzamide groups without any capping group. The final group contains compounds with substituted 2-aminobenzamide functionalities and that lack a capping group.

Generally, the first group of compounds inhibit HDAC1, HDAC2, and HDAC3 in the low to submicromolar range. For instance, compound 19f, which has the 3-indolyl ring as a capping group, showed very good inhibitory activity against HDAC1, -2, and -3 with IC$_{50}$ values (0.13 µM, 0.28 µM, 0.31 µM, respectively). It was found that 19f was more potent than the reference inhibitors MS-275, Mocetinostat, CI994 and RGFP-966. Modification in

the capping group has different effects on the HDAC activity. For example, compound 19k with an N-methyl-3-indolyl ring has similar inhibitory profile with IC$_{50}$ values of 0.14 μM, 0.56 μM, and 0.59 μM for HDAC1, HDAC2, and HDAC3, respectively). Similarly, 19e, which has a benzothiophene capping group, showed IC$_{50}$ values of 0.21 μM, 0.71 μM, and 0.84 μM against HDAC1, HDAC2, and HDAC3, respectively. On the other hand, other capping groups, like phenethyl, 4-chlorophenethyl or 2-pyridyl, resulted in a reduced inhibitory activity, as in the case of compound 19b or slightly decreased activities, as in the case of compound 19a and 19d (Table 1).

Interestingly, the replacement of the pyrazine linker with pyrimidine resulted in a significant decrease of inhibitory activity, as in the case of compound 19c compared to compound 19d, or a slight decrease of HDAC1, HDAC2, and HDAC3 inhibitory activities, as in the case of compound 19j compared to compound 19k. It was also noticed that replacing the methylene connecting the indole capping group and piperazine with an ethylene resulted in a slight decrease in the HDAC inhibitory activity, as in the case of compound 19g compared with 19f (Table 1).

In the second group of the designed compounds, we investigated the effect of different substitution patterns of the 2-aminobenzamide on HDAC selectivity in the presence of 3-indolyl or (N-methyl)-3-indolyl capping groups. In line with reported studies, it was observed that the substitution of 2-aminobenzamides with aromatic or heterocyclic rings at position-5 improved HDAC subtype selectivity. For instance, compound 21a, which has a 2-thienyl ring at the position-5, has high selectivity for HDAC1 and HDAC2 (0.26 μM, 2.47 μM, respectively) over HDAC3. In addition, 21a is more potent than the reference inhibitors MS-275, Mocetinostat, CI994 and RGFP-966. In a similar manner, compounds 21b,c with 4- or 2-fluorophenyl substituents have a significant selectivity toward HDAC1/HDAC2 over HDAC3 compared to the parent unsubstituted derivative 19g. Compound 21b and 21c displayed submicromolar IC$_{50}$ values in the case of HDAC1, and HDAC2 and only weak or no inhibition of HDAC3 (Table 1).

On the contrary, substitution of the 2-aminobenzamide with halogens did not result in marked improvement on HDAC subtype selectivity. For example, compound 19l and 19m, having mono- or disubstituted fluorophenyl, have almost similar subtype selectivity compared to their unsubstituted parent derivative 19k. In the case of compound 19i having a mono chloro substituent, it showed a decrease in HDAC inhibition compared to the unsubstituted parent derivative 19g.

The third group of synthesized compounds lacks the capping group and any substitution on the 2-aminobenzamide group. Compounds 19n and 19o showed only very weak enzymatic activity against HDAC1, HDAC2, and HDAC3.

The last group of inhibitors contains different substitution patterns on the phenyl ring of the ZBG and no capping group. Generally, the compounds possessing aromatic substituents at position-5, like 2-thienyl, 3-thienyl, 4-flourophenyl, and 2-fluorophenyl, showed good HDAC subtype selectivity and potency. Compound 29b showed strong inhibitory activity against HDAC1 and HDAC2 (IC$_{50}$; 0.07 μM, 0.26 μM, respectively), with little activity against HDAC3 (IC$_{50}$; 6.1 μM). Replacing the aromatic ring with trifluoromethyl group, as in compound 27a, diminished the HDAC inhibitory activity (Table 1). On the other hand, substitution of the phenyl group with a fluorine atom at position-4, resulted in a slight increase of HDAC3 selectivity over HDAC1 and HDAC2, as in case of compound 23a with IC$_{50}$ values for HDAC1, HDAC2, and HDAC3 being 3.30 μM, 2.17 μM, and 0.40 μM, respectively. Similarly, replacing the fluorine atom with a chlorine atom, as in compound 25a, resulted in complete loss of inhibitory activity against HDAC1/HDAC2 and decreased activity against HDAC3 (IC$_{50}$ 8.7 μM). Furthermore, replacing the fluorine atom with electron donating groups, like the methyl or methoxy group, resulted in a dramatic loss of HDAC inhibitory activity, as in the case of compound 27b,c (Table 1).

2.3. Molecular Docking Studies

To rationalize the binding mode of the synthesized compounds, we performed molecular docking studies using crystal structures of HDAC1 (PDB ID: 4BKX, apo-form), HDAC2 (PDB ID: 4LY1, co-crystallized with a 2-aminobenzamide), and HDAC3 (PDB ID: 4A69, apo-form) (Supplementary Figure S1).

The first group of the designed compounds (19a–19g), bearing different capping groups and an unsubstituted 2-aminobenzamide moiety, showed similar binding modes in HDAC1-3, as exemplified by the obtained docking results of compound of 19f in HDAC1/HDAC2 (Figure 3A,C). As observed in the resolved crystal structures of HDAC2 in a complex with 2-aminobenzamide derivatives (e.g., PDB 4LYI for HDAC2), the novel derivatives were able to chelate the catalytic zinc ion in a similar bidentate fashion through their carbonyl oxygen and the free amino group of the 2-aminobenzamide moiety (a cut off distance of 2.7 Å was determined for bidentate chelation in this study). In addition, the ZBG showed hydrogen bonds with the conserved H140/145/134, H141/146/135, G149/154/143, and Y303/308/298 in HDAC1, HDAC2, and HDAC3, respectively (Figure 3). The central pyrazine group of compound 19f was placed in the acetyl-lysine tunnel, consisting of G149/154/143, F150/155/144, H178/183/172, F205/210/200, L271/276/266 in HDAC1, HDAC2, and HDAC3, respectively. The attached basic piperazine group shows a salt bridge with the conserved aspartate residue located at the rim of the binding pocket (D99 in HDAC1, D104 in HDAC2, D93 in HDAC3). Meanwhile, the aromatic capping group was found to undergo aromatic interactions with the conserved H28 in HDAC1, H33 in HDAC2, and H22 in HDAC3, respectively.
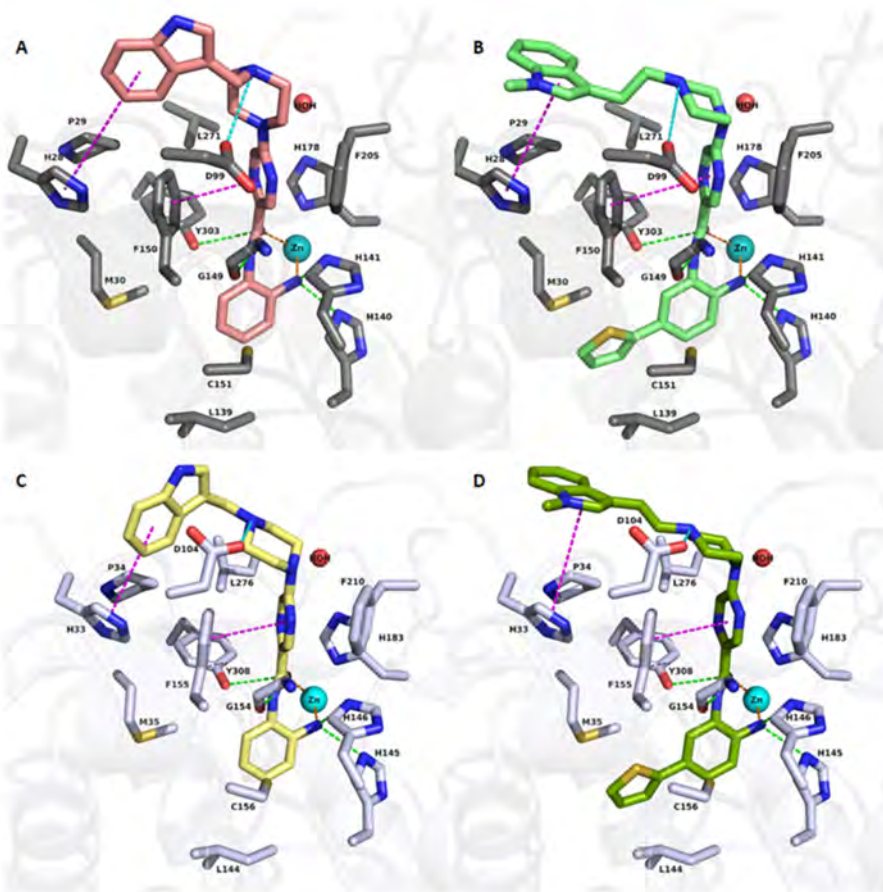
Figure 3. Docking poses of 19f (**A**, salmon colored sticks), 21a (**B**, light green colored sticks), in HDAC1 (PDB ID 4BKX), 19f (**C**, yellow colored sticks), 21a (**D**, dark green colored sticks), in HDAC2

(PDB ID 4LY1). Hydrogen bonds (green dashed lines), metal coordination (orange dashed lines), ionic interactions (cyan dashed lines) and aromatic interactions (magenta dashed lines) between inhibitors and the protein are shown. Relevant residues are shown in stick representation with dark grey carbon atoms in HDAC1and white carbon atoms in HDAC2. The zinc ion is shown as a cyan colored sphere. The conserved water molecule is shown as a red sphere. The zinc-carbonyl oxygen and zinc-amino distances, respectively, are: 2.54 Å and 2.45 Å for 19f/HDAC1, 2.51 Å and 2.44 Å for 21a/HDAC1, 2.17 and 2.27 Å for 19f/HDAC2, 2.22 Å and 2.29 Å for 21a/HDAC2.

The second group of compounds, bearing different substituents at the 2-aminobenzamide scaffold in the presence of the 3-indolyl or (N-methyl)-3-indolyl capping group, shows a different binding mode in the class I HDAC subtypes. As previously observed, substitution of the 2-aminobenzamide moiety by a 5-thienyl ring leads to a selectivity for HDAC1/2 over HDAC3 [44]. Docking results of 21a in HDAC1 and 2 (Figure 3) show that the thienyl moiety is embedded in the foot pocket of HDAC2, where it undergoes hydrophobic interactions with M35, L144, C156 in HDAC2. Meanwhile, HDAC3 has a narrower foot pocket created by pushing the L133 by Y107 in HDAC3 (replaced by S113/118 in HDAC1/2) [45], which does not allow the accommodation of bulky substituents (e.g., thiophene rings) as also substantiated by the docking results in HDAC3 (Supplementary Figure S2).

Compounds bearing no or small substituents, like fluoro substituents, at the 4- and 5- position of the benzamide moiety (19l, 19m, 19i and 19h) regain the inhibitory activity on HDAC3. Docking results show a similar binding mode in class I HDAC subtypes, where the 2-aminobenzamide moiety is placed in the foot pocket while showing a bidentate chelation of the zinc ion, as exemplified by compound 19l in Supplementary Figure S3.

A similar finding was observed with the last group of designed compounds containing different substitution on ZBG and no capping group. Aromatic substituents, like a thienyl or fluorophenyl moieties, at position-5 could not fit into the foot pocket of HDAC3 while showing a similar binding mode in HDAC1/HDAC2 (Figure 4). Hence, compounds having aromatic substituents on ZBG show good HDAC1/HDAC2 selectivity over HDAC3 as observed, for example, in compounds 21a and 29b (Figure 3B,D and Figure 4A,C).

While a small fluoro substituent at position 4 is well tolerated in the foot pocket as observed in compound 23a (Figure 4), larger or bulkier groups, like chloro (25a), and methyl (27b) methoxy (27c), and trifluoromethyl groups (27a) resulted in a significant loss in the inhibitory activity toward the HDAC1/-2/-3 subtypes. Docking poses of these derivatives, as exemplified by compound 25a in HDAC2 (Supplementary Figure S4), reveal that these substituents do not fit well in the foot pocket and result in clashes with surrounding residues (G143 and G305).

In addition to the docking study, we performed molecular dynamics (MD) simulations for the most promising inhibitors 19f, 21a, 23a, 29b and HDAC1, 2 and 3 crystal structures using Amber18 (University of California, San Francisco) to investigate the stability of the predicted binding modes. In all cases the bidentate zinc-chelation of the compounds was preserved during the MD for the studied four potent inhibitors.

The analysis of the MD simulations for the capless compounds 23a and 29b indicated a stable binding mode in HDAC1/HDAC2 and HDAC3 in terms of root-mean-square-deviation (RMSD) (Supplementary Figures S5 and S6) and the interaction of the basic piperazine and the conserved aspartate residue (D106 in HDAC1, D104 in HDAC2, D93 in HDAC3). The obtained docking poses for 23a and 29b (Figure 4) were preserved during the MD in all three HDAC subtypes. In the case of compounds 19f and 21a the solvent-exposed capping groups can adopt several energetically favorable conformations interacting with different parts of the rim region (Supplementary Figures S7 and S8). This is in accordance with the observed X-ray structures of cocrystallized flexible HDAC inhibitors (such as SAHA) where the capping group was found to bind to different regions of the rim. Hence, the RMSD of the 19f and 21a showed higher deviation throughout the MD simulation (Supplementary Figures S7 and S8). The observed flexibility of the capping group might

also explain the similar inhibitory activities of the corresponding capless inhibitors. Further in silico studies are needed to find more suitable capping groups that have higher potency and selectivity. Further opportunities for chemical optimization arise via the search for bioisosteric groups for the aminopyrazine structure.
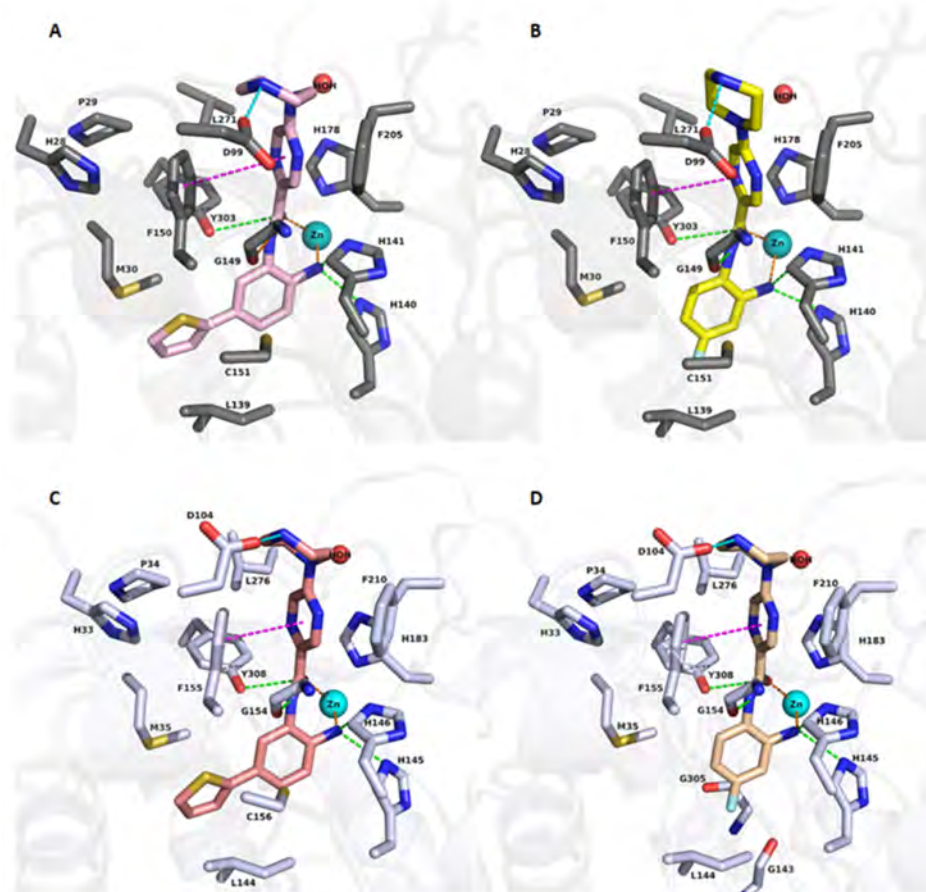
Figure 4. Docking poses of 29b (**A**, pink colored sticks), 23a (**B**, yellow colored sticks), in HDAC1 (PDB ID 4BKX) and 29b (**C**, salmon colored sticks), 23a (**D**, creme colored sticks) in HDAC2, (PDB ID 4LY1). Hydrogen bonds (green dashed lines), metal coordination (orange dashed lines), ionic interactions (cyan dashed lines) and aromatic interactions (magenta dashed lines) between inhibitors and the protein are shown. Relevant residues are shown in stick representation with dark grey carbon atoms in HDAC1 and white carbon atoms in HDAC2. The zinc ion is shown as a cyan colored sphere. The conserved water molecule is shown as a red sphere. The zinc-carbonyl oxygen and zinc-amino distances, respectively, are 2.43 Å and 2.41 Å for 29b/HDAC1, 2.39 Å and 2.58 Å for 23a/HDAC1, 2.22 and 2.28 Å for 29b/HDAC2, 2.23 Å and 2.41 Å for 23a/HDAC2.

2.4. Cellular Assays to Analyze Our New Inhibitors

2.4.1. Tests with Non-Transformed Cells

HDACi should have low toxicity to normal mammalian cells [23]. Therefore, we tested the potential cytotoxicity of the most promising inhibitors in a human epithelial kidney cell line (HEK293) that was derived from normal tissue. The cells were incubated for 48 h with the HDACi at a concentration of 50 μM, and cell viability was determined by the Alamar Blue assay. Most of the tested inhibitors caused only relatively low cytotoxicity in the human cell system and only 50 μM of 29b and 29c produced a significant reduction of cell viability (Table 3).

Table 3. Cytotoxicity studies in human HEK293 Cells.

Name	% Viability	SD	Name	% Viability	SD
19a	73.1	3.4	19m	52.5	0.5
19b	78.6	6.8	21a	94.4	5.5
19c	78.7	7.5	21b	71.0	4.1
19d	67.7	7.3	21c	72.3	5.8
19e	50.9	4.0	23a	67.0	3.4
19f	76.1	8.0	23b	58.7	6.5
19g	71.8	3.0	23c	55.7	1.5
19h	54.5	2.8	25b	83.7	4.4
19i	47.5	1.5	29a	65.8	6.8
19j	62.5	5.8	29b	2.4	0.0
19k	71.4	3.0	29c	2.2	0.1
19l	20.1	0.4	29d	54.0	2.2

2.4.2. Biological Tests with Leukemic Cells

Based on the in vitro activities and the low cellular toxicity for HEK293 cells, we selected the potent HDAC1/-2/-3 inhibitor 19f as well as the HDAC1/HDAC2 selective inhibitors 29b and 21a for further biological characterization in acute myeloid leukemia (AML) cells. The inhibitors were tested on FLT3-ITD positive MV4-11 cells (2 FLT3-ITD alleles). We chose such cells because FLT3-ITD positive AML is a clinically unresolved issue [46–51].

We measured the induction of early (increased exposure of phosphatidylserine on the cell surface and therefore positive staining for annexin-V-FITC) and late apoptosis (positivity for annexin-V and accumulation of propidium iodide, PI) by flow cytometry. Incubation of MV4-11 cells with the inhibitors showed that 0.5 µM 19f caused early and late apoptosis in nearly the whole MV4-11 cell population. We found that 0.5 µM 29b led to apoptosis in about half of the MV4-11 cell population and 21a slightly increased the number of MV4-11 cells in late apoptosis (Figure 5). Due to these data, we focused further analyses on 19f.

To extend these analyses, we incubated MV4-11 cells and MOLM-13 cells (1 FLT3 wild-type allele and 1 FLT3-ITD allele) with 19f. To compare the potency of 19f with an established class I HDACi, we chose the 2-aminobenzamide MS-275. This agent, which specifically inhibits HDAC1, -2, and -3, is tested in clinical trials [51] (https://www.cancer.gov/about-cancer/treatment/clinical-trials/intervention/entinostat, accessed date 10 November 2021). We used 1 µM of 19f and 1 µM MS-275, because this is the maximal clinically achievable concentration of MS-275 in patients [52]. We found that 19f was more effective than MS-275 and those cytotoxic effects of these compounds that occurred were time- and dose-dependently (Figures 6A and 7D). We found that 19f (IC$_{50}$ for apoptosis induction 255 nM) was at least 4-fold more effective than the HDACi MS-275 (IC$_{50}$ for apoptosis induction 1307 nM) in MV4-11 (Figure 6E). In MOLM-13 cells, 19f displayed a higher potency 4-fold (IC$_{50}$ for apoptosis induction 397 nM) than the HDACi MS-275 (IC$_{50}$ for apoptosis induction 1127 nM). The IC$_{50}$ values for growth inhibition of MV4-11 and MOLM-13 cells after 48 h were around 0.3 µM (Figure 6E).
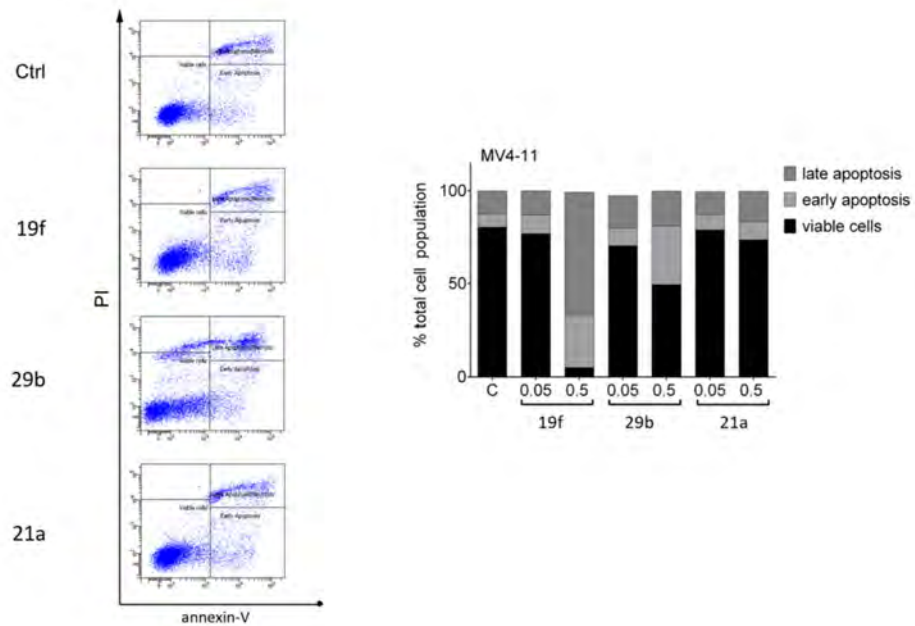
Figure 5. Impact of 19f, 21a and 29b on the survival of MV4-11 cells. The cells were treated with 0.5 μM of 19f, 21a, and 29b for 48 h or solvent (Ctrl). The left panel shows the original flow cytometry scans (x-axis, annexin-V-FITC; y-axis, propidium iodide, PI). The right panel shows the percentage distributions of intact, early apoptotic, and late apoptotic cells. Experiments were performed three times independently.
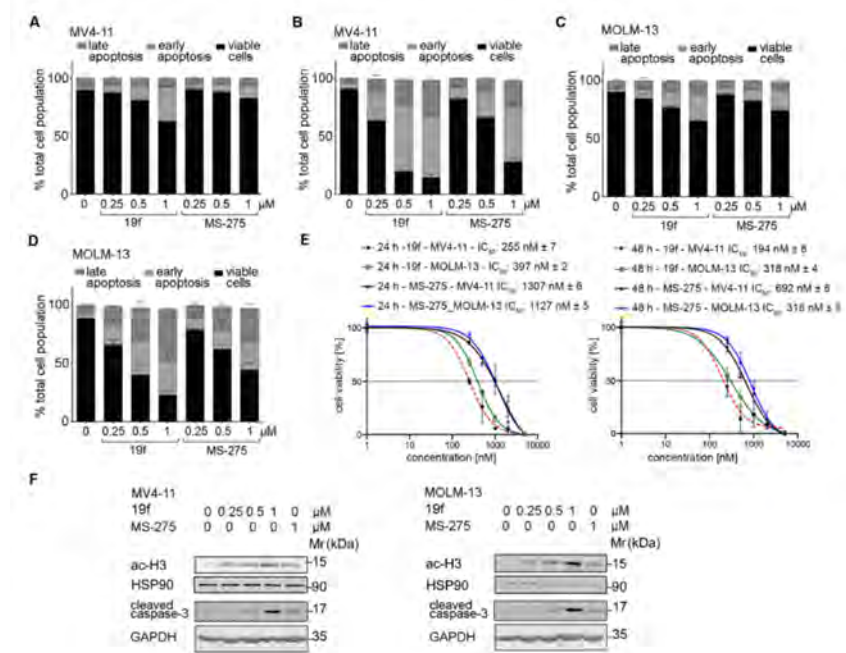
Figure 6. Pro-apoptotic effects of 19f and MS-275 in MV4-11 and MOLM-13 cells. A, B MV4-11 cells were treated with 0.25, 0.5, 1 μM 19f or MS-275 for 24 h (**A**) or 48 h (**B**) and analyzed for annexin-V/PI by flow cytometry. (**C,D**) The same experiments were conducted with MOLM-13 cells. (**E**) IC_{50} values were determined for 19f. (**F**) Immunoblot was done with the stated antibodies and lysates of MV4-11 and MOLM-13 cells that were incubated with the HDACi for 24 h. Cells were incubated with 0.25, 0.5, 1 μM 19f, or 1 μM MS-275. Graphs show representatives of three independent experiments.
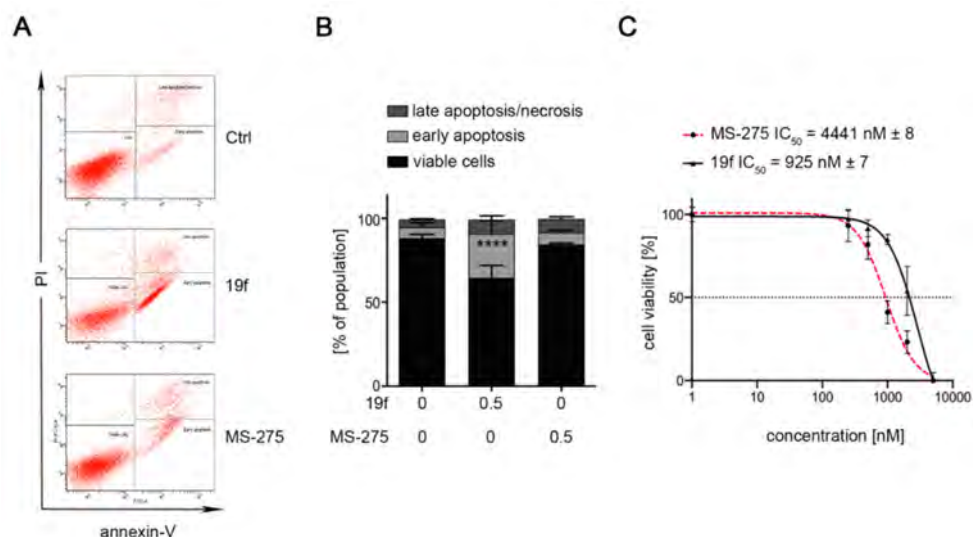
Figure 7. Cytotoxicity of MS-275 and 19f in leukemic HEL cells expressing JAK2V617F. (**A**,**B**) HEL cells were treated with 0.5 μM of MS-275 or 19f for 48 h. (**B**) Cells were stained with annexin V-FITC/PI and analyzed via flow cytometry. Graphs show mean $\pm$ SD of three independent experiments (one-way ANOVA; two-way ANOVA; Bonferroni correction; **** $p < 0.0001$). (**C**) HEL cells were treated with increasing concentrations of MS-275 or 19f from 0.25 μM to 5 μM for 24 h. IC_{50} values were determined for 19f. Results represent three independent experiments.

Immunoblot analyses of MV4-11 and MOLM-13 cells illustrated that 19f triggered the expected accumulation of acetylated histone H3 dose-dependently and more potently than MS-275 did. This was associated with the processing of the ultimate death executioner enzyme caspase-3 to its cleaved active form (Figure 6F).

Compound 19f was also superior to MS-275 in human erythroleukemia (HEL) cells. This erythroleukemia cell model carries a mutation in Janus kinase-2 (JAK2V617F) and HDACi are considered as therapeutic options to control the transformation of this disease into AML [53]. While 0.5 μM MS-275 did not cause apoptosis in HEL cell cultures, 0.5 μM 19f significantly induced apoptosis to 26% (Figure 7A). Dose escalation studies revealed an IC_{50} of 4441 nM for MS-275 and IC_{50} of 925 nM for 19f for toxic effects on HEL cells (Figure 7B).

2.4.3. In Silico Prediction of Pharmacokinetic and Tox Data

To analyze the further in vivo potential of the most promising candidates, 19f and 21a, we calculated several physicochemical properties and predicted pharmacokinetic parameters (Table 4). For predicting the properties the PreADMET (https://preadmet.bmdrc.kr/admetox/, accessed on 10 Novermber 2021) web service was used. The in silico pharmacokinetic data (e.g., human intestinal absorption (HIA%), plasma protein binding) as well as physicochemical data (e.g., water solubility, AlogP) showed that 19f has high predicted oral bioavailability, reduced plasma protein binding and better solubility compared to the reference Entinostat (MS-275). The toxicity prediction using ProTox-II (https://tox-new.charite.de/protox_II/, accessed on 10 November 2021) showed a very low toxicity of 19f (LD_{50} 1500 mg/kg compared to 22 mg/kg for MS-275). ProTox-II uses molecular similarity, fragment propensities, the most frequent features and (fragment similarity based cross-validation) machine-learning, based on a total of 33 models for the prediction of various toxicity endpoints, such as acute toxicity, hepatotoxicity, cytotoxicity, carcinogenicity, mutagenicity, immunotoxicity, adverse outcomes pathways and toxicity targets. None of the toxicity targets included in ProTox-II were predicted for 19f.

Table 4. In silico ADME and Tox prediction for the most promising candidates 19f and 21a as well as the reference inhibitor MS-275. For predicting the properties PreADMET (https://preadmet.bmdrc.kr/admetox/ accessed date 10 Novermber 2021) and ProTox-II (https://tox-new.charite.de/protox_II/ accessed date 10 Novermber 2021) web applications were used.

	MS-275	**19f**	**21a**
Human intestinal absorption%	92.54	93.53	96.14
AlogP98 value	2.07	0.78	3.11
Plasma Protein Binding%	91.07	34.78	77.36
Pure water solubility mg/L	19.92	434.20	3.69
CYP_2C19_inhibition	None	None	None
CYP_2C9_inhibition	Inhibitor	Inhibitor	Inhibitor
CYP_2D6_inhibition	None	None	Non
CYP_2D6_substrate	None	Substrate	Substrate
CYP_3A4_inhibition	Inhibitor	None	None
CYP_3A4_substrate	Substrate	Substrate	Substrate
hERG_inhibition	high risk	moderate risk	high risk
Pgp inhibition	None	None	None
Predicted LD_{50}	22 mg/kg	1500 mg/kg	600 mg/kg
Toxicity prediction ProTox-II	0/17	0/17	1/17

3. Conclusions

A new series of 2-aminobenzamides was synthesized based on different lead structures and biologically tested for their inhibition against HDAC1, HDAC2, and HDAC3. Docking studies were carried out to guide the design of linker and capping groups, as well as the 2-aminobenzamide substitution. Of the various capping groups, indole and N-methylindole were found to be the best choices. Docking studies showed that the indole capping group, e.g., in the potent inhibitor 19f, interacts with the conserved F150/H28 in HDAC1, F150/H33 in HDAC2, and F150/H22 in HDAC3, respectively. In the case of 21a and 29b, the 2-thienyl group on the 2-aminobenzamide fits perfectly to the foot pocket in HDAC1/HDAC2, whereas in the case of HDAC3 the narrow footpocket does not allow such bulky substituents. In the case of HDAC3, the docking solutions showed that inhibitors with bulky substitutions on the 2-aminobenzamide ring could not bind to the zinc ion due to the smaller foot pocket. The most potent compounds, 19f and 29b, were subjected to a cellular biological assay against the cancer cell lines MV4-11, MOLM-13, and HEL. The inhibitors showed strong hyperacetylation of the HDAC1-3 substrate histone H3 in agreement with the in vitro HDAC inhibitory data. The best inhibitor 19f strongly induced apoptosis in these leukemic cells and was found to be superior to the clinically evaluated HDACi MS-275. This work demonstrates that we successfully synthesized and evaluated novel class-I HDACi. Of these, 19f turned out as a specific inhibitor of HDAC1, HDAC2, and HDAC3 with superior activity and promising physicochemical properties.

4. Materials and Methods

4.1. Chemistry

4.1.1. General

All of the specifications regarding the standard materials, equipment and devices used in the experimental methods are included in the Supplementary Materials. In addition, the experimental procedures for synthesis of intermediates are included in the Supplementary Materials.

4.1.2. General Procedure for Amide Coupling

A mixture of the appropriate carboxylic acid (1.0 eq.) and HATU (1.2 eq.) was dissolved in dry DMF (5 mL) and stirred at RT for 30 min. The corresponding amine (0.9 eq.) and DIPEA (5.0 eq.) in THF (3 mL) were added and the reaction mixture was stirred for 18 h at RT. The reaction mixture was diluted with EtOAc (15 mL) and the reaction mixture was washed with 1 N NH_4Cl and saturated $NaHCO_3$, respectively. The organic extracts were washed with brine, dried over anhydrous Na_2SO_4, filtered and concentrated under vacuum. The residue was purified by using MPLC ($CHCl_3$:MeOH) to provide the corresponding amide. Reaction yields, and chromatographic and spectrometric data of the final compounds are reported below.

4.1.3. General Procedure for the Preparation of Final Target Compounds X through N-Boc Cleavage

The N-Boc-protected aniline derivative (1 mmol) was solubilized at 0 ^{0}C in dry DCM (5 mL), and then TFA (5 mL) was added. The reaction mixture was stirred at RT for 30 min. The solvent was evaporated to dryness, the residue was dissolved in 1 mL MeOH, 1 N NaOH (10 mL) was added, and the mixture was stirred for 1 h, before being extracted with EtOAc. The organic extracts were washed with brine, dried over anhydrous Na_2SO_4, filtered and concentrated under vacuum. The residue was purified by using MPLC ($CHCl_3$:MeOH) to provide the corresponding amide. Reaction yields, chromatographic and spectrometric data of the final compounds are reported below.

4.1.4. Spectral Analysis of Final Compounds

N-(2-Aminophenyl)-5-(4-phenethylpiperazin-1-yl)pyrazine-2-carboxamide (19a).
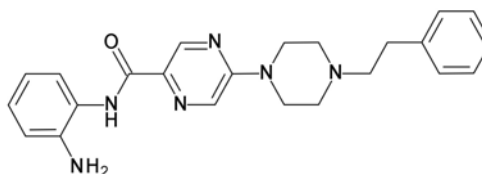
^{1} H NMR (400 MHz, DMSO-d$_6$) δ 9.58 (s, 1H, -CO-NH-Ar), 8.70 (d, J = 1.3 Hz, 1H, Ar-H of Pyrazine), 8.34 (d, J = 1.4 Hz, 1H, Ar-H of Pyrazine), 7.46 (dd, J = 7.9, 1.5 Hz, 1H, Ar-H), 7.30–7.21 (m, 4H, Ar-H), 7.20–7.14 (m, 1H, Ar-H), 6.92 (td, J = 7.6, 1.6 Hz, 1H, Ar-H), 6.80 (dd, J = 8.0, 1.5 Hz, 1H, Ar-H), 6.62 (td, J = 7.5, 1.5 Hz, 1H, Ar-H), 4.82 (s, 2H, -NH$_2$), 3.72 (t, J = 5.0 Hz, 4H, Piperazine Hs), 2.77 (dd, J = 9.5, 6.1 Hz, 2H, -N-CH$_2$CH$_2$-Ar), 2.57–2.54 (m, 6H, -N-CH$_2$CH$_2$-Ar + Piperazine Hs). ^{13}C NMR (101 MHz, DMSO) δ 162.32, 155.54, 142.41, 141.98, 140.76, 133.14, 129.19, 129.09, 128.68, 126.30, 125.99, 124.79, 117.50, 117.23, 59.98, 52.65, 44.41, 33.10. HRMS m/z: 403.2239 [M + H]$^+$; calculated $C_{23}H_{27}N_6O^+$: 403.2246. HPLC: rt 5.68 min (purity 97.6%), yield: 73%.

N-(2-Aminophenyl)-5-(4-(4-chlorophenethyl)piperazin-1-yl)pyrazine-2-carboxamide (19b).
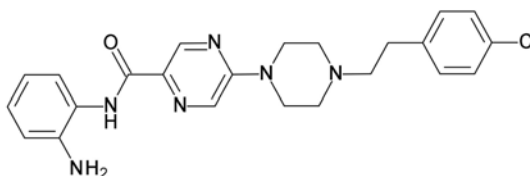
^{1} H NMR (400 MHz, DMSO-d$_6$) δ 9.59 (s, 1H, -CO-NH-Ar), 8.70 (d, J = 1.3 Hz, 1H, Ar-H of Pyrazine), 8.35 (d, J = 1.4 Hz, 1H, Ar-H of Pyrazine), 7.46 (dd, J = 7.9, 1.5 Hz, 1H, Ar-H), 7.35–7.25 (m, 4H, Ar-H), 6.92 (td, J = 7.6, 1.6 Hz, 1H, Ar-H), 6.80 (dd, J = 7.9, 1.5 Hz, 1H, Ar-H), 6.63 (td, J = 7.6, 1.5 Hz, 1H, Ar-H), 4.83 (s, 2H, -NH$_2$), 3.71 (t, J = 5.0 Hz, 4H, Piperazine Hs), 2.77 (t, J = 7.6 Hz, 2H, -N-CH$_2$CH$_2$-Ar), 2.56 (q, J = 6.8, 4.8 Hz, 6H, -N-CH$_2$CH$_2$-Ar + Piperazine Hs). ^{13}C NMR (101 MHz, DMSO) δ 162.32, 155.53, 142.41, 141.98,

139.86, 133.15, 130.99, 130.92, 129.19, 128.56, 125.99, 124.79, 117.51, 117.23, 59.55, 52.60, 44.39, 32.25. MS m/z: 435.26 [M − H]$^-$, 437.61 [M + H]$^+$, HRMS m/z: 459.1680 [M+Na]$^+$; calculated $C_{24}H_{25}N_7O^+$: 459.1676. HPLC: rt 6.57 min (purity 97%), yield: 70%.

N-(2-aminophenyl)-2-(4-(pyridin-2-yl-methyl)piperazin-1-yl)pyrimidine-5-carboxamide (19c).
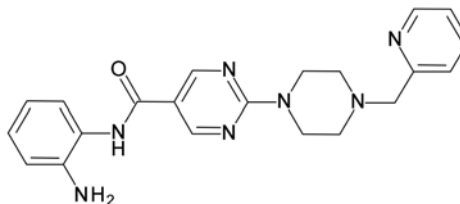
^{1}H NMR (400 MHz, DMSO-d$_6$) δ 9.48 (s, 1H, -CO-NH-Ar), 8.89 (s, 2H, Ar-H of Pyrimidine), 8.58–8.51 (m, 1H, Ar-H), 7.81 (td, J = 7.7, 1.8 Hz, 1H, Ar-H), 7.49 (dt, J = 7.8, 1.1 Hz, 1H, Ar-H), 7.32 (t, J = 6.3 Hz, 1H, Ar-H), 7.12 (dd, J = 7.8, 1.5 Hz, 1H, Ar-H), 6.95 (ddd, J = 8.0, 7.2, 1.6 Hz, 1H, Ar-H), 6.75 (dd, J = 8.0, 1.4 Hz, 1H, Ar-H), 6.56 (td, J = 7.5, 1.4 Hz, 1H, Ar-H), 5.05 (s, 2H, -NH$_2$), 4.00–3.76 (m, 6H, N-CH$_2$-pyridine + Piperazine Hs), 2.78–2.61 (m, 4H, Piperazine Hs). ^{13}C NMR (101 MHz, DMSO) δ 161.81, 158.53, 149.30, 143.75, 137.02, 127.31, 126.98, 123.32, 123.20, 122.71, 116.80, 116.48, 116.30, 64.01, 52.94, 43.93. MS m/z: 388.40 [M − H]$^-$, 390.20 [M + H]$^+$, HRMS m/z: 390.2034 [M + H]$^+$; calculated $C_{21}H_{24}N_7O^+$: 390.2042. HPLC: rt 5.78 min (purity 99.8%), yield: 73%.

N-(2-Aminophenyl)-5-(4-(pyridin-2-ylmethyl)piperazin-1-yl)pyrazine-2-carboxamide (19d).
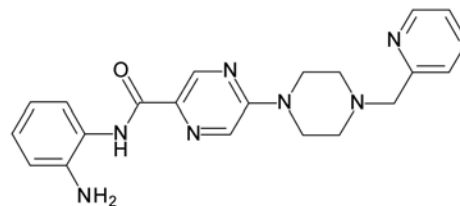
^{1}H NMR (400 MHz, DMSO-d$_6$) δ 9.58 (s, 1H, -CO-NH-Ar), 8.69 (d, J = 1.3 Hz, 1H, Ar-H of Pyrazine), 8.49 (ddd, J = 4.9, 1.8, 0.9 Hz, 1H, Ar-H), 8.33 (d, J = 1.4 Hz, 1H, Ar-H of Pyrazine), 7.77 (td, J = 7.7, 1.9 Hz, 1H, Ar-H), 7.51–7.42 (m, 2H, Ar-H), 7.26 (ddd, J = 7.5, 4.8, 1.2 Hz, 1H, Ar-H), 6.96–6.87 (m, 1H, Ar-H), 6.79 (dd, J = 8.0, 1.5 Hz, 1H, Ar-H), 6.62 (td, J = 7.6, 1.5 Hz, 1H, Ar-H), 4.83 (s, 2H, -NH$_2$), 3.76–3.73 (m, 4H, Piperazine Hs), 3.66 (s, 2H, N-CH$_2$-pyridine), 2.57–2.54 (m, 4H, Piperazine Hs). ^{13}C NMR (101 MHz, DMSO) δ 162.31, 158.44, 155.51, 149.30, 142.39, 142.00, 136.99, 133.16, 129.17, 126.00, 124.80, 124.78, 123.32, 122.69, 117.50, 117.22, 64.01, 52.72, 44.42. MS m/z: 440.38 [M − H]$^-$, 388.84 [M + H]$^+$, HRMS m/z: 390.2037 [M + H]$^+$; calculated $C_{21}H_{24}N_7O^+$: 390.2042. HPLC: rt 11.33 min (purity 95%), yield: 74%.

N-(2-Aminophenyl)-5-(4-(benzo[b]thiophen-3-ylmethyl)piperazin-1-yl)pyrazine-2-carboxamide (19e).
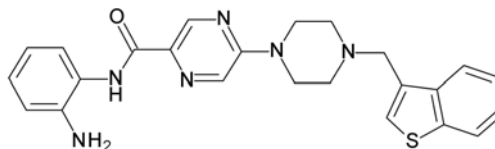
^{1}H NMR (400 MHz, DMSO-d$_6$) δ 9.58 (s, 1H, -CO-NH-Ar), 8.69 (d, J = 1.3 Hz, 1H, Ar-H of Pyrazine), 8.33 (d, J = 1.4 Hz, 1H, Ar-H of Pyrazine), 8.09–7.84 (m, 2H, Ar-H), 7.63 (s, 1H, Ar-H), 7.53–7.29 (m, 3H, Ar-H), 6.98–6.87 (m, 1H, Ar-H), 6.80 (dd, J = 8.0, 1.5 Hz, 1H, Ar-H), 6.62 (td, J = 7.6, 1.5 Hz, 1H, Ar-H), 4.84 (s, 2H, -NH$_2$), 3.90–3.61 (m, 6H, N-CH$_2$-benzothiophene + Piperazine Hs), 2.57–2.55 (m, 4H, Piperazine Hs). MS m/z: 443.41 [M − H]$^-$,

445.02 [M + H]$^+$, HRMS m/z: 445.1810 [M + H]$^+$; calculated C$_{24}$H$_{25}$N$_6$OS$^+$: 445.1810. HPLC: rt 7.19 min (purity 97.4%), yield: 75%.

5-(4-((1H-indol-3-yl)methyl)piperazin-1-yl)-N-(2-aminophenyl)pyrazine-2-carboxamide (19f).
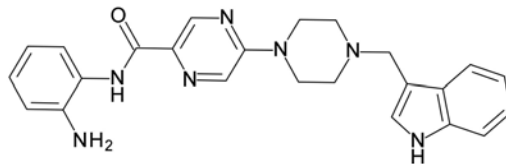
^{1}H NMR (400 MHz, DMSO-d$_6$) δ 10.93 (s, 1H,-NH indole), 9.56 (s, 1H, -CO-NH-Ar), 8.67 (d, J = 1.3 Hz, 1H, Ar-H of Pyrazine), 8.31 (d, J = 1.4 Hz, 1H, Ar-H of Pyrazine), 7.65 (d, J = 7.9 Hz, 1H, Ar-H), 7.45 (d, J = 7.9, 1H, Ar-H), 7.34 (d, J = 8.1 Hz, 1H, Ar-H), 7.24 (d, J = 2.3 Hz, 1H, Ar-H), 7.10–7.02 (m, 1H, Ar-H), 7.02–6.93 (m, 1H, Ar-H), 6.91 (td, J = 7.9, 1.5 Hz, 1H, Ar-H), 6.79 (dd, J = 7.9, 1.4 Hz, 1H, Ar-H), 6.62 (td, J = 7.6, 1.5 Hz, 1H, Ar-H), 4.81 (s, 2H, -NH$_2$), 3.70–3.67 (m, 6H, -N-CH$_2$-Indole + Piperazine Hs), 2.60–2.50 (m, 4H, Piperazine Hs). ^{13}C NMR (101 MHz, DMSO) δ 162.32, 155.48, 142.39, 141.98, 136.76, 133.07, 129.17, 128.04, 125.99, 124.79, 121.44, 119.46, 118.95, 117.50, 117.21, 111.83, 53.32, 52.38, 44.47. MS m/z: 426.41 [M − H]$^−$, 428.26 [M + H]$^+$, HRMS m/z: 428.2198 [M + H]$^+$; calculated C$_{24}$H$_{26}$N$_7$O$^+$: 428.2198. HPLC: rt 7.89 min (97.6%), yield: 25%.

5-(4-(2-(1.H-indol-3-yl)ethyl)piperazin-1-yl)-N-(2-aminophenyl)pyrazine-2-carboxamide (19g).
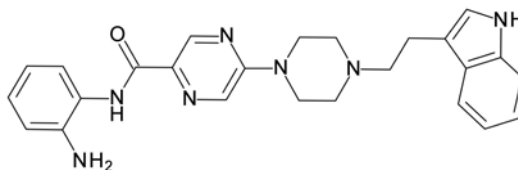
^{1}H NMR (400 MHz, DMSO-d$_6$) δ 10.76 (s, 1H, -NH of indole), 9.59 (s, 1H, -CO-NH-Ar), 8.71 (d, J = 1.3 Hz, 1H, Ar-H of Pyrazine), 8.36 (d, J = 1.4 Hz, 1H, Ar-H of Pyrazine), 7.52 (dd, J = 7.8, 1.1 Hz, 1H, Ar-H), 7.46 (dd, J = 7.9, 1.5 Hz, 1H, Ar-H), 7.32 (dt, J = 8.1, 1.0 Hz, 1H, Ar-H), 7.16 (d, J = 2.4 Hz, 1H, Ar-H), 7.04 (ddd, J = 8.1, 7.0, 1.2 Hz, 1H, Ar-H), 6.99–6.88 (m, 2H, Ar-H), 6.80 (dd, J = 8.0, 1.5 Hz, 1H, Ar-H), 6.62 (td, J = 7.5, 1.5 Hz, 1H, Ar-H), 4.83 (s, 2H, -NH$_2$), 3.75 (s, 4H, Piperazine Hs), 2.95–2.81 (m, 2H, -N-CH$_2$CH$_2$-indole), 2.66–2.60 (m, 6H, -N-CH$_2$CH$_2$-indole + Piperazine Hs). ^{13}C NMR (101 MHz, DMSO) δ 162.33, 155.56, 142.43, 141.99, 136.63, 133.12, 129.19, 127.67, 125.99, 124.80, 122.95, 121.27, 118.72, 118.58, 117.51, 117.23, 112.89, 111.77, 59.14, 52.75, 44.48, 22.85. MS m/z: 440.38 [M − H]$^−$, 442.19 [M + H]$^+$, HRMS m/z: 464.2173 [M+Na]$^+$; calculated C$_{25}$H$_{27}$N$_7$ONa$^+$: 464.2174. HPLC: rt 6.54 min (purity 98.3%), yield: 76%.

5-(4-(2-(1H-indol-2-yl)ethyl)piperazin-1-yl)-N-(2-amino-4,5-difluorophenyl)pyrazine-2-carboxamide (19h).
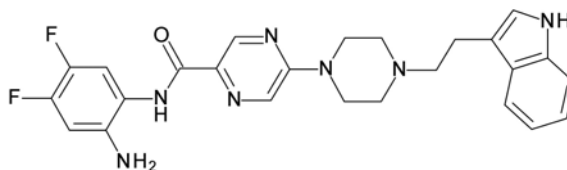
^{1}H NMR (400 MHz, DMSO-d$_6$) δ 10.76 (s, 1H, NH of indole), 9.64 (s, 1H, CO-NH-Ar), 8.70 (d, J = 1.3 Hz, 1H, Ar-H of Pyrazine), 8.34 (d, J = 1.2 Hz, 1H, Ar-H of Pyrazine), 7.63–7.47 (m, 2H, Ar-H), 7.32 (d, J = 8.0 Hz, 1H, Ar-H), 7.16 (s, 1H, Ar-H), 7.12–6.86 (m, 2H, Ar-H), 6.77 (dd, J = 12.8, 8.2 Hz, 1H, Ar-H), 5.02 (s, 2H, NH$_2$), 3.82–3.69 (m, 4H, Piperazine Hs), 2.91–2.87 (m, 2H, -N-CH$_2$CH$_2$-Ar), 2.69–2.62 (m, 6H, -N-CH$_2$CH$_2$-Ar + Piperazine

Hs). ^{13}C NMR (101 MHz, DMSO) δ 162.56, 155.59, 142.62, 136.63, 132.65, 129.20, 127.67, 122.95, 121.27, 118.72, 118.58, 113.34, 113.14, 112.89, 111.77, 104.61, 104.41, 59.22, 52.75, 44.47, 22.91. MS m/z: 478.43 [M + H]. HRMS m/z: 478.2163 [M + H]$^+$; calculated C$_{25}$H$_{26}$F$_2$N$_7$O$^+$: 478.2166. HPLC: rt 7.18 min (purity 98.3%), yield: 32%.

5-(4-(2-(1H-indol-3-yl)ethyl)piperazin-1-yl)-N-(2-amino-4-chlorophenyl)pyrazine-2-carboxamide (19i).
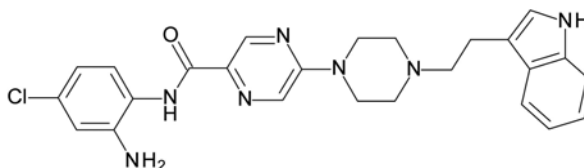
^{1}H NMR (400 MHz, DMSO-d$_6$) δ 10.76 (s, 1H, -NH of indole), 9.59 (s, 1H, -CO-NH-Ar), 8.69 (d, J = 1.3 Hz, 1H, Ar-H of Pyrazine), 8.35 (d, J = 1.3 Hz, 1H, Ar-H of Pyrazine), 7.52 (d, J = 7.8 Hz, 1H, Ar-H), 7.41 (d, J = 8.5 Hz, 1H, Ar-H), 7.32 (d, J = 8.1 Hz, 1H, Ar-H), 7.16 (s, 1H, Ar-H), 7.00 (dt, J = 34.2, 7.5 Hz, 2H, Ar-H), 6.83 (s, 1H, Ar-H), 6.66–6.57 (m, 1H, Ar-H), 5.16 (s, 2H, -NH$_2$), 3.84–3.67 (m, 4H, Piperazine Hs), 2.97–2.81 (m, 2H, -N-CH$_2$CH$_2$-Ar), 2.72–2.52 (m, 6H, -N-CH$_2$CH$_2$-Ar + Piperazine Hs). ^{13}C NMR (101 MHz, DMSO) δ 162.60, 155.56, 144.03, 142.54, 136.63, 132.97, 129.98, 129.17, 127.67, 126.63, 123.32, 122.96, 121.27, 118.72, 118.58, 116.55, 115.90, 112.87, 111.77, 59.11, 52.73, 44.45, 22.83. MS m/z: 476.26 [M + H]$^+$. HRMS m/z: 498.1782 [M+Na]$^+$; calculated C$_{25}$H$_{26}$ClN$_7$ONa$^+$: 498.1785. HPLC: rt 11.32 min (purity 96.9%), yield: 32%.

N-(2-aminophenyl)-2-(4-((1-methyl-1H-indol-3-yl)methyl)piperazin-1-yl)pyrimidine-5-carboxamide (19j).
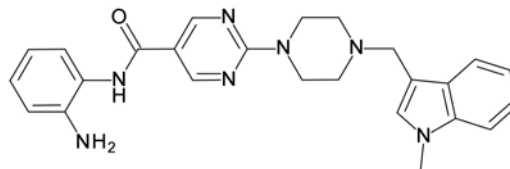
^{1}H NMR (400 MHz, DMSO-d$_6$) δ 9.44 (s, 1H, -CO-NH-Ar), 8.85 (s, 2H, Ar-H of Pyrimidine), 7.66 (dt, J = 7.9, 1.0 Hz, 1H, Ar-H), 7.39–7.35 (m, 1H, Ar-H), 7.23 (s, 1H, Ar-H), 7.15–7.09 (m, 2H, Ar-H), 7.02 (ddd, J = 8.0, 7.0, 1.0 Hz, 1H, Ar-H), 6.94 (td, J = 7.6, 1.6 Hz, 1H, Ar-H), 6.74 (dd, J = 8.0, 1.5 Hz, 1H, Ar-H), 6.55 (td, J = 7.5, 1.5 Hz, 1H, Ar-H), 4.90 (s, 2H, -NH$_2$), 3.82 (t, J = 5.3 Hz, 4H, Piperazine Hs), 3.74 (s, 3H, N-CH$_3$), 3.66 (s, 2H, N-CH$_2$-Indole), 2.45 (t, J = 5.3 Hz, 4H, Piperazine Hs). MS m/z: 440.42 [M − H]$^-$. HRMS m/z: 442.2349 [M + H]$^+$; calculated C$_{25}$H$_{28}$N$_7$O$^+$: 442.2355. HPLC: rt 7.96 min (purity 97.7%), yield: 60%.

N-(2-aminophenyl)-5-(4-((1-methyl-1H-indol-3-yl)methyl)piperazin-1-yl)pyrazine-2-carboxamide (19k).
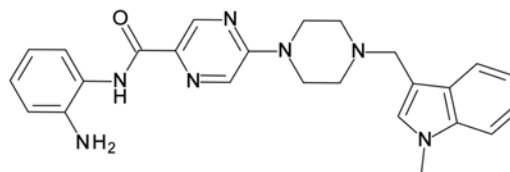
^{1}H NMR (400 MHz, DMSO-d$_6$) δ 9.56 (s, 1H, -CO-NH-Ar), 8.67 (d, J = 1.3 Hz, 1H, Ar-H of Pyrazine), 8.31 (d, J = 1.4 Hz, 1H, Ar-H of Pyrazine), 7.66 (d, J = 7.9 Hz, 1H, Ar-H), 7.45 (dd, J = 7.9, 1.5 Hz, 1H, Ar-H), 7.38 (d, J = 8.2 Hz, 1H, Ar-H), 7.24 (s, 1H, Ar-H), 7.13 (ddd, J = 8.2, 7.0, 1.2 Hz, 1H, Ar-H), 7.02 (ddd, J = 7.9, 7.0, 1.0 Hz, 1H, Ar-H), 6.95–6.86 (m, 1H, Ar-H), 6.79 (dd, J = 8.0, 1.5 Hz, 1H, Ar-H), 6.62 (td, J = 7.6, 1.5 Hz, 1H, Ar-H), 4.81

(s, 2H, -NH$_2$), 3.74 (s, 3H, -NCH$_3$), 3.71–3.68 (m, 6H, N-CH$_2$-Indole + Piperazine Hs), 2.51–2.48 (m, 4H, Piperazine Hs). ^{13}C NMR (101 MHz, DMSO) δ 162.31, 155.49, 142.40, 141.97, 137.18, 133.04, 129.53, 129.15, 128.38, 125.98, 124.79, 124.77, 121.54, 119.67, 119.04, 117.50, 117.22, 110.02, 53.21, 52.42, 44.51, 32.74. MS m/z: 440.38 [M − H]$^-$, 442.04 [M + H]$^+$, HRMS m/z: 442.2350 [M + H]$^+$; calculated C$_{25}$H$_{28}$N$_7$O$^+$: 442.2355, HPLC: rt 14.22 min (purity 95.4%), yield: 56%.

N-(2-amino-4,5-difluorophenyl)-2-(4-((1-methyl-1H-indol-3-yl)methyl)piperazin-1-yl) pyrimidine-5-carboxamide (19l).
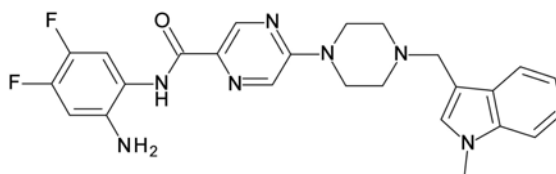
^{1}H NMR (400 MHz, DMSO-d$_6$) δ 9.60 (s, 1H, CO-NH-Ar), 8.66 (d, J = 1.3 Hz, 1H, Ar-H of Pyrazine), 8.30 (d, J = 1.3 Hz, 1H, Ar-H of Pyrazine), 7.66 (d, J = 7.8 Hz, 1H, Ar-H), 7.54 (dd, J = 12.4, 8.7 Hz, 1H, Ar-H), 7.37 (d, J = 8.2 Hz, 1H, Ar-H), 7.23 (s, 1H, Ar-H), 7.17–7.08 (m, 1H, Ar-H), 7.06–6.96 (m, 1H, Ar-H), 6.76 (dd, J = 12.8, 8.2 Hz, 1H, Ar-H), 5.01 (s, 2H, NH$_2$), 3.77–3.59 (m, 9H, N-CH$_2$-Indole +-N-CH$_3$ + Piperazine Hs), 2.58–2.45 (m, 4H, Piperazine Hs). 13C NMR (101 MHz, DMSO) δ 162.54, 155.52, 142.59, 139.40, 137.18, 132.56, 129.52, 129.17, 128.38, 121.53, 120.61, 120.56, 119.67, 119.04, 113.31, 113.11, 110.02, 104.60, 104.40, 53.20, 52.42, 44.51, 32.74. MS m/z: 476.30 [M − H]. HRMS m/z: 500.1979 [M+Na]$^+$; calculated C$_{25}$H$_{25}$F$_2$N$_7$ONa$^+$: 500.1986. HPLC: rt 7.94 min (purity 98.8%), yield: 30%.

N-(2-Amino-4-fluorophenyl)-5-(4-(2-(1-methyl-1H-indol-3-yl)ethyl)piperazin-1-yl) pyrazine-2-carboxamide (19m).
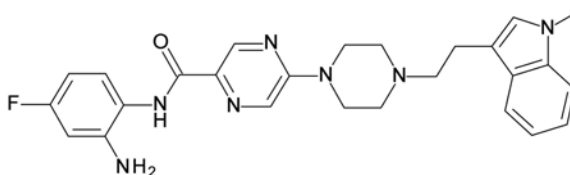
^{1}H NMR (400 MHz, DMSO-d$_6$) δ 9.53 (s, 1H, -CO-NH-Ar), 8.69 (d, J = 1.3 Hz, 1H, Ar-H of Pyrazine), 8.35 (d, J = 1.4 Hz, 1H, Ar-H of Pyrazine), 7.53 (dt, J = 7.9, 1.0 Hz, 1H, Ar-H), 7.36 (d, J = 8.2 Hz, 1H, Ar-H), 7.30 (dd, J = 8.7, 6.3 Hz, 1H, Ar-H), 7.16–7.08 (m, 2H, Ar-H), 7.00 (ddd, J = 7.9, 6.9, 1.0 Hz, 1H, Ar-H), 6.56 (dd, J = 11.1, 2.9 Hz, 1H, Ar-H), 6.38 (td, J = 8.6, 2.9 Hz, 1H, Ar-H), 5.16 (s, 2H, -NH$_2$), 3.79–3.73 (m, 4H, Piperazine Hs), 2.88 (dd, J = 9.8, 5.8 Hz, 2H, -N-CH$_2$CH$_2$-Ar), 2.70–2.55 (m, 6H, -N-CH$_2$CH$_2$-Ar + Piperazine Hs). ^{13}C NMR (101 MHz, DMSO) δ 162.73, 159.76, 155.55, 144.96, 144.84, 142.46, 137.02, 133.11, 129.15, 127.99, 127.42, 127.37, 127.26, 121.42, 120.30, 118.97, 118.68, 112.28, 109.94, 103.06, 102.84, 102.63, 102.39, 59.16, 52.75, 44.47, 32.66, 22.67. HRMS m/z: 474.2420 [M + H]$^+$; calculated C$_{26}$H$_{29}$N$_7$FO$^+$: 474.2417. HPLC: rt 8.05 min (purity 93.7%), yield: 66%.

N-(2-aminophenyl)-2-(4-methylpiperazin-1-yl)pyrimidine-5-carboxamide (19n).
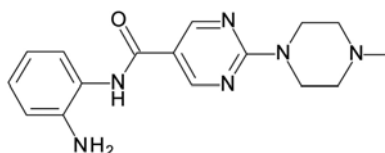
^{1}H NMR (400 MHz, DMSO-d$_6$) δ 9.47 (s, 1H, -CO-NH-Ar), 8.87 (s, 2H, Ar-H of Pyrimidne), 7.15–7.08 (m, 1H, Ar-H), 6.99–6.90 (m, 1H, Ar-H), 6.74 (dd, J = 8.0, 1.4 Hz, 1H, Ar-H), 6.56 (td, J = 7.6, 1.4 Hz, 1H, Ar-H), 4.91 (s, 2H, -NH$_2$), 3.88–3.78 (m, 4H, Piperazine Hs), 2.43–2.33 (m, 4H, Piperazine Hs), 2.22 (s, 3H, -N-CH$_3$). ^{13}C NMR (101 MHz, DMSO) δ

163.06, 161.84, 158.55, 143.74, 127.31, 126.96, 123.23, 116.81, 116.48, 116.32, 54.66, 46.00, 43.72. MS m/z: 313.36 [M + H]. HRMS m/z: 313.1770 [M + H]$^+$; $C_{16}H_{20}N_6O^+$: 313.1776. HPLC: rt 5.58 min (purity 100%), yield: 55%.

N-(2-aminophenyl)-5-(4-methylpiperazin-1-yl)pyrazine-2-carboxamide (19o).
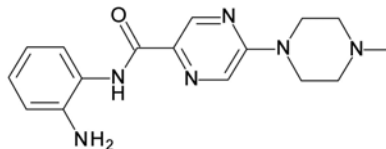
^{1}H NMR (400 MHz, DMSO-d_6) δ 9.58 (s, 1H, -CO-NH-Ar), 8.69 (d, J = 1.3 Hz, 1H, Ar-H of Pyrazine), 8.34 (d, J = 1.4 Hz, 1H, Ar-H of Pyrazine), 7.45 (dd, J = 7.9, 1.4 Hz, 1H, Ar-H), 6.96–6.87 (m, 1H, Ar-H), 6.80 (dd, J = 8.0, 1.4 Hz, 1H, Ar-H), 6.62 (td, J = 7.7, 1.4 Hz, 1H, Ar-H), 4.82 (s, 2H, -NH$_2$), 3.76–3.68 (m, 4H, Piperazine Hs), 2.45–2.37 (m, 4H, Piperazine Hs), 2.22 (s, 3H, -NCH$_3$). ^{13}C NMR (101 MHz, DMSO) δ 162.32, 155.54, 142.40, 142.00, 133.13, 129.19, 125.99, 124.81, 117.49, 117.22, 54.57, 46.15, 44.29. MS m/z: 313.36[M + H]. HRMS m/z: 313.1770 [M + H]$^+$; $C_{16}H_{20}N_6O^+$: 313.1776. HPLC: rt 5.91 min (purity 99.7%), yield: 66%.

N-(2-Amino-5-(thiophen-2-yl)phenyl)-5-(4-(2-(1-methyl-1H-indol-3-yl)ethyl)piperazin-1-yl)pyrazine-2-carboxamide (21a).
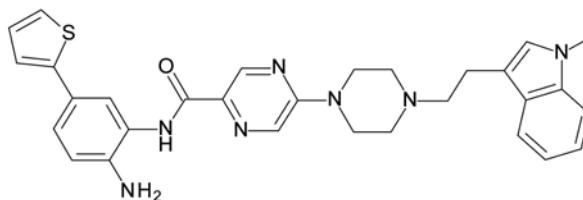
^{1}H NMR (400 MHz, DMSO-d_6) δ 9.67 (s, 1H, -CO-NH-Ar), 8.73 (d, J = 1.3 Hz, 1H, Ar-H of Pyrazine), 8.37 (d, J = 1.4 Hz, 1H, Ar-H of Pyrazine), 7.78 (d, J = 2.2 Hz, 1H, Ar-H), 7.54 (dt, J = 7.9, 1.0 Hz, 1H, Ar-H), 7.39–7.31 (m, 2H, Ar-H), 7.25–7.22 (m, 2H, Ar-H), 7.16–7.09 (m, 2H, Ar-H), 7.04 (dd, J = 5.1, 3.6 Hz, 1H, Ar-H), 7.00 (ddd, J = 8.0, 7.0, 1.0 Hz, 1H, Ar-H), 6.83 (d, J = 8.3 Hz, 1H, Ar-H), 5.08 (s, 2H, -NH$_2$), 3.77 (t, J = 5.1 Hz, 4H, Piperazine Hs), 3.72 (s, 3H, -NCH$_3$), 2.93–2.83 (m, 2H, -N-CH$_2$CH$_2$-Ar), 2.70–2.56 (m, 6H, -N-CH$_2$CH$_2$-Ar + Piperazine Hs). ^{13}C NMR (101 MHz, dmso) δ 162.59, 155.57, 144.77, 142.55, 142.03, 137.02, 133.02, 129.20, 128.63, 127.99, 127.42, 124.81, 123.82, 123.40, 122.27, 121.61, 121.42, 118.98, 118.68, 117.39, 112.28, 109.94, 59.16, 52.75, 44.47, 32.66, 22.67. MS m/z: 536.52 [M − H]$^−$, 538.48 [M + H]$^+$, HRMS m/z: 538.2386 [M + H]$^+$; calculated $C_{30}H_{32}N_7OS^+$: 538.2389. HPLC: rt 9.64 min (95%), yield: 65%.

5-(4-(2-(1H-indol-3-yl)ethyl)piperazin-1-yl)-N-(4-amino-4′-fluoro-[1,1′-biphenyl]-3-yl)pyrazine-2-carboxamide (21b).

^{1}H NMR (400 MHz, DMSO-d_6) δ 10.76 (s, 1H, -NH of indole), 9.67 (s, 1H, CO-NH-Ar), 8.72 (d, J = 1.3 Hz, 1H, Ar-H of Pyrazine), 8.37 (d, J = 1.3 Hz, 1H, Ar-H of Pyrazine), 7.77 (s, 1H, Ar-H), 7.60–7.48 (m, 3H, Ar-H), 7.32 (d, J = 8.0 Hz, 1H, Ar-H), 7.28–7.13 (m, 4H, Ar-H), 7.06–6.94 (m, 2H, Ar-H), 6.88 (d, J = 8.3 Hz, 1H, Ar-H), 5.02 (s, 2H, -NH$_2$),

3.84–3.68 (m, 4H, Piperazine Hs), 2.97–2.80 (m, 2H, -N-CH$_2$CH$_2$-Ar), 2.67–2.59 (m, 6H, -N-CH$_2$CH$_2$-Ar + Piperazine Hs). ^{13}C NMR (101 MHz, DMSO) δ 162.54, 160.29, 155.58, 142.52, 141.79, 137.28, 136.63, 133.05, 129.20, 128.34, 127.83, 124.93, 124.29, 123.19, 122.96, 121.27, 118.72, 118.58, 117.53, 116.04, 115.83, 112.90, 111.77, 59.14, 52.76, 44.49, 22.85.MS m/z: 536.16 [M + H]. HRMS m/z: 536.2573 [M + H]$^+$; calculated C$_{31}$H$_{31}$FN$_7$O $^+$: 536.2574. HPLC: rt 9.01 min (purity 96.3%), yield: 88%.

5-(4-(2-(1H-indol-3-yl)ethyl)piperazin-1-yl)-N-(4-amino-2′-fluoro-[1,1′-biphenyl]-3-yl)pyrazine-2-carboxamide (21c).
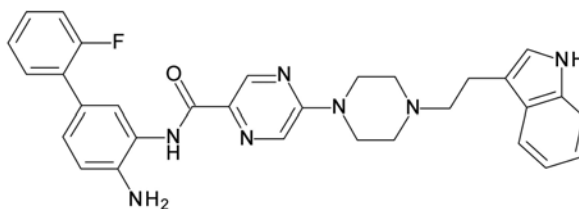
^{1} H NMR (400 MHz, DMSO-d$_6$) δ 10.76 (s, 1H, -NH of indole), 9.68 (s, 1H, CO-NH-Ar), 8.72 (s, 1H, Ar-H of Pyrazine), 8.37 (s, 1H, Ar-H of Pyrazine), 7.69 (s, 1H, Ar-H), 7.53–7.15 (m, 8H, Ar-H), 7.05 (t, J = 8 Hz, 1H, Ar-H), 6.96 (t, J = 8 Hz, 1H, Ar-H), 6.89 (d, J = 8.0 Hz, 1H, Ar-H), 5.09 (s, 2H, -NH$_2$), 3.77–3.73 (m, 4H, Piperazine Hs), 3.02–2.76 (m, 2H, -N-CH$_2$CH$_2$-Ar), 2.76–2.49 (m, 6H, -N-CH$_2$CH$_2$-Ar + Piperazine Hs). 13C NMR (101 MHz, DMSO) δ 162.57, 158.27, 155.57, 142.52, 142.17, 136.63, 133.06, 130.55, 130.51, 129.19, 127.67, 125.49, 125.22, 125.19, 124.45, 123.86, 122.95, 121.31, 118.72, 118.58, 116.99, 116.56, 116.33, 112.90, 111.77, 59.14, 52.76, 44.49, 22.85. MS m/z: 536.36 [M + H]. HRMS m/z: 558.2393 [M+Na]$^+$; calculated C$_{31}$H$_{30}$FN$_7$ONa$^+$: 558.2393. HPLC: rt 10.75 min (purity 96.4%), yield: 85%.

N-(2-Amino-4-fluorophenyl)-5-(piperazin-1-yl)pyrazine-2-carboxamide (23a).
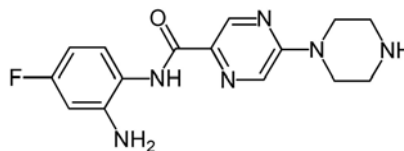
^{1} H NMR (400 MHz, DMSO-d$_6$) δ 9.51 (s, 1H, -CO-NH-Ar), 8.66 (d, J = 1.3 Hz, 1H, Ar-H of Pyrazine), 8.29 (d, J = 1.4 Hz, 1H, Ar-H of Pyrazine), 7.29 (dd, J = 8.7, 6.3 Hz, 1H, Ar-H), 6.56 (dd, J = 11.1, 2.9 Hz, 1H, Ar-H), 6.37 (td, J = 8.6, 2.9 Hz, 1H, Ar-H), 5.15 (s, 2H, -NH$_2$), 3.72–3.58 (m, 4H, Piperazine Hs), 3.29 (s, 1H, NH), 2.92–2.68 (m, 4H, Piperazine Hs). MS m/z: 315.46 [M − H]$^-$. ^{13}C NMR (101 MHz, DMSO) δ 162.75, 162.12, 159.74, 155.61, 144.93, 144.82, 142.46, 129.03, 127.33, 127.23, 120.33, 103.06, 102.84, 102.64, 102.39, 45.68, 45.53. HRMS m/z: 317.1525 [M + H]$^+$; calculated C$_{15}$H$_{18}$FN$_6$O$^+$: 317.1526. HPLC: rt 3.72 min (purity 97.9%), yield: 30%.

4-(5-((2-Amino-5-fluorophenyl)carbamoyl)pyrazin-2-yl)-1-((1-methyl-1H-indol-3-yl)methyl)piperazin-1-ium chloride (23b).
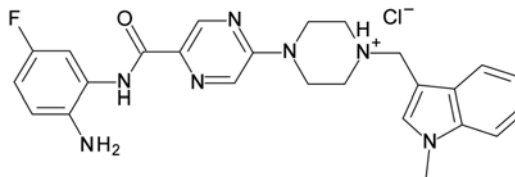
^{1} H NMR (400 MHz, DMSO-d$_6$) δ 11.22 (s, 1H, Piperazinium H), 10.27 (s, 1H, -CO-NH-Ar), 8.76 (d, J = 1.3 Hz, 1H, Ar-H of Pyrazine), 8.43 (d, J = 1.5 Hz, 1H, Ar-H of Pyrazine), 7.84 (dt, J = 7.9, 1.0 Hz, 1H, Ar-H), 7.63 (s, 1H, Ar-H), 7.55 (dd, J = 10.3, 2.9 Hz, 1H, Ar-H), 7.51–7.46 (m, 1H, Ar-H), 7.39–7.32 (m, 1H, Ar-H), 7.22 (ddd, J = 8.2, 7.0, 1.2 Hz, 1H, Ar-H),

7.14 (ddd, J = 8.0, 7.0, 1.0 Hz, 1H, Ar-H), 7.08 (td, J = 8.4, 3.0 Hz, 1H, Ar-H), 4.67 (d, J = 14.2 Hz, 2H, -N-CH$_2$-Indole), 4.50 (s, 2H, -NH$_2$), 3.82 (s, 3H, -N-CH$_3$), 3.49 (t, J = 12.3 Hz, 4H, Piperazine Hs), 3.36–2.93 (m, 4H, Piperazine Hs). HRMS m/z: 460.2260 [M + H]$^+$; calculated C$_{25}$H$_{27}$FN$_7$O$^+$: 460.2261. HPLC: rt 7.47 min (purity 96.7%), yield: 56%.

N-(2-Amino-5-fluorophenyl)-5-(4-(2-(1-methyl-1H-indol-3-yl)ethyl)piperazin-1-yl)pyrazine-2-carboxamide (23c).
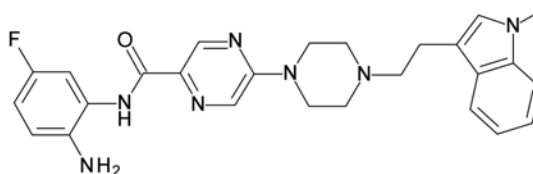
^{1}H NMR (400 MHz, DMSO-d$_6$) δ 9.72 (s, 1H, -CO-NH-Ar), 8.72 (d, J = 1.3 Hz, 1H, Ar-H of Pyrazine), 8.38 (d, J = 1.4 Hz, 1H, Ar-H of Pyrazine), 7.59 (dd, J = 10.8, 3.0 Hz, 1H, Ar-H), 7.53 (dt, J = 7.9, 1.0 Hz, 1H, Ar-H), 7.38–7.32 (m, 1H, Ar-H), 7.17–7.08 (m, 2H, Ar-H), 7.00 (ddd, J = 7.9, 7.0, 1.0 Hz, 1H, Ar-H), 6.83 (dd, J = 8.8, 5.9 Hz, 1H, Ar-H), 6.76 (td, J = 8.5, 3.0 Hz, 1H, Ar-H), 4.73 (s, 2H, -NH2), 3.79–3.74 (m, 4H, Piperazine Hs), 3.72 (s, 3H, -NCH$_3$), 2.88 (dd, J = 9.0, 6.6 Hz, 2H, -N-CH$_2$CH$_2$-Ar), 2.67–2.58 (m, 6H, -N-CH$_2$CH$_2$-Ar + Piperazine Hs). ^{13}C NMR (101 MHz, DMSO) δ 162.26, 142.59, 129.28, 127.42, 121.42, 120.29, 118.97, 118.68, 117.04, 109.94, 59.14, 52.74, 44.45, 32.66, 22.67. MS m/z: 472.56 [M − H]$^-$, 474.50 [M + H]$^+$, HRMS m/z: 474.2414 [M + H]$^+$; calculated C$_{26}$H$_{29}$FN$_7$O$^+$: 474.2417 HPLC: rt 7.44 min (purity 96.6%), yield: 68%.

N-(2-amino-4-chlorophenyl)-5-(piperazin-1-yl)pyrazine-2-carboxamide (25a).
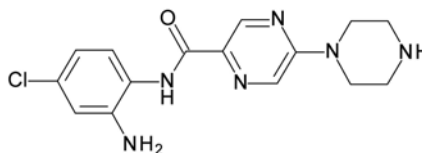
^{1}H NMR (400 MHz, DMSO-d$_6$) δ 9.57 (s, 1H, -CO-NH-Ar), 8.67 (d, J = 1.3 Hz, 1H, Ar-H of Pyrazine), 8.30 (d, J = 1.3 Hz, 1H, Ar-H of Pyrazine), 7.41 (d, J = 8.5 Hz, 1H, Ar-H), 6.83 (d, J = 2.4 Hz, 1H, Ar-H), 6.62 (dd, J = 8.5, 2.4 Hz, 1H, Ar-H), 5.15 (s, 2H, -NH$_2$), 3.65–3.60 (m, 4H, Piperazine Hs), 3.29 (s, 1H, Piperazine NH), 2.84–2.74 (m, 4H, Piperazine Hs). ^{13}C NMR (101 MHz, DMSO) δ 162.63, 155.63, 143.99, 142.55, 129.94, 129.04, 126.58, 123.36, 118.29, 116.55, 115.90, 45.75, 45.63. MS m/z: 333.34 [M + H] $^+$. HRMS m/z: 333.1230 [M + H]$^+$; calculated C$_{15}$H$_{18}$ClN$_6$O$^+$: 333.1230. HPLC: rt 4.77 min (purity 96.6%), yield: 90%.

N-(2-amino-4,5-difluorophenyl)-5-(piperazin-1-yl)pyrazine-2-carboxamide (25b).
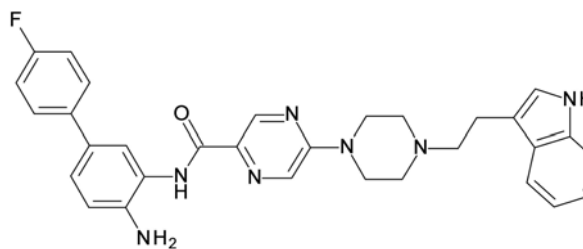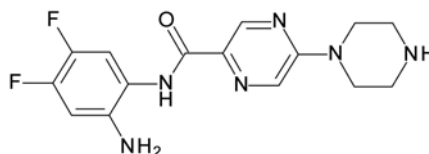

^{1}H NMR (400 MHz, DMSO-d$_6$) δ 9.62 (s, 1H, CO-NH-Ar), 8.67 (d, J = 1.3 Hz, 1H, Ar-H of Pyrazine), 8.30 (d, J = 1.3 Hz, 1H, Ar-H of Pyrazine), 7.55 (dd, J = 12.4, 8.7 Hz, 1H, Ar-H), 6.77 (dd, J = 12.8, 8.2 Hz, 1H, Ar-H), 5.02 (s, 2H, NH$_2$), 3.70–3.60 (m, 4H, Piperazine Hs), 3.30 (s, 1H, NH), 2.85–2.75 (m, 4H, Piperazine Hs). ^{13}C NMR (101 MHz, DMSO) δ 162.58, 155.66, 142.63, 139.28, 132.36, 129.09, 120.61, 113.28, 113.08, 104.62, 104.42, 45.68, 45.53. MS m/z: 335.60 [M + H]. HRMS m/z: 335.1430 [M + H]$^+$; calculated C$_{15}$H$_{17}$F$_2$N$_6$O $^+$: 335.1431. HPLC: rt 3.57 min (purity 95.6%), yield: 50%.

N-(2-amino-5-(trifluoromethyl)phenyl)-5-(piperazin-1-yl)pyrazine-2-carboxamide (27a).
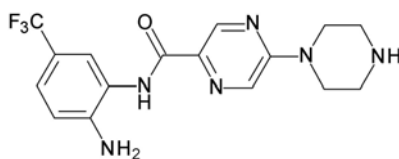
^{1} H NMR (400 MHz, DMSO-d$_6$) δ 9.65 (s, 1H, CO-NH-Ar), 8.68 (d, J = 1.2 Hz, 1H, Ar-H of Pyrazine), 8.31 (d, J = 1.0 Hz, 1H, Ar-H of Pyrazine), 7.73 (d, J = 1.9 Hz, 1H, Ar-H), 7.23 (d, J = 8.4 Hz, 1H, Ar-H), 6.89 (d, J = 8.2 Hz, 1H, Ar-H), 5.57 (s, 2H, NH2), 3.72–3.57 (m, 4H, Piperazine Hs), 3.35 (s, 1H, NH), 2.86–2.71 (m, 4H, Piperazine Hs). ^{13}C NMR (101 MHz, DMSO) δ 162.98, 155.64, 146.18, 142.66, 132.53, 129.05, 126.77, 124.08, 123.56, 123.20, 122.44, 116.18, 45.70, 45.57.MS m/z: 367.46 [M + H]. HRMS m/z: 367.1493 [M + H]$^+$; calculated C$_{16}$H$_{18}$F$_3$N$_6$O $^+$: 367.1494. HPLC: rt 7.16 min (purity 95.7%), yield: 80%.

N-(2-amino-4-methylphenyl)-5-(piperazin-1-yl)pyrazine-2-carboxamide (27b).
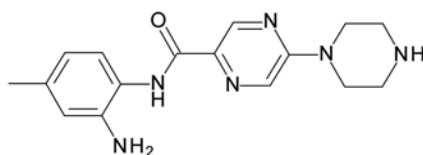
^{1} H NMR (400 MHz, DMSO-d$_6$) δ 9.48 (s, 1H, CO-NH-Ar), 8.66 (d, J = 1.3 Hz, 1H, Ar-H of Pyrazine), 8.29 (d, J = 1.2 Hz, 1H, Ar-H of Pyrazine), 7.29 (d, J = 8.0 Hz, 1H, Ar-H), 6.60 (s, 1H, Ar-H), 6.43 (d, J = 8.2 Hz, 1H, Ar-H), 4.74 (s, 2H, NH$_2$), 3.69–3.57 (m, 4H, Piperazine Hs), 3.22 (s, 1H, NH), 2.79–2.76 (m, 4H, Piperazine Hs), 2.16 (s, 3H, CH$_3$). ^{13}C NMR (101 MHz, DMSO) δ 162.32, 155.62, 142.36, 141.92, 135.04, 132.91, 129.03, 124.87, 122.24, 118.19, 117.60, 45.74, 45.61, 21.23.HRMS m/z: 313.1771 [M + H]$^+$; calculated C$_{16}$H$_{21}$N$_6$O$^+$: 313.1776. HPLC: rt 3.01 min (purity 98.2%), yield: 85%.

N-(2-amino-4-methoxyphenyl)-5-(piperazin-1-yl)pyrazine-2-carboxamide (27c).
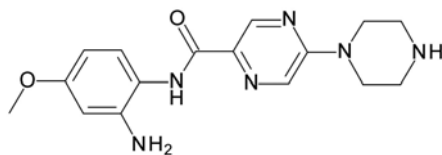
^{1} H NMR (400 MHz, DMSO-d$_6$) δ 9.41 (s, 1H, CO-NH-Ar), 8.65 (d, J = 1.2 Hz, 1H, Ar-H of Pyrazine), 8.28 (d, J = 1.2 Hz, 1H, Ar-H of Pyrazine), 7.20 (d, J = 8.7 Hz, 1H, Ar-H), 6.36 (d, J = 2.8 Hz, 1H, Ar-H), 6.19 (dd, J = 8.7, 2.8 Hz, 1H, Ar-H), 4.86 (s, 2H, NH$_2$), 3.68–3.55 (m, 7H, Piperazine Hs + OCH$_3$), 3.32 (s, 1H, NH), 2.87–2.68 (m, 4H, Piperazine Hs). ^{13}C NMR (101 MHz, DMSO) δ 162.51, 158.10, 155.59, 143.98, 142.31, 133.02, 129.01, 126.67, 117.62, 102.75, 101.90, 55.31, 45.70, 45.56. MS m/z: 329.38 [M + H]$^+$. HRMS m/z: 329.1725 [M + H]$^+$; calculated C$_{16}$H$_{21}$N$_6$O$_2$$^+$: 329.1725. HPLC: rt 3.14 min (purity 100%), yield: 82%.

N-(2-amino-5-(thiophen-3-yl)phenyl)-5-(4-methylpiperazin-1-yl)pyrazine-2-carboxamide (29a).
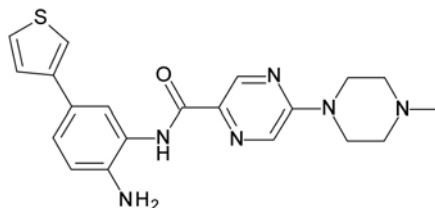
¹ H NMR (400 MHz, DMSO-d$_6$) δ 9.65 (s, 1H, CO-NH-Ar), 8.71 (d, J = 1.3 Hz, 1H, Ar-H of Pyrazine), 8.35 (d, J = 1.3 Hz, 1H, Ar-H of Pyrazine), 7.77 (d, J = 2.1 Hz, 1H, Ar-H), 7.57–7.51 (m, 2H, Ar-H), 7.39 (dd, J = 4.2, 2.3 Hz, 1H, Ar-H), 7.30 (dd, J = 8.3, 2.1 Hz, 1H, Ar-H), 6.83 (d, J = 8.3 Hz, 1H, Ar-H), 4.96 (s, 2H, NH2), 3.77–3.66 (m, 4H, Piperazine Hs), 2.46–2.36 (m, 4H, Piperazine Hs), 2.22 (s, 3H, CH$_3$). ¹³C NMR (101 MHz, DMSO) δ 162.52, 155.56, 142.47, 142.25, 141.65, 133.10, 129.21, 127.00, 126.25, 124.99, 124.70, 124.17, 123.04, 118.31, 117.34, 54.57, 46.16, 44.30. MS m/z: 395.20 [M + H]. HRMS m/z: 395.1652 [M + H]$^+$; calculated C$_{20}$H$_{23}$N$_6$OS $^+$: 395.1654. HPLC: rt 6.88 min (purity 100%), yield: 80%.

N-(2-Amino-5-(thiophen-2-yl)phenyl)-5-(piperazin-1-yl)pyrazine-2-carboxamide (29b).
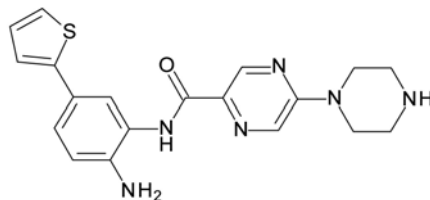
¹ H NMR (400 MHz, DMSO-d$_6$) δ 9.65 (s, 1H, -CO-NH-Ar), 8.70 (d, J = 1.3 Hz, 1H, Ar-H of Pyrazine), 8.32 (d, J = 1.4 Hz, 1H, Ar-H of Pyrazine), 7.78 (d, J = 2.2 Hz, 1H, Ar-H), 7.35 (dd, J = 5.1, 1.1 Hz, 1H, Ar-H), 7.27–7.21 (m, 2H, Ar-H), 7.04 (dd, J = 5.1, 3.6 Hz, 1H, Ar-H), 6.83 (d, J = 8.3 Hz, 1H, Ar-H), 5.07 (s, 2H, -NH$_2$), 3.72–3.60 (m, 4H, Piperazine Hs), 2.82–2.71 (m, 4H, Piperazine Hs). ¹³C NMR (101 MHz, dmso) δ 162.60, 155.62, 144.77, 142.55, 141.99, 132.76, 129.10, 128.63, 124.84, 123.82, 123.41, 122.23, 121.61, 117.40, 45.61, 45.42. MS m/z: 379.36 [M − H]$^-$, 381.39 [M + H]$^+$, HRMS m/z: 381.1494 [M + H]$^+$; calculated C$_{19}$H$_{21}$N$_6$OS$^+$: 381.1497. HPLC: rt 7.20 min (purity 98.5%), yield: 76%.

N-(4-amino-4′-fluoro-[1,1′-biphenyl]-3-yl)-5-(piperazin-1-yl)pyrazine-2-carbox- amide (29c).
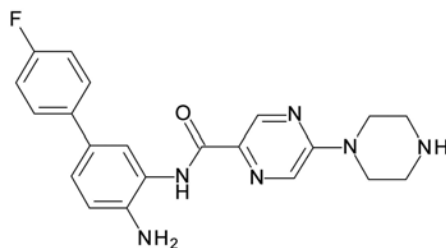
¹ H NMR (400 MHz, DMSO-d$_6$) δ 9.65 (s, 1H, CO-NH-Ar), 8.70 (d, J = 1.3 Hz, 1H, Ar-H of Pyrazine), 8.32 (d, J = 1.2 Hz, 1H, Ar-H of Pyrazine), 7.77 (s, 1H, Ar-H), 7.58–7.53 (m, 2H, Ar-H), 7.25–7.17 (m, 3H, Ar-H), 6.87 (d, J = 8.3 Hz, 1H, Ar-H), 5.02 (s, 2H, NH$_2$), 3.71–3.59 (m, 4H, Piperazine Hs), 3.27 (s, 1H, NH), 2.86–2.74 (m, 4H, Piperazine Hs). ¹³C NMR (101 MHz, DMSO) δ 162.56, 160.29, 155.64, 142.52, 141.75, 137.29, 132.76, 129.08, 128.35, 127.90, 124.96, 124.25, 123.13, 117.54, 116.07, 45.69, 45.54. MS m/z: 393.47 [M + H]$^+$. HRMS m/z: 393.1837 [M + H]$^+$; calculated C$_{21}$H$_{22}$FN$_6$O$^+$: 393.1839. HPLC: rt 7.07 min (purity 99.6%), yield: 88%.

N-(4-amino-2′-fluoro-[1,1′-biphenyl]-3-yl)-5-(4-methylpiperazin-1-yl)pyrazine-2-carboxamide (29d).
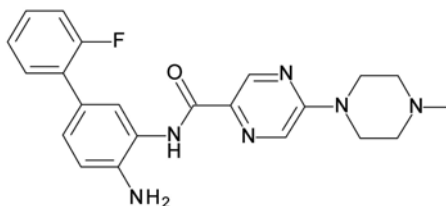
^{1} H NMR (400 MHz, DMSO-d$_6$) δ 9.67 (s, 1H, CO-NH-Ar), 8.70 (s, 1H, Ar-H of Pyrazine), 8.35 (s, 1H, Ar-H of Pyrazine), 7.68 (s, 1H, Ar-H), 7.44 (td, J = 7.9, 1.7 Hz, 1H, Ar-H), 7.34–7.11 (m, 4H, Ar-H), 6.88 (d, J = 8.3 Hz, 1H, Ar-H), 5.09 (s, 2H, NH$_2$), 3.77–3.65 (m, 4H, Piperazine Hs), 2.64–2.35 (m, 4H, Piperazine Hs), 2.21 (s, 3H, CH$_3$). ^{13}C NMR (101 MHz, DMSO) δ 162.55, 160.70, 158.27, 155.56, 142.49, 142.18, 133.08, 130.55, 129.19, 126.63, 125.50, 125.19, 124.44, 123.85, 116.99, 116.56, 116.33, 54.57, 46.15, 44.30. HRMS m/z: 407.1992 [M + H]$^+$; calculated C$_{22}$H$_{24}$FN$_6$O$^+$: 407.1995. HPLC: rt 7.44 min (purity 97.9%), yield: 85%.

4.2. Biological Evaluation

4.2.1. In Vitro HDAC Inhibition Assay

Recombinant human HDAC1, HDAC2, and HDAC3/NCOR1 were purchased from ENZO Life Sciences AG (Lausen, CH). Recombinant human HDAC 4, HDAC5, HDAC7, HDAC9 and HDAC11 were produced by Barinka lab in Prague, as described before [43,54]. Recombinant human HDAC8 was produced by Romier et al. (IGBMC, Univ. Strasbourg), as described in [55].

The in vitro testing on recombinant HDACs 1-3 were performed with a fluorogenic peptide derived from p53 (Ac-RHKK(Acetyl)-AMC). The measurements were performed in an assay buffer (50 mM Hepes, 150 mM NaCl, 5 mM MgCl$_2$, 1 mM TCEP and 0.2 mg/mL BSA, pH 7.4 adjusted with NaOH) at 37 °C. Inhibitors at different concentrations were incubated with 10 nM HDAC1, 3 nM HDAC2 or 3 nM HDAC3 (final concentration) for at least 5 min. The reaction was started with the addition of the fluorogenic substrate (20 μM final concentration) and incubated for 30 min for HDAC2 and HDAC3 and 90 min for HDAC1. The reaction was stopped with a solution of 1 mg/mL trypsin and 20 μM SAHA in 1 mM HCl and incubated for 1 h at 37 °C. The fluorescence intensity was recorded with an Envision 2104 Multilabel Plate Reader (PerkinElmer, Waltham, MA, USA) with an excitation wavelength of 380 ± 8 nm and an emission wavelength of 430 ± 8 nm. The received fluorescence intensities were normalized with uninhibited reaction as 100% and the reaction without enzyme as 0%. A nonlinear regression analysis was done to determine the IC50 value.

The determination of dose response curves for HDAC4, 5, 7 and 9 was performed as previously described [43] with compound 4 as substrate (Abz-SRGGK(thio-TFA)FFRR-NH2). The substrate concentration was 50 μM and the enzyme concentration was 10 nM for HDAC4 and HDAC5, 5 nM for HDAC7 and 20 nM for HDAC9. HDAC11 inhibition assay was performed as described before [56]. The fluorescence intensity was recorded with an Envision 2104 Multilabel Plate Reader (PerkinElmer, Waltham, MA) with an excitation wavelength of 330 ± 75 nm and an emission wavelength of 430 ± 8 nm.

The enzyme inhibition of HDAC8 was determined by using a reported homogenous fluorescence assay 2 [57], The enzymes were incubated for 90 min at 37 °C, with the fluorogenic substrate ZMAL (Z (Ac)Lys-AMC) in a concentration of 10.5 μM and increasing concentrations of inhibitors. Fluorescence intensity was measured at an excitation wavelength of 390 nm and an emission wavelength of 460 nm in a microtiter plate reader (BMG Polarstar).

4.2.2. Cellular Assay

To determine the cytotoxicity of the developed compounds on the human epithelial kidney, cell line HEK293 was used. HEK293 cells (DSMZ Braunschweig, ACC305) were incubated at 37 °C in a humidified incubator with 5% CO$_2$ in Dulbecco's Modified Eagle Medium (DMEM) supplemented with 10% FCS and 5 mM glutamine. Cells were seeded out at 1.5 x 103 cells per well in a 96-well cell culture plate (TPP, Switzerland). The compounds to be tested were added immediately to the medium at 50 μM. After 24 h, Alamar Blue reagent (Invitrogen, CA) was added according to the manufacturer's instructions and incubated again for 21 h before samples were analyzed. Detection of viable cells which convert the resazurine reagent into the highly fluorescent resorufin was performed by

using a FLUOstarOPTIMA microplate reader (BMG Labtec) with the following filter set: Ex 530 nm/Em 590 nm. Measurements were performed in triplicate and data are means with standard deviation <12%. Daunorubicin was used as a positive control and an IC50 value of 12.55 ± 0.07 μM was measured.

All leukemic cells were kept in RPMI-1640 medium supplemented with 10% FBS and 1%penicillin/streptomycin (Sigma-Aldrich, Taufkirchen, Germany) under standard culture conditions at 37 °C and a 5% CO_2 humidified atmosphere. Cells were authenticated as mentioned by us [51].

4.3. Computational Studies

Protein structures were retrieved from the Protein Data bank (PDB) (PDB ID: 4BKX, 4LY1. 4A69) [58]. The HDAC1 (PDB ID: 4BKX) in apo-form and HDAC3 (PDB ID: 4A69) in apo-form were minimized with the ligand of HDAC2 (PDB ID: 4LY1) and BG-45 molecules [59], respectively. All protein structures were prepared using the Protein Preparation Wizard module in Schrödinger Suite [60]. Hydrogen atoms and missing side chains were added. With the exception of a conserved water molecule bound to a conserved histidine in HDAC1, 2 and 3, all water molecules were removed from the X-ray structures. The protonation states and tautomeric forms of the amino acids were optimized using PROPKA tool at pH 7.0. The potential energy of the three optimized structures was minimized using OPLS3e force-field [61]. Ligands were prepared using the LigPrep module in Schrödinger Suite using OPLS3e force-field. Conformations of prepared ligands were generated using the Confgen tool in Schrödinger Suite by applying 64 conformers per each ligand and minimizing the conformers. Molecular docking studies were conducted by applying the Glide program in Schrödinger Suite. The grid box was generated with 10*10*10 Å size using the Receptor Grid Generation module in Schödinger19. Standard Precision (SP) mode with flexible ligand sampling was utilized for docking. To validate the docking protocol, re-docking studies were done. The RMSD values of the re-docking studies corresponding to the binding mode in HDAC1, HDAC2 and HDAC3 are observed as 0.17, 0.29, 0.28 Å, respectively. Docking poses were visualized in the MOE2018.01 program [62].

Molecular dynamics (MD) simulations were carried out using Amber18 [63]. MD systems were generated using the obtained docking poses of 19f, 21a, 23a, and 29b. First, the antechamber module was used to prepare the topologies and force field parameters of the ligands using the general Amber Force Field (GAFF) [63] and AM1-BCC as the atomic charges method semi empirical (AM1), and bond charge correction (BCC) [64,65]. Then, MD systems were generated using the TLeaP package and the ff03 force field for protein and GAFF for the ligands. The systems were solvated with the TIP3P solvation model. The octahedral box was generated with 10 Å. The prepared systems were used to run MD simulation. The simulation protocol includes different steps. Initially, two minimization steps were carried out. In each step, 4000 iterations, including the first 3000 steepest descent and 1000 conjugate gradient, were subjected to the MD systems. First, only solvent atoms were minimized in the first minimization step, while protein and ligand atoms were kept in their initial coordinates with a force constant of 10 kcal mol -1Å -1. Then, in the second minimization, the whole system, including the protein and ligand, were minimized. Subsequently, the system was heated from 0 K to 300 K through 100 ps MD. The complex atoms were again restrained with a force constant of 10 kcal mol -1Å -1 to prevent the large structural deviation. Next, the density was evaluated during 100ps MD. Afterwards, the systems were equilibrated through 200 ps MD before the MD step. The SHAKE algorithm was used to restrain all bonds involving hydrogens [66]. Temperature was controlled by Langevin Dynamics using a collision frequency of 2 ps-1 and pressure of 1 bar. In the MD step, 100 ns MD simulation were performed for each system. The trajectories were analyzed using the CPPTRAJ module and VMD [67].

4.4. PAINS Filter

All the herein described compounds were filtered for pan-assay interference compounds (PAINS) [68]. For this purpose, PAINS1, PAINS2 and PAINS3 filters, as implemented in Schrödinger's Canvas program, were employed. None of the compounds were flagged as a PAIN.

4.5. In Silico Prediction of Pharmacokinetic and Tox Data

For the in silico prediction the PreADMET web application was used (https://preadmet.bmdrc.kr/admetox/ accessed date 10 November 2021). The PreADMET approach is based on different classes of molecular descriptors that are considered for generating the quantitative structure property relationship or binary classification models. The following properties were calculated: human intestinal absorption (% HIA) [69], plasma protein binding, water solubility, AlogP classification models which were used to predict the inhibition of several cytochromes, hERG and para-glycoprotein (p-gp). To predict the human toxicity the ProTox-II approach [70] which is available as web service (https://tox-new.charite.de/protox_II/ accessed date 10 November 2021) was used. ProTox-II uses molecular similarity, fragment propensities, most frequent features and (fragment similarity based cross-validation) machine-learning, based on a total of 33 models for the prediction of various toxicity endpoints, such as acute toxicity, hepatotoxicity, cytotoxicity, carcinogenicity, mutagenicity, immunotoxicity, adverse outcomes (Tox21) pathways and toxicity targets.

References

1. Yoo, C.B.; Jones, P.A. Epigenetic therapy of cancer: Past, present and future. *Nat. Rev. Drug Discov.* **2006**, *5*, 37–50. [CrossRef] [PubMed]
2. Sadakierska-Chudy, A.; Filip, M. A comprehensive view of the epigenetic landscape. Part II: Histone post-translational modification, nucleosome level, and chromatin regulation by ncRNAs. *Neurotox. Res.* **2015**, *27*, 172–197. [CrossRef] [PubMed]
3. Fan, J.; Krautkramer, K.A.; Feldman, J.L.; Denu, J.M. Metabolic regulation of histone post-translational modifications. *ACS Chem. Biol.* **2015**, *10*, 95–108. [CrossRef] [PubMed]
4. Chadha, S.; Wang, L.; Hancock, W.W.; Beier, U.H. Sirtuin-1 in immunotherapy: A Janus-headed target. *J. Leukoc. Biol.* **2019**, *106*, 337–343. [CrossRef]
5. Pant, K.; Peixoto, E.; Richard, S.; Gradilone, S.A. Role of Histone Deacetylases in Carcinogenesis: Potential Role in Cholangiocarcinoma. *Cells* **2020**, *9*, 780. [CrossRef]
6. Fraga, M.F.; Ballestar, E.; Villar-Garea, A.; Boix-Chornet, M.; Espada, J.; Schotta, G.; Bonaldi, T.; Haydon, C.; Ropero, S.; Petrie, K.; et al. Loss of acetylation at Lys16 and trimethylation at Lys20 of histone H4 is a common hallmark of human cancer. *Nat. Genet.* **2005**, *37*, 391–400. [CrossRef]
7. Gryder, B.E.; Sodji, Q.H.; Oyelere, A.K. Targeted cancer therapy: Giving histone deacetylase inhibitors all they need to succeed. *Future Med. Chem.* **2012**, *4*, 505–524. [CrossRef]
8. Cappellacci, L.; Perinelli, D.R.; Maggi, F.; Grifantini, M.; Petrelli, R. Recent progress in histone deacetylase inhibitors as anticancer agents. *Curr. Med. Chem.* **2020**, *27*, 2449–2493. [CrossRef]
9. Wagner, F.F.; Weïwer, M.; Lewis, M.C.; Holson, E.B. Small molecule inhibitors of zinc-dependent histone deacetylases. *Neurotherapeutics* **2013**, *10*, 589–604. [CrossRef]
10. Mann, B.S.; Johnson, J.R.; Cohen, M.H.; Justice, R.; Pazdur, R. FDA approval summary: Vorinostat for treatment of advanced primary cutaneous T-cell lymphoma. *Oncologist* **2007**, *12*, 1247–1252. [CrossRef]
11. Chien, W.; Lee, D.H.; Zheng, Y.; Wuensche, P.; Alvarez, R.; Wen, D.L.; Aribi, A.M.; Thean, S.M.; Doan, N.B.; Said, J.W. Growth inhibition of pancreatic cancer cells by histone deacetylase inhibitor belinostat through suppression of multiple pathways including HIF, NFkB, and mTOR signaling in vitro and in vivo. *Mol. Carcinog.* **2014**, *53*, 722–735. [CrossRef]
12. Sivaraj, D.; Green, M.M.; Gasparetto, C. Panobinostat for the management of multiple myeloma. *Future Oncol.* **2017**, *13*, 477–488. [CrossRef]
13. Arrowsmith, C.H.; Bountra, C.; Fish, P.V.; Lee, K.; Schapira, M. Epigenetic protein families: A new frontier for drug discovery. *Nat. Rev. Drug Discov.* **2012**, *11*, 384–400. [CrossRef]
14. Chifotides, H.T.; Bose, P.; Verstovsek, S. Givinostat: An emerging treatment for polycythemia vera. *Expert Opin. Investig. Drugs* **2020**, *29*, 525–536. [CrossRef]
15. Weichert, W.; Röske, A.; Gekeler, V.; Beckers, T.; Stephan, C.; Jung, K.; Fritzsche, F.R.; Niesporek, S.; Denkert, C.; Dietel, M.; et al. Histone deacetylases 1, 2 and 3 are highly expressed in prostate cancer and HDAC2 expression is associated with shorter PSA relapse time after radical prostatectomy. *Br. J. Cancer* **2008**, *98*, 604–610. [CrossRef]
16. Li, Y.; Seto, E. HDACs and HDAC Inhibitors in Cancer Development and Therapy. *Cold Spring Harb. Perspect. Med.* **2016**, *6*, a026831. [CrossRef]
17. Fritzsche, F.R.; Weichert, W.; Röske, A.; Gekeler, V.; Beckers, T.; Stephan, C.; Jung, K.; Scholman, K.; Denkert, C.; Dietel, M.; et al. Class I histone deacetylases 1, 2 and 3 are highly expressed in renal cell cancer. *BMC Cancer* **2008**, *8*, 381. [CrossRef]
18. Stypula-Cyrus, Y.; Damania, D.; Kunte, D.P.; Cruz, M.D.; Subramanian, H.; Roy, H.K.; Backman, V. HDAC up-regulation in early colon field carcinogenesis is involved in cell tumorigenicity through regulation of chromatin structure. *PLoS ONE* **2013**, *8*, e64600. [CrossRef]
19. Cao, L.-L.; Yue, Z.; Liu, L.; Pei, L.; Yin, Y.; Qin, L.; Zhao, J.; Liu, H.; Wang, H.; Jia, M. The expression of histone deacetylase HDAC1 correlates with the progression and prognosis of gastrointestinal malignancy. *Oncotarget* **2017**, *8*, 39241–39253. [CrossRef]
20. Azad, N.S.; el-Khoueiry, A.; Yin, J.; Oberg, A.L.; Flynn, P.; Adkins, D.; Sharma, A.; Weisenberger, D.J.; Brown, T.; Medvari, P.; et al. Combination epigenetic therapy in metastatic colorectal cancer (mCRC) with subcutaneous 5-azacitidine and entinostat: A phase 2 consortium/stand Up 2 cancer study. *Oncotarget* **2017**, *8*, 35326–35338. [CrossRef]
21. Lee, B.C.; Yvette, K.; Bociek, R.G.; Peter, L.; Lia, G.; Amanda, C.; Rachel, S.; Peter, O.; Scott, C.; Lori, K.; et al. ENGAGE- 501: Phase II study of entinostat (SNDX-275) in relapsed and refractory Hodgkin lymphoma. *Haematologica* **2016**, *101*, 968–975.
22. Batlevi, C.L.; Crump, M.; Andreadis, C.; Rizzieri, D.; Assouline, S.E.; Fox, S.; van der Jagt, R.H.C.; Copeland, A.; Potvin, D.; Chao, R.; et al. A phase 2 study of mocetinostat, a histone deacetylase inhibitor, in relapsed or refractory lymphoma. *Br. J. Haematol.* **2017**, *178*, 434–441. [CrossRef] [PubMed]
23. Muller, S.; Kramer, O.H. Inhibitors of HDACs–Effective Drugs Against Cancer? *Curr. Cancer Drug Targets* **2010**, *10*, 210–228. [CrossRef] [PubMed]
24. Ungerstedt, J.S. Epigenetic Modifiers in Myeloid Malignancies: The Role of Histone Deacetylase Inhibitors. *Int. J. Mol. Sci.* **2018**, *19*, 3091. [CrossRef]
25. Gryder, B.E.; Wu, L.; Woldemichael, G.M.; Pomella, S.; Quinn, T.R.; Park, P.M.C.; Cleveland, A.; Stanton, B.Z.; Song, Y.; Rota, R.; et al. Chemical genomics reveals histone deacetylases are required for core regulatory transcription. *Nat. Commun.* **2019**, *10*, 3004–3004. [CrossRef]

26. Zhang, L.; Zhang, J.; Jiang, Q.; Zhang, L.; Song, W. Zinc binding groups for histone deacetylase inhibitors. *J. Enzym. Inhib. Med. Chem.* **2018**, *33*, 714–721. [CrossRef]

27. Micelli, C.; Rastelli, G. Histone deacetylases: Structural determinants of inhibitor selectivity. *Drug Discov. Today* **2015**, *20*, 718–735. [CrossRef]

28. Zhan, P.; Itoh, Y.; Suzuki, T.; Liu, X. Strategies for the discovery of target-specific or isoform-selective modulators. *J. Med. Chem.* **2015**, *58*, 7611–7633. [CrossRef]

29. Perrin, J.; Werner, T.; Kurzawa, N.; Rutkowska, A.; Childs, D.D.; Kalxdorf, M.; Poeckel, D.; Stonehouse, E.; Strohmer, K.; Heller, B.; et al. Identifying drug targets in tissues and whole blood with thermal-shift profiling. *Nat. Biotechnol.* **2020**, *38*, 303–308. [CrossRef]

30. Becher, I.; Werner, T.; Doce, C.; Zaal, E.A.; Tögel, I.; Khan, C.A.; Rueger, A.; Muelbaier, M.; Salzer, E.; Berkers, C.R.; et al. Thermal profiling reveals phenylalanine hydroxylase as an off-target of panobinostat. *Nat. Chem. Biol.* **2016**, *12*, 908–910. [CrossRef]

31. Shen, S.; Kozikowski, A.P. Why Hydroxamates May Not Be the Best Histone Deacetylase Inhibitors—What Some May Have Forgotten or Would Rather Forget? *ChemMedChem* **2016**, *11*, 15–21. [CrossRef]

32. Lee, S.J.; Choi, S.-E.; Lee, H.B.; Song, M.-W.; Kim, Y.H.; Jeong, J.Y.; Kang, Y.; Kim, H.J.; Kim, T.H.; Jeon, J.Y.; et al. A Class I Histone Deacetylase Inhibitor Attenuates Insulin Resistance and Inflammation in Palmitate-Treated C2C12 Myotubes and Muscle of HF/HFr Diet Mice. *Front. Pharmacol.* **2020**, *11*, 601448. [CrossRef]

33. Cai, J.; Wei, H.; Hong, K.H.; Wu, X.; Cao, M.; Zong, X.; Li, L.; Sun, C.; Chen, J.; Ji, M. Discovery and preliminary evaluation of 2-aminobenzamide and hydroxamate derivatives containing 1, 2, 4-oxadiazole moiety as potent histone deacetylase inhibitors. *Eur. J. Med. Chem.* **2015**, *96*, 1–13. [CrossRef]

34. Ning, Z.Q.; Li, Z.B.; Newman, M.J.; Shan, S.; Wang, X.H.; Pan, D.S.; Zhang, J.; Dong, M.; Du, X.; Lu, X.P. Chidamide (CS055/HBI-8000): A new histone deacetylase inhibitor of the benzamide class with antitumor activity and the ability to enhance immune cell-mediated tumor cell cytotoxicity. *Cancer Chemother. Pharmacol.* **2012**, *69*, 901–909. [CrossRef]

35. Pan, D.-S.; Yang, Q.-J.; Fu, X.; Shan, S.; Zhu, J.-Z.; Zhang, K.; Li, Z.-B.; Ning, Z.-Q.; Lu, X.-P. Discovery of an orally active subtype-selective HDAC inhibitor, chidamide, as an epigenetic modulator for cancer treatment. *MedChemComm* **2014**, *5*, 1789–1796. [CrossRef]

36. Wagner, F.F.; Lundh, M.; Kaya, T.; McCarren, P.; Zhang, Y.L.; Chattopadhyay, S.; Gale, J.P.; Galbo, T.; Fisher, S.L.; Meier, B.C.; et al. An Isochemogenic Set of Inhibitors To Define the Therapeutic Potential of Histone Deacetylases in beta-Cell Protection. *ACS Chem. Biol.* **2016**, *11*, 363–374. [CrossRef]

37. Weïwer, M.; Lewis, M.C.; Wagner, F.F.; Holson, E.B. Therapeutic potential of isoform selective HDAC inhibitors for the treatment of schizophrenia. *Future Med. Chem.* **2013**, *5*, 1491–1508. [CrossRef]

38. Tang, D.; Xu, L.; Zhang, M.; Dorfman, R.G.; Pan, Y.; Zhou, Q.; Zhou, L.; Wang, Y.; Li, Y.; Yin, Y.; et al. Metformin facilitates BG45-induced apoptosis via an anti-Warburg effect in cholangiocarcinoma cells. *Oncol. Rep.* **2018**, *39*, 1957–1965. [CrossRef]

39. Liu, J.; Yu, Y.; Kelly, J.; Sha, D.; Alhassan, A.-B.; Yu, W.; Maletic, M.M.; Duffy, J.L.; Klein, D.J.; Holloway, M.K.; et al. Discovery of Highly Selective and Potent HDAC3 Inhibitors Based on a 2-Substituted Benzamide Zinc Binding Group. *ACS Med. Chem. Lett.* **2020**, *11*, 2476–2483. [CrossRef]

40. Moradei, O.M.; Mallais, T.C.; Frechette, S.; Paquin, I.; Tessier, P.E.; Leit, S.M.; Fournel, M.; Bonfils, C.; Trachy-Bourget, M.-C.; Liu, J. Novel aminophenyl benzamide-type histone deacetylase inhibitors with enhanced potency and selectivity. *J. Med. Chem.* **2007**, *50*, 5543–5546. [CrossRef]

41. Wagner, F.F.; Weiwer, M.; Steinbacher, S.; Schomburg, A.; Reinemer, P.; Gale, J.P.; Campbell, A.J.; Fisher, S.L.; Zhao, W.N.; Reis, S.A.; et al. Kinetic and structural insights into the binding of histone deacetylase 1 and 2 (HDAC1, 2) inhibitors. *Bioorg. Med. Chem.* **2016**, *24*, 4008–4015. [CrossRef] [PubMed]

42. Arts, J.; King, P.; Mariën, A.; Floren, W.; Beliën, A.; Janssen, L.; Pilatte, I.; Roux, B.; Decrane, L.; Gilissen, R.; et al. JNJ-26481585, a Novel "Second-Generation" Oral Histone Deacetylase Inhibitor, Shows Broad-Spectrum Preclinical Antitumoral Activity. *Clin. Cancer Res.* **2009**, *15*, 6841–6851. [CrossRef] [PubMed]

43. Zessin, M.; Kutil, Z.; Meleshin, M.; Nováková, Z.; Ghazy, E.; Kalbas, D.; Marek, M.; Romier, C.; Sippl, W.; Bařinka, C.; et al. One-Atom Substitution Enables Direct and Continuous Monitoring of Histone Deacylase Activity. *Biochemistry* **2019**, *58*, 4777–4789. [CrossRef] [PubMed]

44. Lauffer, B.E.L.; Mintzer, R.; Fong, R.; Mukund, S.; Tam, C.; Zilberleyb, I.; Flicke, B.; Ritscher, A.; Fedorowicz, G.; Vallero, R.; et al. Histone Deacetylase (HDAC) Inhibitor Kinetic Rate Constants Correlate with Cellular Histone Acetylation but not Transcription and Cell Viability. *J. Biol. Chem.* **2013**, *288*, 26926–26943. [CrossRef]

45. Cao, F.; Zwinderman, M.R.H.; Dekker, F.J. The Process and Strategy for Developing Selective Histone Deacetylase 3 Inhibitors. *Molecules* **2018**, *23*, 551. [CrossRef]

46. Yan, B.; Chen, Q.; Shimada, K.; Tang, M.; Li, H.; Gurumurthy, A.; Khoury, J.D.; Xu, B.; Huang, S.; Qiu, Y. Histone deacetylase inhibitor targets CD123/CD47-positive cells and reverse chemoresistance phenotype in acute myeloid leukemia. *Leukemia* **2019**, *33*, 931–944. [CrossRef]

47. Mori, M.; Kaneko, N.; Ueno, Y.; Yamada, M.; Tanaka, R.; Saito, R.; Shimada, I.; Mori, K.; Kuromitsu, S. Gilteritinib, a FLT3/AXL inhibitor, shows antileukemic activity in mouse models of FLT3 mutated acute myeloid leukemia. *Investig. New Drugs* **2017**, *35*, 556–565. [CrossRef]

48. Schlenk, R.F.; Kayser, S. Midostaurin: A Multiple Tyrosine Kinases Inhibitor in Acute Myeloid Leukemia and Systemic Mastocytosis. In *Small Molecules in Hematology*; Martens, U.M., Ed.; Springer International Publishing: Cham, Switzerland, 2018; pp. 199–214.

49. Cioccio, J.; Claxton, D. Therapy of acute myeloid leukemia: Therapeutic targeting of tyrosine kinases. *Expert Opin. Investig. Drugs* **2019**, *28*, 337–349. [CrossRef]

50. Beyer, M.; Henninger, S.J.; Haehnel, P.S.; Mustafa, A.-H.M.; Gurdal, E.; Schubert, B.; Christmann, M.; Sellmer, A.; Mahboobi, S.; Drube, S.; et al. Identification of a highly efficient dual type I/II FMS-like tyrosine kinase inhibitor that disrupts the growth of leukemic cells. *Cell Chem. Biol.* **2021**, *29*, 1–14. [CrossRef]

51. Beyer, M.; Romanski, A.; Mustafa, A.-H.M.; Pons, M.; Büchler, I.; Vogel, A.; Pautz, A.; Sellmer, A.; Schneider, G.; Bug, G.; et al. HDAC3 Activity is Essential for Human Leukemic Cell Growth and the Expression of β-catenin, MYC, and WT1. *Cancers* **2019**, *11*, 1436. [CrossRef]

52. Kiweler, N.; Wünsch, D.; Wirth, M.; Mahendrarajah, N.; Schneider, G.; Stauber, R.H.; Brenner, W.; Butter, F.; Krämer, O.H. Histone deacetylase inhibitors dysregulate DNA repair proteins and antagonize metastasis-associated processes. *J. Cancer Res. Clin. Oncol.* **2020**, *146*, 343–356. [CrossRef]

53. Padrnos, L.; Mesa, R. Novel agents for the treatment of polycythemia vera: An insight into preclinical research and early phase clinical trials. *Expert Opin. Investig. Drugs* **2020**, *29*, 809–817. [CrossRef]

54. Kutil, Z.; Novakova, Z.; Meleshin, M.; Mikesova, J.; Schutkowski, M.; Barinka, C. Histone Deacetylase 11 Is a Fatty-Acid Deacylase. *ACS Chem. Biol.* **2018**, *13*, 685–693. [CrossRef]

55. Marek, M.; Shaik, T.B.; Heimburg, T.; Chakrabarti, A.; Lancelot, J.; Ramos-Morales, E.; Da Veiga, C.; Kalinin, D.; Melesina, J.; Robaa, D.; et al. Characterization of Histone Deacetylase 8 (HDAC8) Selective Inhibition Reveals Specific Active Site Structural and Functional Determinants. *J. Med. Chem.* **2018**, *61*, 10000–10016. [CrossRef]

56. Kutil, Z.; Mikešová, J.; Zessin, M.; Meleshin, M.; Nováková, Z.; Alquicer, G.; Kozikowski, A.; Sippl, W.; Bařinka, C.; Schutkowski, M. Continuous Activity Assay for HDAC11 Enabling Reevaluation of HDAC Inhibitors. *ACS Omega* **2019**, *4*, 19895–19904. [CrossRef]

57. Heimburg, T.; Kolbinger, F.R.; Zeyen, P.; Ghazy, E.; Herp, D.; Schmidtkunz, K.; Melesina, J.; Shaik, T.B.; Erdmann, F.; Schmidt, M.; et al. Structure-Based Design and Biological Characterization of Selective Histone Deacetylase 8 (HDAC8) Inhibitors with Anti-Neuroblastoma Activity. *J. Med. Chem.* **2017**, *60*, 10188–10204. [CrossRef]

58. Berman, H.M.; Westbrook, J.; Feng, Z.; Gilliland, G.; Bhat, T.N.; Weissig, H.; Shindyalov, I.N.; Bourne, P.E. The protein data bank. *Nucleic Acids Res.* **2000**, *28*, 235–242. [CrossRef]

59. Minami, J.; Suzuki, R.; Mazitschek, R.; Gorgun, G.; Ghosh, B.; Cirstea, D.; Hu, Y.; Mimura, N.; Ohguchi, H.; Cottini, F. Histone deacetylase 3 as a novel therapeutic target in multiple myeloma. *Leukemia* **2014**, *28*, 680–689. [CrossRef]

60. *Schrödinger Release 2019-1: Maestro, Protein Preparation Wizard, Prime, Epik, Ligprep, Confgen, Glide*; Schrödinger LLC.: New York, NY, USA, 2019.

61. Harder, E.; Damm, W.; Maple, J.; Wu, C.; Reboul, M.; Xiang, J.Y.; Wang, L.; Lupyan, D.; Dahlgren, M.K.; Knight, J.L. OPLS3: A force field providing broad coverage of drug-like small molecules and proteins. *J. Chem. Theory Comput.* **2016**, *12*, 281–296. [CrossRef]

62. *Molecular Operating Environment (MOE), 2019.01*; Chemical Computing Group: Montreal, QC, Canada, 2019.

63. Case, D.; Betz, R.; Cerutti, D.; Cheatham, T., III; Darden, T.; Duke, R.; Giese, T.; Gohlke, H.; Goetz, A.; Homeyer, N.; et al. *AMBER 2016*; University of California: San Francisco, CA, USA, 2016.

64. Jakalian, A.; Bush, B.L.; Jack, D.B.; Bayly, C.I. Fast, efficient generation of high-quality atomic charges. AM1-BCC model: I. Method. *J. Comput. Chem.* **2000**, *21*, 132–146. [CrossRef]

65. Jakalian, A.; Jack, D.B.; Bayly, C.I. Fast, efficient generation of high-quality atomic charges. AM1-BCC model: II. Parameterization and validation. *J. Comput. Chem.* **2002**, *23*, 1623–1641. [CrossRef]

66. Ryckaert, J.-P.; Ciccotti, G.; Berendsen, H.J. Numerical integration of the cartesian equations of motion of a system with constraints: Molecular dynamics of n-alkanes. *J. Comput. Phys.* **1977**, *23*, 327–341. [CrossRef]

67. Roe, D.R.; Cheatham, T.E., III. PTRAJ and CPPTRAJ: Software for processing and analysis of molecular dynamics trajectory data. *J. Chem. Theory Comput.* **2013**, *9*, 3084–3095. [CrossRef]

68. Baell, J.B.; Holloway, G.A. New Substructure Filters for Removal of Pan Assay Interference Compounds (PAINS) from Screening Libraries and for Their Exclusion in Bioassays. *J. Med. Chem.* **2010**, *53*, 2719–2740. [CrossRef]

69. Zhao, Y.H.; Le, J.; Abraham, M.H.; Hersey, A.; Eddershaw, P.J.; Luscombe, C.N.; Boutina, D.; Beck, G.; Sherborne, B.; Cooper, I.; et al. Evaluation of human intestinal absorption data and subsequent derivation of a quantitative structure–activity relationship (QSAR) with the Abraham descriptors. *J. Pharm. Sci.* **2001**, *90*, 749–784. [CrossRef]

70. Drwal, M.N.; Banerjee, P.; Dunkel, M.; Wettig, M.R.; Preissner, R. ProTox: A web server for the in silico prediction of rodent oral toxicity. *Nucleic Acids Res.* **2014**, *42*, W53–W58. [CrossRef]

3.2. Development of Pyrazine-Anilinobenzamides as Histone Deacetylase HDAC1-3 Selective Inhibitors and Biological Testing Against Pancreas Cancer Cell Lines

Mohamed Abdelsalam, Hany S Ibrahim, Lukas Krauss, Matthes Zessin, Anita Vecchio, Sieglinde Hastreiter, Mike Schutkowski, Günter Schneider, Wolfgang Sippl

Abstract

Class I histone deacetylase (HDAC) enzymes are key regulators of cell proliferation and are frequently dysregulated in cancer cells. Here we describe the synthesis of a novel series of class-I selective HDAC inhibitors containing anilinobenzamide moieties as ZBG connected with a central (piperazin-1-yl)pyrazine moiety. Compounds were tested in vitro against class-I HDAC1, 2, and 3 isoforms. Some highly potent HDAC inhibitors were obtained and were tested in pancreatic cancer cells and showed promising activity. Moreover, we summarize how the growth-inhibitory effects of these compounds can be determined in murine pancreatic cancer cell lines.

Chapter 10

Development of Pyrazine-Anilinobenzamides as Histone Deacetylase HDAC1–3 Selective Inhibitors and Biological Testing Against Pancreas Cancer Cell Lines

Mohamed Abdelsalam, Hany S. Ibrahim, Lukas Krauss, Matthes Zessin, Anita Vecchio, Sieglinde Hastreiter, Mike Schutkowski, Günter Schneider, and Wolfgang Sippl

Abstract

Class I histone deacetylase (HDAC) enzymes are key regulators of cell proliferation and are frequently dysregulated in cancer cells. Here we describe the synthesis of a novel series of class-I selective HDAC inhibitors containing anilinobenzamide moieties as ZBG connected with a central (piperazin-1-yl)pyrazine moiety. Compounds were tested in vitro against class-I HDAC1, 2, and 3 isoforms. Some highly potent HDAC inhibitors were obtained and were tested in pancreatic cancer cells and showed promising activity. Moreover, we summarize how the growth-inhibitory effects of these compounds can be determined in murine pancreatic cancer cell lines.

Key words Class-I histone deacetylases inhibitors, HDAC, Anilinobenzamides, Capping group, Pancreas cancer

1 Introduction

Classical zinc-dependent HDAC inhibitors (HDACis) can be classified into four major groups based on their structures. These are hydroxamates, benzamides, cyclic peptides, and short-chain fatty acids [1, 2]. To date, four HDACis have been approved for the treatment of haematological malignancies [3]. Many other HDACis are currently in clinical trials [4]. Recently, anilinobenzamides have received extensive attention as selective class-I HDACis. Anilinobenzamides have improved class-I HDAC isoform selectivity and strongly inhibit HDAC1, 2 and 3 while they are poorly active or inactive against HDAC8 [5]. The ortho-aminoanilide group acts

---

Authors Mohamed Abdelsalam, Hany S. Ibrahim and Lukas Krauss have contributed equally to this chapter.

IC$_{50}$ (HDAC1)   0.9   µM
IC$_{50}$ (HDAC2)   0.9   µM
IC$_{50}$ (HDAC3)   1.2   µM
IC$_{50}$ (HDAC8)   > 20   µM

IC$_{50}$ (HDAC1)   0.125 µM
IC$_{50}$ (HDAC2)   0.340 µM
IC$_{50}$ (HDAC3)   0.370 µM
IC$_{50}$ (HDAC8)   14.0   µM

IC$_{50}$ (HDAC1)   0.15 µM
IC$_{50}$ (HDAC2)   0.29 µM
IC$_{50}$ (HDAC3)   1.66 µM
IC$_{50}$ (HDAC8)   > 10 µM

IC$_{50}$ (HDAC1)   0.08 µM
IC$_{50}$ (HDAC2)   0.34 µM
IC$_{50}$ (HDAC3)   2.0 µM

IC$_{50}$ (HDAC1)   0.02 µM
IC$_{50}$ (HDAC2)   0.1   µM

IC$_{50}$ (HDAC1)   0.007 µM
IC$_{50}$ (HDAC2)   0.026 µM
IC$_{50}$ (HDAC3)   1.0   µM
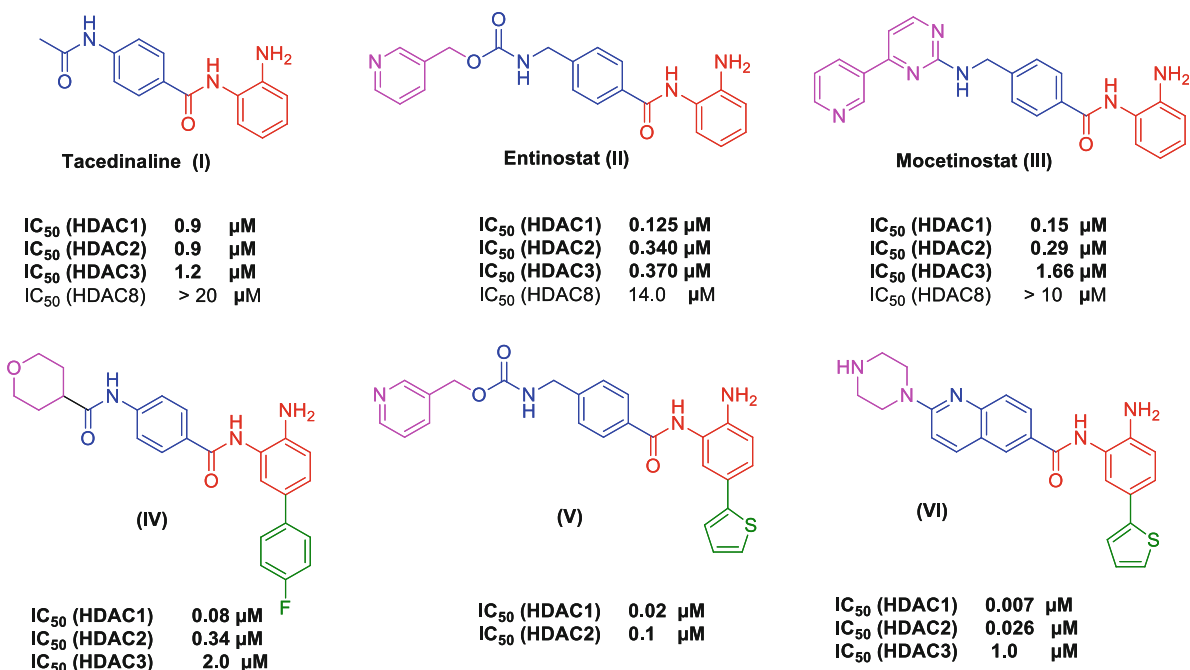
Fig. 1 Representative examples of selective HDAC1, 2, and 3 inhibitors containing 2-aminobenzamide moiety as Zinc binding group, connected to different linkers and capping groups

as ZBG instead of the hydroxamate group in other inhibitors. This replacement allows them to afford selectivity towards HDAC1–3 isoforms [5]. Tacedinaline (CI-994, I), entinostat (MS-275, II), and mocetinostat (MGCD0103, III) are among the first identified members of the anilinobenzamide class (Fig. 1) [6–8]. Entinostat and mocetinostat are currently in phase II trials for treatment of different haematological malignancies including AML or CML as monotherapy or in combination therapy [9, 10].

There is more than 80% sequence homology between HDAC1/2 isoforms. Therefore, it is challenging to design an inhibitor that could preferentially discriminate between both isoforms. HDAC3 shares around 50% sequence homology with both HDAC1/2 isoforms [11]. In crystal structures of HDAC1, 2, and 3, it was shown that there is an internal cavity (so-called foot pocket) near to the catalytic region that could be occupied by bulky aromatic groups, while in the case of HDAC3, this region is occupied by a bulkier tyrosine residue, limiting access to this foot pocket [11]. In this concern another strategy to improve the isoform selectivity towards HDAC1/2 is the addition of aromatic moiety like phenyl or thienyl ring in the position-5 of anilinobenzamide part to fill the foot pocket. For instance, compounds (IV-VI) showed potent activity and high selectivity against HDAC1/2 isoforms over HDAC3 (Fig. 1) [12–14].

Here, we describe the synthetic approaches to develop isoform selective HDAC1–3 inhibitors based on the general pharmacophoric elements of the highly potent pan-HDACi quisinostat
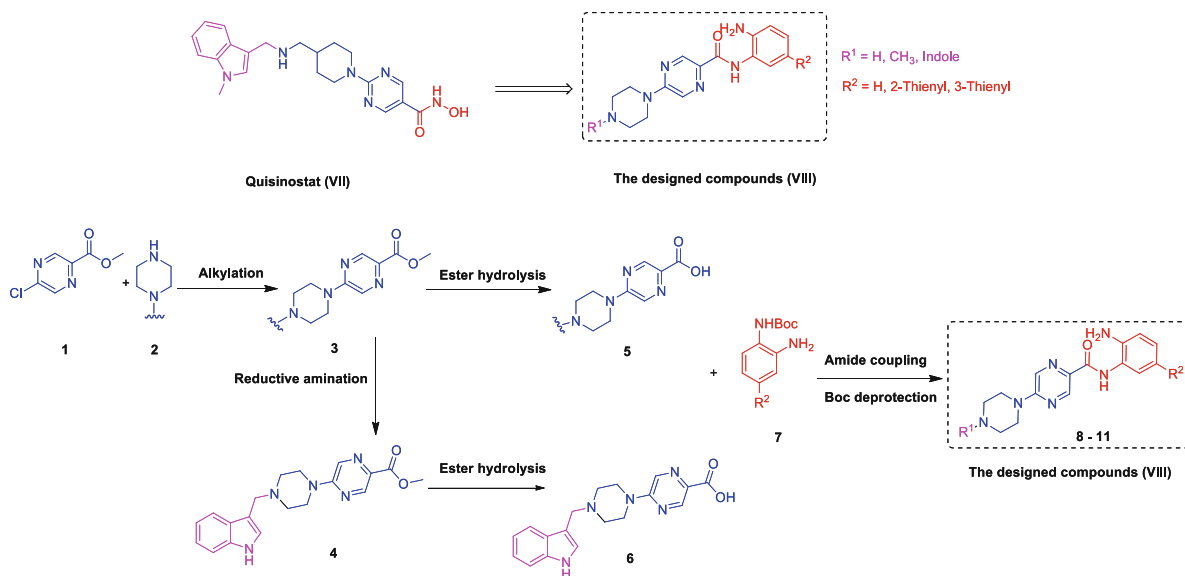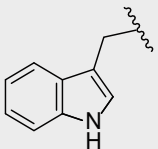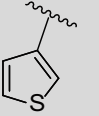
Fig. 2 Scheme showing the synthesis of novel selective HDAC1,2,3 inhibitors (**8–11**) through the modification of general scaffold of Quisinostat (**VII**) by replacing the hydroxamic acid moiety with 2-aminobenzamide group

(JNJ-26481585, VII) (Fig. 2) [15]. The design of the novel compounds is achieved through the replacement of hydroxamic acid functionality with an anilinobenzamide core as ZBG (Fig. 2). Furthermore, 2- or 3-thienyl substituents were introduced on the anilinobenzamide scaffold to improve the selectivity toward HDAC1/2 isoforms (Fig. 2). In addition, the piperazinyl-pyrazine group was used as a linker connecting the anilinobenzamide core and indole capping groups. Also, it was interesting to study the effect of the absence of the capping group on the HDAC isoform selectivity. Therefore, several compounds were prepared lacking such capping group (Fig. 2).

The general synthesis of planned compounds involves three-step synthesis (Fig. 2). Firstly, different piperazinylpyrazine linkers were synthesized via a direct alkylation reaction between the methyl 5-chloropyrazine-2-carboxylate and the appropriate substituted piperazine derivative. The 3-indolyl capping group can be connected to the piperazine linker through a reductive amination reaction using indole-3-carboxaldehyde. The resultant esters were subjected to alkaline hydrolysis to afford the corresponding carboxylic acids. Finally, the carboxylic acids were coupled with the appropriate substituted mono-Boc-protected-*o*-phenylenediamine derivatives, followed by Boc-deprotection, to afford the 2-anilinobenzamides.

All synthesized compounds were tested for their inhibitory activity against human HDAC1, 2, and 3 using a recently developed continuous enzymatic assay. In addition, several reported HDAC1–3 inhibitors (CI-994 and MS-275) were included as reference compounds (Table 1). The unsubstituted anilinobenzamide

Table 1
Inhibitory activity of the synthesized compounds against class I HDACs

Cpd. No.	R^1	R^2	HDAC1 (IC_{50} μM)	HDAC2 (IC_{50} μM)	HDAC3 (IC_{50} μM)
8		H	0.13 ± 0.01	0.28 ± 0.01	0.31 ± 0.01
9	H		0.07 ± 0.01	0.26 ± 0.01	6.1 ± 0.7
10	CH_3		0.04 ± 0.01	0.79 ± 0.02	6% @ 1 μM
11	CH_3		0.11 ± 0.01	0.18 ± 0.06	4.4 ± 0.1
CI994	–	–	37% @ 1 μM	36% @ 1 μM	32% @ 1 μM
MS-275	–	–	0.93 ± 0.1	0.95 ± 0.03	1.8 ± 0.1

n.d. not determined

(**8**) bearing the 3-indolyl ring as a capping group showed good inhibitory activity against HDAC1, 2 and 3 with IC_{50} values (0.13 μM, 0.28 μM, 0.31 μM, respectively). Interestingly, removal of the capping group and modification of the anilinobenzamide scaffold resulted in significant improvement in the HDAC activity and selectivity. For instance, compound **9** having a 2-thienyl ring at position-5 of the phenyl ring of the ZBG showed potent IC_{50} values against HDAC1 and HDAC2 (IC_{50}; 0.07 μM, 0.26 μM, respectively) with little activity against HDAC3 (IC_{50}; 6.1 μM). Compound **10** was the most potent and selective inhibitor among the synthesized compounds with IC_{50} values against HDAC1 and 2 (IC_{50}; 0.04 μM, 0.79 μM respectively). The most potent inhibitors **8–10** were further tested in selected murine pancreatic ductal adenocarcinoma (PDAC) cell lines F2612 and F5061 using the Cell-Titer-Glo luminescent cell viability assay. When indicated, HDAC2 or HDAC3 was genetically knocked out as described previously [16], before seeding them for compound testing. IC_{50} values were calculated from the measured dose-response curves. The IC_{50} values of **8** and **9** were found in the low micromolar to submicromolar range (Fig. 3) whereas the in vitro highly potent HDAC1 inhibitor **10** gave an IC_{50} value above 5 μM (data not shown). The reference inhibitor MS-275 (entinostat) also resulted in a weaker inhibition compared to **8** and **9**. Only small changes in the IC_{50} values were observed when comparing HDAC2-proficient

Dose-Response of 8

HDAC3$^{+/+}$ (E8d)<-> HDAC3$^{-/-}$ (T8d)   HDAC2$^{+/+}$ (E8d) <-> HDAC2$^{-/-}$ (T8d)

Dose-Response of 9

HDAC3$^{+/+}$ (E8d)<-> HDAC3$^{-/-}$ (T8d)   HDAC2$^{+/+}$ (E8d) <-> HDAC2$^{-/-}$ (T8d)
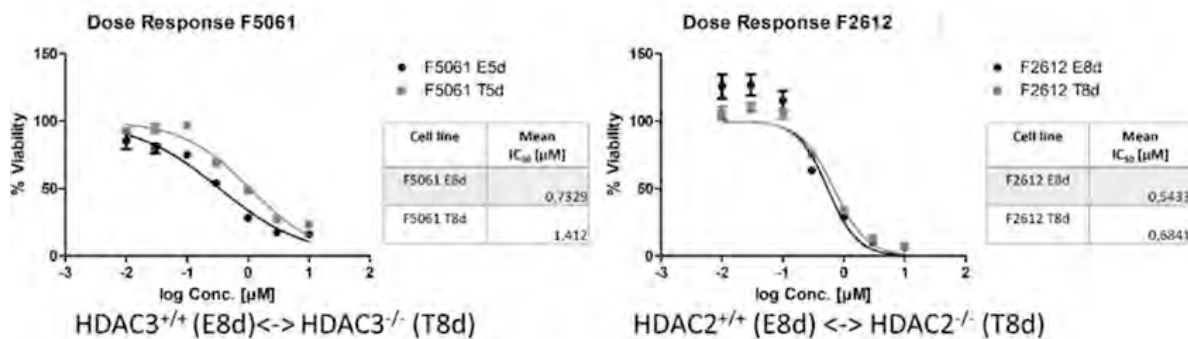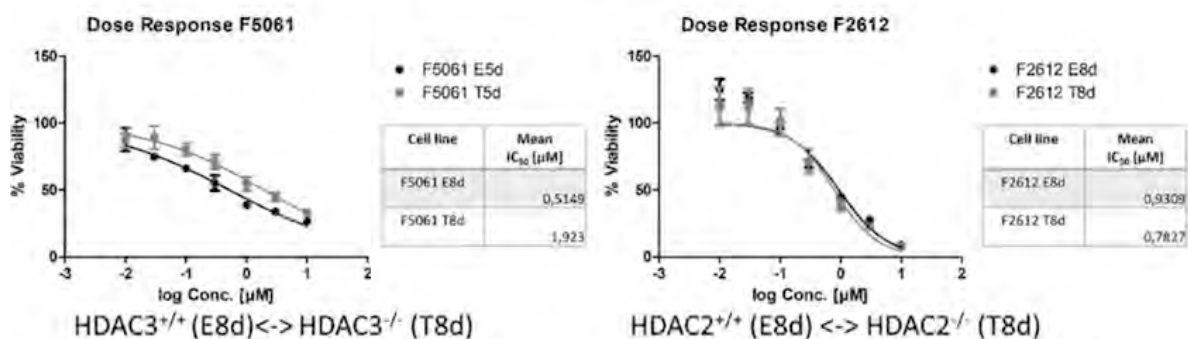
Graphs show one replicate as a representative

Fig. 3 Dose-response curves of HDAC2-proficient/deficient F2612 and HDAC3-proficient/deficient F5061 murine pancreatic ductal adenocarcinoma cell lines treated with the novel synthesized HDAC1,2,3 inhibitors 8 and 9

and deficient F2612 cells, but when comparing the IC$_{50}$ values of HDAC3-proficient and deficient F5061 cells, a shift towards a higher IC$_{50}$ value was observed in the HDAC3-deficient cells, suggesting that sensitivity towards these compounds in the tested cell lines might be driven by HDAC3. After determining an effective dose-range, further experiments to validate the potency and activity of HDACi compounds can be conducted such as measuring differences in the histone H3 acetylation marks (e.g., Western blot of H3K9ac, H3K27ac in treated and untreated cells) [17].

2   Materials

Materials and reagents were purchased from Sigma-Aldrich Co., Ltd. and abcr GmbH. All solvents were analytically pure and dried before use.

2.1 Component for Alkylation	1. Reaction mixture: Methyl 5-chloropyrazine-2-carboxylate (**1**) (10.0 mmol), toluene, piperazine derivative (**2**) (30.0 mmol).
	2. Chloroform, anhydrous sodium sulfate.
2.2 Components for Reductive Amination	1. Reaction mixture: piperazine derivative (**3**) (5.0 mmol), dichloromethane, indole-3-carboxaldehyde (5.0 mmol), glacial acetic acid, sodium triacetoxy borohydride (15 mmol).
	2. 1 M aqueous sodium hydroxide.
2.3 Components for Synthesis of Different Carboxylic Acids Through Ester Hydrolysis	1. Reaction mixture: Ester (**3** or **4**) (1.0 mmol), methanol, 1 M aqueous sodium hydroxide (2.5 mmol).
	2. 1 M Aqueous hydrochloric acid.
2.4 Components for Amide Coupling	1. Reaction mixture: carboxylic acid (**5** or **6**) (1.0 mmol), N,N-dimethylformamide, O-(7-azabenzotriazol-1-yl)-N,N,N′,N′-tetramethyluronium hexafluorophosphate HATU (1.2 mmol), DIPEA (5.0 mmol), the appropriate amine (0.9 mmol).
	2. Ethyl acetate.
	3. 2 M aqueous ammonium chloride, 1 M aqueous sodium bicarbonate, brine.
2.5 Components for Cleavage of Boc Group	1. Reaction mixture: N-Boc-protected amine (**7**) (1 mmol), dichloromethane, trifluoroacetic acid.
	2. 1 M aqueous sodium hydroxide.
2.6 Chromatography Equipment	1. Thin layer chromatography was carried out on aluminum sheets coated with silica gel 60 F254 (Merck, Darmstadt, Germany).
	2. For medium pressure chromatography (MPLC), silica gel Biotage® SNAP ultra HP-sphere 25 μm was used.
	3. Eluents for chromatography: Chloroform: Methanol (9:1) and (8:2).
2.7 Enzymatic Testing of HDAC Inhibitors	1. Recombinant human HDAC1, HDAC2, and HDAC3/NCOR1 were purchased from ENZO Life Sciences AG (Lausen, CH).
	2. Substrate Ac-RHKK(Ac)-AMC was synthesized via solid phase peptide synthesis in house. Prepare a 5 mM stock solution in DMSO.
	3. HDAC-assay buffer: 50 mM 2-[4-(2-hydroxyethyl)piperazin-1-yl]ethane-1-sulfonic acid (HEPES), 140 mM NaCl and 10 mM KCl, pH 7.4 adjusted with NaOH, supplemented

with 1 mM Tris(2-carboxyethyl)phosphine (TCEP) and 0.2 mg/mL bovine serum albumin (BSA).

4. Stop solution: Trypsin from bovine pancreas 40 U/mg (MERCK, Darmstadt, Germany), suberoylanilide hydroxamic acid (SAHA). Prepare the stop solution with a concentration of 1 mg/mL Trypsin with 40 µM SAHA in 1 mM HCl directly before use.

5. Black 384 fluorescence well plate and plate sealer.

2.8 Cell Culture

1. Cells were generated from genetically engineered mouse models (GEMM) as described *(16)*.

2. Cell media: Dulbecco's Eagle medium (high glucose) (Sigma-Aldrich, Munich, Germany) supplemented with 10% FBS, 1% penicillin/streptomycin (PenStrep).

3. 4-Hydroxytamoxifen (Sigma-Aldrich, Munich, Germany).

4. Genotype of F2612: FSF-KrasG12D/+, FSF-Trp53del/+, Pdx1-Flp, R26CAG-FSF-CreERT2/FSF-CreERT2, Hdac2loxP/loxP, Genotype of F5061: FSF-KrasG12D/+, FSF-Trp53del/+, Pdx1-Flp, R26CAG-FSF-CreERT2/FSF-CreERT2, Hdac3loxP/loxP.

2.9 Viability Assay

1. Cell-Titer-Glo Luminescent Cell Viability Assay (Promega, Walldorf, Germany).

2. White 96-well plates (Corning, Costar, Corning, NY, USA).

3. FLUOstar OPTIMA microplate reader (BMG LABTECH, Ortenberg, Germany).

3 Methods

3.1 Alkylation

1. Stir the reaction mixture containing the alkylation components at 130 °C for 2 h.

2. After completion of the reaction as indicated by TLC, pour the mixture into ice cold water and extract the product with chloroform.

3. Wash the organic layer with brine then dry it over anhydrous sodium sulphate.

4. Finally, concentrate the organic layer under reduced pressure to obtain the targeted products (**3**).

3.2 Reductive Amination

1. Stir the reaction mixture at room temperature for 5 h.

2. Quench the mixture by adding 1 M aqueous sodium hydroxide and stir it for another 30 min.

3. Extract the formed suspension with dichloromethane and wash the combined organic layer with brine.

4. Concentrate the organic layer under reduced pressure and purify the obtained solid by MPLC using (CHCl$_3$: MeOH) (9:1).

3.3 Synthesis of Different Carboxylic Acids Through Ester Hydrolysis

1. Stir the reaction mixture at 70 °C for 3 h.

2. Let the reaction mixture to cool to room temperature then acidify the mixture by the dropwise addition of 1 M aqueous hydrochloric acid.

3. Filter the formed precipitate and dry it under vacuum to get the corresponding carboxylic acid as HCl salts (**5** and **6**) (*see* **Note 1**).

3.4 Preparation of Aminobenzamides by Amide Coupling of the Appropriate Carboxylic Acids and Corresponding Amines, Followed by Boc-Deprotection

1. Stir the reaction mixture at room temperature for 18 h (*see* **Note 2**).

2. Dilute the reaction mixture with ethyl acetate.

3. Wash the organic layer with 2 M aqueous ammonium chloride, 1 M sodium bicarbonate and brine.

4. Dry the combined organic extracts over anhydrous sodium sulfate and concentrate the solvent under reduced pressure.

5. Purify the obtained residue by MPLC using (chloroform: methanol) (9:1) to get the corresponding amide.

6. For the preparation of free aminobenzamide derivatives (**8–11**), dissolve the purified product (N-Boc-protected amide derivative) in dichloromethane, then add trifluoroacetic acid at 0 °C.

7. Stir the reaction mixture at room temperature for 30 min, then evaporate the reaction mixture under a vacuum.

8. To remove the excess trifluoroacetic acid, add 1 M aqueous solution of sodium hydroxide to the obtained residue and then extract with ethyl acetate (*see* **Note 3**).

9. Clean the obtained product by using MPLC (CHCl$_3$: MeOH) (8:2) to obtain the corresponding amide (**8–11**).

3.5 Enzymatic Testing of HDAC Inhibitors

1. The enzyme inhibition was determined by using a reported homogenous fluorescence assay *(17)*.

2. Prepare a serial dilution of the compound for 8 concentrations in HDAC assay buffer with a factor of threefold of the final assay concentration. Possible final compound concentrations are 0.006, 0.02, 0.06, 0.2, 0.6, 2, 6, 20 μM. Keep the DMSO concentration constant and not above 5% final concentration.

3. Add 7 μL of every compound concentration in quadruplicates to the 384 fluorescence well plate. Add also 7 μL of a buffer/ DMSO mixture according to the DMSO concentration in your dilution series in quadruplicates to the plate for negative and positive control.

4. Prepare threefold enzyme in HDAC assay buffer and add 7 μL to each compound containing well and to the wells designated for the positive controls. Add 7 μL HDAC assay buffer to the wells designated for the negative control. Possible final HDAC concentrations are 3 nM for HDAC2 and HDAC3 and 10 nM for HDAC1.

5. Incubate the plate for 5 min at room temperature while shaking.

6. Prepare threefold substrate in HDAC assay buffer and add 7 μL to each well designated for the inhibitor assay to start the enzymatic reaction. Using a multichannel pipette for step 4 and 6 is highly recommended.

7. Cover the plate with a plate sealer and incubate the plate at 37 °C for 30 min for HDAC2 and 3 and 90 min HDAC1.

8. Add 21 μL stop solution to all wells used for the inhibitor measurement, seal the plate with the plate sealer and incubate it for 60 min at 37 °C.

9. Measure the fluorescence intensity at wavelengths that belong to AMC fluorescence, e.g., at an excitation wavelength of 390 nm and an emission wavelength of 460 nm in a microtiter plate reader (Envision 2104 Multilabel Plate Reader).

3.6 Biological Assessment with a Proliferation Assay

1. Murine cell lines grow in Dulbecco's Eagle medium supplemented with 10% FBS, 1% penicillin/streptomycin (PenStrep) at 37 °C and 5% CO_2. Every third or fourth day (depending on the cell confluence), the cells have to be split in a 1:10 ratio into new cell culture flask.

2. Seed cells in a white 96-well plate at a density of 2×10^3 cells per well in 100 μL growth medium (see above).

3. 24 h after seeding, dilute compounds in a dilution series (1:3 ratio) in cell culture media with sixfold the final test concentrations: e.g.: 60uM - > 20 μM - > 6,66 μM - > 2,22 μM - > 0,74 μM - > 0,25 μM - > 0.08 μM.

4. Treat cells with the prepared dilution series by adding 20 μL of the dilutions to their designated wells and incubate the cells at 37 °C and 5% CO_2 for 72 h (*see* **Note 4**).

5. Measure cell growth using the Cell-Titer-Glo Luminescent Cell Viability Assay (*see* **Note 5**) according to manufacturer's instructions (*see* **Note 6**).

6. Normalize measured values to control cell measurements and calculate the desired IC_{50} -values (*see* **Note 7**) by using, e.g., GraphPadPrism (*see* **Note 8**).

7. Compare the different calculated IC_{50} values, as in our example (Fig. 3).

4   Notes

1. In the event that no precipitate is formed, try to reduce the amount of solvent by concentration under reduced pressure and leave the mixture to cool. The product will start to precipitate.

2. For monitoring the progress of reaction by TLC, before spotting try first to dilute 1 drop of the reaction mixture with ethyl acetate (1.0 mL), followed by drying TLC sheet for 2 min at 50 °C. Otherwise the DMF may overlap with the product.

3. It is better to make the aminobenzamide derivative as a free base instead of TFA salt before purification by MPLC.

4. Control cells were treated with 0.1% DMSO diluted in growth media. In the HDACi vehicle, 0.1% DMSO is equivalent to the highest HDACi dilution.

5. Cell-Titer-Glo Luminescent Cell Viability Assay lyses cells and measures the present ATP levels in the cell lysate which is proportional to the total number of cells in each well. The assay contains luciferin and luciferase, which converts luciferin to oxyluciferin using ATP. The conversion of luciferin to oxyluciferin generates a luminescent signal which can be measured using adequate detection devices (e.g., FLUOstar OPTIMA microplate reader).

6. In the described setting, 25 µL of Cell-Titer-Glo assay per well is sufficient to induce a linear signal. Alternatively, other assays to measure cell viability can be used instead such as the MTT assay. MTT assay can be performed according to the manufacturer's instructions, but if the media contains a pH indicator, it should be carefully removed before adding twice (2×100 µL) the solubilization solution (alternative to solubilization solution: 1:1 EtOH/DMSO solution). For MTT assay, cells can be seeded in transparent 96-well plates.

7. The measurement of the DMSO treated cells was set at 100%. To obtain IC_{50} values you have to repeat the experiment thrice and calculate the mean of the measured values.

8. Normalized measurements can be copied into GraphPadPrism in triplicates, and concentration values should be log transformed.

Acknowledgments

References

1. Wagner FF, Wesmall Yi UM, Lewis MC et al (2013) Small molecule inhibitors of zinc-dependent histone deacetylases. Neurotherapeutics 10(4):589–604. https://doi.org/10.1007/s13311-013-0226-1

2. Melesina J, Simoben CV, Praetorius L et al (2021) Strategies to design selective histone deacetylase inhibitors. ChemMedChem 16(9):1336–1359. https://doi.org/10.1002/cmdc.202000934

3. Sarkar R, Banerjee S, Amin SA et al (2020) Histone deacetylase 3 (HDAC3) inhibitors as anticancer agents: a review. Eur J Med Chem 192:112171. https://doi.org/10.1016/j.ejmech.2020.112171

4. Mottamal M, Zheng SL, Huang TL et al (2015) Histone deacetylase inhibitors in clinical studies as templates for new anticancer agents. Molecules 20(3):3898–3941. https://doi.org/10.3390/molecules20033898

5. Yang FF, Zhao N, Ge D et al (2019) Next-generation of selective histone deacetylase inhibitors. RSC Adv 9(34):19571–19583. https://doi.org/10.1039/c9ra02985k

6. Prakash S, Foster BJ, Meyer M et al (2001) Chronic oral administration of CI-994: a phase 1 study. Investig New Drugs 19(1):1–11. https://doi.org/10.1023/a:1006489328324

7. Saito A, Yamashita T, Mariko Y et al (1999) A synthetic inhibitor of histone deacetylase, MS-27-275, with marked in vivo antitumor activity against human tumors. Proc Natl Acad Sci U S A 96(8):4592–4597. https://doi.org/10.1073/pnas.96.8.4592

8. Batlevi CL, Crump M, Andreadis C et al (2017) A phase 2 study of mocetinostat, a histone deacetylase inhibitor, in relapsed or refractory lymphoma. Br J Haematol 178(3):434–441. https://doi.org/10.1111/bjh.14698

9. San Jose-Eneriz E, Gimenez-Camino N, Agirre X et al (2019) HDAC inhibitors in acute myeloid leukemia. Cancers (Basel) 11(11):1794. https://doi.org/10.3390/cancers11111794

10. Fratta E, Montico B, Rizzo A et al (2016) Epimutational profile of hematologic malignancies as attractive target for new epigenetic therapies. Oncotarget 7(35):57327–57350. https://doi.org/10.18632/oncotarget.10033

11. Ho TCS, Chan AHY, Ganesan A (2020) Thirty years of HDAC inhibitors: 2020 insight and hindsight. J Med Chem 63(21):12460–12484. https://doi.org/10.1021/acs.jmedchem.0c00830

12. Wagner FF, Weiwer M, Steinbacher S et al (2016) Kinetic and structural insights into the binding of histone deacetylase 1 and 2 (HDAC1, 2) inhibitors. Bioorg Med Chem 24(18):4008–4015. https://doi.org/10.1016/j.bmc.2016.06.040

13. Moradei OM, Mallais TC, Frechette S et al (2007) Novel aminophenyl benzamide-type histone deacetylase inhibitors with enhanced potency and selectivity. J Med Chem 50(23):5543–5546. https://doi.org/10.1021/jm701079h

14. Min C, Moore N, Shearstone JR et al (2017) Selective inhibitors of histone deacetylases 1 and 2 synergize with Azacitidine in acute myeloid leukemia. PLoS One 12(1):e0169128. https://doi.org/10.1371/journal.pone.0169128

15. Arts J, King P, Marien A et al (2009) JNJ-26481585, a novel "second-generation" Oral histone deacetylase inhibitor, shows broad-spectrum preclinical antitumoral activity. Clin Cancer Res 15(22):6841–6851. https://doi.org/10.1158/1078-0432.Ccr-09-0547

16. Bayer S, Wirth M (2017) Engineering of conditional class I Hdac knockout mice and generation of a time-spatial knockout by a dual recombination system. Methods Mol Biol 1510:193–209. https://doi.org/10.1007/978-1-4939-6527-4_14

17. Ibrahim HS, Abdelsalam M, Zeyn Y et al (2022) Synthesis, molecular docking and biological characterization of pyrazine linked 2-aminobenzamides as new class I selective histone deacetylase (HDAC) inhibitors with anti-leukemic activity. Int J Mol Sci 23(1):369. https://doi.org/10.3390/ijms23010369

3.3. Docking, Binding Free Energy Calculations and In Vitro Characterization of Pyrazine Linked 2-Aminobenzamides as Novel Class I Histone Deacetylase (HDAC) Inhibitors

Emre F. Bülbül, Jelena Melesina, Hany S. Ibrahim, **Mohamed Abdelsalam**, Anita Vecchio, Dina Robaa, Matthes Zessin, Mike Schutkowski and Wolfgang Sippl

Abstract

Class I histone deacetylases, HDAC1, HDAC2, and HDAC3, represent potential targets for cancer treatment. However, the development of isoform-selective drugs for these enzymes remains challenging due to their high sequence and structural similarity. In the current study, we applied a computational approach to predict the selectivity profile of developed inhibitors. Molecular docking followed by MD simulation and calculation of binding free energy was performed for a dataset of 2-aminobenzamides comprising 30 previously developed inhibitors. For each HDAC isoform, a significant correlation was found between the binding free energy values and in vitro inhibitory activities. The predictive accuracy and reliability of the best preforming models were assessed on an external test set of newly designed and synthesized inhibitors. The developed binding free-energy models are cost-effective methods and help to reduce the time required to prioritize compounds for further studies.

Article

Docking, Binding Free Energy Calculations and In Vitro Characterization of Pyrazine Linked 2-Aminobenzamides as Novel Class I Histone Deacetylase (HDAC) Inhibitors

Emre F. Bülbül [1] , **Jelena Melesina** [1], **Hany S. Ibrahim** [1,2] , **Mohamed Abdelsalam** [1,3] , **Anita Vecchio** [1], **Dina Robaa** [1], **Matthes Zessin** [4], **Mike Schutkowski** [4] **and Wolfgang Sippl** [1,*]

[1] Department of Medicinal Chemistry, Institute of Pharmacy, Martin-Luther University of Halle-Wittenberg, 06120 Halle (Saale), Germany; emre.bulbul@pharmazie.uni-halle.de (E.F.B.); jelenamelesina@gmail.com (J.M.); hany.ibrahim@pharmazie.uni-halle.de (H.S.I.); mohamed.abdelsalam@pharmazie.uni-halle.de (M.A.); anitavecchio95@gmail.com (A.V.); dina.robaa@pharmazie.uni-halle.de (D.R.)

[2] Department of Pharmaceutical Chemistry, Faculty of Pharmacy, Egyptian Russian University, Cairo 11829, Egypt

[3] Department of Pharmaceutical Chemistry, Faculty of Pharmacy, Alexandria University, Alexandria 21521, Egypt

[4] Department of Enzymology, Institute of Biochemistry and Biotechnology, Martin-Luther-University of Halle-Wittenberg, 06120 Halle (Saale), Germany; matthes.zessin@googlemail.com (M.Z.); mike.schutkowski@biochemtech.uni-halle.de (M.S.)

[*] Correspondence: wolfgang.sippl@pharmazie.uni-halle.de

Abstract: Class I histone deacetylases, HDAC1, HDAC2, and HDAC3, represent potential targets for cancer treatment. However, the development of isoform-selective drugs for these enzymes remains challenging due to their high sequence and structural similarity. In the current study, we applied a computational approach to predict the selectivity profile of developed inhibitors. Molecular docking followed by MD simulation and calculation of binding free energy was performed for a dataset of 2-aminobenzamides comprising 30 previously developed inhibitors. For each HDAC isoform, a significant correlation was found between the binding free energy values and in vitro inhibitory activities. The predictive accuracy and reliability of the best preforming models were assessed on an external test set of newly designed and synthesized inhibitors. The developed binding free-energy models are cost-effective methods and help to reduce the time required to prioritize compounds for further studies.

Keywords: docking; binding free energy; 2-aminobenzamide; HDAC1; HDAC2; HDAC3 inhibitors

1. Introduction

Epigenetic mechanisms are controlled by chemical transformations on DNA or histone proteins [1,2], which are driven by post-translational modifications (PTM) such as methylation, sumoylation, ubiquitinylation, acetylation and others [3]. Histone deacetylases (HDACs) and histone acetyltransferases (HATs) are enzymes that are strongly involved in post-translational modifications of lysine residues of histone proteins. HDACs remove acetyl or rather acyl moieties from the N-terminal lysine residues of histones and non-histone proteins. Hence, they play a pivotal role in multiple biological processes. Due to their important role, HDACs have become promising targets for various diseases such as cancer, inflammation, parasitic infections, and neurodegenerative diseases [4,5].

So far, 18 human HDACs have been identified and subdivided into 4 classes: class I (HDAC1-3, HDAC8), class IIa (HDACs 4, 5, 7 and 9), class IIb (HDACs 6 and 10), class III (Sirtuins) and class IV (HDAC11). Class I, II and IV are called zinc-dependent HDACs, while class III is mostly called sirtuins, and they require NAD^+ for their catalytic activity. Sirtuins are structurally different from the zinc-dependent HDACs [6].

To date, five HDAC inhibitors have been approved for the treatment of cutaneous and peripheral T-cell lymphoma and multiple myeloma. Several others are in clinical trials [7–11]. Most HDAC inhibitors have a common structural pharmacophore. Mostly, they contain a zinc binding group (ZBG), a linker group and a cap group [6]. The aminobenzamide scaffold is one of the most studied ZBGs. According to the released HDAC2 X-ray structure in complex with a 2-aminobenzamide derivative, this ZBG chelates the zinc ion in a bidentate manner, whereas hydrogen bonds with the neighboring histidine and catalytic tyrosine residues further stabilize the zinc coordination [12–14]. These inhibitors also often have a foot pocket targeting group that occupies an internal cavity characteristic to class I HDACs [15].

Since it is challenging and expensive to solve X-ray structures for all ligands of interest, molecular modelling tools are regularly applied to predict their binding modes. Reliable estimation of the protein–ligand interactions has become a promising structure-based drug design strategy. Different approaches have been developed to increase the accuracy of predicting the biological activity of small molecules [16–21]. Molecular docking and molecular dynamics studies are used to predict the binding mode of the ligands as well as the binding affinity of protein–ligand complexes. Although docking methods often correctly estimate the binding poses of ligands, their binding affinity prediction still remains a big challenge [20,22]. Thus, rescoring using binding free-energy calculations is a more popular method to rank the compounds according to their binding affinity [23]. Molecular mechanics (MM) energies combined with the Poisson-Boltzman (PB) or Generalized Born (GB) and surface area continuum solvation (SA) methods are frequently used to predict the binding free energy of the ligand. MMPBSA and MMGBSA methods are based on molecular dynamics simulations. Hence, they increase the accuracy as well as the computational time and cost [24].

In the current study, we tested whether binding free energy calculations can be used to find predictive models for a series of 2-aminobenzamide inhibitors recently reported by us [25]. We expected that the binding free energy calculations would be able to provide successful predictive models using a single frame or a small number of snapshots taken from the MD simulations. Such models repeatedly proved to be useful for the development of inhibitors of diverse epigenetic targets [26–28]. Thus, they can be useful for the design of novel HDAC inhibitors having 2-aminobenzamide scaffold. Additionally, such models can be used as a post-docking filter for screening large databases.

2. Results

2.1. Diversity Analysis of Studied Dataset

In this study, we focused on a particular series of inhibitors covering a reasonable biological activity range to develop a robust prediction model. The compounds chosen as a training set in this study are shown in Table 1 [25]. These compounds have a 2-aminobenzamide moiety as zinc binding group (ZBG). Either a pyrimidine or pyrazine scaffold was used as a linker group. The linker group is connected via a piperazine moiety to the cap group that includes various substituents.

We first analyzed the diversity of the selected compounds. Principal component analysis (PCA) defines the chemical space of the compound data set describing the applicability domain (AD) of the established QSAR model [22,29,30]. The applicability domain can be utilized to determine the limitation of the model. In this study, PCA (PCA1, PCA2 and PCA3) calculated from the descriptors (a_acc, b_1rotN, b_ar, PEOE_VSA_POL, logP(o/w)) was used to define the AD of the training set compounds for which IC_{50} values were. The two-dimensional (2D) plots of the variations of the training set are shown in Figure 1. The PCA analysis indicated that the studied inhibitors were homogeneously distributed within the chemical space. The 3D graphical representation of the training set is shown in Figure 1B to visualize the position of the molecules.

Table 1. Inhibitory activity of synthesized compounds of the training set against HDAC1-3 [25].
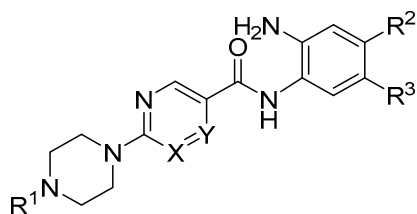
Cpd. No.	Substituents					IC$_{50}$ (μM) or % Inhibition at Given Concentration		
	X	Y	R1	R2	R3	HDAC1	HDAC2	HDAC3
19a	CH	N		H	H	0.51 ± 0.05	0.80 ± 0.07	1.12 ± 0.07
19b	CH	N		H	H	26% @ 2 μM	30% @ 2 μM	65% @ 2 μM
19c	N	CH		H	H	34% @ 2 μM	20% @ 2 μM	27% @ 2 μM
19d	CH	N		H	H	0.52 ± 0.07	1.43 ± 0.08	1.06 ± 0.04
19e	CH	N		H	H	0.21 ± 0.07	0.71 ± 0.04	0.84 ± 0.03
19f	CH	N		H	H	0.13 ± 0.01	0.28 ± 0.01	0.31 ± 0.01
19g	CH	N		H	H	0.31 ± 0.03	0.96 ± 0.05	0.49 ± 0.06
19h	CH	N		F	F	0.81 ± 0.07	0.74 ± 0.03	0.57 ± 0.02
19i	CH	N		Cl	H	3.0 ± 0.2	2.7 ± 0.2	1.9 ± 0.1
19j	N	CH		H	H	0.45 ± 0.06	0.93 ± 0.04	1.75 ± 0.06
19k	CH	N		H	H	0.14 ± 0.02	0.56 ± 0.04	0.59 ± 0.03

Table 1. *Cont.*
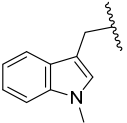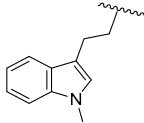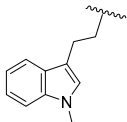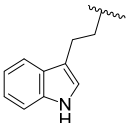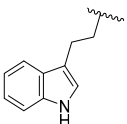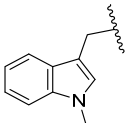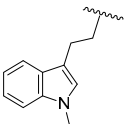
Cpd. No.	Substituents					IC$_{50}$ (µM) or % Inhibition at Given Concentration		
	X	Y	R1	R2	R3	HDAC1	HDAC2	HDAC3
19l	CH	N		F	F	0.29 ± 0.03	0.56 ± 0.02	0.81 ± 0.05
19m	CH	N		F	H	0.40 ± 0.06	1.48 ± 0.19	0.40 ± 0.02
19n	N	CH	CH$_3$	H	H	5% @ 1 µM	7% @ 1 µM	13% @ 1 µM
19o	CH	N	CH$_3$	H	H	27% @ 1 µM	15% @ 1 µM	30% @ 1 µM
21a	CH	N		H	2-Thienyl	0.26 ± 0.01	2.47 ± 0.22	0% @ 1 µM
21b	CH	N		H	4-F-C$_6$H$_4$	0.70 ± 0.08	0.77 ± 0.06	0% @ 1 µM
21c	CH	N		H	2-F-C$_6$H$_4$	0.76 ± 0.07	0.76 ± 0.04	15 ± 1
23a	CH	N	H	F	H	3.30 ± 0.18	2.17 ± 0.18	0.40 ± 0.01
23b	CH	N		H	F	0.27 ± 0.03	0.50 ± 0.03	0.50 ± 0.02
23c	CH	N		H	F	0.33 ± 0.02	1.37 ± 0.08	0.59 ± 0.04
25a	CH	N	H	Cl	H	0% @ 1 µM	0% @ 1 µM	8.7 ± 0.4
25b	CH	N	H	F	F	4.3 ± 0.3	4.2 ± 0.15	1.6 ± 0.1
27a	CH	N	H	H	CF$_3$	0% @ 1 µM	0% @ 1 µM	0% @ 1 µM
27b	CH	N	H	CH$_3$	H	0% @ 1 µM	0% @ 1 µM	0% @ 1 µM
27c	CH	N	H	OCH$_3$	H	20.0 ± 1.0	14.0 ± 2.0	14.0 ± 1.0
29a	CH	N	CH$_3$	H	3-Thienyl	0.11 ± 0.01	0.18 ± 0.06	4.4 ± 0.1
29b	CH	N	H	H	2-Thienyl	0.07 ± 0.01	0.26 ± 0.01	6.1 ± 0.7
29c	CH	N	H	H	4-F-C$_6$H$_4$	0.16 ± 0.03	0.34 ± 0.01	6.7 ± 0.5
29d	CH	N	CH$_3$	H	2-F-C$_6$H$_4$	0.18 ± 0.01	0.26 ± 0.07	12.0 ± 1.0

Table 1. *Cont.*

Cpd. No.	Substituents					IC$_{50}$ (µM) or % Inhibition at Given Concentration		
	X	Y	R1	R2	R3	HDAC1	HDAC2	HDAC3
CI994	–	–	–	–	–	37% @ 1 µM	36% @ 1 µM	32% @ 1 µM
RGFP-966	–	–	–	–	–	16 ± 2	11 ± 1	1.3 ± 0.1
MS-275	–	–	–	–	–	0.93 ± 0.1	0.95 ± 0.03	1.8 ± 0.1
Mocetinostat	–	–	–	–	–	0.33 ± 0.04	0.34 ± 0.01	0.93 ± 0.05

n.d. not determined, – no substituents.
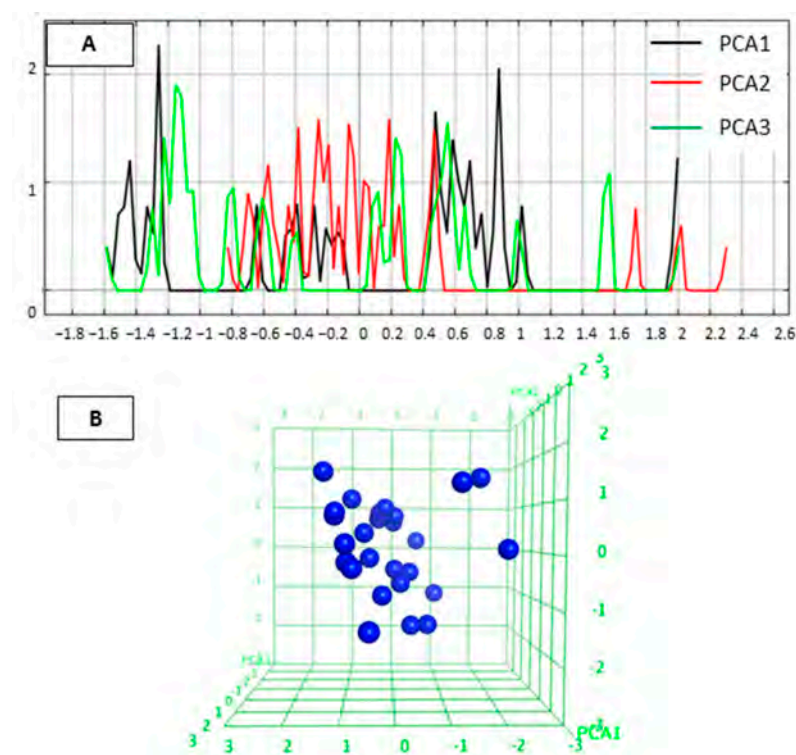
Figure 1. (**A**) 2D plots for visualization of the variation of three most important PCA in test set. Black color represents PCA1, red color PCA2 and green color PCA3. (**B**) 3D plot of the chemical space occupied by the training set (blue).

2.2. Analysis of Protein-Inhibitor Complexes

To understand the binding mode of 2-aminobenzamide derivatives, the X-ray structures of HDAC2 in complex with similar inhibitors (PDB ID: 3MAX, 4LY1, 5IX0, 5IWG) were first analyzed. Analysis revealed that the inhibitors occupy the 11 Å long acetyl lysine substrate channel as well as the 14 Å internal cavity called the foot pocket [15]. At the bottom of the acetyl lysine substrate channel, the ligand binds in a bidentate manner to the Zn^{+2} ion through its carbonyl and free amino group. In addition, the free amino group interacts with neighboring histidine (H145 and H146) as well as tyrosine (Y308) residues. The interaction of amide-NH with glycine (G154) was observed in all HDAC2 X-ray structures in complex with 2-aminobenzamides. The aromatic linker attached to the benzamide moiety connecting the zinc binding group to the cap group is placed between two phenylalanine residues (F155 and F210) (Figure 2). The water-mediated hydrogen bond interaction with histidine (H183) was observed in HDAC2 (PDB ID 4LY1, 5IWG and 5IX0) inhibitor complexes.
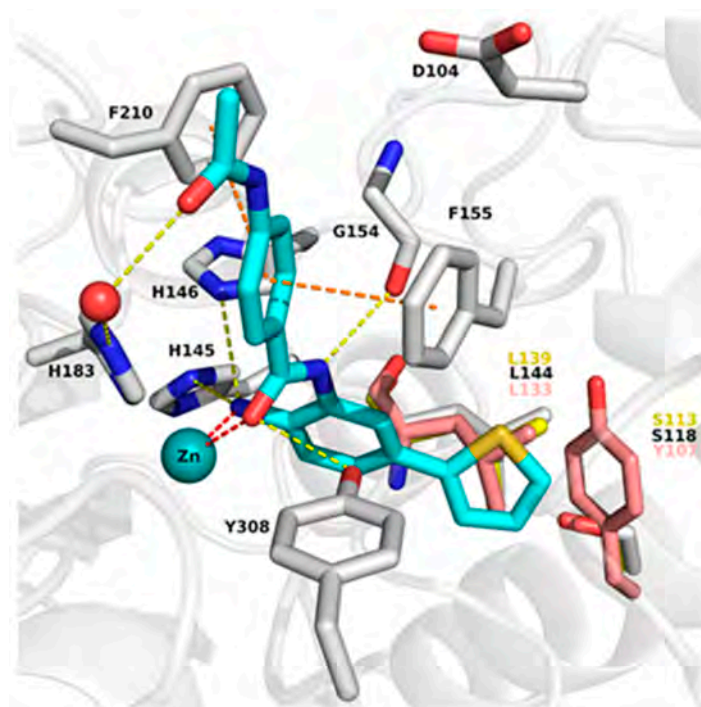
Figure 2. Comparison of the binding pocket of HDAC2 (white carbon atoms) with HDAC1 (yellow carbon atoms) and HDAC3 (salmon carbon atoms). Only the part of the foot pocket that differs in HDAC3 compared to HDAC1 and HDAC2 is shown for all three isoforms, and residues are labeled in the same colors as the carbon atoms. The protein backbone is shown as white ribbon. The zinc ion is shown as cyan sphere and the water molecule as red sphere. The ligand is shown as sticks with cyan carbon atoms. Protein–ligand interactions are shown as dashed lines: zinc coordination in red, hydrogen bonds in yellow, and aromatic interactions in orange.

The binding pocket of HDAC1 is very similar to HDAC2, whereas in HDAC3 the bulky Y107 amino acid residue situated in the foot pocket replaces the serine residues observed in HDAC1/2 (S113 and S118 in HDAC1 and HDAC2, respectively). Hence, in HDAC3 the side chain of Y107 pushes the L133 residue, causing a smaller size of the foot pocket compared to HDAC1/2. This conformational change of the L133 residue (L144 in HDAC2) may block the entry of bulky substituents into the foot pocket (Figure 2).

After careful analysis of the HDAC2 crystal structures in complex with 2-aminobenzamide, we conducted redocking (the ability to reproduce the binding mode of co-crystallized ligand) and cross-docking (the ability to correctly predict the binding mode of the other crystallized ligands) studies to find an appropriate docking protocol (Figure S1 and Table S1, Supplementary Materials). The structure PDB ID 4LY1 was chosen to dock the training set since it showed the best re- and cross-docking results, i.e., the lowest RMSD (root mean square deviation) values (Table S1). The co-crystallized ligand of HDAC2 (PDB ID 4LY1) exhibits high inhibitory activity against HDAC1 and HDAC2 [13]. Thus, the ligand from PDB ID 4LY1 was docked in HDAC1 (PDB ID: 4BKX [31]) and the complex was used for further analysis. Since this ligand does not show any inhibitory activity against HDAC3, the selective HDAC3 compound BG45 [32] was docked to HDAC3 (PDB ID: 4A69 [33]) and used for further analysis. Subsequently, the generated protein–ligand complexes were subjected to 100 ns MD simulation to check the stability of the ligands and protein–ligand interactions.

Analysis of the MD simulation of HDAC1, HDAC2 and HDAC3-inhibitor complexes revealed that protein and ligand remained mostly stable throughout the MD simulation (Figures S2–S4, Supplementary Materials). In addition, most protein-ligand interactions

were maintained throughout the 100 ns simulation time (Figure 3). The active site residues did not show significant fluctuations during the 100 ns simulations (Figure 3), with the exception of the catalytic tyrosine residue (Y303, Y308 and Y298 in HDAC1, 2 and 3, respectively) for which some flexibility was observed. More detailed analysis showed that the zinc binding group of the inhibitors maintained its bidentate chelation with the zinc ion through its free amino group and carbonyl oxygen as well as the hydrogen bond interactions with H140/145/134, H141/146/135 and G149/G154/143 in HDAC1/2/3, respectively, during the simulation. Due to the flexibility of the catalytic tyrosine residue, the observed hydrogen bond interaction with the carbonyl group was not always maintained, especially in case of HDAC1 and -2. In addition, the phenyl linker group mostly kept the aromatic interactions with the phenylalanine residues in HDAC1/2 (F150/155 and F205/210 in HDAC1/2, respectively). In HDAC3, it could be observed that the π–π interactions became less stable after 60 ns, which can be attributed to the fluctuation of F200. The thiophene ring located at the foot pocket of HDAC1 and HDAC2 stayed stable by making hydrophobic interaction with the neighboring residues in both subtypes. Meanwhile, the solvent-exposed amide cap group of the HDAC1,2 ligand underwent some small fluctuations in HDAC1 and HDAC2.
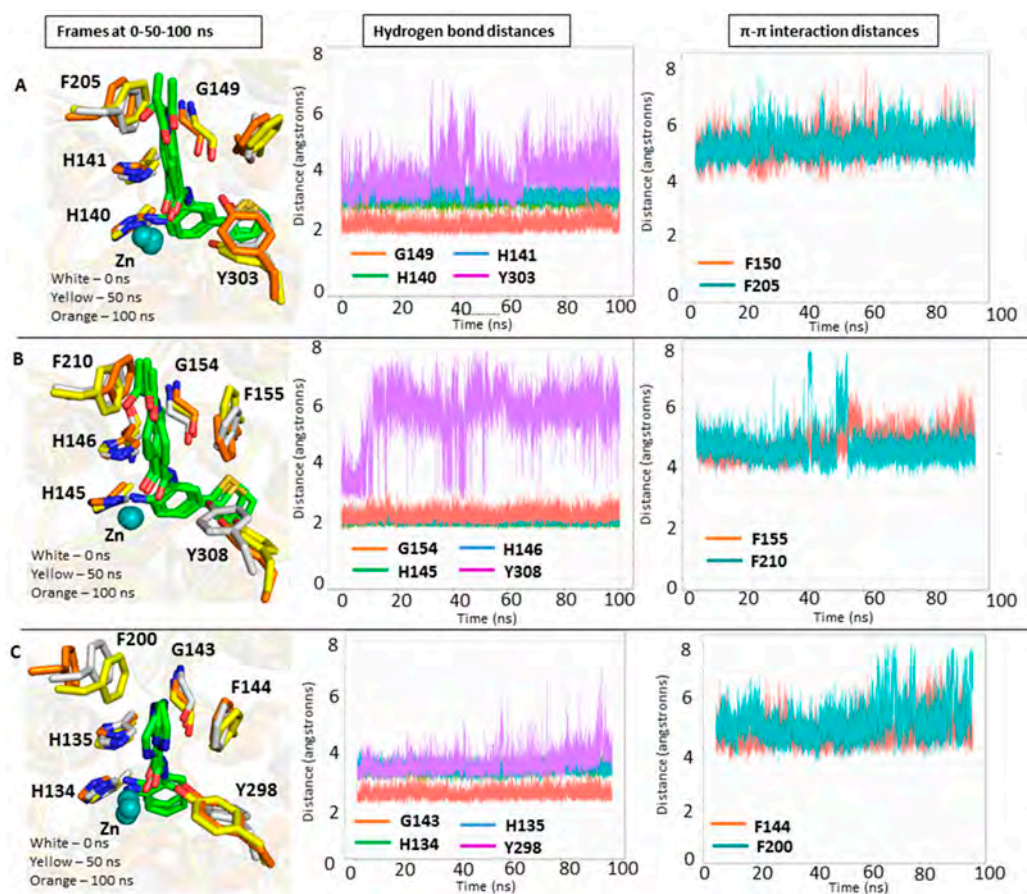
Figure 3. Results of the MD simulations of HDAC1, 2, 3 in complex with inhibitors. Shown are the frames of the MD simulations at 0 ns (white carbon atoms), 50 ns (yellow carbon atoms), and 100 ns (orange carbon atoms) on the left side. In the middle, distance analysis of specified hydrogen bonds between inhibitor and HDAC are shown. On the right side, the distance analysis of aromatic π–π interactions between inhibitor and HDAC are shown. HDAC1 (**A**), HDAC2 (**B**), HDAC3 (**C**). Zinc ions are shown as cyan spheres. Ligands are shown in stick representation and their carbon atoms are colored green in HDAC1, HDAC2 and HDAC3. For clarity, only relevant amino acid residues are shown.

2.3. Docking Results of the Training Set

The docking results of the 30 compounds from the training set (published previously in [25]) demonstrated that they show a similar binding mode in the binding pocket of HDAC1, HDAC2 and HDAC3 (Figure 4). The compounds chelate the zinc ion and form hydrogen bonds with H140/145/134, H141/146/135, Y303/308/298, and G149/154/143 in HDAC1/2/3, respectively. Their pyrazine and pyrimidine linker groups are accommodated into the hydrophobic tunnel making π–π interactions with F150/155/144 and F205/210/200 in HDAC1/2/3, respectively. The piperazine unit shows ionic interaction with the conserved D99/104/93 in HDAC1/2/3, respectively. The cap group is surface-exposed and occupies the hydrophobic cavity, which consists of F150/155/144, P29/34/23 and H28/33/22 in HDAC1/2/3, respectively. A significant difference was observed for compounds having bulky substituents such as thiophene or phenyl groups attached to the 2-aminobenzamide moiety in the foot pocket region. These bulky substituents cannot enter into the foot pocket of HDAC3 because of the aforementioned steric hindrance.
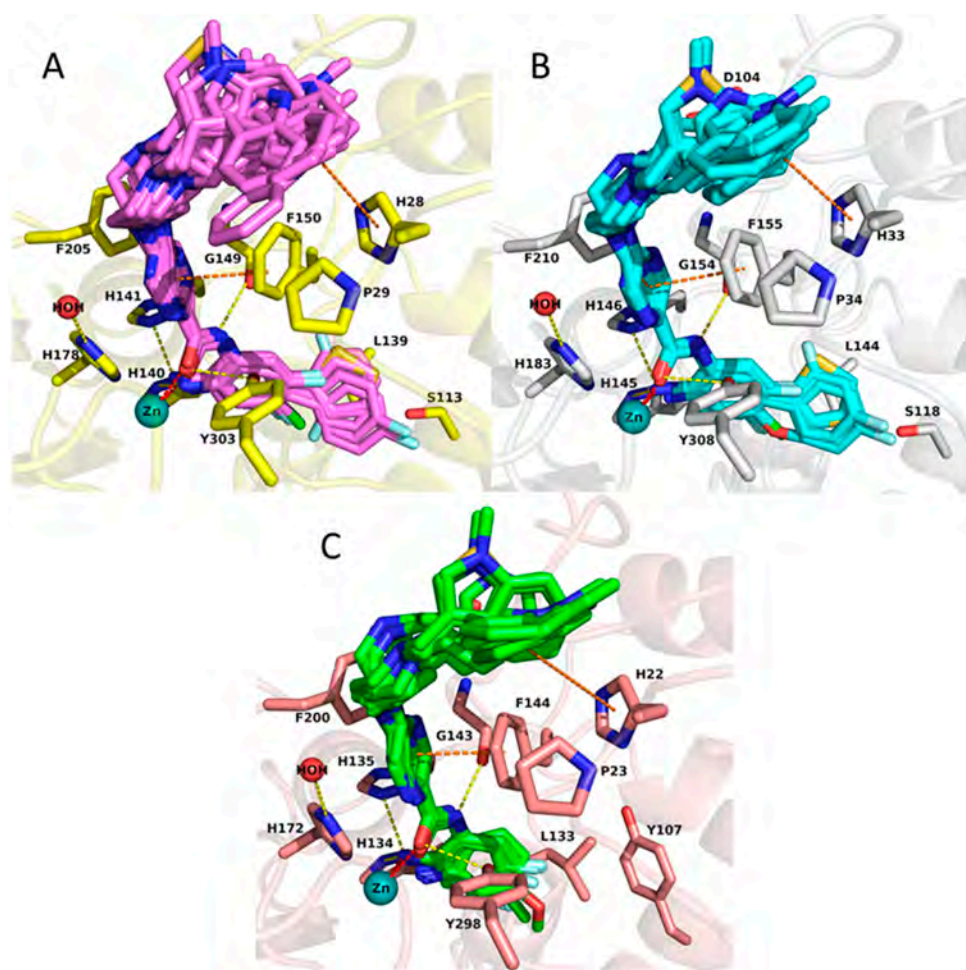
Figure 4. Docking poses of studied inhibitors having IC$_{50}$ values obtained for HDAC1 (**A**), HDAC2 (**B**), HDAC3 (**C**). The carbon atoms of the shown residues are colored as following: yellow in HDAC1, white in HDAC2 and salmon in HDAC3. Zinc ions are shown as cyan spheres, water molecules as red spheres. Inhibitors are shown in stick representation and their carbon atoms are colored pink, cyan and green in HDAC1, HDAC2 and HDAC3, correspondingly. Zinc coordination is shown as red dashed lines, hydrogen bonds as yellow, and aromatic interactions as orange.

Although the docking poses of the studied inhibitors were reasonable, a correlation between the docking scores and pIC_{50} was poor ($R^2 = 0.13$ for HDAC1, $R^2 = 0.11$ for HDAC2, $R^2 = 0.35$ for HDAC3). The correlation between the docking scores and pIC_{50} was computed using the QSAR tool in MOE program [34]. Due to the low correlation observed between docking scores and pIC_{50}, we decided to rescore the docking poses by means of binding free energy (BFE) calculations.

2.4. Rescoring of Docking Poses Using MM-GB/SA and MM-PB/SA

The total energy was calculated using six different parameter settings and six different frame settings (see Methods part for details). In total, 108 models (36 models for each protein) were established and evaluated by computing the correlation coefficient (R^2) between biological data and energy values (Figure 5). Only compounds that have measured IC_{50} values were considered (22 compounds for HDAC1, 23 compounds for HDAC2 and 22 compounds for HDAC3). Further details for established models are shown in Table S2.
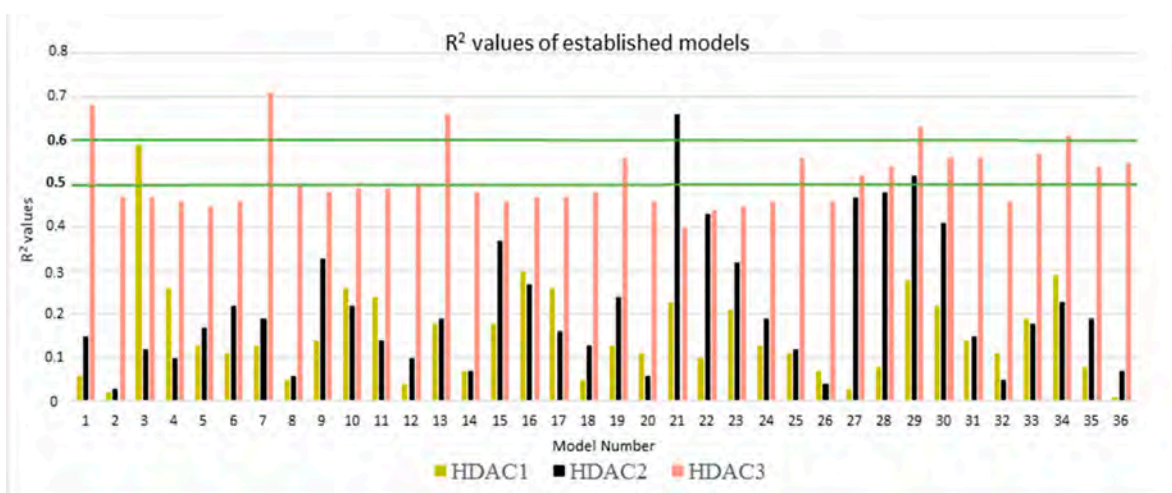
Figure 5. The R^2 values of established predictive models for HDAC1 (dark yellow bars), HDAC2 (black bars) and HDAC3 (salmon bars). Green lines represent the thresholds for model selection.

To evaluate the obtained models, first, the energy terms showing R^2 value less than 0.5 were skipped for HDAC1 and HDAC2. This threshold was increased to 0.6 for HDAC3 due to numerous good correlations for this isoform. In the next step, the leave-one-out cross-validation method was applied. The selected models were judged according to their R^2, RMSE (root mean square error), Q^2_{LOO} (leave-one-out cross-validation), and QMSE (crossed-root mean square error). The statistical parameters of the best models selected for each protein are viewed in Table 2. More details are given in Tables S3–S5.

Table 2. Best performing models of HDAC1, HDAC2 and HDAC3.

Protein	N	Model Number	Solvation Model	Frame	R^2	RMSE	Q^2LOO	QMSE
HDAC1	22	3	GB1	MD1-50	0.59	0.29	0.51	0.32
HDAC2	23	21	GB8	MD1-50	0.66	0.24	0.60	0.26
HDAC3	22	7	GB2	Emin1	0.71	0.29	0.65	0.32

R^2 (correlation coefficient), RMSE (root mean square error), Q^2_{LOO} (leave-one-out cross-validation), QMSE (crossed-root mean square error), Emin1 (single frame after the first energy minimization step), MD1-50 (average energy of every fifth frame between frame 1–50 during the MD simulation).

In the case of HDAC1, model 3 outperformed the other models by means of the R^2 value (Figure 5). This model was established using the total calculated energy from the GB1 model considering only frames 1–50 of the MD step. This model showed a correlation coefficient R^2 of 0.59 and an RMSE of 0.29. The cross-validation values calculated by using the leave-one-out method were calculated as Q^2_{LOO} 0.51 and QMSE 0.32 (Table 2). Among the established HDAC2 models, model 21 exhibited the highest R^2 value of 0.66 (Figure 5). Model 21 was established with the combination of the GB8 model and different intervals (frames 1–50) of the MD simulation. This model showed R^2 of 0.66, RMSE of 0.24, Q^2_{LOO} of 0.60 and QMSE of 0.26 (Table 2). During the analysis of the HDAC3 models, five models showing R^2 of more than 0.6 emerged (Figure 5). Based on the analysis of the R^2 and cross-validation results, we selected Model 7 with the lowest RMSE and QMSE values and highest R^2 and Q^2_{LOO} values (Table 2). Thus, out of the 108 developed models, three best-performing models (one best model per HDAC subtype) were selected based on their R^2, RMSE, Q^2_{LOO}, QMSE parameters. Their correlation plots are shown in Figure 6.
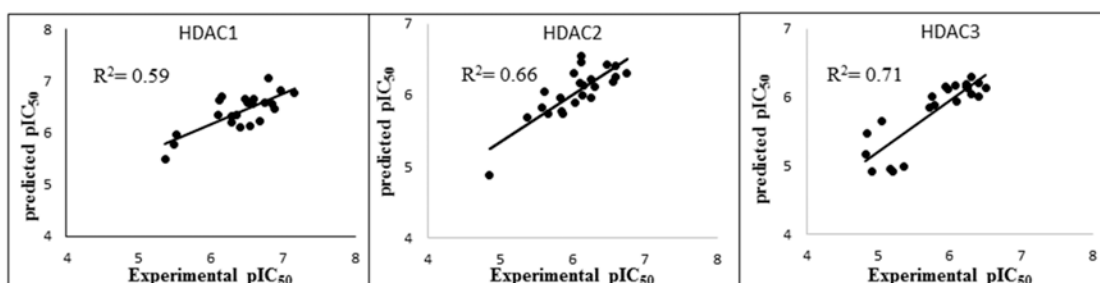
Figure 6. The correlation plots of the best binding free-energy models showing correlation between the predicted data and experimental data for each HDAC subtype.

In addition to the good correlation coefficients observed in the regression models, we noticed that the best models could discriminate the compounds in the training set (30 compounds) according to their activity. With IC_{50} cut off values of 1 µM, 1 µM and 2 µM for HDAC1, 2, and 3, respectively, models could separate highly active compounds from less active ones. For HDAC1, the BFE values of all the compounds showing IC_{50} less than 1 µM were calculated lower than −68.4 kcal/mol, and only one compound with non-determined IC_{50} value (19c) crossed this threshold with a BFE value of −68.9 kcal/mol (Table S3). For HDAC2 all compounds showing IC_{50}, less than 1 µM had calculated BFE values less than −110.2 kcal/mol and only two slightly less potent compounds 19m and 21a crossed this threshold (Table S4). For HDAC3, all compounds having IC_{50} less than 2 µM except 19i, 19l and 25b had calculated BFE values less than −55.4 kcal/mol, and only three compounds with non-determined IC_{50} values 19b, 19c and 19n crossed the threshold (Table S5). The discriminating power of the models is visualized in the box plots shown in Figure 7.
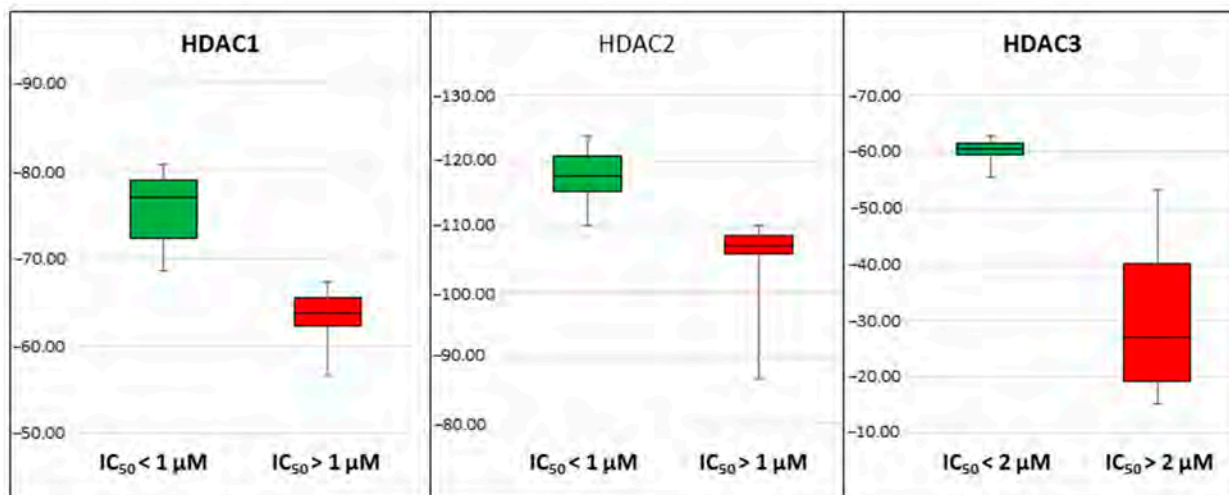
Figure 7. Box plots showing binding free-energy distributions (values given in kcal/mol) obtained for studied compounds.

2.5. Evaluation of Novel Designed HDAC1-2-3 Inhibitors

Novel derivatives of scaffold A, pyrimidine/pyrazine-piperazine scaffold, (30a, 30b, 30c and 30d) (Figure 8A, Table 3) were designed starting from the lead compound 29b in the training set in an attempt to improve selectivity for HDAC1 over HDAC2 and 3. Instead of the attachment of the long or bulky groups, a small methyl and acetyl group was added to increase the interaction with the residues at the rim of the pocket. In addition, the hydrophobicity of the secondary amine 29b was increased by the tertiary amine formation or conversion to an acetamido group.
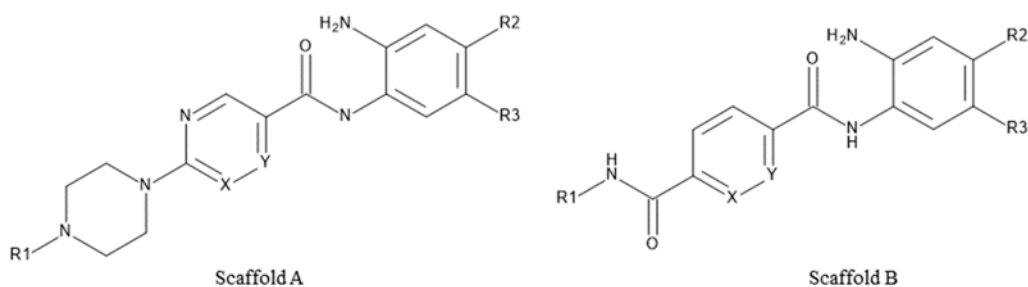
Figure 8. General structure of the test set molecules.

On the other hand, in an attempt to test the impact of an inverse amide combination with hydrophobic cap group on HDAC1, 2 and 3 inhibitory activity, compounds of scaffold B (31a, 31b, 31c, Figure 8B) were designed by combining structural features of 23a, the cocrystallized ligand in HDAC2 (PDB ID: 4LY1) and entinostat. Here, a fluoro-substituted 2-aminobenzamide moiety was chosen as a foot-pocket targeting scaffold, since it previously showed a favorable effect on HDAC3 selectivity. Additionally, a substituted inverse amide scaffold was chosen as a capping group.

The established best three models for HDAC1-3 were evaluated using this test set of novel derivatives in order to assess their reliability and predictive accuracy. The test set involved seven compounds having two scaffolds (Scaffold A and Scaffold B, Figure 8, Table 3).

Table 3. Structures of the novel inhibitors (test set).

Cpd. No.	Scaffold	Substituents				
		X	Y	R1	R2	R3
30a	A	N	CH	$-CH_3$	H	2-Thienyl
30b	A	CH	N	$-CH_3$	H	2-Thienyl
30c	A	CH	N	(acetyl)	H	2-Thienyl
30d	A	CH	N	(acetyl)	H	H
31a	B	CH	CH	(benzyl)	F	H
31b	B	CH	CH	(pyridinylmethyl)	F	H
31c	B	CH	CH	(pyridinylmethyl)	F	H

The chemical space of the test set was analyzed in a similar way as for the training set. The 2D and 3D distribution of the test set were shown in Figure 9. The designed compounds occupy the similar PCA space with the training set and homogeneously distributed within the PCA space.
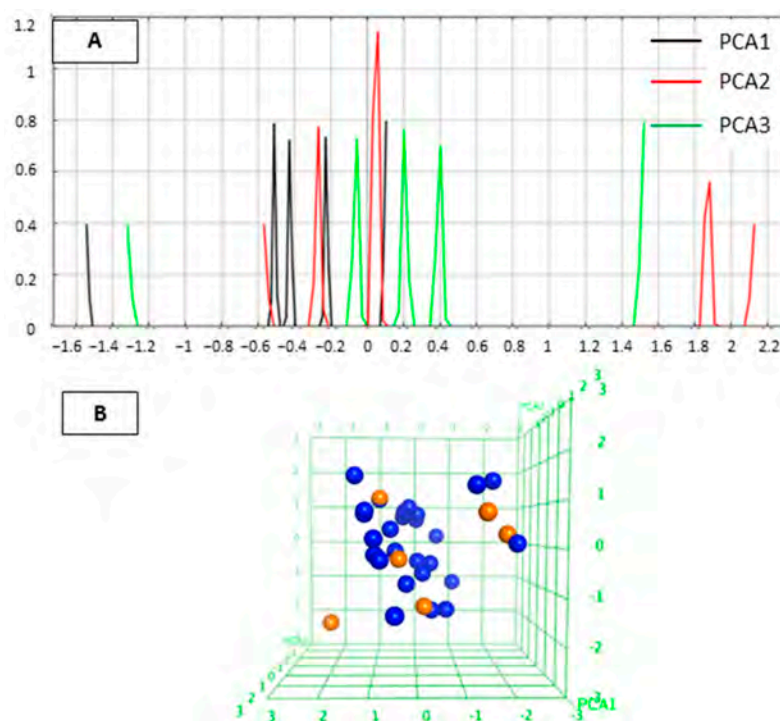
Figure 9. (**A**) 2D plots for visualization of the variation of three most important PCA in test set. Black color represents PCA1, red color PCA2 and green color PCA3. (**B**) 3D plot of the chemical space occupied by the training set (blue) and test set (orange).

First, the test set was docked to HDAC1-3 using the same protocol as for the training set. The expected binding modes, previously observed for reference compounds and compounds of the training set, were obtained for all compounds in HDAC1 and HDAC2, as well as for compounds 30d, 31a, 31b and 31c in HDAC3. Compounds having the 2-thienyl substituent at the foot pocket targeting group (30a, 30b, 30c) did not fit well into the pocket of HDAC3 due to the steric hindrance that is mentioned in Section 2.2. As an example, the docking pose of 30c in HDAC2 is shown in Figure 10. This compound chelated the zinc ion and established hydrogen bonds with H145, H146, Y308 and G154. The pyrimidine linker formed pi–pi interactions with F155 and F210 at the hydrophobic tunnel. Interestingly, the amide at scaffold B (31a, 31b and 31c), which is exemplified by the docking poses of 31a in Figure S5, lost the interaction with D99/104/93 in HDAC1/2/3, respectively, resulting in significantly reduced activity, although the aromatic cap group that was accommodated into hydrophobic tunnel consisted of F150/155/144, P29/34/23 and H28/33/22 in HDAC1/2/3, respectively.
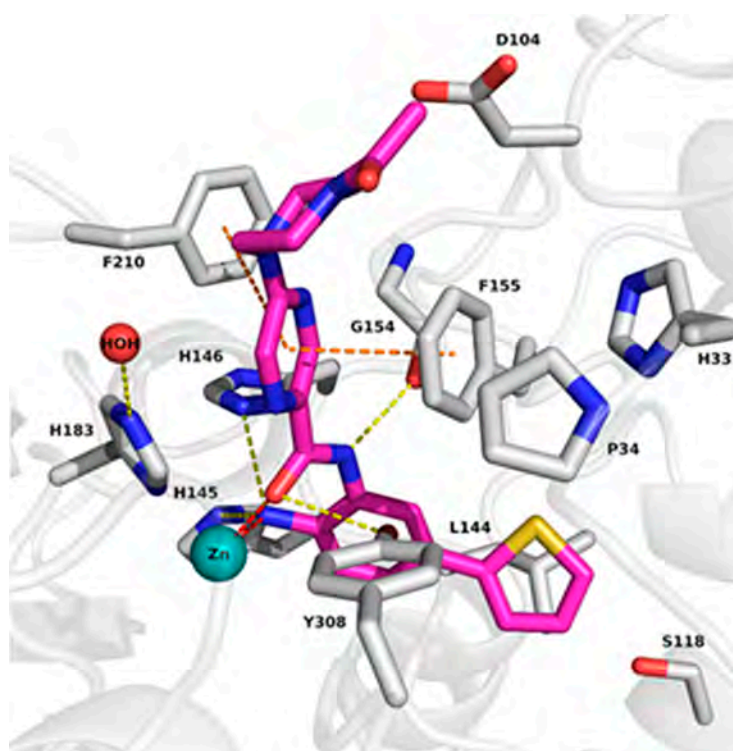
Figure 10. Docking pose of **30c** inHDAC2. The carbons of shown protein amino acid residues are white. Zinc ion is shown as cyan sphere, water molecule as red sphere, the ligand is shown in stick representation with magenta-colored carbon atoms. Zinc coordination is shown as red dashed lines, hydrogen bonds as yellow dashed lines and aromatic interactions as orange dashed lines.

The obtained docking poses were submitted to BFE calculations and the activities of the compounds were predicted using the three best models for HDAC1-3. The prediction results (Table 4, Tables S6–S8) demonstrated that the compounds in all HDAC isoforms can be correctly classified as active or weakly active/inactive taking into consideration the cutoff values established for the training set (see Section 2.4). The difference of experimental and predicted pIC_{50} was also less than <1.3 log units. Only compound 30b and 30c in HDAC1 and compound 30d in HDAC2 exhibited a bigger difference (>1 log unit) between predicted and experimentally observed pIC_{50} values, but still the compounds were correctly grouped into the activity class.

Table 4. Experimental and predicted activities (pIC$_{50}$ or inhibition percent at a given concentration) of the test set compounds against HDAC1-3s.

Cpd. No.	Scaffold	Experimental HDAC1 pIC$_{50}$	Predicted HDAC1 pIC$_{50}$)	Difference Experimental—Predicted HDAC1 pIC$_{50}$	Experimental HDAC2 pIC$_{50}$	Predicted HDAC2 pIC$_{50}$	Difference Experimental—Predicted HDAC2 pIC$_{50}$	Experimental HDAC3 pIC$_{50}$	Predicted HDAC3 pIC$_{50}$
30a	A	6.49	6.55	0.06	6.21	6.00	0.21	8% @1 µM 38% @10 µM	5.06
30b	A	7.40	6.31	1.09	6.10	6.24	0.14	6% @1 µM 35% @10 µM	5.01
30c	A	7.72	6.50	1.22	5.96	5.95	0.01	4% @1 µM 30% @10 µM	4.98
30d	A	5.72	5.70	0.02	4.62	5.89	1.27	15% @1 µM 72% @10 µM	5.98
31a	B	4% @1 µM 31% @10 µM	5.58		10% @1 µM 37% @10 µM	5.52		21% @1 µM 65% @10 µM	5.81
31b	B	0% @1 µM 27% @10 µM	5.77		13% @1 µM 30% @10 µM	5.29		19% @1 µM 59% @10 µM	5.80
31c	B	6% @1 µM 36% @10 µM	5.68		14% @1 µM 51% @10 µM	5.52		25% @1 µM 66% @10 µM	5.79

The compounds are correctly classed based on the BFE predicted activity group. Since only % inhibition was measured for the weakly active compounds from scaffold B, one can only constitute that it rightly predicts that the compounds are rather weakly active. It is not possible to deduce an IC$_{50}$ range based solely on the % inhibition data.

3. Discussion

In this study, we demonstrated that the binding free energy (BFE) calculations can be used as a post-docking filter for the docking poses derived from a dataset of 2-aminobenzamide derivatives tested against HDAC1-2-3. The different setups were used to estimate the binding free energies of the protein–ligand complexes.

Redocking and cross-docking studies were performed to find the most accurate docking setup. To test the ligand flexibility and stability of the protein-inhibitor complexes we ran in addition 100 ns MD simulations. The predicted ligand-binding mode was stable and the initial ligand–protein interactions were retained throughout the whole simulation time, except for one hydrogen bond interaction with the catalytic tyrosine (Y303, Y308, Y298 in HDAC1/2/3, respectively). The increased flexibility of the catalytic tyrosine was observed in all cases. Interestingly, the conformational flexibility of the catalytic tyrosine was also reported in other HDAC2 X-ray structures in complex with a 2-substituted benzamide (PDB ID: 7KBH [35]). It might be possible that this conformational flexibility of the catalytic tyrosine can be utilized to design 6-substituted 2-aminobenzamide derivatives with pronounced selectivity in future studies.

In the second part of the study, the docking protocols for each enzyme were defined by applying the redocking and crossdocking studies. The determined docking protocols were used to understand the binding mode of the studied inhibitors. Although the docking poses correspond to the experimentally observed binding modes of similar inhibitors, the obtained docking scores unfortunately did not give a significant correlation with the experimental activities.

In the last step, the selected docking poses were rescored by performing the GPU-based binding free-energy calculations with different setups. The MM-GB/SA and MM-PB/SA values were analyzed to test whether BFE results correctly rank the compounds according to their experimental activities. Leave-one-out cross-validation studies were performed to find the best model that can explain the activity in terms of energy. We found that different energy terms gave good correlation with the biological activity in different isoforms. GB1 model and 50 frames derived from short MD for HDAC1, GB8 model and 50 frames derived from short MD for HDAC2 and GB2 model after the first minimization for HDAC3 were chosen as the best models based on the computed R^2, RMSE, Q^2_{LOO} and

QMSE values. Additionally, the chosen models discriminated the compounds according to their activity. The rescoring of the docking poses using the GPU-based binding free energy calculations demonstrated better agreement with the experimental activity than the docking scores. The chosen models were evaluated by utilizing the test set. The selected models discriminated the inhibitors well into more active and less active, and predicted their experimentally observed activity values with high accuracy for the compounds with scaffold A. In the case of compounds with scaffold B, the model predicted them to be less active with pIC_{50} values below 6.0. Since we did not determine the exact IC_{50} value for these less-active inhibitors, a quantitative analysis of the prediction accuracy was not possible. The determined percentage of inhibition at 1 and 10 µM suggests that the compounds are active in the single-digit micromolar range and therefore less interesting. In general, the developed rescoring models can be used as primary filters to identify the most promising compounds for synthesis and in vitro testing.

4. Materials and Methods

4.1. Training Set and Diversity Analysis

The ligand data include 30 compounds recently synthesized in our group and tested against human HDAC1-3 [25]. Their chemical structures are listed in Table 1. The same numbering system was used to name the compounds as shown in the original publication by Ibrahim et al. [25]. The dataset was prepared using the Ligprep tool in Schrödinger suite with default settings [36]. Subsequently, the output of the ligand preparation step was subjected to the confgen tool [36] for the conformational enrichment by generating 64 conformers per each ligand where the output conformers were finally minimized using the OPLS3e force field [37]. Conformational enrichment is crucial to enhance the possibility to find the most likely docking poses.

The diversity of the compounds determines the limitations of the quantitative structure–activity relationship (QSAR) model. To understand the applicability domain of the studied molecules, we analyzed the most important three principal components using the principal component analysis (PCA) [38] implemented in MOE [34]. The various 2D descriptors, including number of H-bond acceptor atoms (a_acc), number of rotatable single bonds (b_1rotN), number of aromatic bonds (b_ar), total polar van der Waals surface area (PEOE_VSA_POL), logarithmic octanol/water partition coefficient (logP (o/w)), were calculated in MOE. The important descriptors that show no correlation between descriptors were selected using the Contingency module in MOE. The selected descriptors (a_acc, b_1rotN, b_ar, PEOE_VSA_POL, logP(o/w)) were applied for linear transformation by PCA. The first three principal components can explain about 100 % variation of the original space. Then, the selected first three components were used to establish a plot showing the distribution of the studied molecules.

4.2. Preparation of Protein-Inhibitor Complexes

X-ray crystal structures of HDAC1 (PDB ID: 4BKX [31]), HDAC2 (PDB ID: 3MAX, 4LY1, 5IX0, 5IWG [12–14]) and HDAC3 (PDB ID: 4A69 [33]) were downloaded from the Protein Data Bank (PDB, rcsb.org, [39]) and analyzed in MOE. The complex of HDAC2 with an inhibitor having 2-aminobenzamide scaffold (PDB ID: 4LY1, [13]) was chosen for further investigations due to the ligand's similarity to studied compounds and good cross-docking results (Table S1). Since no crystal structure is available for the complex of HDAC1 with a 2-aminobenzamide derivative, the available crystal structure of this isoform was minimized with the ligand taken from HDAC2 to imitate induced fit effect. On the other hand, the same ligand shows no activity on HDAC3 [13]. Hence, the selective HDAC3 inhibitor BG45 was chosen and minimized with HDAC3 due to its similarity to the synthesized compounds [32]. Subsequently, protein structures were prepared using the protein preparation wizard of Schrödinger suite [36]. Hydrogen bonds and missing side chains were automatically added, and bond orders were assigned. The solvent molecules (except one conserved water molecule W617) and ions (except the catalytic Zn^{+2} ion) were

removed. The protonation states at pH 7.4 and residue tautomers were optimized. Then, protein–ligand complexes were minimized using the OPLS3e force-field to remove steric clashes [37].

To check the stability of the generated complexes, 100 ns MD simulations were performed. It revealed that the protein, ligand and zinc ion were stable during the whole 100 ns simulation. Although the amide cap group of the ligand in HDAC1 and HDAC2 caused small fluctuation more than 2 Å, the other components of the ligand (ZBG, foot pocket group, linker group) were stable. In addition, the bidentate zinc coordination between zinc and ligand were conserved during 100 ns simulation (Figures S2–S4).

4.3. Molecular Docking

Docking studies were performed using Glide in Schrödinger Suite [36]. The active site of the proteins was defined with 10 Å radius grid box around the ligand. Standard precision (SP) mode was applied for docking. Ten docking poses were subjected for further post-docking minimization. The other settings were used as default. The docking results were visually analyzed in MOE program [34]. Before docking the novel inhibitors, we evaluated the accuracy of the docking setup by performing redocking and cross-docking of ligands from HDAC2 crystal structures (PDB IDs 3MAX, 4LY1, 5IWG and 5IX0). The docking protocol showed low RMSD values in the range between 0.2 and 1.1 Å, demonstrating that the protocol is appropriate for these proteins and ligands. In addition, molecular docking studies of the synthesized compounds were also performed for HDAC1 and HDAC3.

4.4. Molecular Dynamics (MD) Simulations

GPU-based MD simulations were performed using AMBER16 [40]. Each ligand was prepared in Antechamber module utilizing the semi-empirical Austin Model1 with bond charge correction (AM1-BCC) [41,42]. In addition, atom types and bond types were assigned, and residue topology files were generated. Then, protein–ligand complexes were prepared using the tLEaP module of AMBER. General amber force field (GAFF) and the Duan force field (ff03.r1) were used for ligand and protein, respectively [43–45]. The prepared protein–ligand complexes were solvated by TIP3P solvation model, and a margin of 10 Å. Moreover, the 12-6-4LJ ionic model was applied for the zinc ion [46]. Two minimization steps including the two substeps in each minimization were done. In the first step, 4000 iterations (2000 cycles of steepest descent and then 2000 conjugate gradient) were performed by restraining the protein residues, ligand and water molecules to their initial geometries (force constant of 10 kcal $\times$ mol^{-1} $\times$ Å^{-2}) to relieve the bad contacts. In the second step, 4000 iterations (2000 cycles of steepest descent and then 2000 conjugate gradient) without restraints were applied to remove the steric clashes in the entire complex. Then, the system was heated at 300 K through 100 ps of MD while restraining the protein–ligand complex (force constant of 10 kcal $\times$ mol^{-1} $\times$ Å^{-2}). The system was equilibrated with a period of 200 ps. Afterwards, a 1 ns (or 100 ns for initial complexes) MD simulation was run with a time step of 2 fs. Through the equilibration and MD step, the entire complex was kept at 300 K by the Langevin thermostat dynamics using the collision frequency of 2 ps [47]. The pressure of the system was maintained at 1 bar using isotropic pressure scaling with a relaxation time of 2 ps. A nonbonded cut-off distance was 10 Å. The particle mesh Ewald (PME) method was applied to calculate the full electrostatic energy of the system [48,49]. The SHAKE algorithm was utilized to constrain all bonds involving hydrogens [50]. Finally, after the MD job, the third energy minimization with 4000 iterations (2000 cycles of steepest descent and then 2000 conjugate gradient) was performed. The CPPTRAJ module of AMBER was used to analyze the MD snapshots.

4.5. Binding Free Energy (BFE) Calculations

The protein–ligand complexes were prepared as described in Section 4.2. Binding free energy (BFE) calculations were done for the docked inhibitors against HDAC1/2/3 in AMBER16 program [40]. The MMPBSA.py script was used for BFE calculations. Different

radii sets (GB ^{HCT} (igb = 1), GB ^{OBC} (igb = 2), GB ^{OBC2} (igb = 5), and GBn (igb = 8) as well as PB_mbondi (mbondi) and PB_parse (parse) were tested [51–55]. The MM-GB(PB)/SA methods combine molecular mechanics and solvent models. In addition, six different methods listed were considered to analyze the results: (1) single frame at the first minimization step (Emin1), (2) single frame at the second minimization step (Emin2), (3) single frame at the third minimization after MD (Emin3), (4) frames 1–50 during MD (MD-1) with an interval of 5, (5) frames 51–100 during MD with an interval of 5 (MD-2), (6) frames 101–500 with an interval of 5 during MD (MD-3).

The binding free energies of protein–ligand complexes can be obtained from the difference between complex energy and the sum of the protein and ligand components (Equation (1)) [22].

$$\Delta G_{bind} = G_{complex} - (G_{protein} + G_{ligand}) \tag{1}$$

The binding free energies in Equation (1) can be obtained as the sum of the gas phase energy (E_{MM}), free solvation enegies (ΔG_{sol}) and entropy ($-T\Delta S$) (Equation (2)) [56].

$$G_{molecule} = E_{MM} + \Delta G_{sol} - T\Delta S \tag{2}$$

The molecular mechanics energy (E_{MM}) is calculated as the sum of E_{int} (internal), E_{ele} (electrostatic), E_{vdw} (van der Waals). The internal energies (E_{int}) calculate the bond, angle and dihedral energies, while the electrostatic energies (E_{ele}) take into account the interactions between atoms occurring as a result of positive and negative atomic charges. Van der Waals (E_{vdw}) interactions were calculated taking into account the interactions among atoms. Solvation energies are the sum of polar solvent contributions ($G_{PB/GB}$) and nonpolar solvent contributions (G_{SA}) (Equation (3)).

$$\Delta G_{bind} = (E_{int} + E_{ele} + E_{vdw}) + (\Delta G_{PB/GB} + \Delta G_{SA}) - T\Delta S \tag{3}$$

The conformational entropy change ($-T\Delta S$) is often considered to determine the total binding free energies. The absolute temperature is expressed as T and entropy of the molecule as S. However, including the entropy changes to the BFE calculation increases the computational cost, and does not always improve the accuracy of the calculation [22,57]. Hence, the conformational entropy change was not included to the calculation. Only enthalpy values (ΔH) were considered to find the correlation between binding enthalpies and biological data (Equation (4)).

$$\Delta H = (E_{MM}) + (\Delta G_{sol}) \tag{4}$$

To evaluate models, the R^2 values of the each energy terms against biological data were computed by the Contingency tool in MOE [34].

4.6. Test Set

The external test data included seven newly designed and synthesized compounds that were tested against human HDAC1-3. They were used to explore the reliability and predictive power of the selected QSAR models for HDAC1-3. Their chemical structures are listed in Figure 8 and Table 3. The test dataset was prepared using the same settings as mentioned in Section 4.1.

4.7. Experimental Data of the Synthesized Compounds

All the experimental methods and analytical data for the newly synthesized inhibitors are provided in the Supplementary Materials (p. S24, Scheme SI and SII, [25]).

4.8. Biological Assay of the Synthesized Compounds

HDAC1, 2, 3 inhibitory activity for the novel inhibitors was performed as previously reported [25]. To keep the test number small, we applied a two-step screening. In a first screening, the % inhibition values for two concentrations (1 and 10 μM) were determined for

all compounds. We then generated the exact IC_{50} value only for the most potent inhibitors in the training and test set with % of inhibition at 1μM above 50%.

A fluorogenic peptide derived from p53 (Ac-RHKK(Acetyl)-AMC) was used as substrate. The measurements were performed in an assay buffer (50 mM Hepes, 150 mM NaCl, 5 mM $MgCl_2$, 1 mM TCEP and 0.2 mg/mL BSA, pH 7.4 adjusted with NaOH) at 37 °C. Inhibitors at different concentrations were incubated with 10 nM HDAC1, 3 nM HDAC2 or 3 nM HDAC3 (final concentration) for at least 5 min. The reaction was started with the addition of the fluorogenic substrate (20 μM final concentration) and incubated for 30 min for HDAC2 and HDAC3 and 90 min for HDAC1. The reaction was stopped with a solution of 1 mg/mL trypsin in 1 mM HCl and incubated for 1 h at 37 °C. The fluorescence intensity was recorded with an Envision 2104 Multilabel Plate Reader (PerkinElmer, Waltham, MA) with an excitation wavelength of 380 ± 8 nm and an emission wavelength of 430 ± 8 nm. The received fluorescence intensities were normalized with uninhibited reaction as 100% and the reaction without enzyme as 0%. A nonlinear regression analysis was done to determine the IC_{50} value.

Supplementary Materials: The following supporting information can be downloaded at: https://www.mdpi.com/article/10.3390/molecules27082526/s1, Figure S1: Comparison of the redocking results for HDAC2 X-rays in complex with inhibitors, Figure S2: 100 ns MD results for the HDAC1-inhibitor complex, Figure S3: 100 ns MD results for the HDAC2-inhibitor complex, Figure S4: 100 ns MD results for the HDAC3-inhibitor complex, Figure S5: Docking poses of 31a in HDAC2, Table S1: RMSD results taken from the cross-docking, Table S2: R^2 values of all models generated for HDAC1, HDAC2 and HDAC3, Table S3: The docking scores, binding free energy results of the best model and in vitro data in HDAC1, MODEL 3, Table S4: The docking scores, binding free energy results of the best model and in vitro data in HDAC2, MODEL21, Table S5: The docking scores, binding free energy results of the best model and in vitro data in HDAC3, MODEL7, Table S6: The docking scores, binding free energy results, and prediction results of the test set in HDAC1, Table S7: The docking scores, binding free energy results, and prediction results of the test set in HDAC2, Table S8: The docking scores, binding free energy results, and prediction results of the test set in HDAC3, p. S14: Synthetic methods [25]

Author Contributions: E.F.B. did the docking, molecular dynamic simulations and binding free calculations and wrote the manuscript. J.M. supervised the docking experiments and revised the manuscript. H.S.I., A.V. and M.A. synthesized the tested inhibitors. M.Z. carried out the enzymatic HDAC testing. D.R. carried out the MD simulations and revised the manuscript. M.S. and W.S. designed and supervised the synthesis and experiments and wrote the manuscript. All authors have read and agreed to the published version of the manuscript.

Institutional Review Board Statement: Not applicable.

Informed Consent Statement: Not applicable.

Data Availability Statement: Not applicable.

Conflicts of Interest: The authors declare no conflict of interest.

Sample Availability: Not applicable.

References

1. Keating, S.T.; Plutzky, J.; El-Osta, A. Epigenetic Changes in Diabetes and Cardiovascular Risk. *Circ. Res.* **2016**, *118*, 1706–1722. [CrossRef] [PubMed]
2. Goldberg, A.D.; Allis, C.D.; Bernstein, E. Epigenetics: A landscape takes shape. *Cell* **2007**, *128*, 635–638. [CrossRef] [PubMed]

3. Navarro Quiroz, E.; Chavez-Estrada, V.; Macias-Ochoa, K.; Ayala-Navarro, M.F.; Flores-Aguilar, A.S.; Morales-Navarrete, F.; de la Cruz Lopez, F.; Gomez Escorcia, L.; Musso, C.G.; Aroca Martinez, G.; et al. Epigenetic Mechanisms and Posttranslational Modifications in Systemic Lupus Erythematosus. *Int. J. Mol. Sci.* **2019**, *20*, 5679. [CrossRef] [PubMed]
4. Felice, C.; Lewis, A.; Armuzzi, A.; Lindsay, J.O.; Silver, A. Review article: Selective histone deacetylase isoforms as potential therapeutic targets in inflammatory bowel diseases. *Aliment. Pharmacol. Ther.* **2015**, *41*, 26–38. [CrossRef]
5. Micelli, C.; Rastelli, G. Histone deacetylases: Structural determinants of inhibitor selectivity. *Drug Discov. Today* **2015**, *20*, 718–735. [CrossRef]
6. 6. Melesina, J.; Simoben, C.V.; Praetorius, L.; Bülbül, E.F.; Robaa, D.; Sippl, W. Strategies To Design Selective Histone Deacetylase Inhibitors. *ChemMedChem* **2021**, *16*, 1336–1359. [CrossRef]
7. Ning, Z.Q.; Li, Z.; Newman, M.J.; Shan, S.; Wang, X.; Pan, S.; Zhang, J.; Dong, M.; Du, X.; Lu, X. Chidamide (CS055/HBI-8000): A new histone deacetylase inhibitor of the benzamide class with antitumor activity and the ability to enhance immune cell-mediated tumor cell cytotoxicity. *Cancer Chemother. Pharmacol.* **2012**, *69*, 901–909. [CrossRef]
8. Dong, M.; Ning, Z.; Xing, P.; Xu, J.; Cao, H.; Dou, G.; Meng, Z.; Shi, Y.; Lu, X.; Feng, F. Phase I study of chidamide (CS055/HBI-8000), a new histone deacetylase inhibitor, in patients with advanced solid tumors and lymphomas. *Cancer Chemother. Pharmacol.* **2012**, *69*, 1413–1422. [CrossRef]
9. Atadja, P. Development of the pan-DAC inhibitor panobinostat (LBH589): Successes and challenges. *Cancer Lett.* **2009**, *280*, 233–241. [CrossRef]
10. Ito, T.; Ouchida, M.; Morimoto, Y.; Yoshida, A.; Jitsumori, Y.; Ozaki, T.; Sonobe, H.; Inoue, H.; Shimizu, K. Significant growth suppression of synovial sarcomas by the histone deacetylase inhibitor FK228 in vitro and in vivo. *Cancer Lett.* **2005**, *224*, 311–319. [CrossRef]
11. Kijima, M.; Yoshida, M.; Sugita, K.; Horinouchi, S.; Beppu, T. Trapoxin, an antitumor cyclic tetrapeptide, is an irreversible inhibitor of mammalian histone deacetylase. *J. Biol. Chem.* **1993**, *268*, 22429–22435. [CrossRef]
12. Wagner, F.F.; Weïmer, M.; Steinbacher, S.; Schomburg, A.; Reinemer, P.; Gale, J.P.; Campbell, A.J.; Fisher, S.L.; Zhao, W.; Reis, S.A.; et al. Kinetic and structural insights into the binding of histone deacetylase 1 and 2 (HDAC1, 2) inhibitors. *Bioorg. Med. Chem.* **2016**, *24*, 4008–4015. [CrossRef]
13. Lauffer, B.E.; Mintzer, R.; Fong, R.; Mukund, S.; Tam, C.; Zilberleyb, I.; Flicke, B.; Ritscher, A.; Fedorowicz, G.; Vallero, R.; et al. Histone deacetylase (HDAC) inhibitor kinetic rate constants correlate with cellular histone acetylation but not transcription and cell viability. *J. Biol. Chem.* **2013**, *288*, 26926–26943. [CrossRef] [PubMed]
14. Bressi, J.C.; Jennings, A.J.; Skene, R.; Wu, Y.; Melkus, R.; Jong, R.D.; O'Connell, S.; Grimshaw, C.E.; Navre, M.; Gangloff, A.R. Exploration of the HDAC2 foot pocket: Synthesis and SAR of substituted N-(2-aminophenyl)benzamides. *Bioorg. Med. Chem. Lett.* **2010**, *20*, 3142–3145. [CrossRef] [PubMed]
15. Wang, D.F.; Wiest, O.; Helquist, P.; Lan-Hargest, H.; Wiech, L.N. On the function of the 14 A long internal cavity of histone deacetylase-like protein: Implications for the design of histone deacetylase inhibitors. *J. Med. Chem.* **2004**, *47*, 3409–3417. [CrossRef] [PubMed]
16. Durrant, J.D.; McCammon, J.A. Molecular dynamics simulations and drug discovery. *BMC Biol.* **2011**, *9*, 71. [CrossRef]
17. Armen, R.S.; Chen, J.; Brooks, C.L., 3rd. An Evaluation of Explicit Receptor Flexibility in Molecular Docking Using Molecular Dynamics and Torsion Angle Molecular Dynamics. *J. Chem. Theory Comput.* **2009**, *5*, 2909–2923. [CrossRef]
18. Moitessier, N.; Englebienne, P.; Lee, D.; Lawandi, J.; Corbeil, C.R. Towards the development of universal, fast and highly accurate docking/scoring methods: A long way to go. *Br. J. Pharmacol.* **2008**, *153* (Suppl. 1), S7–S26. [CrossRef]
19. Gilson, M.K.; Zhou, H.X. Calculation of protein-ligand binding affinities. *Annu. Rev. Biophys. Biomol. Struct.* **2007**, *36*, 21–42. [CrossRef]
20. Warren, G.L.; Andrews, C.W.; capelli, A.; Clarke, B.; Lalonde, J.; Lambert, M.H.; Lindvall, M.; Nevins, N.; Semus, S.F.; Senger, S.; et al. A critical assessment of docking programs and scoring functions. *J. Med. Chem.* **2006**, *49*, 5912–5931. [CrossRef]
21. Sherman, W.; Day, T.; Jacobson, M.P.; Friesner, R.A.; Farid, R. Novel procedure for modeling ligand/receptor induced fit effects. *J. Med. Chem.* **2006**, *49*, 534–553. [CrossRef] [PubMed]
22. Karaman, B.; Sippl, W. Docking and binding free energy calculations of sirtuin inhibitors. *Eur. J. Med. Chem.* **2015**, *93*, 584–598. [CrossRef] [PubMed]
23. Cournia, Z.; Allen, B.; Sherman, W. Relative Binding Free Energy Calculations in Drug Discovery: Recent Advances and Practical Considerations. *J. Chem. Inf. Model.* **2017**, *57*, 2911–2937. [CrossRef]
24. Genheden, S.; Ryde, U. The MM/PBSA and MM/GBSA methods to estimate ligand-binding affinities. *Expert Opin. Drug Discov.* **2015**, *10*, 449–461. [CrossRef] [PubMed]
25. Ibrahim, H.S.; Abdelsalam, M.; Zeyn, Y.; Zessin, M.; Mustafa, A.-H.M.; Fischer, M.A.; Zeyen, P.; Sun, P.; Bülbül, E.F.; Vecchio, A.; et al. Synthesis, Molecular Docking and Biological Characterization of Pyrazine Linked 2-Aminobenzamides as New Class I Selective Histone Deacetylase (HDAC) Inhibitors with Anti-Leukemic Activity. *Int. J. Mol. Sci.* **2022**, *23*, 369. [CrossRef] [PubMed]
26. Simoben, C.V.; Ghazy, E.; Zeyen, P.; Darwish, S.; Schmidt, M.; Romier, C.; Robaa, D.; Sippl, W. Binding Free Energy (BFE) Calculations and Quantitative Structure–Activity Relationship (QSAR) Analysis of *Schistosoma mansoni* Histone Deacetylase 8 (*sm*HDAC8) Inhibitors. *Molecules* **2021**, *26*, 2584. [CrossRef]

27. Slynko, I.; Schmidtkunz, K.; Rumpf, T.; Klaeger, S.; Heinzlmeir, S.; Najar, A.; Metzger, E.; Kuster, B.; Schüle, R.; Jung, M.; et al. Identification of Highly Potent Protein Kinase C-Related Kinase 1 Inhibitors by Virtual Screening, Binding Free Energy Rescoring, and in vitro Testing. *ChemMedChem* **2016**, *11*, 2084–2094. [CrossRef]

28. Wichapong, K.; Rohe, A.; Platzer, C.; Slynko, I.; Erdrmann, F.; Schmidt, M.; Sippl, W. Application of Docking and QM/MM-GBSA Rescoring to Screen for Novel Myt1 Kinase Inhibitors. *J. Chem. Inf. Model.* **2014**, *54*, 881–893. [CrossRef]

29. Brandmaier, S.; Novotarskyi, S.; Sushki, I.; Tetko, I.V. From descriptors to predicted properties: Experimental design by using applicability domain estimation. *Altern. Lab. Anim.* **2013**, *41*, 33–47. [CrossRef]

30. Netzeva, T.I.; Worth, A.P.; Aldenberg, T. Current status of methods for defining the applicability domain of (quantitative) structure-activity relationships. The report and recommendations of ECVAM Workshop 52. *Altern. Lab. Anim.* **2005**, *33*, 155–173. [CrossRef]

31. *Schrödinger Release 2019-1*; Schrödinger LLC: New York, NY, USA, 2019; Available online: https://www.schrodinger.com/platform#product-list-collapse (accessed on 1 February 2022).

32. Harder, E.; Damm, W.; Maple, J.; Wu, C.; Reboul, M.; Xiang, J.Y.; Wang, K.; Lupyan, D.; Dahigren, M.K.; Knight, J.L.; et al. OPLS3: A Force Field Providing Broad Coverage of Drug-like Small Molecules and Proteins. *J. Chem. Theory Comput.* **2016**, *12*, 281–296. [CrossRef] [PubMed]

33. Millard, C.J.; Watson, P.J.; Celardo, I.; Gordiyenko, Y.; Cowley, S.M.; Robinson, C.V.; Fairall, L.; Schwabe, J.W.R. Class I HDACs share a common mechanism of regulation by inositol phosphates. *Mol. Cell* **2013**, *51*, 57–67. [CrossRef] [PubMed]

34. Watson, P.J.; Fairall, L.; Santos, G.M.; Schwabe, J.W.R. Structure of HDAC3 bound to co-repressor and inositol tetraphosphate. *Nature* **2012**, *481*, 335–340. [CrossRef] [PubMed]

35. Berman, H.M.; Westbrook, J.; Feng, Z.; Gilliland, G.; Bhat, T.N.; Weissig, H.; Shindyalov, I.N.; Bourne, P.E. The Protein Data Bank. *Nucleic Acids Res.* **2000**, *28*, 235–242. [CrossRef] [PubMed]

36. *Molecular Operating Environment (MOE)*; Chemical Computing Group (CCG): Montreal, QC, Canada, 2012; Available online: https://www.chemcomp.com/Products.htm (accessed on 1 February 2022).

37. Minami, J.; Suzuki, R.; Mazitschek, R.; Gorgun, G.; Ghosh, B.; Cirstea, D.; Hu, Y.; Mimura, N.; Ohguchi, H.; Cottini, F.; et al. Histone deacetylase 3 as a novel therapeutic target in multiple myeloma. *Leukemia* **2014**, *28*, 680–689. [CrossRef]

38. Song, L.F.; Lee, T.-S.; Zhu, C.; York, D.M.; Merz, K.M., Jr. Using AMBER18 for Relative Free Energy Calculations. *J. Chem. Inf. Model.* **2019**, *59*, 3128–3135. [CrossRef]

39. Jakalian, A.; Jack, D.B.; Bayly, C.I. Fast, efficient generation of high-quality atomic charges. AM1-BCC model: II. Parameterization and validation. *J. Comput. Chem.* **2002**, *23*, 1623–1641. [CrossRef]

40. Jakalian, A.; Jack, D.B.; Bayly, C.I. Fast, efficient generation of high-quality atomic charges. AM1-BCC model: I. Method. *J. Comput. Chem.* **2000**, *21*, 132–146. [CrossRef]

41. Wang, J.; Wolf, R.M.; Caldwell, J.W.; Kollman, P.A.; Case, D.A. Development and testing of a general amber force field. *J. Comput. Chem.* **2004**, *25*, 1157–1174. [CrossRef]

42. Lee, M.C.; Duan, Y. Distinguish protein decoys by using a scoring function based on a new AMBER force field, short molecular dynamics simulations, and the generalized born solvent model. *Proteins* **2004**, *55*, 620–634. [CrossRef]

43. Duan, Y.; Wu, C.; Chowdhury, S.; Lee, M.C.; Xiong, G.; Zhang, W.; Yang, R.; Cieplak, P.; Luo, R.; Lee, T.; et al. A point-charge force field for molecular mechanics simulations of proteins based on condensed-phase quantum mechanical calculations. *J. Comput. Chem.* **2003**, *24*, 1999–2012. [CrossRef] [PubMed]

44. Li, P.; Song, L.F.; Merz, K.M., Jr. Parameterization of highly charged metal ions using the 12-6-4 LJ-type nonbonded model in explicit water. *J. Phys. Chem. B* **2015**, *119*, 883–895. [CrossRef] [PubMed]

45. Pastor, R.W.; Brooks, B.R.; Szabo, A. An analysis of the accuracy of Langevin and molecular dynamics algorithms. *Mol. Phys.* **1988**, *65*, 1409–1419. [CrossRef]

46. Sagui, C.; Pedersen, L.G.; Darden, T.A. Towards an accurate representation of electrostatics in classical force fields: Efficient implementation of multipolar interactions in biomolecular simulations. *J. Chem. Phys.* **2004**, *120*, 73–87. [CrossRef] [PubMed]

47. Toukmaji, A.; Sagui, C.; Boar, J.; Datden, T. Efficient particle-mesh Ewald based approah to fixed and induced dipolar interactions. *J. Chem. Phys.* **2000**, *113*, 10913. [CrossRef]

48. Ryckaert, J.P.; Ciccotti, G.; Berendsen, H.J.C. Numerical integration of the cartesan equations of motion of a system with constraints: Molecular dynamics of n-alkanes. *J. Comput. Phys.* **1977**, *23*, 327–341. [CrossRef]

49. Mongan, J.; Simmerling, C.; McCammon, A.; Case, D.A.; Onufriev, A. Generalized Born model with a simple, robust molecular volume correction. *J. Chem. Theory Comput.* **2007**, *3*, 156–169. [CrossRef]

50. Onufriev, A.; Bashford, D.; Case, D.A. Exploring protein native states and large-scale conformational changes with a modified generalized born model. *Proteins* **2004**, *55*, 383–394. [CrossRef]

51. Feig, M.; Onufriev, A.; Lee, M.S.; Case, D.A.; Brooks, C.L. Performance comparison of generalized born and Poisson methods in the calculation of electrostatic solvation energies for protein structures. *J. Comput. Chem.* **2004**, *25*, 265–284. [CrossRef]

52. Hawkins, G.D.; Cramer, C.J.; Truhlar, D.G. Parametrized Models of Aqueous Free Energies of Solvation Based on Pairwise Descreening of Solute Atomic Charges from a Dielectric Medium. *J. Phys. Chem.* **1996**, *100*, 19824–19839. [CrossRef]

53. Hawkins, G.D.; Cramer, C.J.; Truhlar, D.G. Pairwise solute descreening of solute charges from a dielectric medium. *Chem. Phys. Lett.* **1995**, *246*, 122–129. [CrossRef]

54. Kollman, P.A.; Massova, I.; Reyes, C.; Kuhn, B.; Huo, S.; Chong, L.; Lee, M.; Lee, T.; Duan, Y.; Wang, W.; et al. Calculating structures and free energies of complex molecules: Combining molecular mechanics and continuum models. *Acc. Chem. Res.* **2000**, *33*, 889–897. [CrossRef] [PubMed]
55. Hou, T.J.; Wang, J.; Li, Y.; Wang, W. Assessing the Performance of the Molecular Mechanics/Poisson Boltzmann Surface Area and Molecular Mechanics/Generalized Born Surface Area Methods. II. The Accuracy of Ranking Poses Generated From Docking. *J. Comput. Chem.* **2011**, *32*, 866–877. [CrossRef] [PubMed]
56. Carey, R.N.; Wold, S.; Westgard, J.O. Principal component analysis: An alternative to "referee" methods in method comparison studies. *Anal. Chem.* **1975**, *47*, 1824–1829. [CrossRef]
57. Liu, J.; Yu, Y.; Kelly, J.; Sha, D.; Alhassan, A.B.; Yu, Q.; Maletic, M.M.; Duffy, J.L.; Klein, D.J.; Holloway, M.K.; et al. Discoveery of highly selective and potent HDAC3 inhibitors based on a 2-substituted benzamide zinc binding group. *ACS Med. Chem. Lett.* **2020**, *11*, 2476–2483. [CrossRef]

3.4. Design and synthesis of bioreductive prodrugs of class I histone deacetylase inhibitors and their biological evaluation in virally transfected acute myeloid leukemia cells

Mohamed Abdelsalam, Mariia Zmyslia, Karin Schmidtkunz, Anita Vecchio, Sebastian Hilscher, Hany S. Ibrahim, Mike Schutkowski, Manfred Jung, Claudia Jessen-Trefzer, Wolfgang Sippl

Abstract

Although histone deacetylase (HDAC) inhibitors show promise in treating various types of hematologic malignancies, they have some limitations, including poor pharmacokinetics and off-target side effects, which may be a reason to exclude many of them from further drug development. Prodrug design has shown promise as an approach to improve pharmacokinetic properties and also to improve target tissue specificity. In the present work, several bioreducible prodrugs for class I HDACs were designed and synthesized based on known selective HDAC inhibitors. The zinc-binding group of the HDAC inhibitors was masked with various nitroarylmethyl residues to make them substrates of nitroreductase (NTR). The developed prodrugs showed very weak HDAC inhibitory activity compared to their parent inhibitors. The prodrugs were also tested against wild-type and NTR-transfected THP1 cells. Cellular assays showed that both 2-nitroimidazole-based prodrugs **5** and **6** were best activated by the NTR prodrug system and exhibited potent activity against NTR-THP1 cells. Compound **6** showed the highest cellular activity (GI_{50} = 77 nM) and also exhibited a moderate selectivity window. Moreover, activation of the prodrug by NTR was confirmed by LC-MS analysis, which showed the release of the parent inhibitor after incubation of prodrug **6** with *E. coli* NTR. Thus, compound **6** can be considered as a novel prodrug selective for class I HDACs with good bioreductive properties, which could be used as a good starting point for increasing selectivity and for further optimization.

Design and synthesis of bioreductive prodrugs of class I histone deacetylase inhibitors and their biological evaluation in virally transfected acute myeloid leukemia cells

Mohamed Abdelsalam [a,b], Mariia Zmyslia [c], Karin Schmidtkunz [d], Anita Vecchio [a], Sebastian Hilscher [e], Hany S. Ibrahim[a,f], Mike Schutkowski [e], Manfred Jung [d,g], Claudia Jessen-Trefzer[c,*], Wolfgang Sippl[a,*]

[a] *Department of Medicinal Chemistry, Institute of Pharmacy, Martin-Luther University of Halle-Wittenberg, 06120, Halle/Saale, Germany*

[b] *Department of Pharmaceutical Chemistry, Faculty of Pharmacy, Alexandria University, Alexandria 21521, Egypt*

[c] *Institute of Organic Chemistry, University of Freiburg, 79104 Freiburg i. Br., Germany*

[d] *Institute of Pharmaceutical Science, University of Freiburg, 79104 Freiburg i. Br., Germany*

[e] *Department of Enzymology, Institute of Biochemistry, Martin-Luther-University of Halle-Wittenberg, 06120 Halle (Saale), Germany*

[f] *Department of Pharmaceutical Chemistry, Faculty of Pharmacy, Egyptian Russian University, Badr City, Cairo 11829, Egypt*

[g] *CIBSS – Centre for Integrative Biological Signalling Studies, University of Freiburg, 79104 Freiburg i. Br., Germany*

*Corresponding authors: Dr. Claudia Jessen-Trefzer, E-mail address: claudia.jessen-trefzer@pharmazie.uni-freiburg.de Prof. Dr. Wolfgang Sippl, E-mail address: wolfgang.sippl@pharmazie.uni-halle.de

Keywords:

Epigenetics, Class I HDACs, 2-Aminobenzamides, Hypoxia, Nitroreductases, Prodrugs, Acute myeloid leukemia (AML)

Abstract

Although histone deacetylase (HDAC) inhibitors show promise in treating various types of hematologic malignancies, they have some limitations, including poor pharmacokinetics and off-target side effects, which may be a reason to exclude many of them from further drug development. Prodrug design has shown promise as an approach to improve pharmacokinetic properties and also to improve target tissue specificity. In the present work, several bioreductive prodrugs for class I HDACs were designed and synthesized based on known selective HDAC inhibitors. The zinc-binding group of the HDAC inhibitors was masked with various nitroarylmethyl residues to make them substrates of nitroreductase (NTR). The developed prodrugs showed very weak HDAC inhibitory activity compared to their parent inhibitors. The prodrugs were also tested against wild-type and NTR-transfected THP1 cells. Cellular assays showed that both 2-nitroimidazole-based prodrugs **5** and **6** were best activated by the NTR prodrug system and exhibited potent activity against NTR-THP1 cells. Compound **6** showed the highest cellular activity (GI_{50} = 77 nM) and also exhibited a moderate selectivity window. Moreover, activation of the prodrug by NTR was confirmed by LC-MS analysis, which showed the release of the parent inhibitor after incubation of prodrug

1

6 with *E. coli* NTR. Thus, compound **6** can be considered as a novel prodrug selective for class I HDACs with good bioreductive properties, which could be used as a good starting point for increasing selectivity and for further optimization.

1. Introduction

Reversible histone acetylation is a key post-translational modification that regulates gene expression by modifying chromatin architecture [1, 2]. This process is controlled by two opposing enzyme families. Histone acetyltransferases (HATs) catalyze the addition of an acetyl or acyl group on the ε-amino group of lysine residues of histone proteins [3]. These modifications result in neutralizing the positive charge on lysine residues, reducing the interactions between histone proteins and DNA, and finally leading to gene-transcription activation [2, 3]. The histone deacetylases (HDACs) remove the acetyl or acyl groups from the modified lysine residues, resulting in the formation of condensed chromatin and transcriptional gene silencing [2, 4]. In humans, eighteen different HDACs have been identified and classified according to their sequence homology to yeast into four classes. Class I (HDAC1, 2, 3, and 8), class II (HDAC4, 5, 6, 7, 9, and 10), and class IV (HDAC11), which are zinc-dependent deacetylases, and class III (sirtuins SIRT1-7), which are NAD^+-dependent deacetylases [4, 5]. Besides acting on modified lysine residues of histones, HDACs have numerous non-histone substrates [2, 5, 6]. Recently, HDACs have gained growing interest as potential therapeutic targets as these enzymes can modify the aberrant epigenetic conditions associated with cancer development [6, 7]. Several HDAC inhibitors (HDACi) have been developed and tested as potential therapies for solid tumors and blood malignancies [8-10]. Most HDACi share a common pharmacophoric feature consisting of three distinct groups as follows: a zinc binding group (ZBG), a capping group, and a linker [11]. The ZBG is responsible for chelating Zn^{2+} ion in the active site of HDACs. Different ZBGs have been used for the development of HDACi, e.g. hydroxamic acids, 2-aminobenzamides, short-chain fatty acids, thiols, alkylhydrazides, and others [12, 13]. In addition, cyclic peptides without a ZBG have been reported as HDACi [14]. To date, four HDACi have been approved by the US Food and Drug Administration (FDA) for the treatment of different types of hematological malignancies. These include the hydroxamate-based inhibitors vorinostat, belinostat, and panobinostat, as well as the thiol-prodrug/depsipeptide (romidepsin) [11]. Although hydroxamic acid is a potent and widely used ZBG, it was observed that hydroxamate-based HDAC inhibitors often lack HDAC-isoform selectivity and show off-target side effects [15, 16]. In addition, they are associated with cellular mutagenicity and genotoxicity [17]. Compared with hydroxamate-based HDACi, the 2-aminobenzamide HDACi exhibit improved class I HDAC selectivity and lower toxicity (**Fig. 1**) [18, 19]. Several clinical studies revealed that hematological toxicities associated with HDACi may limit their therapeutic window, and this is a main reason to exclude several potent candidates from further drug development [20-22]. Therefore, cell-specific inhibition of such epigenetic targets could be a promising strategy to overcome off-target side effects.

I (Tacedinaline; CI994)

IC_{50} (HDAC1) 0.9 μM
IC_{50} (HDAC2) 0.9 μM
IC_{50} (HDAC3) 1.2 μM
IC_{50} (HDAC8) > 20 μM

II

IC_{50} (HDAC1) 0.04 μM
IC_{50} (HDAC2) 0.1 μM
IC_{50} (HDAC3) > 20 μM
IC_{50} (HDAC8) > 20 μM

III (Entinostat; M-S275)

IC_{50} (HDAC1) 0.13 μM
IC_{50} (HDAC2) 0.34 μM
IC_{50} (HDAC3) 0.37 μM

IV

IC_{50} (HDAC1) 0.13 ± 0.01 μM
IC_{50} (HDAC2) 0.28 ± 0.01 μM
IC_{50} (HDAC3) 0.31 ± 0.01 μM
IC_{50} (HDAC8)   > 20 μM

V

IC_{50} (HDAC1) 4.57 ± 0.6 μM
IC_{50} (HDAC2) 6.64 ± 1.4 μM
IC_{50} (HDAC3) 4.01 ± 0.9 μM
IC_{50} (HDAC8)   > 20 μM

VI

IC_{50} (HDAC1) 1.14 ± 0.3 μM
IC_{50} (HDAC2) 6.15 ± 0.8 μM
IC_{50} (HDAC3) 5.22 ± 1.1 μM
IC_{50} (HDAC8)   > 20 μM

Fig. 1: Examples of 2-aminobenzamide-HDAC inhibitors and their inhibitory activity towards different HDAC isoforms [18, 19].

One of the approaches that can be applied to enhance targeted-tissue specificity and to improve drug delivery to selected cell types is the design of prodrugs [23]. Prodrugs are themselves inactive, but through chemical or enzymatic cleavage, the bioactive form of drugs can be released. Also, by exploiting tumor-intrinsic factors, a cancer-specific release might be obtained [23, 24]. One of these factors is hypoxia, which is a deficiency in oxygen supply reaching the tissues and contributes to the chemotherapeutic resistance of tumors [25]. Hypoxia induces high expression of reductase enzymes; therefore, hypoxia has evolved as a promising approach in the design of anticancer agents [26, 27]. Additionally, several hypoxia-activated chemotherapeutic agents are currently in clinical development [26]. The directed enzyme prodrug therapy (DEPT) principle is one of the strategies that can be applied for the selective targeting of exogenous enzymes to cancer cells. This approach allows site-specific release of the active drug by an exogenous enzyme that is either linked to an antibody (ADEPT) or encoded by a gene that is targeted to the tumor site (GDEPT) [28]. Nitroreductase (NTR) is one of the enzymes that can be used for the DEPT approach [28]. NTR is a bacterial oxygen-insensitive homodimeric flavoenzyme encoded by the nfsB gene [29, 30]. The NTR catalyzes the reduction of the nitro group of various nitroaromatic substrates such as 4-nitrobenzyl and 1-methyl-2-nitroimidazolyl carbamates of cytotoxic amines to the corresponding nitroso intermediate, which is further reduced to the hydroxylamine derivative, followed by self-immolation and fragmentation to release the active inhibitor, in addition to a Michael acceptor and CO_2 as side products (**Fig. 2**) [31-33].

There is ample evidence for the presence of reducing enzymes in hypoxic tumors, including but not limited to enzymes able to reduce nitroaromatic compounds [27]. For example a nitroreductase enzyme has been isolated from Walker 256 rat carcinoma cells, which can

3

convert CB 1954 to a cytotoxic DNA interstrand crosslinking agent by reduction of its 4-nitro group to the corresponding hydroxylamino species [34]. Interestingly, inhibition of drug reduction by oxygen through redox cycling mechanism was first demonstrated for nitro compounds and was subsequently shown to be responsible for the hypoxia-selective cytotoxicity of nitroimidazole. In the current study we have worked with a bacterial enzyme (NTR from E. coli), since it is well-known mimic of hypoxic conditions.

1-Methyl-2-nitroimidazole has been identified as a good masking group for NTR substrates, which is characterized by fast unmasking, and it has been further used as a prodrug moiety for the cell-specific delivery of several chemotherapeutic agents [25, 35]. Recently, the NTR-activated prodrug approach has been successfully applied for the design of different epigenetic inhibitors, such as the hydroxamate-based HDACi vorinostat (SAHA) [36] and the lysine-specific histone demethylase 1 (LSD1) tranylcypromine [37]. In the present study we used this system to develop a research tool to study the effects of class I selective HDAC inhibitors in targeted cells which, as non-cytotoxic agents, also allow the study of the effect of the Michael acceptor that is formed upon enzymatic uncaging. We developed different nitroaryl-based NTR prodrugs for class I HDAC inhibitors using previously developed aminobenzamide based HDAC inhibitors. Furthermore, the biological activity of the newly synthesized prodrugs is evaluated against acute myeloid leukemia (AML) cells using an NTR enzyme-prodrug system.
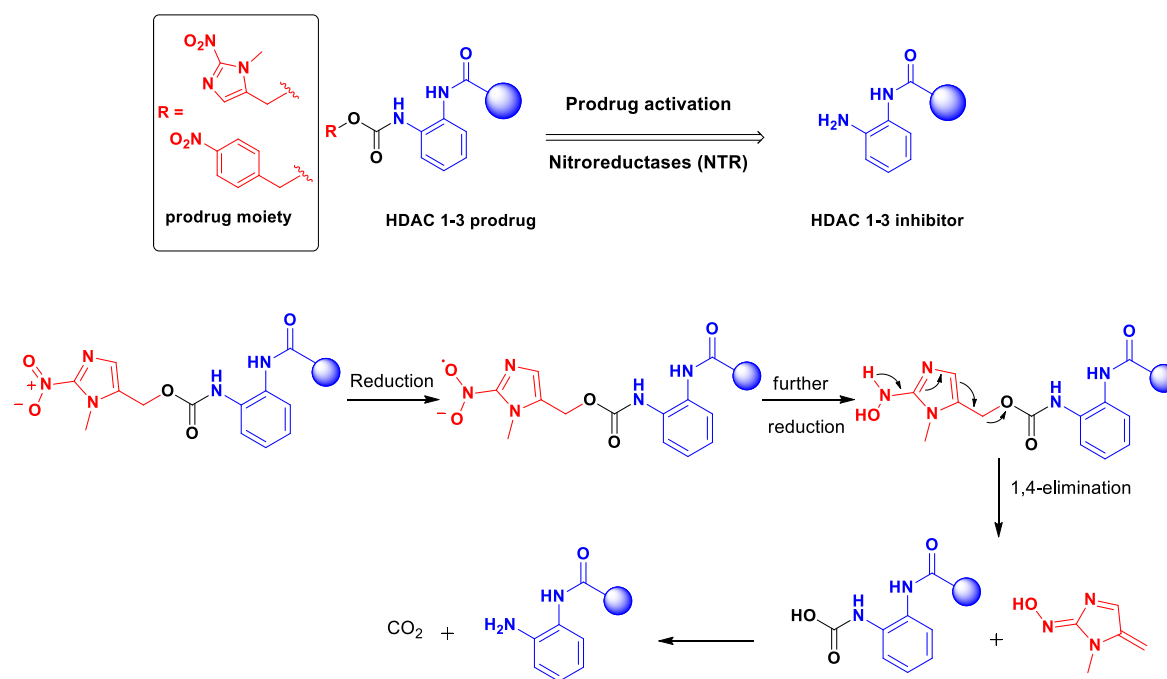
Fig. 2: The rationale for the design of novel class I HDAC prodrugs based on different 2-aminobenzamides and the postulated schematic pathway of HDAC inhibitor release.

4

2. Results and discussion

2.1. Chemistry

For the design of the prodrugs, different reported HDAC1-3 inhibitors (**I–II** and **IV–VI**; **Fig. 1**) were selected, and their aminobenzamide group was masked with different nitroaryl alcohols, such as 4-nitrobenzyl or 1-methyl-2-nitroimidazolyl alcohols (**Fig. 2**), through a carbamate linker. This attachment should result in reducing the binding to the targeted protein (since such sterically demanding groups are not accepted by the narrow HDAC1-3 binding tunnel), and accordingly, the HDAC inhibitory activity of these prodrugs is expected to decrease. In addition, the carbamate linker was chosen as it is in vivo more stable compared to corresponding carbonates or ester groups [38]. Additionally, the carbamic acid formed after the elimination of the nitroaromatic prodrug moiety can undergo fast and irreversible self-immolation, which finally results in the formation of the free aminobenzamide and CO_2, as shown in **Fig. 2** [39].

To obtain the 2-nitroimidazole-based prodrugs, we planned a three-step synthetic scheme. The first step involved the synthesis of different reported 2-aminobenzamides **I–II** and **IV–VI**, which were synthesized according to previously reported procedures [18, 19, 40]. The second step was the synthesis of 1-methyl-2-nitro-1*H*-imidazole-5-methanol (**1**), which was prepared according to our previously reported method [37]. Then, the alcohol intermediate **1** was activated using 4-nitrophenyl chloroformate (**2**) in the presence of pyridine to obtain the corresponding 4-nitrophenyl carbonate derivative **3**. Finally, condensation of the activated nitroimidazole intermediate **3** with the appropriate amine in the presence of hydroxybenzotriazole (HOBt) afforded the corresponding prodrugs **4–8** (**Scheme 1**). Regarding the synthesis of the 4-nitrobenzyl-based prodrugs **10–12**, the commercially available 4-nitrobenzyl chloroformate (**9**) was reacted with the appropriate amine in the presence of potassium carbonate to get the corresponding prodrug **10–12** as shown in **Scheme 2**.

5
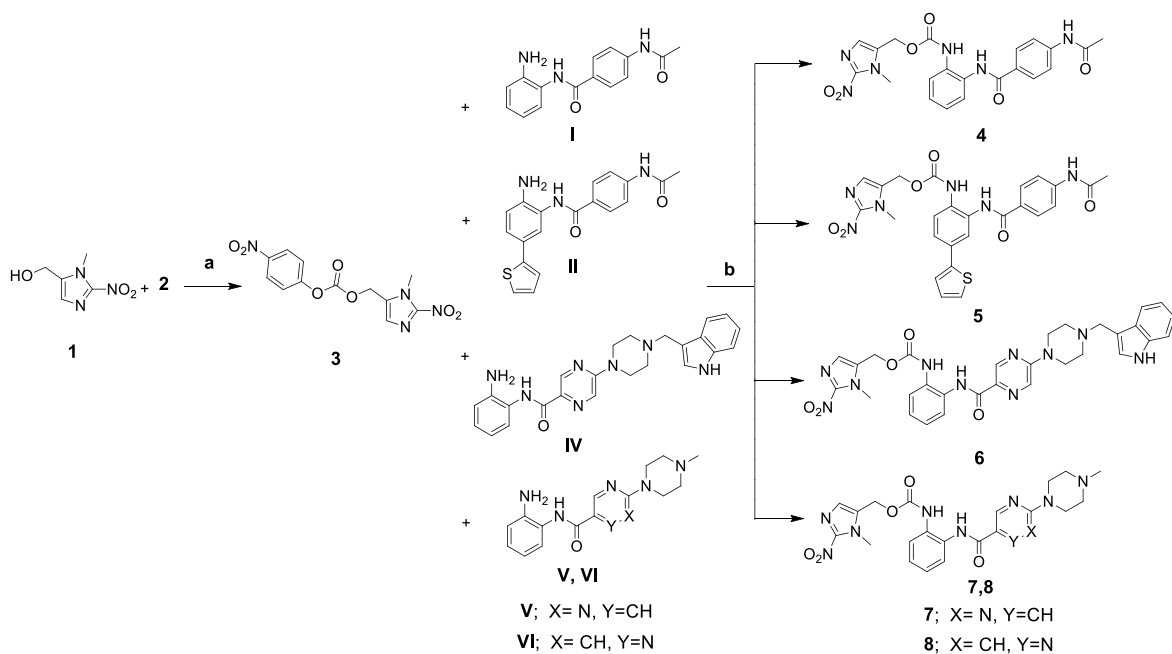
Scheme 1: Synthesis of 1-methyl-2-nitro-1*H*-imidazolyl-based prodrugs **4–8**. Reagents and conditions: (a) 4-nitrophenyl chloroformate (**2**), pyridine, THF, overnight; (b) HOBt, DMF, overnight.
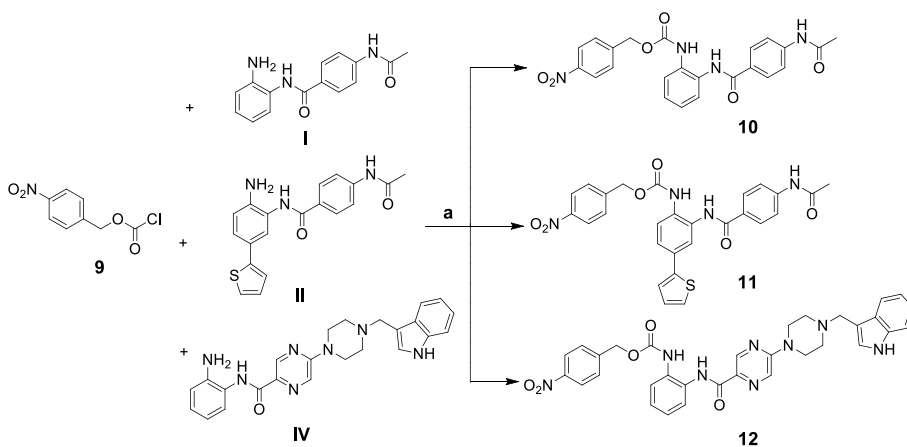
Scheme 2: Synthesis of 4-nitrobenzyl-based prodrugs **10–12**. Reagents and conditions: (a) K_2CO_3, THF, 4 h.
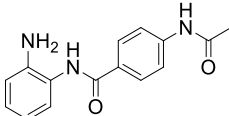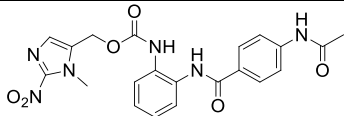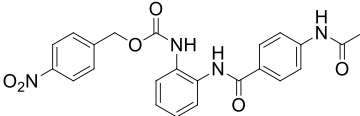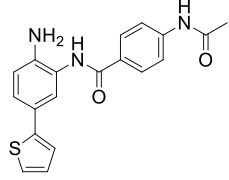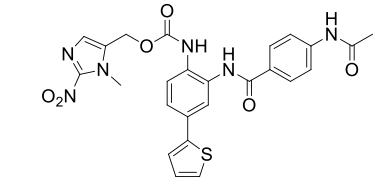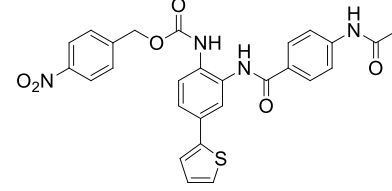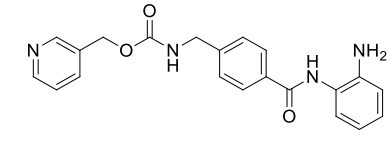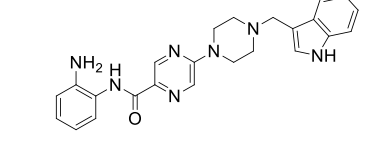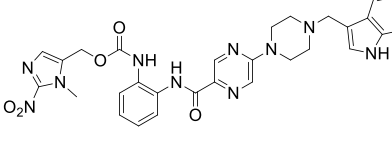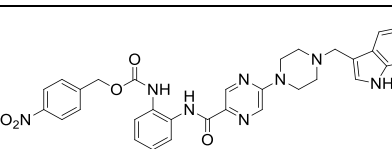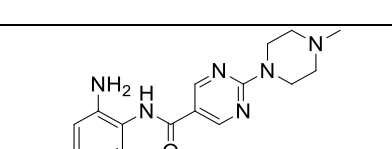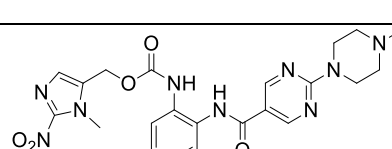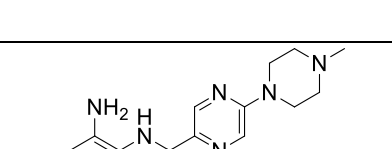
2.2. Biological evaluation
2.2.1. *In vitro* testing of HDAC inhibitory activity

The synthesized prodrugs, in addition to the parent HDAC inhibitors, were tested for their inhibitory activity against human class I HDACs (HDAC1, 2, and 3) using a fluorogenic peptide derived from p53 (Ac-RHKK(Acetyl)-AMC) [41] (**Table 1**). The prodrugs were

6
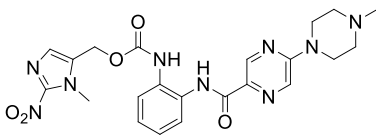
tested against HDAC1, 2, and 3 at three different concentrations (10, 1, and 0.1 µM) (**Table 1, Supp. Information Tables S1-S3**). As previously described [18, 42], compounds **IV–VI** were designed as a novel series of class I HDAC inhibitors based on different structural modifications of the general scaffold of the reported HDAC 1-3 inhibitors tacedinaline (**I**) and entinostat (**III**). For the previously developed HDAC inhibitors [18, 42] we showed target engagement by measuring the hyperacetylation on H3K9 (HDAC1 substrate). For the developed inhibitors the phenyl ring in the middle of tacedinaline was replaced with the more polar pyrazine ring as in the case of compound **VI**, which showed improved inhibitory activity against HDAC1-3 compared to tacedinaline (**Table 1**). On the other hand, the replacement of the phenyl ring with a pyrimidine ring, as in the case of compound **V,** resulted only in a slight decrease in the inhibitory activity against HDAC1 compared to compound **VI**. The second modification involved the replacement of the middle phenyl ring of entinostat with a pyrazine ring, in addition to the replacement of the pyridine ring (capping group) with the bulkier 3-indolyl scaffold as in the case of compound **IV**, which resulted in higher inhibitory activity against HDAC 1-3 compared to the reference inhibitors (**Table 1**). The preliminary testing of the developed prodrugs showed that they exhibited very weak HDAC inhibitory activity compared to the corresponding parent inhibitors.

Table 1: In vitro evaluation of HDAC 1, 2, and 3 inhibition by HDAC inhibitors **I-VI** and the corresponding prodrugs, in addition to % inhibition against NTR-THP1 at 10 µM

Cpd. Id	Chemical structure	HDAC1 IC$_{50}$ µM or % inhibition	HDAC2 IC$_{50}$ µM or % inhibition	HDAC3 IC$_{50}$ µM or % inhibition	% Inhibition NTR-THP1 at 10 µM
(I)		8.8 ± 1.2	7.5 ± 0.8	4.2 ± 0.5	84
4		21 % at 1 µM 8 % at 0.1 µM	7 % at 1 µM 2 % at 0.1 µM	10 % at 1 µM 12 % at 0.1 µM	14
10		17 % at 1 µM 10 % at 0.1 µM	14 % at 1 µM 8 % at 0.1 µM	12 % at 1 µM 7 % at 0.1 µM	19
(II)		0.04 ± 0.006	0.26 ± 0.01	16.4 ± 3.6	88

	Structure				
5		31 % at 1 µM 17 % at 0.1 µM	8 % at 1 µM 2 % at 0.1 µM	11 % at 1 µM 8 % at 0.1 µM	98
11		14 % at 1 µM 9 % at 0.1 µM	7 % at 1 µM 8 % at 0.1 µM	9 % at 1 µM 3 % at 0.1 µM	35
(III)		0.93 ± 0.11	0.95 ± 0.03	1.8 ± 0.1	n.d.
(IV)		0.13 ± 0.01	0.28 ± 0.01	0.31 ± 0.01	93
6		38 % at 1 µM 16 % at 0.1 µM	13 % at 1 µM 3 % at 0.1 µM	15 % at 1 µM 11 % at 0.1 µM	98
12		20 % at 1 µM 12 % at 0.1 µM	5 % at 1 µM 1 % at 0.1 µM	12 % at 1 µM 5 % 0.1 µM	80
(V)		4.6 ± 0.6	6.6 ± 1.4	4.0 ± 0.9	73
7		19 % at 1 µM 17 % at 0.1 µM	8 % at 1 µM 5 % at 0.1 µM	15 % at 1 µM 7 % at 0.1 µM	17
(VI)		1.1 ± 0.3	6.2 ± 0.8	5.2 ± 1.1	88

8

| 8 | | 25 % at 1 μM

20 % at 0.1 μM | 10 % at 1 μM

1 % at 0.1 μM | 16 % at 1 μM

9 % at 0.1 μM | 93 |

n.d. not determined, **( )** the codes for parent inhibitors are written in Latin numbers between brackets.

2.2.2. Cellular testing
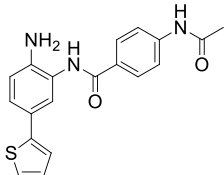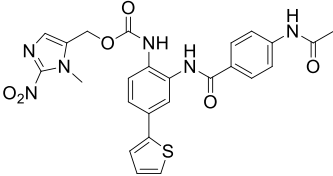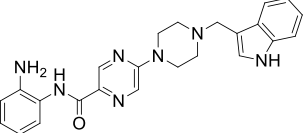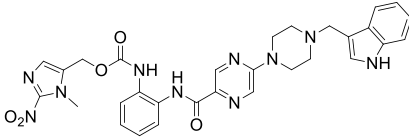
2.2.2.1. Cytotoxic activity against wild-type and NTR-THP1 cells

The prodrugs and their parent inhibitors were then tested in a cell viability assay via a tetrazolium salt-based assay on wild-type THP1 acute myeloid leukemia (AML) cells and THP1 cells that had been lentivirally transfected with the *E. coli* nitroreductase NfsB. We had used this system successfully before to activate bioreductive prodrugs of inhibitors of the lysine-specific demethylase 1 (LSD1)]37[. We pre-screened all compounds at 1, 10, and 50 μM concentrations in the wild-type and transfected cell lines (% inhibition against NTR-THP1 at 10 μM is presented in **Table 1**). When sub-μM inhibition of HDACs *in vitro* and more than 50% inhibition of cell viability were achieved by the prodrugs in the NTR-THP1 cells, a GI_{50} value was determined. For inhibitors **II** and **IV**, the more potent prodrugs **5** and **6**, respectively, were selected.

The two potent prodrugs **5** and **6** were both 2-nitroimidazole rather than nitrobenzyl compounds, which is in line with previous findings on the better activation of the heterocyclic prodrugs. Interestingly, compound **4** and compound **10** show little effect on NTR-THP1 cells at 10 μM (14 and 19% inhibition, **Table 1**), even so compound **4** is a nitroimidazole derivative. Potentially, the core structure (from compound **I**) is binding weakly to NTR and subsequently prodrug activation is hindered. However, regarding compound **5** and **6**, the cellular effects are in the range of the parent HDAC inhibitor, implying almost full conversion (**Table 2**). Whereas the parent HDAC inhibitors have essentially the same activity on both cell lines, we find a selectivity window of 6–12 fold for the prodrugs (**Table 2**). The inhibition in wild-type THP1 cells resulted either from the intrinsic toxicity of the carbamates or from some background reductive activation in the non-transfected cells. Thus, while the selectivity could still be improved, compound **6** is a prodrug with very good bioreductive properties, which leads to highly potent activity against a leukemic cell line and is a great starting point for further optimization.

Table 2: GI_{50} values of the most active prodrugs and the corresponding inhibitors against wild-type and transfected NTR-THP1 cells and their selectivity window

Cpd. Id	Chemical structure	Inhibition of viability in THP1 cells IC_{50} (μM) ± SEM	Inhibition of viability in NTR-THP1 cells IC_{50} (μM) ± SEM	Selectivity window

9

(II)		1.67 ± 0.51	1.62 ± 0.62	1.0
5		12.3 ± 0.7	1.84 ± 0.4	6.7
(IV)		0.034 ± 0.003	0.063 ± 0.013	0.5
6		0.91 ± 0.36	0.077 ± 0.004	11.8

2.2.2.2. Cytotoxic activity against J774A.1 cells

To analyze the therapeutic window of the developed prodrugs, the cytotoxic properties of the prodrugs and the parent inhibitors were determined using a MTT assay protocol against the murine macrophage cell line (J774A.1) after incubation for 72 hours. To quantify cytotoxic activity, the half-maximal inhibitory concentration (IC_{50}) was determined. The results, summarized in **Fig. 3** and **Table 3**, consistently showed that the synthesized prodrugs exhibited significantly higher IC_{50} values compared to the corresponding parent HDAC inhibitors.

The ratio of prodrug IC_{50} to parent compound IC_{50} was calculated, revealing a 4– to 78–fold improvement in reducing cellular cytotoxicity when using the prodrug approach instead of the parent HDAC inhibitors. Compounds **4** and **10** were found to be the least toxic prodrugs against J774A.1 cells. It was not possible to calculate accurate IC_{50} values for both compounds as they demonstrated minimal or no cellular toxicity even at tested concentrations up to 100 μM. At the same time, compound **5** and **6** show moderate toxicity in J77A.1 cells, pointing towards potential off-target effects in this cell line.

Table 3: IC_{50} values for HDAC inhibitors and corresponding prodrugs against J774A.1 cells for a 72-h incubation period determined in the MTT assay.

Cpd. Id	IC_{50} (μM) ± SEM	Prodrug to Parent IC_{50} Ratio
(I)	0.9 ± 0.7	NA
4	NA	NA

10

10	NA	NA
(II)	0.2 ± 0.02	NA
5	15.5 ± 0.6	77.5
(IV)	0.1 ± 0.05	NA
6	2.5 ± 0.6	25
12	0.4 ± 0.04	4
(V)	5.1 ± 0.2	NA
7	61.9 ± 0.5	12.1
(VI)	0.8 ± 0.3	NA
8	23.3 ± 3.7	29.1

11
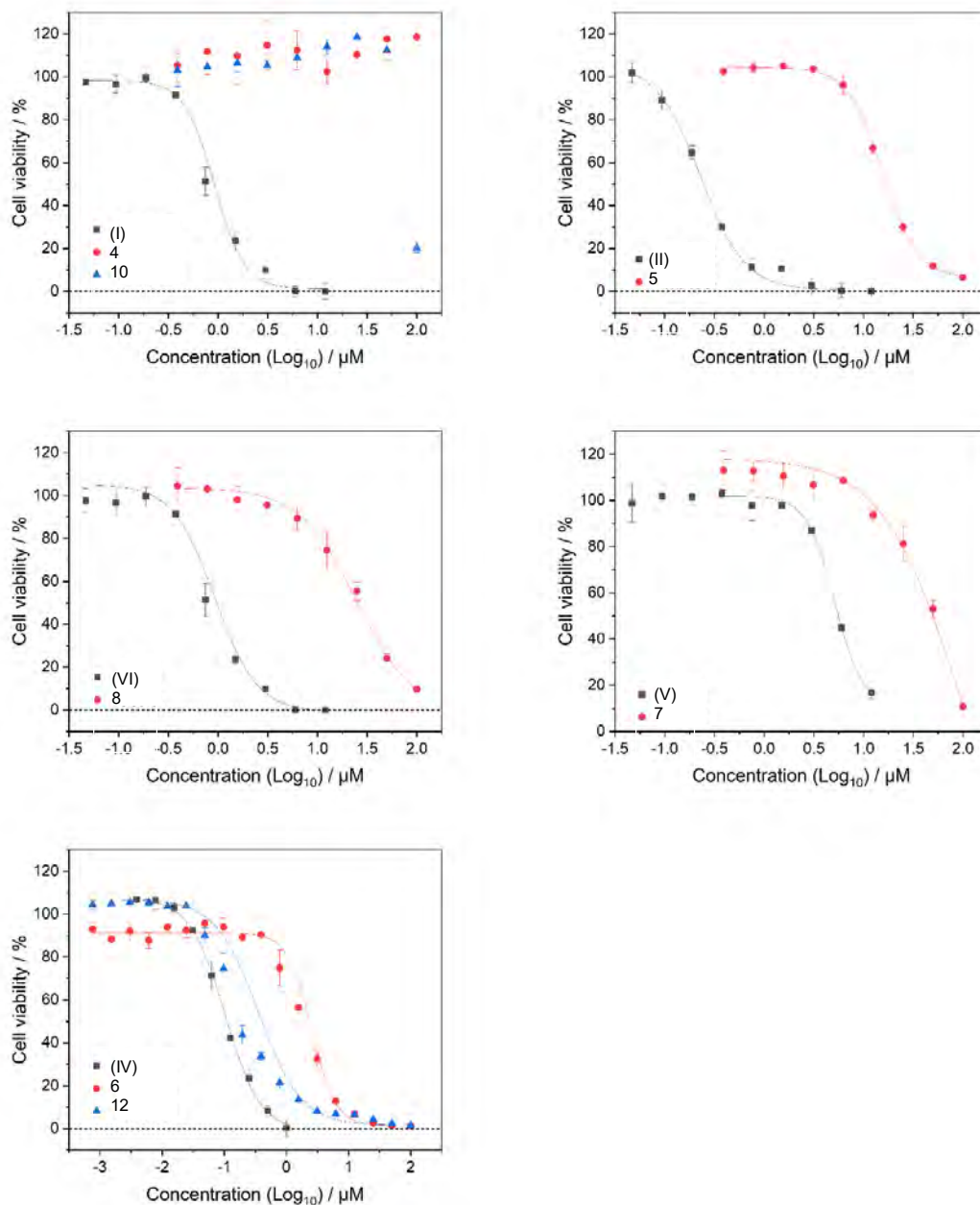
Fig. 3: Dose-response curves against J774A.1 cell line showing cytotoxic activities of HDAC inhibitors and corresponding prodrugs.

2.2.3. In vitro prodrug activation by NTR

An LC-MS analysis was performed to determine the interaction profile of the most promising prodrug **6** with *E. coli* NTR. After 30 minutes of incubation, the prodrug **6** (retention time: 5.6 min, m/z: 611.2473) reacted with NTR, resulting in the formation of the parent inhibitor (**IV**; retention time: 4.16 min, m/z: 428.2193), in addition to other metabolites (**Fig. 4, Table 4**).

12

Table 4: LC-MS of prodrug 6 activated by NTR

	Retention time (min)	m/z
Prodrug 6	5.58	611.2473
Parent HDAC inhibitor IV	4.16	428.2193
Prodrug 6 with NTR	2.95	466.1944
	4.16	428.2193
	5.55	611.2471

13
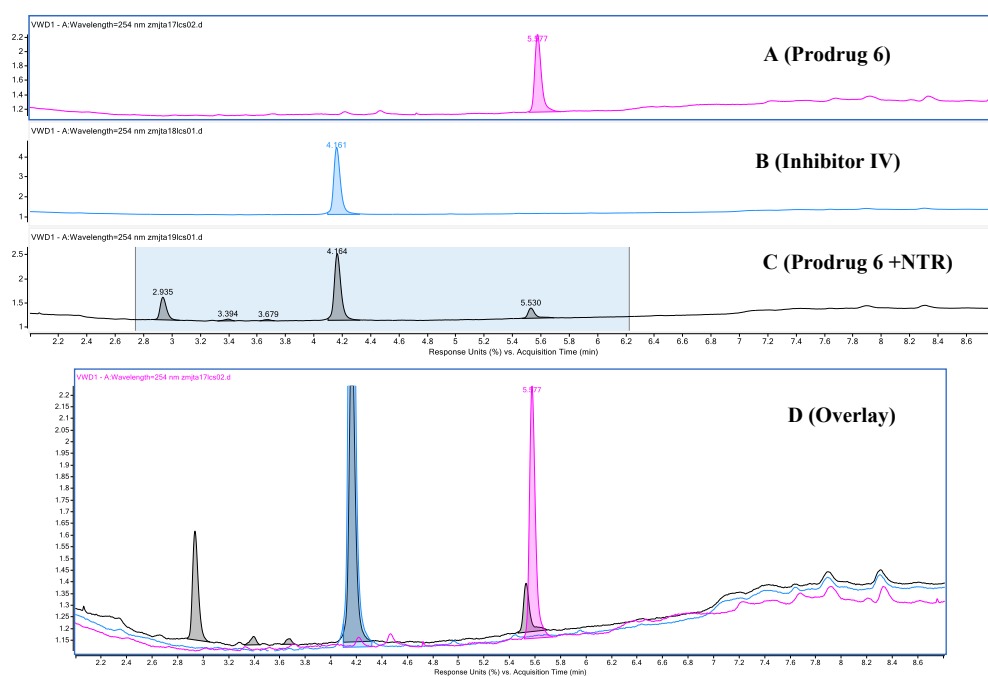
Fig. 4: HPLC chromatogram of the reduction reaction for prodrug **6** catalyzed by NTR at a 30 min reaction time. (A) Chromatogram of **6** without NTR; (B) Chromatogram of the parent inhibitor **IV**; (C) Chromatogram of **6** with NTR showing the release of the inhibitor **IV**; (D) Overlay of the three chromatograms.

14

3. Conclusion

Over recent years, histone deacetylases (HDACs) have gained great interest as key epigenetic modulators involved in the regulation of several cellular processes, and their overexpression has been associated with the initiation and progression of different types of cancer. Several HDAC inhibitors have been approved for the treatment of different subtypes of blood malignancies; however, the majority of them show some limitations, including genotoxicity, mutagenicity, and undesirable adverse effects. One strategy that could be used to overcome such problems and improve drug delivery to selected cell types is the design of prodrugs. In the current study, a novel series of bioreductive nitroaromatic prodrugs for class I HDACs has been designed and synthesized based on different reported HDAC1, 2, and 3 inhibitors. The aminobenzamide part (ZBG) of the selected HDAC inhibitors was masked with different nitroarylmethyl alcohols through a carbamate linker. Such attachment should reduce the binding to the targeted HDACs, which could be explained by the weaker HDAC inhibitory activity of the newly synthesized prodrugs compared to the parent inhibitors. Furthermore, the biological activity of the newly synthesized prodrugs was evaluated against THP1 acute myeloid leukemia cells using a nitroreductase (NTR) prodrug system. This prodrug system catalyzes the reduction of the nitro group of different nitroaromatic substrates of cytotoxic amines to release the active inhibitor selectively in NTR-expressing cells. Cellular testing revealed that two 2-nitroimidazole-based prodrugs (**5** and **6**) were activated by the NTR prodrug system. Both compounds showed cellular effects almost in the range of the corresponding parent inhibitors. Compound **6** showed potent activity against the NTR-THP1 cell in the nanomolar range. In addition, it exhibited a moderate selectivity window. The in vitro prodrug activation by NTR was confirmed by LC-MS analysis, which showed the release of the parent inhibitor after incubation of the prodrug **6** with *E. coli* NTR. This work demonstrates that we successfully synthesized and evaluated a novel class I HDAC prodrug with good bioreductive properties, which can be used as a good starting point to enhance the selectivity and for further optimization. In addition, our model shows the potential to genetically engineer tumor cells with a bacterial nitroreductase for specific activation.

4. Materials and Methods

4.1. General Experimental Information

Materials and reagents were purchased from Sigma-Aldrich Co., Ltd. (Darmstadt, Germany) and abcr GmbH (Karlsruhe, Germany). All solvents were analytically pure and dried before use. Thin-layer chromatography was carried out on aluminum sheets coated with silica gel 60 F254 (Merck, Darmstadt, Germany). For medium-pressure chromatography (MPLC), silica gel 60 (0.036-0.200 mm) was used. Purity was measured by UV absorbance at 254 nm. The elution system used for HPLC consists of MeOH, H_2O, and 0.05% trifluoroacetic acid. The HPLC consisted of a LiChrosorb® RP-18 (5 µm) 100-4.6 Merck column (Merck, Darmstadt, Germany), two LC-10AD pumps, a SPD-M10A VP PDA detector, and a SIL-HT autosampler, all from the manufacturer Shimadzu (Kyoto, Japan). The absorption spectra were recorded with a Shimadzu SPD-M10A diode array detector spectrophotometer (Kyoto, Japan). For the preparative HPLC, a LiChrosorb® RP-18 (7 µm) 250-25 Merck (Merck, Darmstadt, Germany) column was used. The applied mobile phase was a gradient with

15

increasing polarity composed of acetonitrile/water and formic acid. Mass spectrometry analyses were performed with a Finnigan MAT710C (Thermo Separation Products, San Jose, CA, USA) for the ESI MS spectra and with a LTQ (linear ion trap) Orbitrap XL hybrid mass spectrometer (Thermo Fisher Scientific, Bremen, Germany) for the HRMS-ESI (high-resolution mass spectrometry) spectra. For the HRMS analyses, the signal for the isotopes with the highest prevalence was given and calculated. ^{1}H NMR spectra were taken on a Varian Inova 400 using deuterated DMSO as solvent. Chemical shifts were referenced to the residual solvent signals. The following abbreviations and formulas for solvents and reagents were used: ethyl acetate (EtOAc), *N, N*-dimethylformamide (DMF), dimethyl sulfoxide (DMSO), methanol (MeOH), tetrahydrofuran (THF), water (H_2O), sodium sulphate (Na_2SO_4), dichloromethane (DCM), potassium carbonate (K_2CO_3), and hydroxybenzotriazole (HOBt).

4.2. Experimental Procedures and Characterization of Synthesized Compounds

Intermediate **1** and the aniline derivatives **I-II** and **IV-VI** were synthesized according to the previously reported methods [37] and [18, 19, 40], respectively.

(1-Methyl-2-nitro-1*H*-imidazol-5-yl)methyl (4-nitrophenyl) carbonate (3)

4-Nitrophenyl chloroformate (**2**) (492 mg, 2.44 mmol, 1.2 eq.) in dry THF (5 mL) was added slowly to an ice-cold solution of intermediate **1** (320 mg, 2.37 mmol, 1 eq.) in dry THF (15 mL) and pyridine (0.2 mL, 2.44 mmol, 1.2 eq.). The reaction was allowed to warm to room temperature and stirred overnight. The reaction mixture was evaporated to dryness, EtOAc was added, and the solution was washed with HCl (1 M, 15 mL) and brine (15 mL). The combined organic layers were dried over Na$_2$SO4, filtered, and concentrated under reduced pressure. The crude product was purified by MPLC (EtOAc : hexane) to give the product as white solid (yield: 220 mg, 0.68 mmol, 33.8%); ^{1}H NMR (400 MHz, DMSO-d^6) δ 8.32 (d, *J* = 9.1 Hz, 2H), 7.57 (d, *J* = 9.1 Hz, 2H), 7.35 (s, 1H), 5.45 (s, 2H), 3.97 (s, 3H).

General procedure for the preparation of final compounds 4-8.

(1-Methyl-2-nitro-1*H*-imidazol-5-yl)methyl (4-nitrophenyl) carbonate (**3**) (100 mg, 0.31 mmol, 1 eq.) was added to a mixture of HOBt·H$_2$O (60 mg, 0.39 mmol, 1.3 eq.) and the appropriate aniline derivative (**I, II, IV-VI**) (0.31 mmol, 1 eq.) in dry DMF (5 mL), and the resulting reaction mixture was stirred at RT for 18 h. The solvent was removed under reduced pressure. The crude product was purified by MPLC using (DCM: MeOH) to give the corresponding final product.

(1-Methyl-2-nitro-1*H*-imidazol-5-yl)methyl (2-(4-acetamidobenzamido)phenyl)carbamate (4)
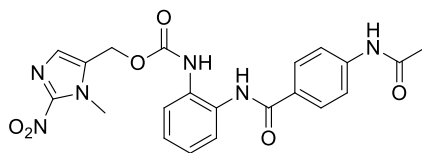
^{1}H NMR (400 MHz, DMSO-d^6) δ 10.20 (s, 1H), 9.72 (s, 1H), 9.00 (s, 1H), 7.89 (d, *J* = 8.8 Hz, 2H), 7.69 (d, *J* = 8.8 Hz, 2H), 7.56 (d, *J* = 7.6 Hz, 1H), 7.50 (dd, *J* = 7.8, 1.6 Hz, 1H), 7.27 (s, 1H), 7.23 – 7.14 (m, 2H), 5.25 (s, 2H), 3.90 (s, 3H), 2.06 (s, 3H); ^{13}C NMR (101

16

MHz, DMSO-d^6) δ 169.2, 165.4, 153.8, 142.9, 133.7, 131.8, 130.73, 130.71, 129.19, 129.13, 128.8, 126.6, 126.0, 125.0, 118.5, 55.9, 34.6, 24.6; HRMS *m/z*: 475.1336 [M + Na]$^+$; calculated C$_{21}$H$_{20}$N$_6$O$_6$Na$^+$: 475.1342; HPLC: rt 9.82 min (98.83%); white solid; yield: 90 mg, 0.2 mmol, 64.3%.

(1-Methyl-2-nitro-1*H*-imidazol-5-yl)methyl   (2-(4-acetamidobenzamido)-4-(thiophen-2-yl)phenyl)carbamate (5)
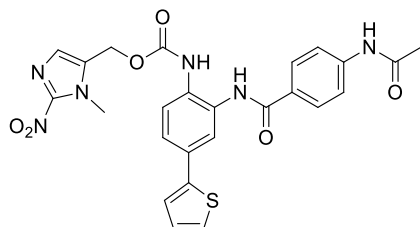
^{1}H NMR (400 MHz, DMSO-d^6) δ 10.21 (s, 1H), 9.81 (s, 1H), 9.10 (s, 1H), 7.92 (d, *J* = 8.8 Hz, 2H), 7.80 (d, *J* = 2.2 Hz, 1H), 7.71 (d, *J* = 8.8 Hz, 2H), 7.63 (d, *J* = 8.5 Hz, 1H), 7.56 – 7.50 (m, 2H), 7.45 (dt, *J* = 3.6, 1.9 Hz, 1H), 7.28 (s, 1H), 7.11 (dt, *J* = 7.9, 4.0 Hz, 1H), 5.26 (s, 2H), 3.92 (s, 3H), 2.07 (s, 3H); ^{13}C NMR (101 MHz, DMSO-d^6) δ 169.2, 165.6, 153.8, 146.5, 143.0, 142.9, 133.6, 131.3, 131.0, 130.98, 130.54, 129.2, 129.0, 128.7, 126.0, 124.0, 123.3, 123.1, 118.5, 56.0, 34.7, 24.6; HRMS *m/z*: 557.1215 [M + Na]$^+$; calculated C$_{25}$H$_{22}$N$_6$O$_6$SNa$^+$: 557.1219; HPLC: rt 12.60 min (97.29%); white solid; yield: 75 mg, 0.14 mmol, 45.2%.

(1-Methyl-2-nitro-1*H*-imidazol-5-yl)methyl   (2-(5-(4-((1*H*-indol-3-yl)methyl)piperazin-1-yl)pyrazine-2-carboxamido)phenyl)carbamate (6)
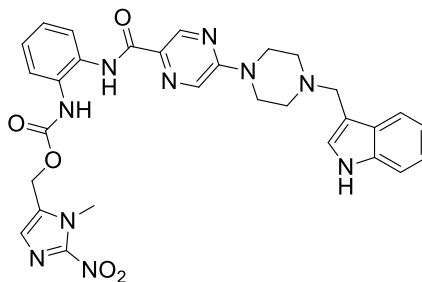
^{1}H NMR (400 MHz, DMSO-d^6) δ 10.93 (s, 1H), 9.83 (s, 1H), 9.40 (s, 1H), 8.67 (s, 1H), 8.24 (s, 1H), 7.95 (d, *J* = 15.2 Hz, 1H), 7.66 (d, *J* = 7.8 Hz, 1H), 7.50 – 7.20 (m, 5H), 7.14 (t, *J* = 7.6 Hz, 1H), 7.06 (t, *J* = 7.3 Hz, 1H), 6.98 (t, *J* = 7.4 Hz, 1H), 5.28 (s, 2H), 3.90 (s, 3H), 3.79 – 3.60 (m, 6H), 2.62 – 2.50 (m, 4H);   HRMS *m/z*: 611.2476 [M + H]$^+$; calculated C$_{30}$H$_{31}$N$_{10}$O$_5$$^+$: 611.2479; HPLC: rt 11.16 min (99.75%); beige solid; yield: 50 mg, 0.08 mmol, 26.3%.

(1-Methyl-2-nitro-1*H*-imidazol-5-yl)methyl   2-(2-(4-methylpiperazin-1-yl)pyrimidine-5-carboxamido)phenylcarbamate (7)

17

^{1}H NMR (400 MHz, DMSO-d^6) δ 9.68 (s, 1H), 9.04 (s, 1H), 8.84 (s, 2H), 7.60 (d, J = 16.6 Hz, 1H), 7.48 (dd, J = 7.9, 1.5 Hz, 1H), 7.26 (s, 1H), 7.21 (td, J = 7.7, 1.6 Hz, 1H), 7.15 (td, J = 7.6, 1.5 Hz, 1H), 5.25 (s, 2H), 3.91 (s, 3H), 3.84 (t, J = 5.0 Hz, 4H), 2.40 (t, J = 5.0 Hz, 4H), 2.24 (s, 3H); HRMS m/z: 496.205 [M + H]$^+$; calculated C$_{22}$H$_{26}$N$_9$O$_5^+$: 496.205; HPLC: rt 8.58 min (92.05%); colourless oil; Yield: 35 mg, 0.07 mmol, 22.9%.

(1-Methyl-2-nitro-1*H*-imidazol-5-yl)methyl (2-(5-(4-methylpiperazin-1-yl)pyrazine-2-carboxamido)phenyl)carbamate formate (8)

^{1}H NMR (400 MHz, DMSO-d^6) δ 9.86 (s, 1H), 9.42 (s, 1H), 8.69 (d, J = 1.1 Hz, 1H), 8.27 (s, 1H), 7.97 (s, 1H), 7.89 (d, J = 8.4 Hz, 1H), 7.60 (d, J = 8.3 Hz, 1H), 7.46 – 7.38 (m, 1H), 7.35 – 7.29 (m, 1H), 7.27 – 7.21 (m, 1H), 7.15 (td, J = 7.7, 1.3 Hz, 1H), 5.29 (s, 2H), 3.90 (s, 3H), 3.79 – 3.62 (m, 4H), 2.55 – 2.49 (m, 4H), 2.30 (s, 3H); HRMS m/z: 496.205 [M + H]$^+$; calculated C$_{22}$H$_{26}$N$_9$O$_5^+$: 496.205; The compound exist as formic acid salt as it was purified using preparative HPLC; HPLC: rt 9.17 min (97.95%); colourless oil; yield: 20 mg.

General procedure for preparation of final compounds 10-12.

A solution of 4-nitrobenzyl chloroformate (**9**) (100 mg, 0.46 mmol, 1 eq.) in 3 mL of THF was added dropwise to a mixture of the appropriate aniline derivative (**I-III**) (0.46 mmol, 1 eq.) and K$_2$CO$_3$ (83 mg, 0.6 mmol, 1.3 eq.) in dry THF (10 mL) at 0º C. The reaction mixture was stirred at RT for 4 h. The reaction mixture was filtered, and the solvent was evaporated under reduced pressure. The obtained residue was purified using MPLC (DCM: MeOH) to give the corresponding product.

4-Nitrobenzyl (2-(4-acetamidobenzamido)phenyl)carbamate (10)

^{1}H NMR (400 MHz, DMSO-d^6) δ 10.20 (s, 1H), 9.73 (s, 1H), 9.13 (s, 1H), 8.20 – 8.14 (m, 2H), 7.92 – 7.86 (m, 2H), 7.68 (d, J = 8.8 Hz, 2H), 7.62 (d, J = 8.8 Hz, 2H), 7.56 (dd, J = 7.8,

18

1.5 Hz, 1H), 7.51 (dd, J = 7.7, 1.7 Hz, 1H), 7.24 – 7.13 (m, 2H), 5.27 (s, 2H), 2.06 (s, 3H); ^{13}C NMR (101 MHz, DMSO-d^6) δ 169.2, 165.4, 154.2, 147.4, 145.0, 142.9, 131.9, 130.8, 129.1, 128.8, 128.7, 127.5, 126.6, 126.0, 125.0, 124.0, 118.5, 65.2, 24.6; HRMS m/z: 471.1274 [M + Na]$^+$; calculated C$_{23}$H$_{20}$N$_4$O$_6$Na$^+$: 471.1280; HPLC: rt 11.66 min (95.69%); white solid; yield: 65 mg, 0.14 mmol, 32.5%.

4-Nitrobenzyl (2-(4-acetamidobenzamido)-4-(thiophen-2-yl)phenyl)carbamate (11)

^{1}H NMR (400 MHz, DMSO-d^6) δ 10.21 (s, 1H), 9.81 (s, 1H), 9.20 (s, 1H), 8.18 (d, J = 8.8 Hz, 2H), 7.92 (d, J = 8.7 Hz, 2H), 7.79 (d, J = 2.1 Hz, 1H), 7.69 (d, J = 8.7 Hz, 2H), 7.66 – 7.60 (m, 3H), 7.55 – 7.49 (m, 2H), 7.45 (dd, J = 3.6, 1.0 Hz, 1H), 7.11 (dd, J = 5.1, 3.6 Hz, 1H), 5.29 (s, 2H), 2.07 (s, 3H); ^{13}C NMR (101 MHz, DMSO-d^6) δ 169.2, 165.6, 154.2, 147.5, 144.9, 143.0, 142.96, 131.4, 131.0, 130.5, 129.2, 129.0, 128.8, 128.6, 127.5, 126.0, 124.0, 123.7, 123.4, 123.1, 118.5, 65.3, 24.6; HRMS m/z: 553.1153 [M + Na]$^+$; calculated C$_{27}$H$_{22}$N$_4$O$_6$SNa$^+$: 553.1158; HPLC: rt 13.78 min (95.31%); white solid; yield: 72 mg, 0.14 mmol, 28.8%.

4-Nitrobenzyl (2-(5-(4-((1H-indol-3-yl)methyl)piperazin-1-yl)pyrazine-2-carboxamido)phenyl)carbamate (12)

^{1}H NMR (400 MHz, DMSO-d^6) δ 10.93 (s, 1H), 9.88 (s, 1H), 9.48 (s, 1H), 8.68 (d, J = 1.3 Hz, 1H), 8.19 – 8.09 (m, 3H), 7.94 (s, 1H), 7.68 – 7.57 (m, 3H), 7.34 (d, J = 8.0 Hz, 2H), 7.26 – 7.21 (m, 2H), 7.15 (td, J = 7.7, 1.5 Hz, 1H), 7.09 – 7.03 (m, 1H), 7.00 – 6.95 (m, 1H), 5.29 (s, 2H), 3.69 (s, 6H), 2.56 – 2.50 (m, 4H); ^{13}C NMR (101 MHz, DMSO-d^6) δ 162.2, 156.3, 155.5, 154.8, 150.4, 147.4, 145.0, 142.7, 136.8, 132.2, 129.2, 128.7, 128.0, 126.4, 126.3, 125.2, 125.1, 125.06, 123.9, 121.4, 119.5, 118.9, 111.8, 110.8, 65.3, 53.5, 52.5, 44.5; HRMS m/z: 607.2412 [M + H]$^+$; calculated C$_{32}$H$_{31}$N$_8$O$_5$$^+$: 607.2417; HPLC: rt 11.87 min (97.29%); beige solid; yield: 55 mg, 0.09 mmol, 19.57%.
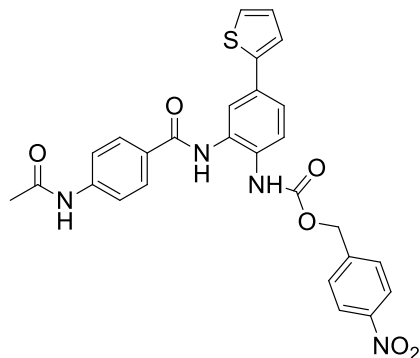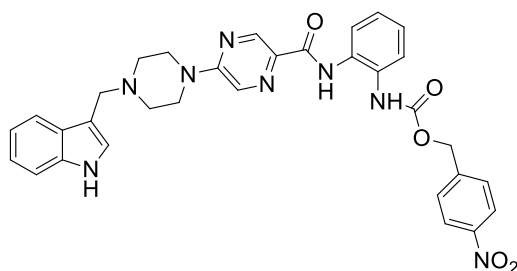
4.3. Biological Evaluation

19

4.3.1. In Vitro HDAC Inhibition Assay

Recombinant human proteins HDAC1, HDAC2, and HDAC3/NCOR1 were purchased from ENZO Life Sciences AG (Lausen, CH). Recombinant human HDAC8 was produced by Romier et al. (IGBMC, Univ. Strasbourg), as described in [43]. The in vitro testing on recombinant HDACs 1-3 was performed with a fluorogenic peptide derived from p53 (Ac-RHKK(Acetyl)-AMC) as reported [18,39]. The measurements were performed in assay buffer (50 mM Hepes, 150 mM NaCl, 5 mM $MgCl_2$, 1 mM TCEP, and 0.2 mg/mL BSA, pH 7.4 adjusted with NaOH) at 37 ˚C. All compounds at different concentrations were incubated with 10 nM HDAC1, 3 nM HDAC2, or 3 nM HDAC3 (final concentration) for at least 5 min. The reaction was first started with the addition of a fluorogenic peptide substrate (20 µM final concentration) and incubated for 30 min for HDAC2 and HDAC3 and 90 min for HDAC1. The reaction was then stopped with a solution of 1 mg/mL trypsin and 20 µM SAHA in 1 mM HCl and incubated for 1 h at 37 ˚C. The fluorescence intensity was measured with an Envision 2104 Multilabel Plate Reader (PerkinElmer, Waltham, MA, USA) with an excitation wavelength of 380 ± 8 nm and an emission wavelength of 430 ± 8 nm. The measured fluorescence intensities were normalized with uninhibited reaction as 100% and the reaction without enzyme as 0%. A nonlinear regression analysis was done to determine the IC_{50} value. The enzyme inhibition of HDAC8 was determined by using a reported homogenous fluorescence assay 2 [44]. The enzyme was incubated for 90 min at 37 ˚C, with the fluorogenic substrate ZMAL (Z (Ac)Lys-AMC) in a concentration of 10.5 µM and increasing concentrations of tested compounds. Fluorescence intensity was reported at an excitation wavelength of 390 nm and an emission wavelength of 460 nm in a microtiter plate reader (BMG Polarstar).

4.3.2. Cellular testing

4.3.2.1. Cytotoxic activity against wild type THP1 and NTR-THP1 cells

The NTR-expressing cell line THP1-NTR was generated in the group of Prof. Miething from the University of Freiburg Medical Center, by lentiviral transfection of wild-type THP1 cells (RRID:CVCL_0006), which was a kind gift of Prof. Lübbert from the University Hospital, Freiburg, with an nfsb gene construct. Both cell lines were cultivated in RPMI1640 medium supplemented with 10% (v/v) FCS, 2 mM L-glutamine and 1% Penicillin/Streptomycin at 37 °C in a humidified atmosphere with 5% CO_2. Cells were diluted to 5×10^4 cells·mL^{-1}, and mixed with compounds to a final DMSO concentration of 0.5% and seeded at 100 µL in 96-well plates in triplicates. After 72 h incubation, the CellTiter 96® AQueous Non-Radioactive Cell Proliferation Assay from Promega was performed according to the manufacturer's instructions. Assay plates were measured at 492 nm on a POLARstar Optima microplate reader (BMG Labtech, Germany). Data was plotted as absorbance units against logarithm of compound concentration using OriginPro 9G (OriginLab, USA). 50% inhibition of viability (GI_{50}) was determined as compound concentration required to reduce the number of metabolic active cells by 50% compared to DMSO control. The assay had already been described [37].

4.3.2.2. Cytotoxic activity against J774A.1 cell line

20

Murine macrophage cell line J774A.1 was maintained under standard conditions at 37°C and 5% CO_2 in DMEM (High glucose) supplemented with 10% fetal bovine serum.

4.3.2.2.1. Cytotoxic properties of active drugs

Cytotoxic properties of active drugs were determined in MTT assay against J774A.1 cells. 2000 cells/well were plated in 96 well plates. Cells were incubated overnight and the medium was removed from assay wells. Subsequently, 100 µL of compounds **I**, **II**, **V**, and **VI** were applied to cells at concentrations of 12 µM, 6 µM, 3 µM, 1.5 µM, 0.75 µM, 0.375 µM, 0.187 µM, 0.094 µM, 0.047 µM, while compound **IV** was applied at concentrations of 1 µM, 0.5 µM, 0.25 µM, 0.125 µM, 0.0625 µM, 0.0313 µM, 0.0156 µM, 0.0078 µM, 0.0039 µM. DMSO at concentration 0.2% (v/v) was used as vehicle control. After 72 h incubation MTT assay was performed. All experiments were conducted in triplicate and repeated at least twice.

4.3.2.2.2. Cytotoxic properties of prodrugs

Cytotoxic properties of prodrugs determined in MTT assay against J774A.1 cells. 2000 cells/well were plated in 96 well plates. Cells were incubated overnight and the medium was removed from assay wells. Subsequently, 100 µL of prodrugs **4**, **5**, **7**, **8**, and **10** were applied to cells at concentrations of 100 µM, 50 µM, 25 µM, 12.5 µM, 6.3 µM, 3.1 µM, 1.6 µM, 0.8 µM, 0.4 µM and 100 µL of prodrugs **6** and **12** at concentrations of 100 µM, 50 µM, 25 µM, 12.5 µM, 6.25 µM, 3.125 µM, 1.563 µM, 0.781 µM, 0.391 µM, 0.195 µM, 0.098 µM, 0.049 µM, 0.024 µM, 0.012 µM, 0.006 µM, 0.003 µM, 0.002 µM, 0.0001 µM. DMSO at concentration 0.5% (v/v) was used as vehicle control. After 72 h incubation MTT assay was performed. All experiments were conducted in triplicate and repeated at least twice.

4.3.2.2.3. MTT Assay

At designated time point medium in assay wells of 96-well cell culture plates was replaced with equal volume (100 µL) of the 0.5 mg/mL MTT solution in phenol free complete culture medium. The plates were incubated for 3 hours at 37°C, 5% CO_2. Upon incubation the medium was carefully removed and formazan crystals were solubilized with 100 µL DMSO for 10 minutes on orbital shaker at 300 rpm. Absorbance was measured with Tecan Spark 10M microplate reader (Tecan Trading AG, Switzerland) at 500 nm and a reference wavelength of 650 nm. The percentage of cell viability was determined using following formula: (OD 500 sample/OD500 control)*100.

4.3.3. In vitro prodrug activation by NTR

In vitro prodrug activation by NTR was performed with an assay mixture containing final concentrations: 200 µM of **6**, 1.5 mM NADH, 1.5 µM FMN and 250 nM NTR. Reactions were carried out in HEPES buffer (50 mM, pH 7.4) containing 2.5% DMSO as co-solvent at 37°C for 30 min at 300 rpm. At designated time aliquots from control and reaction samples were collected and the reaction was stopped by mixing 1:1 with cold acetonitrile (ACN).

Chromatographic separation was achieved using an ACQUITY UPLC BEH C18 Column (130Å, 1.7 µm, 2.1 mm x 100 mm, Dublin, Ireland). Mobile phase A consisted of water supplemented with 0.1% formic acid (FA) and mobile phase B consisted of ACN supplemented with 0.1% FA. Analysis was performed with a flow rate of 0.5 mL/min using

21

the following program: 0-12 min gradient of 10-80% mobile phase B, 12-14 min at 100% mobile phase B. Column temperature was maintained at 50 °C. The mass spectrophotometry study was performed with Agilent 6546 LC/Q-TOF operating in the positive ion mode.

Conflicts of Interest: The authors declare no conflict of interest.

References

1. Fan, J., et al., *Metabolic regulation of histone post-translational modifications.* ACS chemical biology, 2015. **10**(1): p. 95-108.
2. Bannister, A.J. and T. Kouzarides, *Regulation of chromatin by histone modifications.* Cell Research, 2011. **21**(3): p. 381-395.
3. Sun, X.J., et al., *The Role of Histone Acetyltransferases in Normal and Malignant Hematopoiesis.* Front Oncol, 2015. **5**: p. 108.
4. Seto, E. and M. Yoshida, *Erasers of histone acetylation: the histone deacetylase enzymes.* Cold Spring Harb Perspect Biol, 2014. **6**(4): p. a018713.
5. Park, S.-Y. and J.-S. Kim, *A short guide to histone deacetylases including recent progress on class II enzymes.* Experimental & Molecular Medicine, 2020. **52**(2): p. 204-212.
6. Pant, K., et al., *Role of histone deacetylases in carcinogenesis: potential role in cholangiocarcinoma.* Cells, 2020. **9**(3): p. 780.
7. Ropero, S. and M. Esteller, *The role of histone deacetylases (HDACs) in human cancer.* Mol Oncol, 2007. **1**(1): p. 19-25.
8. Lee, M.J., et al., *Histone deacetylase inhibitors in cancer therapy.* Curr Opin Oncol, 2008. **20**(6): p. 639-49.
9. Pramanik, S.D., et al., *Potential of histone deacetylase inhibitors in the control and regulation of prostate, breast and ovarian cancer.* Frontiers in Chemistry, 2022. **10**.
10. Chen, I.-C., B. Sethy, and J.-P. Liou, *Recent Update of HDAC Inhibitors in Lymphoma.* Frontiers in Cell and Developmental Biology, 2020. **8**.
11. Zhang, L., et al., *Zinc binding groups for histone deacetylase inhibitors.* Journal of enzyme inhibition and medicinal chemistry, 2018. **33**(1): p. 714-721.

12.   Wagner, F.F., et al., *Small molecule inhibitors of zinc-dependent histone deacetylases.* Neurotherapeutics, 2013. **10**: p. 589-604.

13.   Melesina, J., et al., *Strategies To Design Selective Histone Deacetylase Inhibitors.* ChemMedChem, 2021. **16**(9): p. 1336-1359.

14.   Vickers, C.J., et al., *Discovery of HDAC Inhibitors That Lack an Active Site Zn(2+)-Binding Functional Group.* ACS Med Chem Lett, 2012. **3**(6): p. 505-8.

15.   Perrin, J., et al., *Identifying drug targets in tissues and whole blood with thermal-shift profiling.* Nature Biotechnology, 2020. **38**(3): p. 303-308.

16.   Becher, I., et al., *Thermal profiling reveals phenylalanine hydroxylase as an off-target of panobinostat.* Nature chemical biology, 2016. **12**(11): p. 908-910.

17.   Shen, S. and A.P. Kozikowski, *Why hydroxamates may not be the best histone deacetylase inhibitors—what some may have forgotten or would rather forget?* ChemMedChem, 2016. **11**(1): p. 15-21.

18.   Ibrahim, H.S., et al., *Synthesis, Molecular Docking and Biological Characterization of Pyrazine Linked 2-Aminobenzamides as New Class I Selective Histone Deacetylase (HDAC) Inhibitors with Anti-Leukemic Activity.* Int J Mol Sci, 2021. **23**(1).

19.   Moradei, O.M., et al., *Novel Aminophenyl Benzamide-Type Histone Deacetylase Inhibitors with Enhanced Potency and Selectivity.* Journal of Medicinal Chemistry, 2007. **50**(23): p. 5543-5546.

20.   Subramanian, S., et al., *Clinical Toxicities of Histone Deacetylase Inhibitors.* Pharmaceuticals, 2010. **3**(9): p. 2751-2767.

21.   Bruserud, O., et al., *Histone Deacetylase Inhibitors in Cancer Treatment: A Review of the Clinical Toxicity and the Modulation of Gene Expression in Cancer Cells.* Current Pharmaceutical Biotechnology, 2007. **8**(6): p. 388-400.

22.   Gao, X., et al., *Efficacy and toxicity of histone deacetylase inhibitors in relapsed/refractory multiple myeloma: Systematic review and meta-analysis of clinical trials.* Exp Ther Med, 2019. **18**(2): p. 1057-1068.

23.   Fan, W., et al., *Histone deacetylase inhibitor based prodrugs.* Eur J Med Chem, 2020. **203**: p. 112628.

24.   Jornada, D.H., et al., *The Prodrug Approach: A Successful Tool for Improving Drug Solubility.* Molecules, 2015. **21**(1): p. 42.

25.   Karnthaler-Benbakka, C., et al., *Targeting a Targeted Drug: An Approach Toward Hypoxia-Activatable Tyrosine Kinase Inhibitor Prodrugs.* ChemMedChem, 2016. **11**(21): p. 2410-2421.

26.   Phillips, R.M., *Targeting the hypoxic fraction of tumours using hypoxia-activated prodrugs.* Cancer Chemother Pharmacol, 2016. **77**(3): p. 441-57.

27.   Wilson, W.R. and M.P. Hay, *Targeting hypoxia in cancer therapy.* Nat Rev Cancer, 2011. **11**(6): p. 393-410.

28.   Tietze, L.F. and K. Schmuck, *Prodrugs for targeted tumor therapies: recent developments in ADEPT, GDEPT and PMT.* Curr Pharm Des, 2011. **17**(32): p. 3527-47.

29.   Williams, E.M., et al., *Nitroreductase gene-directed enzyme prodrug therapy: insights and advances toward clinical utility.* Biochem J, 2015. **471**(2): p. 131-53.

30.   Race, P.R., et al., *Structural and mechanistic studies of Escherichia coli nitroreductase with the antibiotic nitrofurazone. Reversed binding orientations in different redox states of the enzyme.* J Biol Chem, 2005. **280**(14): p. 13256-64.

31.   Lee, M., et al., *Synthesis of an aminopropyl analog of the experimental anticancer drug tallimustine, and activation of its 4-nitrobenzylcarbamoyl prodrug by nitroreductase and NADH.* Bioorganic & Medicinal Chemistry Letters, 1997. **7**(8): p. 1065-1070.

32. Hay, M.P., et al., *Structure− Activity Relationships for 4-Nitrobenzyl Carbamates of 5-Aminobenz [e] indoline Minor Groove Alkylating Agents as Prodrugs for GDEPT in Conjunction with E. c oli Nitroreductase.* Journal of medicinal chemistry, 2003. **46**(12): p. 2456-2466.

33. Skwarska, A., et al., *Development and pre-clinical testing of a novel hypoxia-activated KDAC inhibitor.* Cell Chemical Biology, 2021. **28**(9): p. 1258-1270.e13.

34. Knox, R.J., et al., *The nitroreductase enzyme in walker cells that activates 5-(aziridin-1-yl)-2,4-dinitrobenzamide (CB 1954) to 5-(aziridin-1-YL)-4-hydroxylamino-2-nitrobenzamide is a form of NAD(P)H dehydrogenase (quinone) (EC 1.6.99.2).* Biochemical Pharmacology, 1988. **37**(24): p. 4671-4677.

35. Gruber, T.D., et al., *Cell-Specific Chemical Delivery Using a Selective Nitroreductase–Nitroaryl Pair.* ACS Chemical Biology, 2018. **13**(10): p. 2888-2896.

36. Calder, E.D.D., et al., *Hypoxia-activated pro-drugs of the KDAC inhibitor vorinostat (SAHA).* Tetrahedron, 2020. **76**(21): p. 131170.

37. Herrlinger, E.M., et al., *Nitroreductase-Mediated Release of Inhibitors of Lysine-Specific Demethylase 1 (LSD1) from Prodrugs in Transfected Acute Myeloid Leukaemia Cells.* Chembiochem, 2020. **21**(16): p. 2329-2347.

38. Ghosh, A.K. and M. Brindisi, *Organic Carbamates in Drug Design and Medicinal Chemistry.* Journal of Medicinal Chemistry, 2015. **58**(7): p. 2895-2940.

39. Alouane, A., et al., *Self-Immolative Spacers: Kinetic Aspects, Structure–Property Relationships, and Applications.* Angewandte Chemie International Edition, 2015. **54**(26): p. 7492-7509.

40. Thomas, M., et al., *Synthesis and biological evaluation of glucuronide prodrugs of the histone deacetylase inhibitor CI-994 for application in selective cancer chemotherapy.* Bioorg Med Chem, 2008. **16**(17): p. 8109-16.

41. Zessin, M., et al., *One-Atom Substitution Enables Direct and Continuous Monitoring of Histone Deacylase Activity.* Biochemistry, 2019. **58**(48): p. 4777-4789.

42. Abdelsalam, M., et al., *Development of Pyrazine-Anilinobenzamides as Histone Deacetylase HDAC1–3 Selective Inhibitors and Biological Testing Against Pancreas Cancer Cell Lines*, in *HDAC/HAT Function Assessment and Inhibitor Development: Methods and Protocols*, O.H. Krämer, Editor. 2023, Springer US: New York, NY. p. 145-155.

43. Marek, M., et al., *Characterization of Histone Deacetylase 8 (HDAC8) Selective Inhibition Reveals Specific Active Site Structural and Functional Determinants.* Journal of Medicinal Chemistry, 2018. **61**(22): p. 10000-10016.

44. Heimburg, T., et al., *Structure-Based Design and Biological Characterization of Selective Histone Deacetylase 8 (HDAC8) Inhibitors with Anti-Neuroblastoma Activity.* J Med Chem, 2017. **60**(24): p. 10188-10204.

3.5. N^4-(2-Amino-4-fluorophenyl)-N^1-(3-{2-[2-(3-{[2-(2,6-dioxo-3-piperidyl)-1,3-dioxoisoindolin-4-yl]amino}propoxy)ethoxy]ethoxy}propyl)-terephthalamide

Mohamed Abdelsalam, Matthes Zessin, Matthias Schmidt, Mike Schutkowski
and Wolfgang Sippl

Abstract

The design of proteolysis targeting chimeras (PROTACs) has become a promising technology for modifying a protein of interest (POI) through protein degradation. Herein, we describe the synthetic pathway to develop N^4-(2-amino-4-fluorophenyl)-N^1-(3-{2-[2-(3-{[2-(2,6-dioxo-3-piperidyl)-1,3-dioxoisoindolin-4-yl]amino}propoxy)ethoxy]ethoxy}propyl)terephthalamide, which was designed to work as a selective degrader of histone deacetylase-3 (HDAC3). The newly synthesized compounds were characterized by ^{1}H-NMR, ^{13}C-NMR, IR and HRMS. The title compound was tested in vitro against human class-I HDACs isoforms and showed IC$_{50}$ = 3.4 µM against HDAC3; however, it did not show degradation for the targeted HDACs.

N^4-(2-Amino-4-fluorophenyl)-N^1-(3-{2-[2-(3-{[2-(2,6-dioxo-3-piperidyl)-1,3-dioxoisoindolin-4-yl]amino}propoxy)ethoxy]ethoxy}propyl)terephthalamide

Mohamed Abdelsalam [1,2] , **Matthes Zessin** [1,3] , **Matthias Schmidt** [1] , **Mike Schutkowski** [3] and **Wolfgang Sippl** [1,*]

1 Department of Medicinal Chemistry, Institute of Pharmacy, Martin-Luther-University of Halle-Wittenberg, 06120 Halle (Saale), Germany
2 Department of Pharmaceutical Chemistry, Faculty of Pharmacy, Alexandria University, Alexandria 21521, Egypt
3 Department of Enzymology, Institute of Biochemistry, Martin-Luther-University of Halle-Wittenberg, 06120 Halle (Saale), Germany
* Correspondence: wolfgang.sippl@pharmazie.uni-halle.de

Abstract: The design of proteolysis targeting chimeras (PROTACs) has become a promising technology for modifying a protein of interest (POI) through protein degradation. Herein, we describe the synthetic pathway to develop N^4-(2-amino-4-fluorophenyl)-N^1-(3-{2-[2-(3-{[2-(2,6-dioxo-3-piperidyl)-1,3-dioxoisoindolin-4-yl]amino}propoxy)ethoxy]ethoxy}propyl)terephthalamide, which was designed to work as a selective degrader of histone deacetylase-3 (HDAC3). The newly synthesized compounds were characterized by ^{1}H-NMR, ^{13}C-NMR, IR and HRMS. The title compound was tested in vitro against human class-I HDACs isoforms and showed IC_{50} = 3.4 μM against HDAC3; however, it did not show degradation for the targeted HDACs.

Keywords: PROTACs; HDAC isoforms; HDAC inhibitors; 2-aminobenzamides

1. Introduction

Class-I histone deacetylases (including HDAC1, 2, 3, and 8 isoforms) are among eleven zinc-dependent histone deacetylases that catalyze the hydrolysis of acetyl groups from histone lysine residues [1]. They play an important role in the regulation of gene expression and cell proliferation [2]. Dysregulation of their epigenetic activity has been involved in a wide range of diseases [3–5], including cancer [2]. Several HDAC inhibitors (HDACis) have been developed and identified as potential anticancer therapeutics [6]. Most HDACis share a common pharmacophoric scaffold consisting of three different parts as follows: a zinc binding group (ZBG) that is responsible for chelating of zinc ion in the active site of HDACs, a capping group that usually induce hydrophobic interactions at the rim of the HDAC enzyme, in addition to a linker connecting both groups [7]. HDACis can be classified based on their zinc binding groups (ZBG) into different groups, mainly hydroxamates, 2-aminobenzamides, thiols, cyclic peptides, and others [8]. To date, four HDACis have been approved by US Food and Drug Administration (FDA) for treatment of different hematological malignancies including the hydroxamate-based vorinostat, belinostat and panobinostat, in addition to the cyclic peptide romidepsin [9]. Although the hydroxamic acids exhibit potent ZBG activity, it was observed that hydroxamate-based HDACis lack isoform selectivity, and this might contribute to the off-target side effect associated with such drugs [10,11]. It has been reported that 2-aminobenzamides can enhance class-I HDAC selectivity and strongly inhibit HDAC subtypes HDACs1, -2, and -3 [12]. Tacedinaline (Figure 1) is the first reported 2-aminobenzamide-based HDAC inhibitor, which is currently in a clinical trial (phase II) for treatment of patients with multiple myeloma [13]. BRD3308

is an analog of tacedinaline with higher selectivity against HDAC3 (IC$_{50}$ HDAC3 = 64 nM) (Figure 1) [14].

(A)

(B)

Tacedinaline

IC$_{50}$ (HDAC1) 0.9 µM
IC$_{50}$ (HDAC2) 0.9 µM
IC$_{50}$ (HDAC3) 1.2 µM

BRD 3308

IC$_{50}$ (HDAC1) 1.08 µM
IC$_{50}$ (HDAC2) 1.15 µM
IC$_{50}$ (HDAC3) 0.064 µM

Pomalidomide

(C)

Compound 5
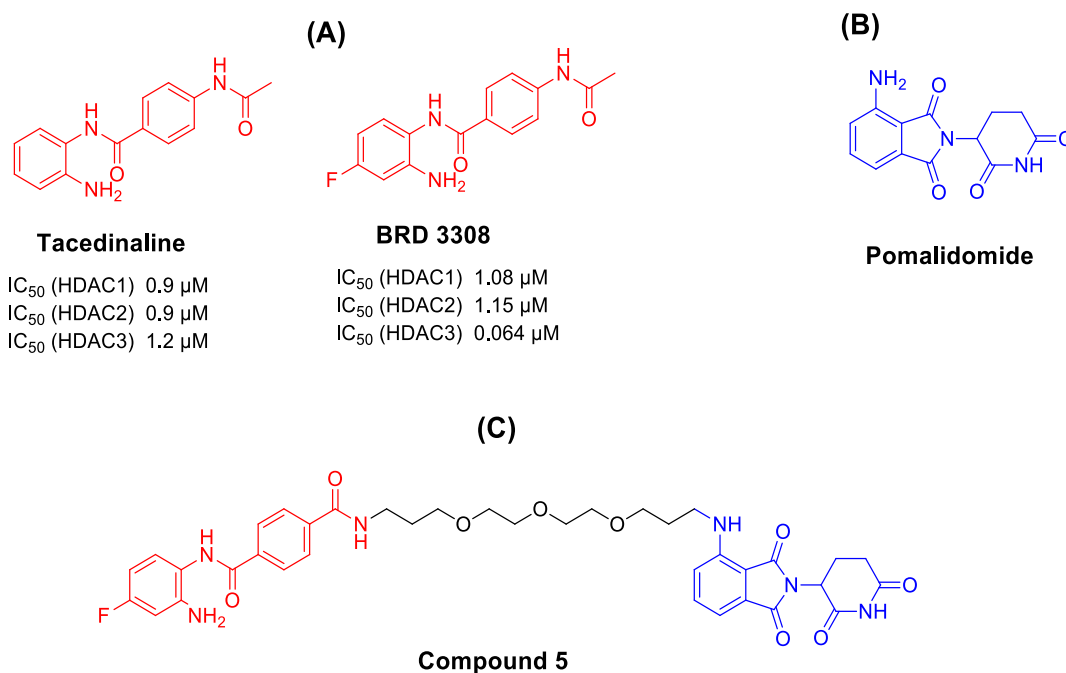
Figure 1. Design of HDACs-PROTACs. (**A**) Examples of 2-aminobenzamide-based HDAC inhibitors. (**B**) Example of CRBN-based E3 ligase ligand. (**C**) Our designed HDAC-PROTACs.

PROTACs are hybrid bifunctional molecules connecting a protein of interest (POI) ligand to an E3 ubiquitin ligase (E3) recruiting ligand using a certain linker [15]. The von Hippel–Lindau (VHL) and cereblon (CRBN) ligands are the most frequently used E3 ligands for PROTACs design [16]. Binding of a PROTACs molecule to both a protein of interest and E3 ligase induce the formation of ternary complex. Formation of such a complex hijacks subsequent ubiquitination of the target protein and degradation via the ubiquitin-proteasome system (UPS) [16]. Due to this characteristic mechanism of action, the PROTACs approach has several advantages compared to conventional inhibitors. Firstly, PROTACs technology has been demonstrated to overcome the problem of resistance encountered in most current therapeutics through elimination of the entire target, which results in deletion of both enzymatic and non-enzymatic activity of the target protein [15]. In addition, the degradation of a POI through PROTACs is a catalytic process which means that only low doses of PROTACs are required; therefore, PROTACs are less prone to target overexpression and mutations [15]. In the past few years, targeting different HDAC isoforms using the PROTAC approach has attracted great interest. In 2018, we reported the development of the first Sirtuin-2 deacetylase degrader [17]. Very recently we have also reported the design of novel HDAC8 degraders [18].

In the present study, we planned to design a selective degrader for class-I HDACs isoforms. For the PROTAC design, the 2-aminobenzamide selective HDAC-3 inhibitor (BRD3308) was chosen and connected to the (CRBN) E3 ligase ligand (pomalidomide) through a polyethylene glycol linker (Figure 1).

2. Results and Discussion

2.1. Chemistry

To obtain the desired compound, a synthetic strategy was used that involved three main steps, as shown in Scheme 1. The first step involved synthesis of the HDAC3 inhibitor part functionalized with carboxylic acid group **3**. This intermediate was synthesized via the

amide coupling reaction between 4-methoxycarbonylbenzoic acid (**1**) and 4-fluorobenzene-1,2-diamine (**2**) using hexafluorophosphate azabenzotriazole tetramethyl uronium (HATU) as a carboxylic acid activating agent and DIPEA, followed by the alkaline hydrolysis of the methyl ester using lithium hydroxide to afford the desired carboxylic acid **3**. The second step included the preparation of the pomalidomide connected to the polyethylene glycol linker functionalized with terminal primary amine intermediate **4**. This intermediate was synthesized according to the previously reported method [19]. Finally, amide coupling between the obtained carboxylic acid (**3**) and the pomalidomide-linker-amine **4** was carried out using the method mentioned above to afford compound **5**.
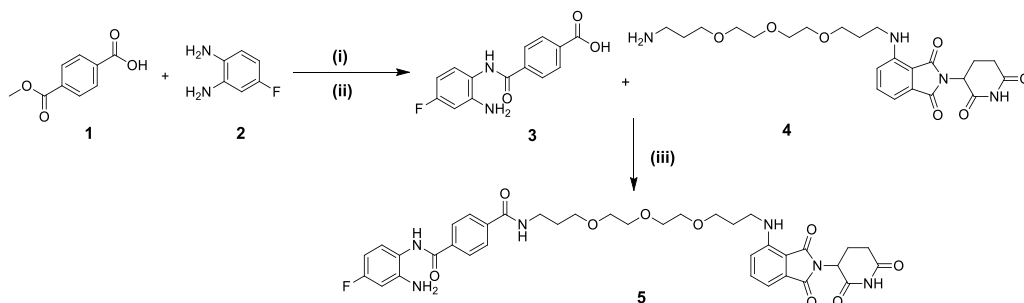
Scheme 1. The synthetic pathway toward the synthesis of compound **5** involved the synthesis of intermediates **3** and **4** followed by amide coupling to obtain the final compound. Reagents and conditions: (**i**) HATU, DIPEA, DMF, RT, 3 h; (**ii**) LiOH.H$_2$O, THF, H$_2$O, RT, 5 h; (**iii**); HATU, DIPEA, DMF, RT, 3 h.

2.2. Biological Evaluation

2.2.1. In Vitro HDAC Inhibition Assay

Compound **5** was subjected to in vitro HDAC inhibition activity against human class-I HDACs (HDAC1, 2, and 3) using a fluorogenic peptide derived from p53 (Ac-RHKK(Acetyl)-AMC) HDAC1-3 isoforms as demonstrated in Table 1 [20]. Compound **5** showed moderate inhibitory activity against HDAC1 and 2, while it showed an IC$_{50}$ = 3.4 µM for HDAC3.

Table 1. Inhibitory activity of compound (**5**) against HDAC 1, 2, and 3.

Cpd. No.	Structure	HDAC1 (IC$_{50}$ µM)	HDAC2 (IC$_{50}$ µM)	HDAC3 (IC$_{50}$ µM)
5		18.0 ± 1	14.0 ± 1	3.4 ± 0.1

2.2.2. Cellular Testing

In addition, compound **5** was tested against a pancreatic cancer cell line (PSN1). In order to evaluate the degradation capability of synthesized PROTAC for HDAC1-3, the cellular levels of HDAC1-3 in PSN1 cell line were analyzed by Western blot. When tested in human HCT116 cells, compound **5** unfortunately showed no degradation of HDAC1-3 (data not shown). Further structural modifications might be tested for compound **5** (e.g., using different linkers with different lengths, further ubiquitin E3 ligase ligands) to obtain the desired degradation activity. In summary, we established a synthetic route for class I HDAC degraders with good yields that can be used for the development of further analogs.

3. Materials and Methods

3.1. General Experimental Information

Materials and reagents were purchased from Sigma-Aldrich Co., Ltd. (Darmstadt, Germany) and abcr GmbH (Karlsruhe, Germany). All solvents were analytically pure and dried before use. Thin layer chromatography was carried out on aluminum sheets coated with silica gel 60 F254 (Merck, Darmstadt, Germany). For medium pressure chromatography (MPLC), silica gel 60 (0.036e0.200 mm) was used. The melting points (mp) were determined on Boëtius hot stage apparatus (VEB Kombinat, NAGEMA, Dresden, GDR). Purity was measured by UV absorbance at 254 nm. The HPLC consisted of a LiChrosorb®® RP-18 (5 μm) 100-4.6 Merck column (Merck, Darmstadt, Germany), two LC-10AD pumps, a SPD-M10A VP PDA detector, and a SIL-HT autosampler, all from the manufacturer Shimadzu (Kyoto, Japan). The absorption spectra were recorded with a SPD-M10A diode array detector Shimadzu spectrophotometer (Kyoto, Japan). Mass spectrometry analyses were performed with a Finnigan MAT710C (Thermo Separation Products, SanJose, CA, USA) for the ESI MS spectra and with a LTQ (linear ion trap) Orbitrap XL hybrid mass spectrometer (Thermo Fisher Scientific, Bremen, Germany) for the HRMS-ESI (high-resolution mass spectrometry) spectra. IR spectra were taken using an FTIR, using potassium bromide (KBr) as a supporting material (ATR method). For the HRMS analyses, the signal for the isotopes with the highest prevalence was given and calculated. ^{1}H NMR spectra were taken on a Varian Inova 400 using deuterated DMSO as solvent. Chemical shifts were referenced to the residual solvent signals. The following abbreviations and formulas for solvents and reagents were used: ethyl acetate (EtOAc), *N,N*-dimethylformamide (DMF), dimethyl sulfoxide (DMSO), methanol (MeOH), tetrahydrofuran (THF), water (H_2O), dichloromethane (DCM), *N,N*-diisopropylethylamine (DIPEA), *O*-(7-azabenzotriazol-1-yl)-*N,N,N′,N′*-tetramethyluronium-hexafluorphosphate (HATU) and hydrochloric acid (HCl), trifluoroacetic acid (TFA).

3.2. Experimental Procedures and Characterization of Synthesized Compounds

4-[(2-Amino-4-fluorophenyl)carbamoyl]benzoic acid (**3**)

A mixture of the 4-methoxycarbonylbenzoic acid (1) (0.145 g, 0.8 mmol, 1 eq.), HATU (0.35 g, 0.92 mmol, 1.15 eq.) was dissolved in dry DMF (5 mL) and stirred at RT for 30 min. 4-Fluorobenzene-1,2-diamine (2) (0.11 g, 0.87 mmol, 1.1 eq.) and DIPEA (0.7 mL, 4.02 mmol, 5 eq.) were added and the reaction mixture was stirred at RT for 3 h. The reaction mixture was diluted with EtOAc (15 mL) and the reaction mixture was washed with 1 N NH_4Cl and 1 N $NaHCO_3$, respectively. The organic extracts were washed with brine, dried over anhydrous Na_2SO_4, filtered and concentrated under vacuum. The residue was purified using MPLC using (DCM—MeOH) to provide the corresponding amide, which was further dissolved in a mixture of 10 mLTHF: H_2O (1:1); then, lithium hydroxide monohydrate (87 mg) was added to the solution and the reaction mixture was stirred at RT for 5 h. The TLC showed that there were no starting materials. Then, the mixture was neutralized using 1N HCl. The precipitated solid was filtered and dried under vacuum to obtain the corresponding carboxylic acid 3 as beige amorphous powder; mp. 275–277 °C; yield (0.11 g, 0.4 mmol, 50% over 2 steps); ^{1}H NMR (400 MHz, DMSO-d^6) δ 13.20 (s, 1H), 9.71 (s, 1H), 8.04 (q, *J* = 8.2 Hz, 4H), 7.15–7.05 (m, 1H), 6.52 (d, *J* = 11.2 Hz, 1H), 6.34 (t, *J* = 8.4 Hz, 1H), 5.24 (s, 2H); ^{13}C NMR (101 MHz, DMSO-d^6) δ 167.2, 165.4, 162.8, 160.4, 145.9, 138.8, 133.5, 129.6, 129.1, 128.5, 119.3, 102.3, 1020, 101.7; IR (KBr, ν, cm^1): 3321, 3234, 3072, 2849, 2675, 2558, 1683, 1639, 1622, 1612; MS-ESI *m/z*: 273.18 [M–H]$^-$; HPLC: rt 9.30 min using MeOH/H_2O/0.05%TFA (purity 96.52%); UV-Vis spectra (MeOH/H_2O/TFA 50: 50: 0.05), λmax: 212 nm (ε = 974 M^{-1} cm^{-1}, log ε = 2.99), 226 nm (ε = 1003 M^{-1} cm^{-1}, log ε = 3.00), 256 nm (ε = 411 M^{-1} cm^{-1}, log ε = 2.61), 287 nm (ε = 300 M^{-1} cm^{-1}, log ε = 2.48).

4-(3-{2-[2-(3-Aminopropoxy)ethoxy]ethoxy}propylamino)-2-(2,6-dioxo-3-piperidyl)-isoindoline-1,3-dione (**4**) was synthesized according to the previously reported method (Supplementary Materials) [19].

N^4-(2-Amino-4-fluorophenyl)-N^1-(3-{2-[2-(3-{[2-(2,6-dioxo-3-piperidyl)-1,3-dioxois-oindolin-4-yl]amino}propoxy)ethoxy]ethoxy}propyl)terephthalamide (**5**)

A mixture of compound **3** (0.11, 0.4 mmol, 1.0 eq.) and HATU (0.167 g, 0.44 mmol, 1.1 eq.) was dissolved in dry DMF (5 mL) and stirred at RT for 30 min. Intermediate 4 (0.21 g, 0.44 mmol, 1.1 eq.) and DIPEA (0.35 mL, 2 mmol, 5.0 eq.) were added and the reaction mixture was stirred at RT for 3 h. The reaction mixture was diluted with ethyl acetate (30 mL) and the reaction mixture was washed with 1 N NH_4Cl and saturated $NaHCO_3$, respectively. The combined organic extracts were washed with brine, dried over anhydrous Na_2SO_4, filtered, and concentrated under vacuum. The residue was purified using MPLC (Chloroform—MeOH) to provide the targeted compound as yellow amorphous powder; mp. 96–98 °C; yield (0.12 g, 0.16 mmol, 40.9%); ^{1}H NMR (400 MHz, DMSO-d^6) δ 11.06 (s, 1H), 9.66 (s, 1H), 8.54 (t, J = 5.5 Hz, 1H), 8.02 (d, J = 8.4 Hz, 2H), 7.92 (d, J = 8.4 Hz, 2H), 7.55 (dd, J = 8.5, 7.2 Hz, 1H), 7.14–7.05 (m, 2H), 7.00 (d, J = 6.9 Hz, 1H), 6.64 (t, J = 5.9 Hz, 1H), 6.53 (dd, J = 11.2, 2.9 Hz, 1H), 6.34 (td, J = 8.5, 2.9 Hz, 1H), 5.23 (s, 2H), 5.03 (dd, J = 12.8, 5.4 Hz, 1H), 3.57–3.42 (m, 12H), 3.39–3.30 (m, 4H), 2.86 (ddd, J = 17.6, 14.1, 5.5 Hz, 1H), 2.62–2.51 (m, 2H), 2.00 (ddd, J = 10.6, 7.2, 4.8 Hz, 1H), 1.83–1.71 (m, 4H); ^{13}C NMR (101 MHz, DMSO-d^6) δ 173.2, 170.5, 169.3, 167.8, 165.9, 165.4, 146.9, 146.1, 146.0, 137.4, 137.1, 136.7, 132.6, 129.1, 128.2, 127.4, 117.5, 110.8, 109.5, 102.6, 102.3, 102.0, 101.7, 70.3, 70.2, 70.1, 70.0, 68.7, 68.7, 49.0, 37.2, 31.4, 29.8, 29.3, 22.6; IR (KBr, ν, cm^{-1}): 3360, 2870, 1693., 1624, 1511; HRMS *m/z*: 733.299 [M + H]$^+$; calculated $C_{37}H_{42}FN_6O_9^+$: 733.299; HPLC: rt 12.26 min using MeOH/H_2O/0.05%TFA (purity 96.59%); UV-Vis spectra (MeOH/H_2O/TFA 50: 50: 0.05), λmax: 229 nm ($ε$ = 2839 M^{-1} cm^{-1}, log $ε$ = 3.45), 260 nm ($ε$ = 1109 M^{-1} cm^{-1}, log $ε$ = 3.04), 420 nm ($ε$ = 569 M^{-1} cm^{-1}, log $ε$ = 2.76).

3.3. Biological Testing

In Vitro HDAC Inhibition Assay

Recombinant human HDAC1, HDAC2, and HDAC3/NCOR1 were purchased from ENZO Life Sciences AG (Lausen, CH). The in vitro testing on recombinant HDACs 1-3 was performed as described in (Supplementary Materials) [12].

Supplementary Materials: The following supporting information can be downloaded online. Synthesis of intermediate **4**, in vitro HDAC inhibitory assay and copies of ^{1}H-NMR, ^{13}C-NMR, HPLC, IR, MS, and UV spectra.

Author Contributions: M.A. carried out the synthesis and analytical characterization and wrote the manuscript, M.Z. carried out the in vitro HDAC testing, M.S. (Matthias Schmidt) contributed in synthesis planning analytical characterization, M.S. (Mike Schutkowski) supervised the in vitro testing, W.S. carried out data analysis, supervised the project and manuscript writing. All authors have read and agreed to the published version of the manuscript.

Data Availability Statement: Not applicable.

Conflicts of Interest: The authors declare no conflict of interest.

References

1. Pant, K.; Peixoto, E.; Richard, S.; Gradilone, S.A. Role of histone deacetylases in carcinogenesis: Potential role in cholangiocarci-noma. *Cells* **2020**, *9*, 780. [CrossRef] [PubMed]
2. Fraga, M.F.; Ballestar, E.; Villar-Garea, A.; Boix-Chornet, M.; Espada, J.; Schotta, G.; Bonaldi, T.; Haydon, C.; Ropero, S.; Petrie, K. Loss of acetylation at Lys16 and trimethylation at Lys20 of histone H4 is a common hallmark of human cancer. *Nat. Genet.* **2005**, *37*, 391–400. [CrossRef] [PubMed]
3. Abel, T.; Zukin, R.S. Epigenetic targets of HDAC inhibition in neurodegenerative and psychiatric disorders. *Curr. Opin. Pharmacol.* **2008**, *8*, 57–64. [CrossRef] [PubMed]

4. Wang, Y.; Miao, X.; Liu, Y.; Li, F.; Liu, Q.; Sun, J.; Cai, L. Dysregulation of Histone Acetyltransferases and Deacetylases in Cardiovascular Diseases. *Oxid. Med. Cell. Longev.* **2014**, *2014*, 641979. [CrossRef] [PubMed]
5. Zeng, C.; Tsoi, L.C.; Gudjonsson, J.E. Dysregulated epigenetic modifications in psoriasis. *Exp. Dermatol.* **2021**, *30*, 1156–1166. [CrossRef] [PubMed]
6. Gryder, B.E.; Sodji, Q.H.; Oyelere, A.K. Targeted cancer therapy: Giving histone deacetylase inhibitors all they need to succeed. *Future Med. Chem.* **2012**, *4*, 505–524. [CrossRef] [PubMed]
7. Zhang, L.; Zhang, J.; Jiang, Q.; Zhang, L.; Song, W. Zinc binding groups for histone deacetylase inhibitors. *J. Enzym. Inhib. Med. Chem.* **2018**, *33*, 714–721. [CrossRef] [PubMed]
8. Wagner, F.F.; Weïwer, M.; Lewis, M.C.; Holson, E.B. Small molecule inhibitors of zinc-dependent histone deacetylases. *Neurotherapeutics* **2013**, *10*, 589–604. [CrossRef] [PubMed]
9. Ho, T.C.S.; Chan, A.H.Y.; Ganesan, A. Thirty Years of HDAC Inhibitors: 2020 Insight and Hindsight. *J. Med. Chem.* **2020**, *63*, 12460–12484. [CrossRef] [PubMed]
10. Perrin, J.; Werner, T.; Kurzawa, N.; Rutkowska, A.; Childs, D.D.; Kalxdorf, M.; Poeckel, D.; Stonehouse, E.; Strohmer, K.; Heller, B. Identifying drug targets in tissues and whole blood with thermal-shift profiling. *Nat. Biotechnol.* **2020**, *38*, 303–308. [CrossRef] [PubMed]
11. Becher, I.; Werner, T.; Doce, C.; Zaal, E.A.; Tögel, I.; Khan, C.A.; Rueger, A.; Muelbaier, M.; Salzer, E.; Berkers, C.R. Thermal profiling reveals phenylalanine hydroxylase as an off-target of panobinostat. *Nat. Chem. Biol.* **2016**, *12*, 908–910. [CrossRef] [PubMed]
12. Ibrahim, H.S.; Abdelsalam, M.; Zeyn, Y.; Zessin, M.; Mustafa, A.-H.M.; Fischer, M.A.; Zeyen, P.; Sun, P.; Bülbül, E.F.; Vecchio, A.; et al. Synthesis, Molecular Docking and Biological Characterization of Pyrazine Linked 2-Aminobenzamides as New Class I Selective Histone Deacetylase (HDAC) Inhibitors with Anti-Leukemic Activity. *Int. J. Mol. Sci.* **2022**, *23*, 369. [CrossRef] [PubMed]
13. Xie, R.; Tang, P.; Yuan, Q. Rational design and characterization of a DNA/HDAC dual-targeting inhibitor containing nitrogen mustard and 2-aminobenzamide moieties. *Medchemcomm* **2018**, *9*, 344–352. [CrossRef] [PubMed]
14. Wagner, F.F.; Lundh, M.; Kaya, T.; McCarren, P.; Zhang, Y.-L.; Chattopadhyay, S.; Gale, J.P.; Galbo, T.; Fisher, S.L.; Meier, B.C.; et al. An Isochemogenic Set of Inhibitors to Define the Therapeutic Potential of Histone Deacetylases in β-Cell Protection. *ACS Chem. Biol.* **2016**, *11*, 363–374. [CrossRef] [PubMed]
15. Sun, X.; Gao, H.; Yang, Y.; He, M.; Wu, Y.; Song, Y.; Tong, Y.; Rao, Y. PROTACs: Great opportunities for academia and industry. *Signal Transduct. Target. Ther.* **2019**, *4*, 64. [CrossRef] [PubMed]
16. Bricelj, A.; Steinebach, C.; Kuchta, R.; Gütschow, M.; Sosič, I. E3 Ligase Ligands in Successful PROTACs: An Overview of Syntheses and Linker Attachment Points. *Front. Chem.* **2021**, *9*, 707317. [CrossRef] [PubMed]
17. Schiedel, M.; Herp, D.; Hammelmann, S.R.; Swyter, S.R.; Lehotzky, A.; Robaa, D.; Oláh, J.; Ovadi, J.; Sippl, W.; Jung, M. Chemically induced degradation of sirtuin 2 (Sirt2) by a proteolysis targeting chimera (PROTAC) based on sirtuin rearranging ligands (SirReals). *J. Med. Chem.* **2018**, *61*, 482–491. [CrossRef] [PubMed]
18. Darwish, S.; Ghazy, E.; Heimburg, T.; Herp, D.; Zeyen, P.; Salem-Altintas, R.; Ridinger, J.; Robaa, D.; Schmidtkunz, K.; Erdmann, F.; et al. Design, Synthesis and Biological Characterization of Histone Deacetylase 8 (HDAC8) Proteolysis Targeting Chimeras (PROTACs) with Anti-Neuroblastoma Activity. *Int. J. Mol. Sci.* **2022**, *23*, 7535. [CrossRef] [PubMed]
19. Cheng, J.; Li, Y.; Wang, X.; Dong, G.; Sheng, C. Discovery of Novel PDEδ Degraders for the Treatment of KRAS Mutant Colorectal Cancer. *J. Med. Chem.* **2020**, *63*, 7892–7905. [CrossRef] [PubMed]
20. Zessin, M.; Kutil, Z.F.; Meleshin, M.; Nováková, Z.; Ghazy, E.; Kalbas, D.; Marek, M.; Romier, C.; Sippl, W.; Bařinka, C. One-atom substitution enables direct and continuous monitoring of histone deacylase activity. *Biochemistry* **2019**, *58*, 4777–4789. [CrossRef] [PubMed]

3.6. Histone Deacetylase (HDAC) Inhibitors for the Treatment of Schistosomiasis

Ehab Ghazy, **Mohamed Abdelsalam**, Dina Robaa, Raymond J. Pierce and Wolfgang Sippl

Abstract

Schistosomiasis is a major neglected parasitic disease that affects more than 240 million people worldwide and for which the control strategy consists of mass treatment with the only available drug, praziquantel. Schistosomes display morphologically distinct stages during their life cycle and the transformations between stages are controlled by epigenetic mechanisms. The targeting of epigenetic actors might therefore represent the parasites' Achilles' heel. Specifically, histone deacetylases have been recently characterized as drug targets for the treatment of schistosomiasis. This review focuses on the recent development of inhibitors for schistosome histone deacetylases. In particular, advances in the development of inhibitors of *Schistosoma mansoni* histone deacetylase 8 have indicated that targeting this enzyme is a promising approach for the treatment of this infection.

Review

Histone Deacetylase (HDAC) Inhibitors for the Treatment of Schistosomiasis

Ehab Ghazy [1,2,†], Mohamed Abdelsalam [1,2,†], Dina Robaa [1], Raymond J. Pierce [3] and Wolfgang Sippl [1,*]

1 Department of Medicinal Chemistry, Institute of Pharmacy, Martin-Luther-University of Halle-Wittenberg, 06120 Halle (Saale), Germany; ehab.ghazy@alexu.edu.eg (E.G.); mohamed.abdelsalam@pharmazie.uni-halle.de (M.A.); dina.robaa@pharmazie.uni-halle.de (D.R.)
2 Department of Pharmaceutical Chemistry, Faculty of Pharmacy, Alexandria University, Alexandria 21521, Egypt
3 Centre d'Infection et d'Immunité de Lille, U1019—UMR9017—CIIL, Institute Pasteur de Lille, CNRS, Inserm, CHU Lille, Univ. Lille, F-59000 Lille, France; raymond.pierce@sfr.fr
* Correspondence: wolfgang.sippl@pharmazie.uni-halle.de
† These authors contributed equally to this work.

Abstract: Schistosomiasis is a major neglected parasitic disease that affects more than 240 million people worldwide and for which the control strategy consists of mass treatment with the only available drug, praziquantel. Schistosomes display morphologically distinct stages during their life cycle and the transformations between stages are controlled by epigenetic mechanisms. The targeting of epigenetic actors might therefore represent the parasites' Achilles' heel. Specifically, histone deacetylases have been recently characterized as drug targets for the treatment of schistosomiasis. This review focuses on the recent development of inhibitors for schistosome histone deacetylases. In particular, advances in the development of inhibitors of *Schistosoma mansoni* histone deacetylase 8 have indicated that targeting this enzyme is a promising approach for the treatment of this infection.

Keywords: schistosomiasis; epigenetic; smHDAC8; hydroxamic acids; HDAC inhibitors; sirtuins

1. Introduction

1.1. HDACs: Functions, Classes, and Therapeutic Potential

Histone acetylation is one of the most studied post-translational modifications. The state of histone acetylation is controlled through the "writers", histone acetyltransferases (HATs) and the "erasers", histone deacetylases (HDACs). HDACs are responsible for the removal of acyl (mostly acetyl) groups from lysine residues. Their substrates include histones and numerous non-histone proteins, such as p53, cytoskeleton proteins, RNA processing enzymes, and proteins involved in cell signaling and apoptosis [1]. So far, 18 different human HDACs isoforms have been identified, differing in size, cellular distribution, substrate, acyl group removed, and mechanism of catalytic activity. HDACs are classified into two major categories; the classical Zn^{2+}-dependent HDACs and sirtuins [1]. Classical histone deacetylases, for which the abbreviation HDACs will refer from now on, comprise 11 enzymes that have a zinc ion in the active site responsible for their catalytic activity. These metalloenzymes have a conserved deacetylase domain but differ in size, cellular localization, and substrates [2]. They are further classified in classes I (HDACs 1–3, 8), IIa (HDACs 4, 5, 7, 9), IIb (HDACs 6, 10), and IV (HDAC11) [3–5]. Non-classical HDACs (class III) are named sirtuins due to their homology to the yeast silent information regulator 2 (SIR2). Unlike HDACs, the seven sirtuin isoforms exert their deacetylase activity by utilizing nicotinamide adenine dinucleotide (NAD^+) as a cofactor; the catalytic reaction involves the cleavage of the nicotinamide moiety and the transfer of the acyl group from the lysine residue to ADP-ribose [6,7]. HDACs and sirtuins are involved in the regulation of different physiological functions, and their uncontrolled activity is linked to many pathological

conditions. As a result, their structure, substrates, biological roles, and relation to disease have been extensively studied, and many informative reviews on HDACs (such as [1,8–13]) and sirtuins (such as [6,7,14–16]) are available. Moreover, HDAC inhibitors (HDACi) were investigated as potential therapeutic agents for several diseases [17–24], with oncology being the most successful field as six HDACi have received regulatory approval for the treatment of different hematological malignancies [1,25].

1.2. Repurposing Anticancer HDACi as Antiparasitic Agents

Neglected parasitic diseases affect millions of people with high morbidity and mortality. Lack of vaccines and a limited number of available drugs have resulted in their extensive use, raising the concern of resistance and consequent treatment failure. Additionally, current therapies sometimes involve long regimes, are usually active against only specific life-cycle forms of the parasites, and occasionally can have severe side effects [26]. As a result, new antiparasitic agents with novel mechanisms of action are urgently needed. One attractive strategy in this regard is the "piggyback" approach aiming to repurpose some drugs, already approved for other human diseases, as potential antiparasitic agents, which could decrease the time and costs to develop novel therapies [27]. Anticancer agents are especially attractive for this approach as tumors and parasites are similar in some aspects such as high metabolic and reproductive activity and the ability to survive within the host immune system [28]. Parasites are characterized by a complex life cycle with several morphologically distinct forms indicating the epigenetic control of gene expression. Indeed, major human parasites depend on HDACs and other epigenetic modulators for their survival and growth; therefore, HDACs were suggested as potential novel targets for antiparasitic therapy [26,29]. While the current work focuses on HDAC inhibitors as potential treatments for schistosomiases, HDACi for other parasitic infections such as malaria [30–35], trypanosomiasis [27,36–38], toxoplasmosis [39,40], leishmaniasis [41–43], and cestode infections [44] have also been reported and reviewed [26,29].

1.3. Schistosomiasis—Key Facts

Schistosomiasis is a parasitic infection that affects around 240 million people worldwide and is prevalent in poor tropical and subtropical regions, mostly in Africa [45]. The infection is caused by blood flukes from the genus *Schistosoma*, mainly *S. mansoni*, *S. haematobium*, and *S. japonicum* [45]. The parasite life cycle involves a specific snail intermediate host where the infective cercariae develop and then infect the human host to become the schistosomula (larvae) which later migrate to the liver and mature into adult male and female worms. Upon pairing, the eggs are then released in the feces to repeat the life cycle [46]. Current treatment and control of schistosomiasis exclusively depends on the antiparasitic agent praziquantel. Although this agent is active against parasitic flatworms, some reports suggested lack of efficacy during mass drug administration programs raising the concern of the development of drug resistance [46]. Therefore, new antischistosomal therapies with novel targets and mechanisms of action are of high interest. Repurposing of HDAC inhibitors against schistosomiasis appears a promising strategy given their previously mentioned success in the oncology field and also the identification of essential histone deacetylases in *S. mansoni* [47].

1.4. SmHDAC8, a Potential Drug Target in Schistosomes

Several orthologs of the human HDACs have been identified and characterized in schistosomes, belonging to classes I (smHDAC1, 3, and 8), II (smHDAC4, 5, and 6), and III (smSirt1, 2, 5, 6, and 7) [48,49]. Members of class I are expressed in all life cycles of the parasite, with the smHDAC8 isoform having the most abundant transcripts [50,51]. Interestingly, the human counterpart (hHDAC8) usually shows a lower level of expression in human cells compared to HDAC1 and 3 [51]. Therefore, it was suggested that this isoform may have a specific function for the parasite and could be an attractive target for novel antischistosomal therapy [50,51]. This was further supported by smHDAC8

knockdown studies demonstrating a significantly reduced viability and fertility of the parasites [52]. Crystal structures of smHDAC8 show that this enzyme adopts the canonical α/β HDAC fold, with specific solvent exposed loops corresponding to insertions in the schistosome HDAC8 sequence. These extensions do not affect the binding site and hence have no direct effect on the catalytic mechanism or ligand binding. SmHDAC8 shares the highest structural similarity with human HDAC8, and both enzymes show a characteristic subpocket in the binding site, dubbed the HDAC8-specific side pocket. This pocket is formed by the catalytic tyrosine residue, the L6 and L1-loop, where the latter loop is significantly shorter than in the other human HDAC isoforms. The HDAC8-specific pocket can hence be exploited for the development of selective inhibitors. When comparing the active sites of sm- and hHDAC8, few differences can be observed, with only one amino acid substitution in the binding site (Met274 in hHDAC8 is replaced by His292 in smHDAC8). Interestingly, crystal structures of smHDAC8 with several inhibitors showed that Phe151, which is located in the lysine binding channel, can adopt two different conformations, namely a flipped-in and a flipped-out conformation. The flipped-out conformation is characterized by Phe151 side chain turned away from the catalytic pocket and Lys20 instead pointing into the active site. This conformation is not found in resolved crystal structures of hHDAC isoforms and is considered to be unlikely also in hHDAC8 [52,53]. It is noteworthy that HDAC8 from other schistosome species (e.g., *S. haematobium*, *S. japonicum*), share a very similar catalytic site architecture, meaning that inhibitors of smHDAC8 will be likely to affect these species in the same way [48]. In Table 1, an overview of the interactions observed for reported smHDAC8 inhibitors in the catalytic pocket of the enzyme is given.

Table 1. Observed interactions of the herein mentioned inhibitors in the binding site of smHDAC8 (vdW = van-der-Waals interaction).

Cpd	PDB ID	Zn²⁺-chelation *	H-bond triad **	F216 (π-π)	F151 (π-π)	K20 (cation-π)	K20 (H-bond)	H292	Y341 (π-π)	P291 (vdW)
1 (J1038)	4BZ8	X	X		X			X (H-bond)		
2 (J1075)	4BZ9	X		X		X				
3	6GXW	X	X			X		X (vdW)	X	
4	6GXU	X	X	X				X (π-π)		
5 (TH31)	5FUE	X	X			X	X	X (H-bond)	X	
6 (TH65)	6HTH	X	X			X	X	X (H-bond)	X	X
8	7P3S	X	X			X		X (π-π)	X	
12	6TLD	X	X					X (H-bond)		
13	6HU3	X	X					X (vdW)	X	X

* Bidetate chelation of catalytic zinc ion. ** Three hydrogen bonds with H141, H142, Y341.

2. Antischistosomal Effect of HDAC Inhibitors

2.1. Pan HDAC Inhibitors

The availability of HDAC inhibitors either as experimental probes or approved drugs was utilized to study phenotypic and molecular effects of HDAC inhibition in schistosomes. The HDAC inhibitor Trichostatin A (TSA) was shown to block the transformation of the free-swimming miracidia into the sporocyst in a concentration dependent manner [54]. From a therapeutic point of view, it is, however, more interesting to target the parasitic stages that live in the human host. Therefore, some HDAC inhibitors were also tested on both larvae and adult worms [55]. Again, treatment with TSA caused an increase in

general levels of protein acetylation in schistosomes and induced mortality and apoptosis in schistosomula maintained in culture. Interestingly, the pan HDACi suberanilohydroxamic acid (SAHA, vorinostat) was not effective in that assay, while TSA was effective only after 2 days of treatment and at higher doses than those routinely used for cancer cell lines [55]. Moreover, another study revealed that some cellular functions, such as DNA replication and control of reactive oxygen species, were affected upon treatment of schistosomula with TSA which might explain the antischistosomal effect of this HDACi [47]. The FDA approved HDAC inhibitors, vorinostat (SAHA), belinostat, panobinostat, and romidepsin, were the major focus of another study as these anticancer agents were tested against several human parasites including Schistosoma mansoni [56]. The four compounds were not active against the schistosomula while panobinostat showed modest inhibition of adult worm pairing and egg production. In contrast, the cyclic tetrapeptide romidepsin showed complete inhibition of pairing and egg production at 10 μM concentration [56].

2.2. Selective smHDAC8 Inhibitors

2.2.1. Hydroxamic Acid Based Inhibitors

A campaign was initiated based on a structure-based virtual screening approach where different commercially available derivatives bearing zinc binding groups were first docked to a homology model of smHDAC8 (later validated through solving the crystal structure) and the selected hits were tested in vitro for their inhibitory activity against schistosomal and human HDACs (smHDAC8, hHDAC1, hHDAC6, and hHDAC8 isoforms) [57]. Among the identified compounds, two hits showed good inhibitory activity against smHDAC8 in the low micromolar range (**1** and **2**, Figure 1). These two hits were then successfully cocrystallized with smHDAC8 and the crystal structure of the complex was solved [52,57]. It was also interesting that the 3-chlorobenzothiophene-2-hydroxamic acid **2** (J1075, Figure 1) exhibited dose-dependent killing of the schistosomula and adult worms as it induced 100% killing of schistosomula at 50 μM within 3 days and was also active at 10 μM. In addition, it was able to induce separation of the male and female worm pairs within 3 days at 50 μM and 5 days at 20 μM [52]. These two hits were then selected to serve as lead compounds for further structure-guided optimization to obtain more potent and selective smHDAC8 inhibitors.

To build on the previous results, a series of hydroxamic acid derivatives were designed and synthesized based on the general scaffold of the micromolar hit (**2**, J1075 [57]) [58]. To achieve better smHDAC8 activity and selectivity, different structural modifications were performed. For instance, the benzothiophene scaffold was changed into different bicyclic systems. Moreover, ring open analogues containing different substituted cinnamic-hydroxamic acid derivatives were synthesized. The newly synthesized compounds were evaluated for their inhibitory activity against schistosomal and major human HDACs isoforms. Several compounds showed potent activity against smHDAC8 ranging from the low micromolar to the nanomolar range. In addition, the most active compounds were further screened for lethality against the schistosomal larval stage. Interestingly, compounds **3** and **4** (Figure 1) showed significant and dose-dependent killing of the larvae with EC_{50} values of 6.5 and 11.8 μM, respectively, and markedly impaired egg laying of adult worm pairs maintained in culture [58].

1 (J1038)

IC$_{50}$ (smHDAC8) = 1.48 μM
IC$_{50}$ (hHDAC8) = 0.97 μM
IC$_{50}$ (hHDAC1) = 27.48 μM
IC$_{50}$ (hHDAC6) = 3.56 μM

2 (J1075)

IC$_{50}$ (smHDAC8) = 4.3 μM
IC$_{50}$ (hHDAC8) = 3.1 μM
IC$_{50}$ (hHDAC1) = 11.6 μM
IC$_{50}$ (hHDAC6) = 1.9 μM
at 50 μM = 100 % reduction of
viability and pairing (3days)

3

IC$_{50}$ (smHDAC8) = 0.44 μM
IC$_{50}$ (hHDAC8) = 0.47 μM
IC$_{50}$ (hHDAC1) = 20.2 μM
IC$_{50}$ (hHDAC6) = 8.2 μM
EC$_{50}$ (Larval stage) = 6.5 μM

4

IC$_{50}$ (smHDAC8) = 0.18 μM
IC$_{50}$ (hHDAC8) = 0.18 μM
IC$_{50}$ (hHDAC1) = 7.7 μM
IC$_{50}$ (hHDAC6) = 3.2 μM
EC$_{50}$ (Larval stage) = 11.8 μM

5 (TH31)

IC$_{50}$ (smHDAC8) = 0.47μM
IC$_{50}$ (hHDAC8) = 0.58 μM
IC$_{50}$ (hHDAC1) = 33.6 μM
IC$_{50}$ (hHDAC6) = 3.0 μM

6 (TH65)

IC$_{50}$ (smHDAC8) = 0.075 μM
IC$_{50}$ (hHDAC8) = 0.026 μM
IC$_{50}$ (hHDAC1) = 6.3 μM
IC$_{50}$ (hHDAC6) = 0.4 μM
at 20 μM = 100 % reduction of
viability (2 days), 90% of pairing
(5 days)

7

IC$_{50}$ (smHDAC8) = 0.092 μM
IC$_{50}$ (hHDAC8) = 0.14 μM
IC$_{50}$ (hHDAC1) = 2.08 μM
IC$_{50}$ (hHDAC6) = 0.6 μM

8

IC$_{50}$ (smHDAC8) = 0.27 μM
IC$_{50}$ (hHDAC8) = 0.32 μM
IC$_{50}$ (hHDAC1) = 18.51 μM
IC$_{50}$ (hHDAC6) = 0.29 μM
EC$_{50}$ (Larval stage) = 3.5 μM

9

IC$_{50}$ (smHDAC8) = 0.40 μM
IC$_{50}$ (hHDAC8) = 0.63 μM
IC$_{50}$ (hHDAC1) = 47.5% at 200 μM
IC$_{50}$ (hHDAC6) = 5.12 μM

10

IC$_{50}$ (smHDAC8) = 0.75 μM
IC$_{50}$ (hHDAC8) = 1.31 μM
IC$_{50}$ (hHDAC1) =15.3% at 200 μM
IC$_{50}$ (hHDAC6) = 7.11 μM

11

IC$_{50}$ (smHDAC8) = 1.02 μM
IC$_{50}$ (hHDAC8) = 2.11 μM
IC$_{50}$ (hHDAC1) = 3.61 μM
at 50 μM > 40 % reduction
of viability

12

IC$_{50}$ (smHDAC8) = 4.44 μM
IC$_{50}$ (hHDAC8) = 12.43 μM
IC$_{50}$ (hHDAC1) = 8.1% at 10 μM
IC$_{50}$ (hHDAC6) = 42.50 μM

13

IC$_{50}$ (smHDAC8)= 0.50 μM
IC$_{50}$ (hHDAC8) = 2.2 μM
IC$_{50}$ (hHDAC1) = 11% at 5 μM
IC$_{50}$ (hHDAC6) = -1.5 μM at 5 μM

Figure 1. Examples of hydroxamic acid-based smHDAC8 inhibitors. IC$_{50}$ values are cited for inhibition of the recombinant enzyme, EC$_{50}$ values refer to viability testing on schistosomula.

In a further study, several benzhydroxamic acid derivatives were designed as open ring analogues of the previously reported hit (**1**, J1038 [57]) [59]. Structure-based design and chemical synthesis were combined to improve the activity against smHDAC8 and selectivity over major human HDAC isoforms. The developed inhibitors were tested in vitro for their inhibitory activity against schistosomal and human HDACs (smHDAC8, hHDAC1, hHDAC6, and hHDAC8 isoforms). Twenty-seven compounds demonstrated an inhibitory activity in the nanomolar range in the in vitro assays. Most of the designed compounds exhibited notable selectivity for smHDAC8 over the human HDAC isoforms tested (HDAC1

and HDAC6). Interestingly, some of these inhibitors also exhibited a preference for smH-DAC8 over human HDAC8. In addition, phenotypic screening showed that compounds **6** and **7** caused a significant dose dependent killing of the schistosome larvae compared to praziquantel, which is known to be less active against larval developmental stages of the parasite [60]. Furthermore, at a concentration of 20 μM, compound **6** caused 90% separation of adult male and female worm pairs after 5 days. Moreover, compound **6** resulted in 80% reduction of egg laying of adult worm pairs at the same concentration [59]. It is worth mentioning that the cytotoxicity studies of the tested compounds against HEK293 (human embryonic kidney) cells showed that the compounds exhibit a relatively low effect on cell proliferation, which indicates that the inhibition of hHDAC8 does not induce intrinsic toxicity [59].

The crystal structure of compound **6** in complex with smHDAC8 showed a similar binding mode as that classically adopted by meta-substituted benzhydroxamic acid derivatives (Figure 2A) [53]. The hydroxamic acid moiety chelates the catalytic zinc ion in a bidendate fashion while undergoing a triad of hydrogen bonds with the catalytic tyrosine and two histidine residues. Phe151 shows a flipped-out conformation and the flipped in Lys20 displays a cation-π interaction with the central phenyl moiety. Meanwhile, the biphenyl capping group is positioned in the HDAC8-specific pocket, displaying π-π interactions with Tyr341 as well as hydrophobic interactions with Pro291.

In a following study, compound **6** was used as a scaffold to get more cellular active compounds against the parasite. The optimization process was guided by docking studies, and the new derivatives were designed through modifying the capping group by replacing the biphenyl ring system with polycyclic rings to target the hydrophobic HDAC8 specific pocket [61]. Several compounds showed potent smHDAC8 and hHDAC8 activity in the nanomolar range with decreased activity against hHDAC1 and 6. The most promising inhibitor, **8,** caused significant dose-dependent killing of the schistosome larvae with EC_{50} value of 3.5 μM and is thus the most potent antischistosomal HDAC inhibitor against this life stage reported so far. In addition, it caused noticeable impairment of egg laying of adult worm pairs. Finally, the developed compounds showed an acceptable safety profile on human HEK239 cells [61]. Inhibitor **8** was also cocrystallized with smHDAC8 confirming the conserved binding mode of benzhydroxamic acid derived inhibitors (Figure 2B). In parallel, the developed inhibitors were analyzed by docking and molecular dynamics simulation in order to rationalize the determined in vitro data [62].

A further study [63] was initiated based on the general scaffold of the previously reported benzhydroxamic acids such as compound **6** [59]. Briefly, a series of isophthalic acid-based HDAC inhibitors were designed as potential selective smHDAC8 inhibitors where a 3-acylbenzohydroxamic acid moiety was connected to different capping groups using an alkoxyamide group as a connecting unit [63]. The alkoxyamide group was previously identified [30,64] as a novel connecting unit which can probably enable charge assisted hydrogen bonds due to the additional polarization of the N–H bond. The work was then extended to include a hydrazide group as another connecting unit. Compounds **9** and **10** showed submicromolar activity against smHDAC8 with IC_{50} values 0.4 and 0.75 μM, respectively, and good selectivity over hHDAC1. Moreover, both compounds showed almost 10-fold selectivity over hHDAC6 and modest preference for smHDAC8 over hHDAC8. Unfortunately, the compounds were found to be inactive against the parasite in the cellular assay.
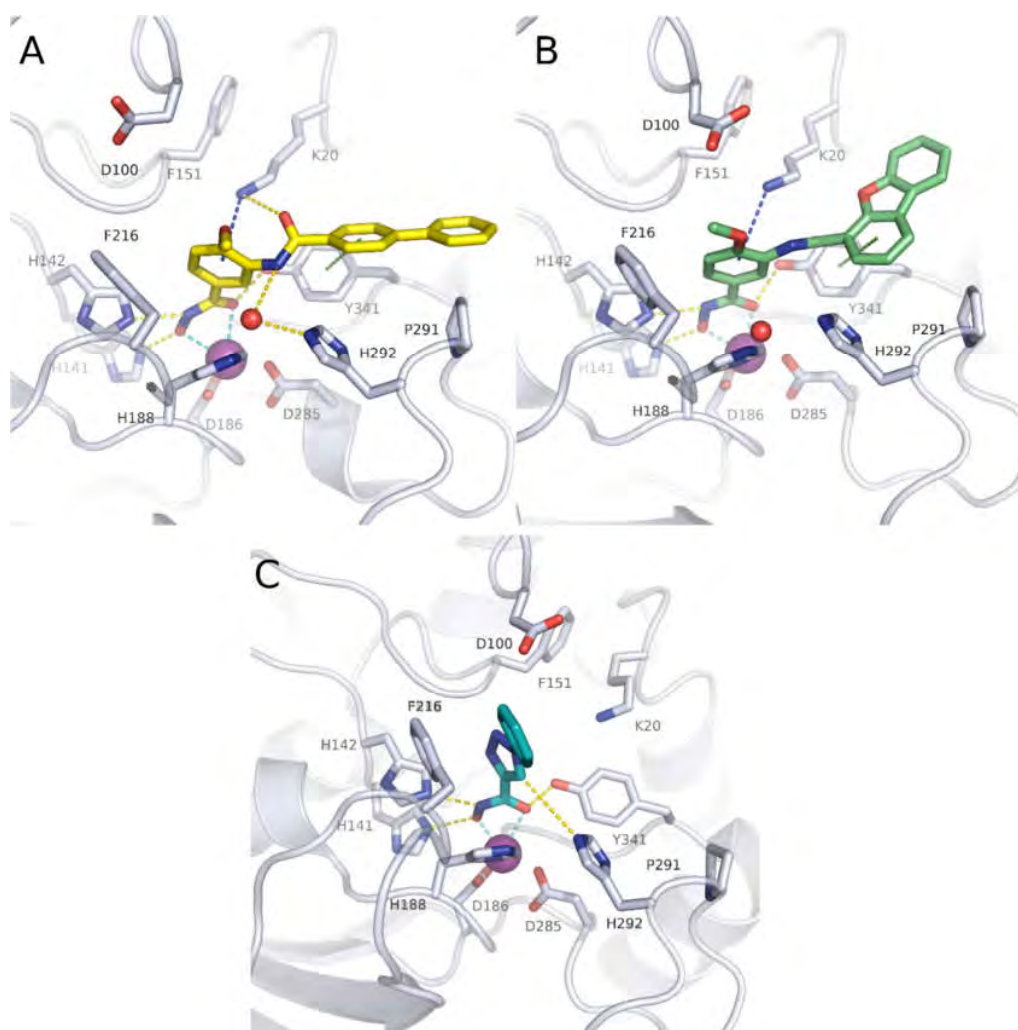
Figure 2. Crystal structures of some smHAC8 inhibitors. (**A**) Crystal structure of smHDAC8 with compound **6** shown as yellow sticks (PDB ID 5HTH); (**B**) crystal structure of smHDAC8 with compound **8** shown as green sticks (PDB ID 7P3S); (**C**) crystal structure of smHDAC8 with compound **12** shown as teal sticks (PDB ID 6TLD). The catalytic zinc ion is shown as purple sphere and water molecules as red spheres. Cyan-dashed lines indicate metal coordination, yellow-dashed line hydrogen bond interactions, green-dashed lines π-π interactions, and blue-dashed line cation-π interactions.

Another series of smHDAC8 inhibitors was designed based on structure-based virtual screening using High Throughput Docking (HTD) and phenotypical characterization of the selected hits [65]. The identified compounds had a hydroxamic acid group coupled to different capping groups such as (spiro)indoline or a tricyclic thieno[3,2-b]indole core [65]. Since the main goal of the study was to obtain compounds with drug like properties and strong activity against the parasite, these hits were then tested against the *S. mansoni* larval stage using an ATP-based viability assay. Seven compounds were found to reduce schistosomula viability in a dose dependant manner with EC_{50} values ranging from 13 to 50 μM under assay conditions. Moreover, further investigations were performed on other parasite developmental stages. Some of the compounds from both classes caused impaired viability of juvenile and adult worms, with compound **11** decreasing the viability of the treated adult *S. mansoni* worm pairs by more than 40% at 50 μM. In addition, some compounds were shown to impact egg production in vitro and induce morphological

alterations of the adult schistosome reproductive systems. Some of the compounds showed activity against smHDAC8 in the low micromolar range [65].

Recently, novel triazole-based hydroxamic acids were identified as smHDAC8 inhibitors with improved selectivity for the smHDAC8 over the human orthologues (HDAC8, HDAC1, and HDAC6) [66]. Crystallographic studies of smHDAC8 complexed with **12** showed that the triazole ring of **12** makes a weak hydrogen bond with the smHDAC8 specific residue His292, an aromatic interaction with its imidazole ring as well as a π-cation interaction with Lys20 of smHDAC8 (Figure 2C). Interestingly, these previous interactions were not observed between **12** and the corresponding amino acids of the human orthologue HDAC8 as, in the case of hHDAC8, the His292 is replaced by Met274. Furthermore, the preferred orientation of the triazole moiety in smHDAC8 allows a π-stacking interaction between the phenyl ring of **12** and Phe216, whereas in the case of hHDAC8 this interaction with the corresponding Phe208 is not observed. To enhance the affinity of the triazole-hydroxamic acid hit **12** toward smHDAC8 and improve its selectivity, some structural modifications were performed on the phenyl ring of **12** by introducing a chlorine atom and an aromatic substituent at positions 5 and 2, respectively, which resulted in compound **13**. Interestingly, compound **13** was found to exhibit a superior smHDAC8 inhibitory activity (IC_{50} = 0.50 μM) compared to the lead compound **12** (IC_{50} = 4.44 μM). Comparison of the crystal structures of smHDAC8/**12** and smHDAC8/**13** revealed that compound **13** is slightly tilted within the active pocket of smHDAC8 compared to compound **12**, in which the triazole ring of **13** is closer to the smHDAC8 specific residue His292. Another observation is that the fluoro-phenyl capping group of **13** is stacked onto the Tyr341 side chain, which is considered as an essential interaction for improving the affinity toward smHDAC8. However, the promising in vitro smHDAC8 activity of the triazole compounds was not translated into schistosomicidal activity as they only showed low activity against the schistosomula, probably due to poor transport of the compounds across the parasite tegument [66].

2.2.2. Non-Hydroxamic Acid Based Inhibitors

The quest for selective inhibitors of smHDAC8 started with a study in which a small-focused library of HDAC inhibitors was screened against the parasitic recombinant enzyme. Besides many active hydroxamic acids, an interesting mercaptoacetamide analogue of SAHA (**14**) was identified as a micromolar smHDAC8 inhibitor. Despite being less active on smHDAC8 than the other hydroxamic acid-based inhibitors, this thiol derivative showed a better selectivity towards hHDAC8 compared to SAHA [67]. To gain more insights, the cocrystallized structure of compound **14** bound to smHDAC8 was solved, representing the first example of a co-complex of histone deacetylases of any origin with a mercaptoacetamide. The crystal structure of smHDAC8 and **14** revealed that this thiol inhibitor is accommodated in the catalytic pocket, where it binds to both the catalytic zinc ion and the catalytic tyrosine Tyr341 via its mercaptoacetamide group. Interestingly, it was also shown that changing the zinc binding warhead results in a different positioning of the hydrophobic alkyl linker and the aromatic capping group common to compound (**14**) and SAHA, which might explain the differences in the activity and the selectivity of **14** toward smHDAC8 over hHDAC8 compared to SAHA. Taking into consideration the inapplicability of free thiol groups for cellular testing, an ester prodrug of the thiol was prepared (compound **15**, Figure 3) and tested against schistosomula. This prodrug induced dose- and time-dependent killing of cultured schistosomula in the range 10–50 μM, as well as induction of apoptosis at concentrations of 20 and 50 μM [67].
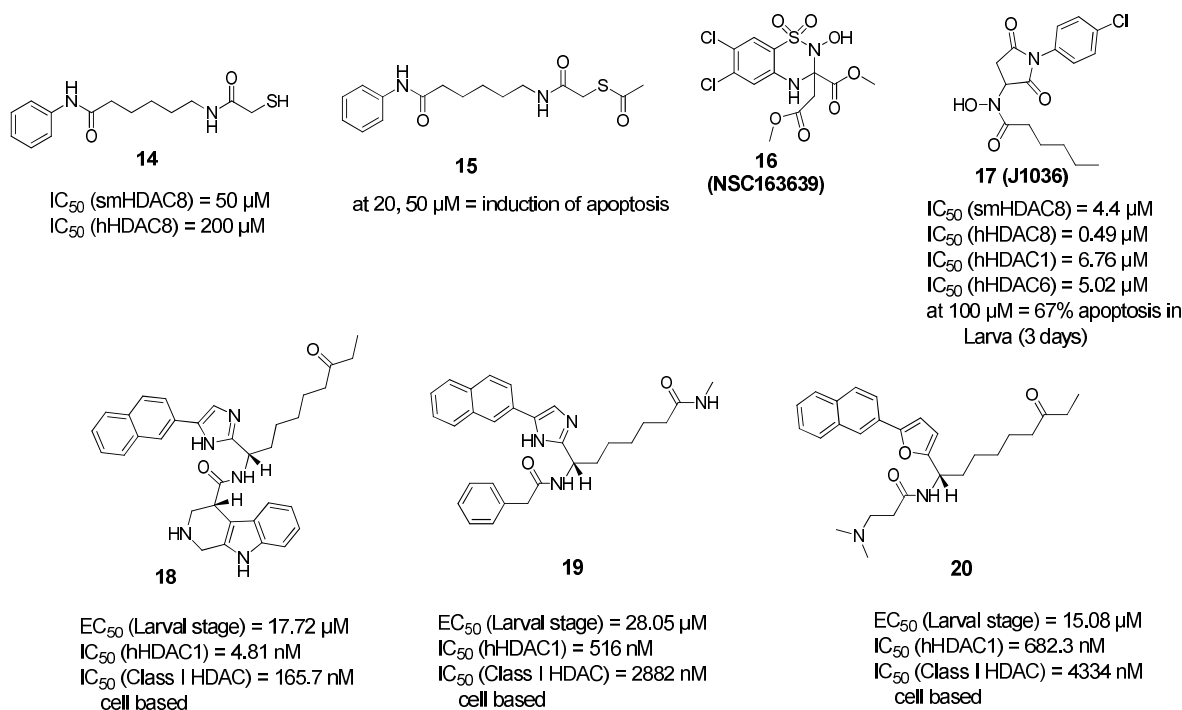
Figure 3. Examples of non-hydroxamic acid smHDAC8 inhibitors.

A virtual screening approach was reported [68] as the authors used the available smHDAC8-inhibitor complexes to develop a structure-based per-residue 3D QSAR (COM-BINEr 2.0) model able to rationalize the crucial smHDAC8-ligand interactions. This model was used to screen the NCI Diversity Set V and identified a benzothiadiazine dioxide derivative (**16**, NSC163639). This compound showed a moderate in vitro smHDAC8 activity (37% inhibition at 30 μM) and some selectivity against human HDACs. To get a primary idea about the structure–activity relationship of this hit, two close analogues were synthesized and their smHDAC8 activity was tested and explained by means of docking studies. The authors suggested, as future work, that attachment of strong zinc binding groups such as a hydroxamic acid moiety through a linker instead of the ester groups in (**16**, NSC163639) could lead to a favorable placement and interactions of the benzothiadiazine moiety in the smHDAC8 active site [68].

Based on another docking-based virtual screening approach, another class of smH-DAC8 inhibitors was identified [69]. Eight compounds having the general scaffold of N-(2,5-dioxopyrrolidin-3-yl)-n-alkylhydroxamic acid were identified and tested in vitro for their inhibitory activity against schistosomal and major human HDACs (smHDAC8, hHDAC1, hHDAC6, and hHDAC8 isoforms) [69]. The newly identified hits exerted a smHDAC8 inhibitory activity with IC_{50} values ranging from 4.4 to 20.3 μM. In addition, they showed activity against hHDAC1, 6, and 8. Among the identified compounds, (**17**, J1036) induced dose-dependent apoptosis in the *S. mansoni* larvae, affecting around 67% of the larvae after 3 days of incubation at a concentration of 100 μM, compared to the effect induced by SAHA (43% apoptosis at a dose of 100 μM). In addition, (**17**, J1036) was successfully cocrystallized with smHDAC8, which confirmed the in silico prediction of this compound. Analysis of the crystal structure of the smHDAC8/J1036 complex showed that the internal hydroxamic acid group was able to chelate the catalytic zinc ion in a bidentate manner, showing an inverted binding mode compared to all the so far reported smHDAC8/hydroxamic acid crystal structures. Besides the chelation of the zinc ion, the n-pentyl chain of J1036 is positioned in the foot pocket, which has not been observed before in the previously reported unsubstituted hydroxamic acids. Such occupancy of the foot pocket by n-alkylhydroxamic acids may offer the chance to develop selective

HDAC inhibitors through further structural optimization. In addition, the newly identified hits are expected to a lower toxicity compared to classical hydroxamic acids, as the toxicity-induced mechanism of the latter is usually caused by formation of the isocyanate via Lossen rearrangement which might be absent for n-alkyl hydroxamic acids due to substitution on the nitrogen atom [69].

In another approach, Guidi et al. performed a high-throughput assay based on the measurement of ATP in the larval stage of *S. mansoni* and screened a small library of class I HDACs inhibitors at a single concentration of 10 μM [70]. Four compounds were selected for further testing in dose response assays where they showed potency against the schistosomula in the range of 10–20 μM. Interestingly, the compounds showed variable activities against class I hHDACs in both in vitro and cell-based assays, which was not surprising taking into consideration the weak zinc binding moieties in the compounds and suggesting a potential selectivity for smHDACs. Upon testing in survival assays on adult worms, three out of the four hits (**18–20**) induced a significant decrease in viability of adult male worms within seven days of compound incubation at concentrations of 10 and 20 μM [70]. Since the three compounds showed a lethal action at 10 μM concentration, a sub-lethal concentration of 5 μM of compounds **19** and **20** was shown to induce a strong reduction in the number of eggs laid by worm pairs after three days of treatment. Compounds **19** and **20** were also found to induce morphological alterations in the female reproductive organs which is consistent with their effect on egg production. Finally, worm lysates treated with compound **18** and **19** showed high level of histone hyperacetylation comparable to the levels observed in case of worms treated with the pan-HDAC inhibitor TSA [70].

2.3. Molecular Pathways Affected by smHDAC8 Inhibitors

Both knockdown studies and the use of selective inhibitors provided a solid proof of evidence that targeting smHDAC8 is a promising antischistosomal therapy. However, the exact molecular mechanisms underlying these anthelmintic effects are yet to be revealed. This necessitated further research to identify smHDAC8 partners and substrates affected upon its inhibition and knockdown. Therefore, the interactome of smHDAC8 was analyzed using two different, but complementary, molecular biology techniques [71]. The combination of yeast two-hybrid (Y2H) screening of an *S. mansoni* cDNA library and co-immunoprecipitation (Co-IP) experiments on adult worm protein extracts identified potential smHDAC8 partner proteins involved in cytosolic and nuclear process such as DNA repair, control of metabolism, protein dephosphorylation, cell cycle regulation, and cytoskeleton organization [71]. Recently, it was suggested that smHDAC8 interaction with SmRho1.1, a schistosomal orthologue of human Ras homolog family member A (RhoA) GTPase, could represent a potential molecular mechanism by which smHDAC8 regulates the cytoskeleton. Indeed, smHDAC8 selective inhibition or knockdown were demonstrated to cause disruption of the parasite actin cytoskeleton organization, more evidently in schistosomula [72].

3. Schistosomal Sirtuins Are Potential Targets for Antischistosomal Therapy

As previously mentioned, the *S. mansoni* genome encodes five sirtuins expressed throughout the life cycle, with some variations in the pattern of expression [49]. To determine whether sirtuins are essential for the parasite survival, different inhibitors of human sirtuins were tested against the parasite larvae and adult worms. Indeed, all tested inhibitors induced a time and dose-dependent mortality of schistosomula. However, three Sirt1/2 inhibitors, namely, salermide, sirtinol, and MS3 caused the most significant decrease in schistosomula viability at 10 μM and killed all the larvae at 20 μM. Moreover, salermide and sirtinol were also shown to cause separation of adult worms in vitro and decrease egg production. Furthermore, salermide caused dose-dependent phenotypic changes in the gonads of adult worms demonstrated by reduction in numbers of germinal cells in the testes of males and disorganization in the ovaries of females. Interestingly, transcriptional knockdown of smSirt1 produced similar phenotypic effects in the ovaries, but not in the

testis, suggesting that the phenotype observed after Salermide treatment may have resulted from inhibition of other sirtuin isoforms [49].

The above data provided a solid proof of evidence of the significance of Sirt1/2 inhibition against different life stages of the parasites. This was followed by another effort to identify novel and selective inhibitors of smSirt2 [73] based on the previous development of an in vitro assay for the determination of smSirt2 deacetylase activity [74]. Here, the GSK Kinetobox library was screened against smSirt2, and some potential hits were identified showing micromolar activity against the parasitic enzyme. One of these hits (TCMDC143295, **21**, Figure 4) was then subjected to an extensive structure–activity relationship study that resulted in compounds **22–24** with better enzymatic activity while also showing selectivity over human Sirt2 (hSirt2) and no general toxicity to human cells. The compounds were also demonstrated to decrease the viability of the parasite larva at 10 and 20 µM and reduce adult worm pairing and egg production [73].

21 (TCMDC-143295)

IC_{50} (smSirt2) = 23.7 µM
IC_{50} (hSirt2) =22% at 25 µM

22

IC_{50} (smSirt2) = 2.3 µM
IC_{50} (hSirt2) =22% at 25 µM

23

IC_{50} (smSirt2) = 3.3 µM
IC_{50} (hSirt2) =30% at 25 µM

24

IC_{50} (smSirt2) = 4.3 µM
IC_{50} (hSirt2) =28% at 25 µM
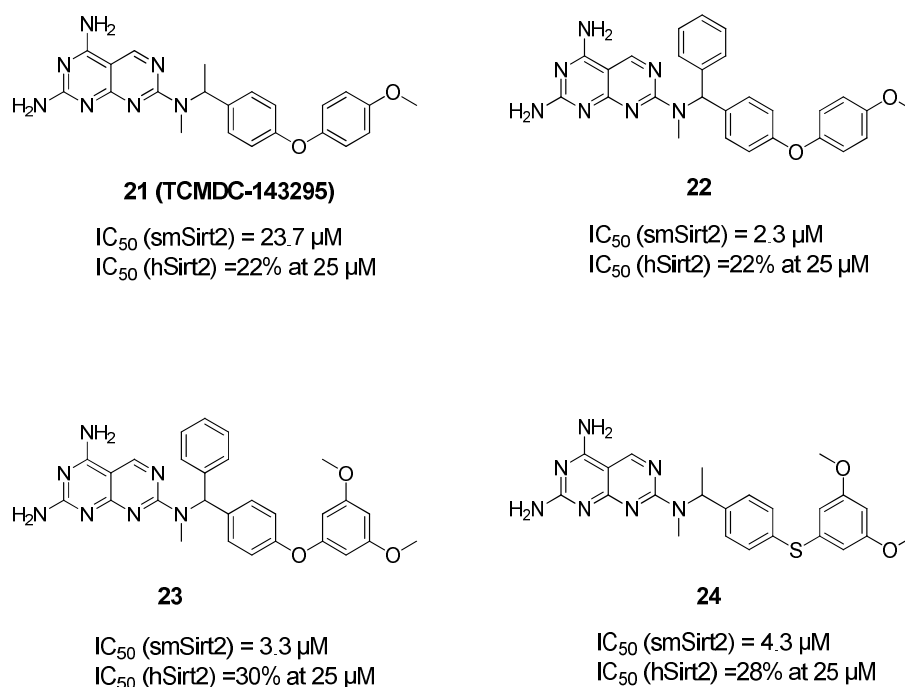
Figure 4. Reported inhibitors of Schistosoma mansoni sirtuins.

4. Summary

Significant progress in semi-automation of phenotypic screening and drug discovery methodologies for schistosomiasis has been achieved over the last decade. Based on published data, smHDAC8 inhibitors appear to have the most promise as schistosomicidal drugs. Unfortunately, numerous compounds with good enzymatic inhibition data show no effect on the parasite, which may be due to poor bioavailability. In addition, so far little is still known about bioavailability and stability of HDACi in animal models of schistosomiasis. Most of the studies investigating the possibility of the use of HDACi for the treatment of schistosomiasis worked entirely with cultured schistosomes. Testing of HDACi in animal models of infection should bring new insights into the killing of schistosomes via HDACi and will in fact be required before considering HDACi for further preclinical trials. On the other hand, it must be mentioned that several compounds reviewed in this work should be regarded as "hits" that still need extensive optimization to be described as "leads" that could then be considered for further preclinical development. Furthermore, numerous HDAC inhibitors are currently being tested in preclinical and clinical trials for the treatment of cancer in combination with other anticancer agents. Likewise, combination

therapies of smHDAC8 inhibitors and other anthelmintic agents could provide promising results. Additionally, the potential of HDACs as therapeutic targets in parasitic diseases is being actively confirmed, such as the very recent identification of *Trypanosoma cruzi* histone deacetylases 2 (tcDAC2) [75] and the development of species selective inhibitors. Therefore, the authors are confident that further HDAC inhibitors will be reported as novel antiparasitic agents in the future.

Institutional Review Board Statement: Not applicable.

Informed Consent Statement: Not applicable.

Data Availability Statement: Not applicable.

Conflicts of Interest: The authors declare no conflict of interest.

References

1. Ho, T.C.S.; Chan, A.H.Y.; Ganesan, A. Thirty Years of HDAC Inhibitors: 2020 Insight and Hindsight. *J. Med. Chem.* **2020**, *63*, 12460–12484. [CrossRef]
2. Park, S.-Y.; Kim, J.-S. A short guide to histone deacetylases including recent progress on class II enzymes. *Exp. Mol. Med.* **2020**, *52*, 204–212. [CrossRef]
3. Bertrand, P. Inside HDAC with HDAC inhibitors. *Eur. J. Med. Chem.* **2010**, *45*, 2095–2116. [CrossRef] [PubMed]
4. Zhang, L.; Zhang, J.; Jiang, Q.; Song, W. Zinc binding groups for histone deacetylase inhibitors. *J. Enzym. Inhib. Med. Chem.* **2018**, *33*, 714–721. [CrossRef] [PubMed]
5. Narita, T.; Weinert, B.; Choudhary, C. Functions and mechanisms of non-histone protein acetylation. *Nat. Rev. Mol. Cell Biol.* **2019**, *20*, 156–174. [CrossRef]
6. Jing, H.; Lin, H. Sirtuins in Epigenetic Regulation. *Chem. Rev.* **2015**, *115*, 2350–2375. [CrossRef]
7. Chen, B.; Zang, W.; Wang, J.; Huang, Y.; He, Y.; Yan, L.; Liu, J.; Zheng, W. The chemical biology of sirtuins. *Chem. Soc. Rev.* **2015**, *44*, 5246–5264. [CrossRef] [PubMed]
8. Zwinderman, M.R.H.; De Weerd, S.; Dekker, F.J. Targeting HDAC Complexes in Asthma and COPD. *Epigenomes* **2019**, *3*, 19. [CrossRef]
9. Mathias, R.; Guise, A.J.; Cristea, I.M. Post-translational Modifications Regulate Class IIa Histone Deacetylase (HDAC) Function in Health and Disease. *Mol. Cell. Proteom.* **2015**, *14*, 456–470. [CrossRef]
10. Yao, Y.-L.; Yang, W.-M. Beyond Histone and Deacetylase: An Overview of Cytoplasmic Histone Deacetylases and Their Nonhistone Substrates. *J. Biomed. Biotechnol.* **2010**, *2011*, 1–15. [CrossRef]
11. Verdin, E.; Ott, M. 50 years of protein acetylation: From gene regulation to epigenetics, metabolism and beyond. *Nat. Rev. Mol. Cell Biol.* **2015**, *16*, 258–264. [CrossRef]
12. Roche, J.; Bertrand, P. Inside HDACs with more selective HDAC inhibitors. *Eur. J. Med. Chem.* **2016**, *121*, 451–483. [CrossRef]
13. Ma, F.; Zhang, C.-Y. Histone modifying enzymes: Novel disease biomarkers and assay development. *Expert Rev. Mol. Diagn.* **2016**, *16*, 297–306. [CrossRef]
14. Bheda, P.; Jing, H.; Wolberger, C.; Lin, H. The Substrate Specificity of Sirtuins. *Annu. Rev. Biochem.* **2016**, *85*, 405–429. [CrossRef] [PubMed]
15. Osborne, B.; Bentley, N.L.; Montgomery, M.K.; Turner, N. The role of mitochondrial sirtuins in health and disease. *Free Radic. Biol. Med.* **2016**, *100*, 164–174. [CrossRef] [PubMed]
16. Chalkiadaki, A.; Guarente, L. The multifaceted functions of sirtuins in cancer. *Nat. Cancer* **2015**, *15*, 608–624. [CrossRef] [PubMed]
17. Danaher, R.J.; Zhang, L.; Donley, C.J.; Laungani, N.A.; Hui, S.E.; Miller, C.S.; Westlund, K.N. Histone deacetylase inhibitors prevent persistent hypersensitivity in an orofacial neuropathic pain model. *Mol. Pain* **2018**, *14*, 1744806918796763. [CrossRef] [PubMed]
18. Hadden, M.J.; Advani, A. Histone Deacetylase Inhibitors and Diabetic Kidney Disease. *Int. J. Mol. Sci.* **2018**, *19*, 2630. [CrossRef] [PubMed]
19. Zhou, Y.; Wang, Q.; Yang, Q.; Tang, J.; Xu, C.; Gai, D.; Chen, X.; Chen, J. Histone Deacetylase 3 Inhibitor Suppresses Hepatitis C Virus Replication by Regulating Apo-A1 and LEAP-1 Expression. *Virol. Sin.* **2018**, *33*, 418–428. [CrossRef]
20. Chen, W.-Y.; Zhang, H.; Gatta, E.; Glover, E.J.; Pandey, S.C.; Lasek, A.W. The histone deacetylase inhibitor suberoylanilide hydroxamic acid (SAHA) alleviates depression-like behavior and normalizes epigenetic changes in the hippocampus during ethanol withdrawal. *Alcohol* **2019**, *78*, 79–87. [CrossRef]

21. Choi, S.Y.; Kee, H.J.; Sun, S.; Seok, Y.M.; Ryu, Y.; Kim, G.R.; Kee, S.-J.; Pflieger, M.; Kurz, T.; Kassack, M.U.; et al. Histone deacetylase inhibitor LMK235 attenuates vascular constriction and aortic remodelling in hypertension. *J. Cell. Mol. Med.* **2019**, *23*, 2801–2812. [CrossRef] [PubMed]
22. Kee, H.J.; Ryu, Y.; Seok, Y.M.; Choi, S.Y.; Sun, S.; Kim, G.R.; Jeong, M.H. Selective inhibition of histone deacetylase 8 improves vascular hypertrophy, relaxation, and inflammation in angiotensin II hypertensive mice. *Clin. Hypertens.* **2019**, *25*, 13. [CrossRef] [PubMed]
23. Romeiro, L.A.S.; Nunes, J.L.D.C.; Miranda, C.D.O.; Cardoso, G.S.H.R.; de Oliveira, A.S.; Gandini, A.; Kobrlova, T.; Soukup, O.; Rossi, M.; Senger, J.; et al. Novel Sustainable-by-Design HDAC Inhibitors for the Treatment of Alzheimer's Disease. *ACS Med. Chem. Lett.* **2019**, *10*, 671–676.e7. [CrossRef]
24. Steelant, B.; Wawrzyniak, P.; Martens, K.; Jonckheere, A.-C.; Pugin, B.; Schrijvers, R.; Bullens, D.M.A.; Vanoirbeek, J.; Krawczyk, K.; Dreher, A.; et al. Blocking histone deacetylase activity as a novel target for epithelial barrier defects in patients with allergic rhinitis. *J. Allergy Clin. Immunol.* **2019**, *144*, 1242–1253. [CrossRef]
25. Sangwan, R.; Rajan, R.; Mandal, P.K. HDAC as onco target: Reviewing the synthetic approaches with SAR study of their inhibitors. *Eur. J. Med. Chem.* **2018**, *158*, 620–706. [CrossRef] [PubMed]
26. Fioravanti, R.; Mautone, N.; Rovere, A.; Rotili, D.; Mai, A. Targeting histone acetylation/deacetylation in parasites: An update (2017–2020). *Curr. Opin. Chem. Biol.* **2020**, *57*, 65–74. [CrossRef]
27. Engel, J.A.; Jones, A.J.; Avery, V.M.; Sumanadasa, S.D.; Ng, S.S.; Fairlie, D.P.; Skinner-Adams, T.; Andrews, K.T. Profiling the anti-protozoal activity of anti-cancer HDAC inhibitors against Plasmodium and Trypanosoma parasites. *Int. J. Parasitol. Drugs Drug Resist.* **2015**, *5*, 117–126. [CrossRef]
28. Oliveira, G. Cancer and parasitic infections: Similarities and opportunities for the development of new control tools. *Rev. da Soc. Bras. Med. Trop.* **2014**, *47*, 1–2. [CrossRef]
29. Hailu, G.S.; Robaa, D.; Forgione, M.; Sippl, W.; Rotili, D.; Mai, A. Lysine Deacetylase Inhibitors in Parasites: Past, Present, and Future Perspectives. *J. Med. Chem.* **2017**, *60*, 4780–4804. [CrossRef]
30. Hansen, F.K.; Sumanadasa, S.D.; Stenzel, K.; Duffy, S.; Meister, S.; Marek, L.; Schmetter, R.; Kuna, K.; Hamacher, A.; Mordmüller, B.; et al. Discovery of HDAC inhibitors with potent activity against multiple malaria parasite life cycle stages. *Eur. J. Med. Chem.* **2014**, *82*, 204–213. [CrossRef]
31. Ontoria, J.M.; Paonessa, G.; Ponzi, S.; Ferrigno, F.; Nizi, E.; Biancofiore, I.; Malancona, S.; Graziani, R.; Roberts, D.; Willis, P.; et al. Discovery of a Selective Series of Inhibitors of Plasmodium falciparum HDACs. *ACS Med. Chem. Lett.* **2016**, *7*, 454–459. [CrossRef] [PubMed]
32. De Vreese, R.; De Kock, C.; Smith, P.J.; Chibale, K.; D'Hooghe, M. Exploration of thiaheterocyclic hHDAC6 inhibitors as potential antiplasmodial agents. *Futur. Med. Chem.* **2017**, *9*, 357–364. [CrossRef]
33. Diedrich, D.; Stenzel, K.; Hesping, E.; Antonova-Koch, Y.; Gebru, T.; Duffy, S.; Fisher, G.; Schöler, A.; Meister, S.; Kurz, T.; et al. One-pot, multi-component synthesis and structure-activity relationships of peptoid-based histone deacetylase (HDAC) inhibitors targeting malaria parasites. *Eur. J. Med. Chem.* **2018**, *158*, 801–813. [CrossRef]
34. Bouchut, A.; Rotili, D.; Pierrot, C.; Valente, S.; Lafitte, S.; Schultz, J.; Hoglund, U.; Mazzone, R.; Lucidi, A.; Fabrizi, G.; et al. Identification of novel quinazoline derivatives as potent antiplasmodial agents. *Eur. J. Med. Chem.* **2019**, *161*, 277–291. [CrossRef] [PubMed]
35. Mackwitz, M.K.W.; Hesping, E.; Antonova-Koch, Y.; Diedrich, D.; Woldearegai, T.G.; Skinner-Adams, A.P.D.T.; Clarke, M.; Schöler, A.; Limbach, L.; Kurz, T.; et al. Structure–Activity and Structure–Toxicity Relationships of Peptoid-Based Histone Deacetylase Inhibitors with Dual-Stage Antiplasmodial Activity. *ChemMedChem* **2019**, *14*, 912–926. [CrossRef]
36. Zuma, A.A.; de Souza, W. Histone deacetylases as targets for antitrypanosomal drugs. *Futur. Sci. OA* **2018**, *4*, FSO325. [CrossRef] [PubMed]
37. Kelly, J.M.; Taylor, M.C.; Horn, D.; Loza, E.; Kalvinsh, I.; Björkling, F. Inhibitors of human histone deacetylase with potent activity against the African trypanosome Trypanosoma brucei. *Bioorg. Med. Chem. Lett.* **2012**, *22*, 1886–1890. [CrossRef] [PubMed]
38. Carrillo, A.K.; Guiguemde, W.A.; Guy, R.K. Evaluation of histone deacetylase inhibitors (HDACi) as therapeutic leads for human African trypanosomiasis (HAT). *Bioorg. Med. Chem.* **2015**, *23*, 5151–5155. [CrossRef]
39. Loeuillet, C.; Touquet, B.; Guichou, J.F.; Labesse, G.; Sereno, D. A Tiny Change Makes a Big Difference in the Anti-Parasitic Activities of an HDAC Inhibitor. *Int. J. Mol. Sci.* **2019**, *20*, 2973. [CrossRef]
40. Araujo-Silva, C.A.; De Souza, W.; Martins-Duarte, E.S.; Vommaro, R.C. HDAC inhibitors Tubastatin A and SAHA affect parasite cell division and are potential anti-Toxoplasma gondii chemotherapeutics. *Int. J. Parasitol. Drugs Drug Resist.* **2021**, *15*, 25–35. [CrossRef]
41. Corpas-López, V.; Díaz-Gavilán, M.; Franco-Montalbán, F.; Merino-Espinosa, G.; López-Viota, M.; López-Viota, J.; Belmonte-Reche, E.; Palacio, J.P.-D.; de Pedro, N.; Gómez-Vidal, J.A.; et al. A nanodelivered Vorinostat derivative is a promising oral compound for the treatment of visceral leishmaniasis. *Pharmacol. Res.* **2019**, *139*, 375–383. [CrossRef]
42. Vaca, H.R.; Celentano, A.M.; Macchiaroli, N.; Kamenetzky, L.; Camicia, F.; Rosenzvit, M.C. Histone deacetylase enzymes as potential drug targets of Neglected Tropical Diseases caused by cestodes. *Int. J. Parasitol. Drugs Drug Resist.* **2019**, *9*, 120–132. [CrossRef] [PubMed]

43. De Souza, L.Â.; Silva, E.B.M.; Agripino, J.D.M.; Onofre, T.S.; Calla, L.F.A.; Heimburg, T.; Ghazy, E.; Bayer, T.; da Silva, V.H.F.; Ribeiro, P.D.; et al. Histone deacetylases inhibitors as new potential drugs against Leishmania braziliensis, the main causative agent of new world tegumentary leishmaniasis. *Biochem. Pharmacol.* **2020**, *180*, 114191. [CrossRef]

44. Vaca, H.R.; Celentano, A.M.; Toscanini, M.A.; Heimburg, T.; Ghazy, E.; Zeyen, P.; Hauser, A.-T.; Oliveira, G.; Elissondo, M.C.; Jung, M.; et al. The potential for histone deacetylase (HDAC) inhibitors as cestocidal drugs. *PLoS Negl. Trop. Dis.* **2021**, *15*, e0009226. [CrossRef]

45. World Health Organization. Schistosomiasis. Available online: https://www.who.int/news-room/fact-sheets/detail/schistosomiasis (accessed on 19 July 2021).

46. Vale, N.; Gouveia, M.J.; Rinaldi, G.; Brindley, P.J.; Gärtner, F.; Costa, J.M.C.d. Praziquantel for Schistosomiasis: Single-Drug Metabolism Revisited, Mode of Action, and Resistance. *Antimicrob. Agents Chemother.* **2017**, *61*, e02582-16. [CrossRef]

47. Anderson, L.; Gomes, M.R.; DaSilva, L.F.; Pereira, A.D.S.A.; Mourão, M.M.; Romier, C.; Pierce, R.; Verjovski-Almeida, S. Histone deacetylase inhibition modulates histone acetylation at gene promoter regions and affects genome-wide gene transcription in Schistosoma mansoni. *PLoS Negl. Trop. Dis.* **2017**, *11*, e0005539. [CrossRef] [PubMed]

48. Scholte, L.L.; Mourão, M.M.; Pais, F.; Melesina, J.; Robaa, D.; Volpini, A.C.; Sippl, W.; Pierce, R.J.; Oliveira, G.; Nahum, L.A. Evolutionary relationships among protein lysine deacetylases of parasites causing neglected diseases. *Infect. Genet. Evol.* **2017**, *53*, 175–188. [CrossRef] [PubMed]

49. Lancelot, J.; Caby, S.; Dubois-Abdesselem, F.; Vanderstraete, M.; Trolet, J.; Oliveira, G.; Bracher, F.; Jung, M.; Pierce, R.J. Schistosoma mansoni Sirtuins: Characterization and Potential as Chemotherapeutic Targets. *PLoS Negl. Trop. Dis.* **2013**, *7*, e2428. [CrossRef]

50. Oger, F.; Dubois, F.; Caby, S.; Noël, C.; Cornette, J.; Bertin, B.; Capron, M.; Pierce, R.J. The class I histone deacetylases of the platyhelminth parasite Schistosoma mansoni. *Biochem. Biophys. Res. Commun.* **2008**, *377*, 1079–1084. [CrossRef]

51. Pierce, R. Targeting Schistosome Histone Modifying Enzymes for Drug Development. *Curr. Pharm. Des.* **2012**, *18*, 3567–3578. [CrossRef]

52. Marek, M.; Kannan, S.; Hauser, A.-T.; Mourão, M.M.; Caby, S.; Cura, V.; Stolfa, D.A.; Schmidtkunz, K.; Lancelot, J.; Andrade, L.; et al. Structural Basis for the Inhibition of Histone Deacetylase 8 (HDAC8), a Key Epigenetic Player in the Blood Fluke Schistosoma mansoni. *PLoS Pathog.* **2013**, *9*, e1003645. [CrossRef]

53. Marek, M.; Shaik, T.B.; Heimburg, T.; Chakrabarti, A.; Lancelot, J.; Morales, E.R.; Da Veiga, C.; Kalinin, D.; Melesina, J.; Robaa, D.; et al. Characterization of Histone Deacetylase 8 (HDAC8) Selective Inhibition Reveals Specific Active Site Structural and Functional Determinants. *J. Med. Chem.* **2018**, *61*, 10000–10016. [CrossRef] [PubMed]

54. Azzi, A.; Cosseau, C.; Grunau, C. Schistosoma mansoni: Developmental arrest of miracidia treated with histone deacetylase inhibitors. *Exp. Parasitol.* **2009**, *121*, 288–291. [CrossRef]

55. Dubois, F.; Caby, S.; Oger, F.; Cosseau, C.; Capron, M.; Grunau, C.; Dissous, C.; Pierce, R.J. Histone deacetylase inhibitors induce apoptosis, histone hyperacetylation and up-regulation of gene transcription in Schistosoma mansoni. *Mol. Biochem. Parasitol.* **2009**, *168*, 7–15. [CrossRef]

56. Chua, M.J.; Arnold, M.; Xu, W.; Lancelot, J.; Lamotte, S.; Späth, G.F.; Prina, E.; Pierce, R.J.; Fairlie, D.; Skinner-Adams, T.; et al. Effect of clinically approved HDAC inhibitors on Plasmodium, Leishmania and Schistosoma parasite growth. *Int. J. Parasitol. Drugs Drug Resist.* **2017**, *7*, 42–50. [CrossRef] [PubMed]

57. Kannan, S.; Melesina, J.; Hauser, A.-T.; Chakrabarti, A.; Heimburg, T.; Schmidtkunz, K.; Walter, A.; Marek, M.; Pierce, R.J.; Romier, C.; et al. Discovery of Inhibitors of Schistosoma mansoni HDAC8 by Combining Homology Modeling, Virtual Screening, and in Vitro Validation. *J. Chem. Inf. Model.* **2014**, *54*, 3005–3019. [CrossRef] [PubMed]

58. Bayer, T.; Chakrabarti, A.; Lancelot, J.; Shaik, T.B.; Hausmann, K.; Melesina, J.; Schmidtkunz, K.; Marek, M.; Erdmann, F.; Schmidt, M.; et al. Synthesis, Crystallization Studies, and in vitro Characterization of Cinnamic Acid Derivatives as Sm HDAC8 Inhibitors for the Treatment of Schistosomiasis. *ChemMedChem* **2018**, *13*, 1517–1529. [CrossRef]

59. Heimburg, T.; Chakrabarti, A.; Lancelot, J.; Marek, M.; Melesina, J.; Hauser, A.-T.; Shaik, T.B.; Duclaud, S.; Robaa, D.; Erdmann, F.; et al. Structure-Based Design and Synthesis of Novel Inhibitors Targeting HDAC8 from Schistosoma mansoni for the Treatment of Schistosomiasis. *J. Med. Chem.* **2016**, *59*, 2423–2435. [CrossRef]

60. Panic, G.; Flores, D.; Ingram-Sieber, K.; Keiser, J. Fluorescence/luminescence-based markers for the assessment of Schistosoma mansoni schistosomula drug assays. *Parasites Vectors* **2015**, *8*, 1–12. [CrossRef]

61. Ghazy, E.; Heimburg, T.; Lancelot, J.; Zeyen, P.; Schmidtkunz, K.; Truhn, A.; Darwish, S.; Simoben, C.V.; Shaik, T.B.; Erdmann, F.; et al. Synthesis, structure-activity relationships, cocrystallization and cellular characterization of novel smHDAC8 inhibitors for the treatment of schistosomiasis. *Eur. J. Med. Chem.* **2021**, *225*, 113745. [CrossRef]

62. Simoben, C.; Ghazy, E.; Zeyen, P.; Darwish, S.; Schmidt, M.; Romier, C.; Robaa, D.; Sippl, W. Binding Free Energy (BFE) Calculations and Quantitative Structure–Activity Relationship (QSAR) Analysis of *Schistosoma mansoni* Histone Deacetylase 8 (*sm*HDAC8) Inhibitors. *Molecules* **2021**, *26*, 2584. [CrossRef] [PubMed]

63. Stenzel, K.; Chakrabarti, A.; Melesina, J.; Hansen, F.K.; Lancelot, J.; Herkenhöhner, S.; Lungerich, B.; Marek, M.; Romier, C.; Pierce, R.J.; et al. Isophthalic Acid-Based HDAC Inhibitors as Potent Inhibitors of HDAC8 fromSchistosoma mansoni. *Arch. Der. Pharm.* **2017**, *350*, 1700096. [CrossRef] [PubMed]

64. Marek, L.; Hamacher, A.; Hansen, F.K.; Kuna, K.; Gohlke, H.; Kassack, M.U.; Kurz, T. Histone Deacetylase (HDAC) Inhibitors with a Novel Connecting Unit Linker Region Reveal a Selectivity Profile for HDAC4 and HDAC5 with Improved Activity against Chemoresistant Cancer Cells. *J. Med. Chem.* **2013**, *56*, 427–436. [CrossRef] [PubMed]

65. Saccoccia, F.; Brindisi, M.; Gimmelli, R.; Relitti, N.; Guidi, A.; Saraswati, A.P.; Cavella, C.; Brogi, S.; Chemi, G.; Butini, S.; et al. Screening and Phenotypical Characterization of Schistosoma mansoni Histone Deacetylase 8 (SmHDAC8) Inhibitors as Multistage Antischistosomal Agents. *ACS Infect. Dis.* **2020**, *6*, 100–113. [CrossRef]
66. Kalinin, D.V.; Jana, S.K.; Pfafenrot, M.; Chakrabarti, A.; Melesina, J.; Shaik, T.B.; Lancelot, J.; Pierce, R.J.; Sippl, W.; Romier, C.; et al. Structure-Based Design, Synthesis, and Biological Evaluation of Triazole-Based smHDAC8 Inhibitors. *ChemMedChem* **2019**, *15*, 571–584. [CrossRef]
67. Stolfa, D.A.; Marek, M.; Lancelot, J.; Hauser, A.-T.; Walter, A.; Leproult, E.; Melesina, J.; Rumpf, T.; Wurtz, J.-M.; Cavarelli, J.; et al. Molecular Basis for the Antiparasitic Activity of a Mercaptoacetamide Derivative That Inhibits Histone Deacetylase 8 (HDAC8) from the Human Pathogen Schistosoma mansoni. *J. Mol. Biol.* **2014**, *426*, 3442–3453. [CrossRef]
68. Ballante, F.; Reddy, D.R.; Zhou, N.J.; Marshall, G.R. Structural insights of SmKDAC8 inhibitors: Targeting Schistosoma epigenetics through a combined structure-based 3D QSAR, in vitro and synthesis strategy. *Bioorg. Med. Chem.* **2017**, *25*, 2105–2132. [CrossRef]
69. Simoben, C.V.; Robaa, D.; Chakrabarti, A.; Schmidtkunz, K.; Marek, M.; Lancelot, J.; Kannan, S.; Melesina, J.; Shaik, T.B.; Pierce, R.J.; et al. A Novel Class of Schistosoma mansoni Histone Deacetylase 8 (HDAC8) Inhibitors Identified by Structure-Based Virtual Screening and In Vitro Testing. *Molecules* **2018**, *23*, 566. [CrossRef]
70. Guidi, A.; Saccoccia, F.; Gennari, N.; Gimmelli, R.; Nizi, E.; Lalli, C.; Paonessa, G.; Papoff, G.; Bresciani, A.; Ruberti, G. Identification of novel multi-stage histone deacetylase (HDAC) inhibitors that impair Schistosoma mansoni viability and egg production. *Parasites Vectors* **2018**, *11*, 668. [CrossRef]
71. Caby, S.; Pagliazzo, L.; Lancelot, J.; Saliou, J.-M.; Bertheaume, N.; Pierce, R.J.; Roger, E. Analysis of the interactome of Schistosoma mansoni histone deacetylase 8. *PLoS Negl. Trop. Dis.* **2017**, *11*, e0006089. [CrossRef]
72. Pagliazzo, L.; Caby, S.; Lancelot, J.; Salomé-Desnoulez, S.; Saliou, J.-M.; Heimburg, T.; Chassat, T.; Cailliau, K.; Sippl, W.; Vicogne, J.; et al. Histone deacetylase 8 interacts with the GTPase SmRho1 in Schistosoma mansoni. *PLoS Negl. Trop. Dis.* **2021**, *15*, e0009503. [CrossRef]
73. Monaldi, D.; Rotili, D.; Lancelot, J.; Marek, M.; Wössner, N.; Lucidi, A.; Tomaselli, D.; Ramos-Morales, E.; Romier, C.; Pierce, R.J.; et al. Structure–Reactivity Relationships on Substrates and Inhibitors of the Lysine Deacylase Sirtuin 2 from Schistosoma mansoni (SmSirt2). *J. Med. Chem.* **2019**, *62*, 8733–8759. [CrossRef] [PubMed]
74. Schiedel, M.; Marek, M.; Lancelot, J.; Karaman, B.; Almlöf, I.; Schultz, J.; Sippl, W.; Pierce, R.J.; Romier, C.; Jung, M. Fluorescence-Based Screening Assays for the NAD++-Dependent Histone Deacetylase smSirt2 from Schistosoma mansoni. *J. Biomol. Screen.* **2014**, *20*, 112–121. [CrossRef] [PubMed]
75. Marek, M.; Ramos-Morales, E.; Picchi-Constante, G.F.; Bayer, T.; Norström, C.; Herp, D.; Sales-Junior, P.A.; Guerra-Slompo, E.P.; Hausmann, K.; Chakrabarti, A.; et al. Species-selective targeting of pathogens revealed by the atypical structure and active site of Trypanosoma cruzi histone deacetylase DAC2. *Cell Rep.* **2021**, *37*. [CrossRef]

4. Further results – not yet published

4.1. Synthesis and in vitro testing of bifunctional HDAC degraders

As previously reported in study **3.5**, compound **5** was designed and synthesized as a class I HDAC degrader. However, it did not show any notable degradation of HDAC1, 2, or 3. Several factors can affect the design and accordingly the degradation ability of PROTACs such as the protein of interest warheads, the length and composition of the linker [168, 169], the recruited E3 ligase [170], and the attachment point of the linker to both warheads [171, 172]. The previously mentioned factors contribute to the formation of the ternary complex, which is essential for the polyubiquitination and subsequent degradation of the POI. Therefore, it was interesting to try different HDAC warheads such as the unsubstituted or substituted 2-aminobenzamides in addition to the hydroxamate-based (SAHA) HDAC inhibitors (**Figure 12**). Another modification was to use different E3 ligase ligands such as the Von Hippel-Lindau (VHL) ligand, which is among the most utilized E3 recruiting ligands in PROTAC's development (**Figure 12**) [173]. Furthermore, we planned to replace the E3 ligase ligands with the adamantly moiety to design hydrophobic tag-based degraders (**Figure 12**). Additionally, variable linkers were used for the design of the planned degraders.
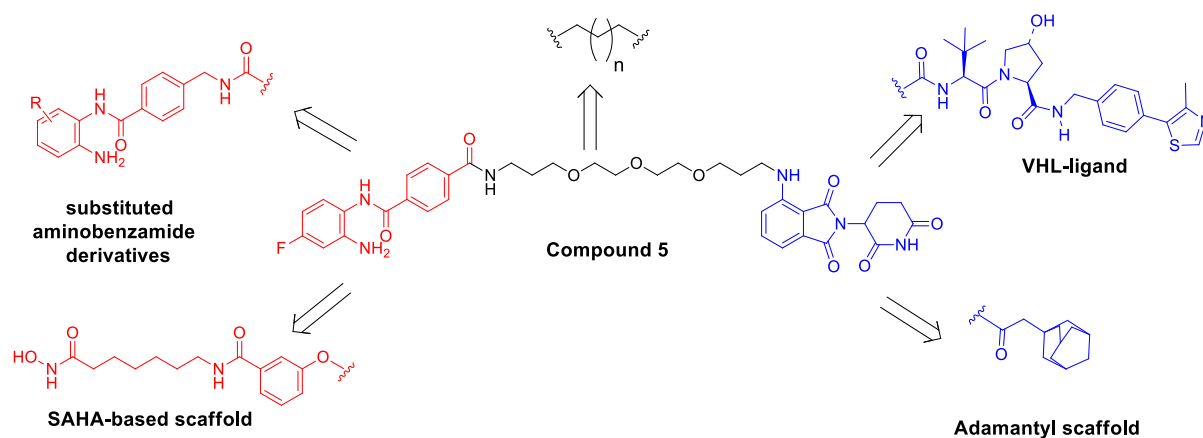
Figure 12: Different planned strategies for the design of different HDAC degraders.

In total, 13 novel heterobifunctional molecules were synthesized using different HDAC inhibitor parts as well as different E3 ligase ligands or hydrophobic adamantly scaffold. The developed compounds can be divided, according to the utilized HDAC warheads, into two main groups. The first group of degraders was designed based on different substituted 2-aminobenzamide scaffolds as in the case of compounds **MA26-28**, **MA61**, and **MA64-MA66** (**Figures 13, 14**). The second group contains the hydroxamic acid derivative (SAHA) as the HDAC inhibitor part as in the case of compounds **MA54-MA59 (Figures 16-19)**.

In order to obtain the first group of the planned degraders, different synthetic strategies were applied that involved three main steps as demonstrated in **Figures 13** and **14**. The first step included the synthesis of the 2-aminobenzamide-containing HDAC warheads functionalized with either a free carboxylic acid group as in the case of intermediates **3**, **8**, and **12** (**Figure 13**) or with a free amino group as in the case of intermediates **16** and **18a,b** (**Figure 14**).

In most cases, these 2-aminobenzamide scaffolds were used for amide coupling with the counterpart linkers without prior protection of the aromatic amino group as in the case of intermediates **6** and **16**. This could be explained by the reduced reactivity of such aromatic amines compared with the aliphatic amines used in the coupling reactions, especially in the presence of an electron-withdrawing group in the meta-position such as the fluoro atom, as in the case of intermediates **6** and **8**, which usually results in decreasing the electron density and hence the reactivity. The second step involved the synthesis of the pomalidomide connected to a polyethylene glycol linker (intermediate **13**) (**Figure 13**), which was prepared as previously described in **study 3.5** [174], or the VHL ligand connected to dicarboxylic acid alkyl linkers (intermediates **22a,b**) as shown in **Figure 14**. The VHL ligand **20** was synthesized as previously described [175]. The third step involved the amide coupling reaction between the appropriate HDAC inhibitor part and the corresponding E3 ligase ligand or the hydrophobic adamantly scaffold to get the final compounds (**MA26-28**, **MA61**, and **MA64-MA66**). In general, two different amide coupling reactions were utilized to obtain the desired intermediates and final compounds. The first method was the activation of the carboxylic acid to the corresponding acid chloride using thionyl chloride followed by reaction with the appropriate amine as in the case of intermediates **3** and **10**. The second and most common method used herein involved the reaction between the appropriate carboxylic acid and the amine derivative in the presence of the coupling reagent HATU (Hexafluorophosphate Azabenzotriazole Tetramethyl Uronium) and DIPEA (*N*, *N*-Diisopropylethylamine) as a base to get the corresponding amide.
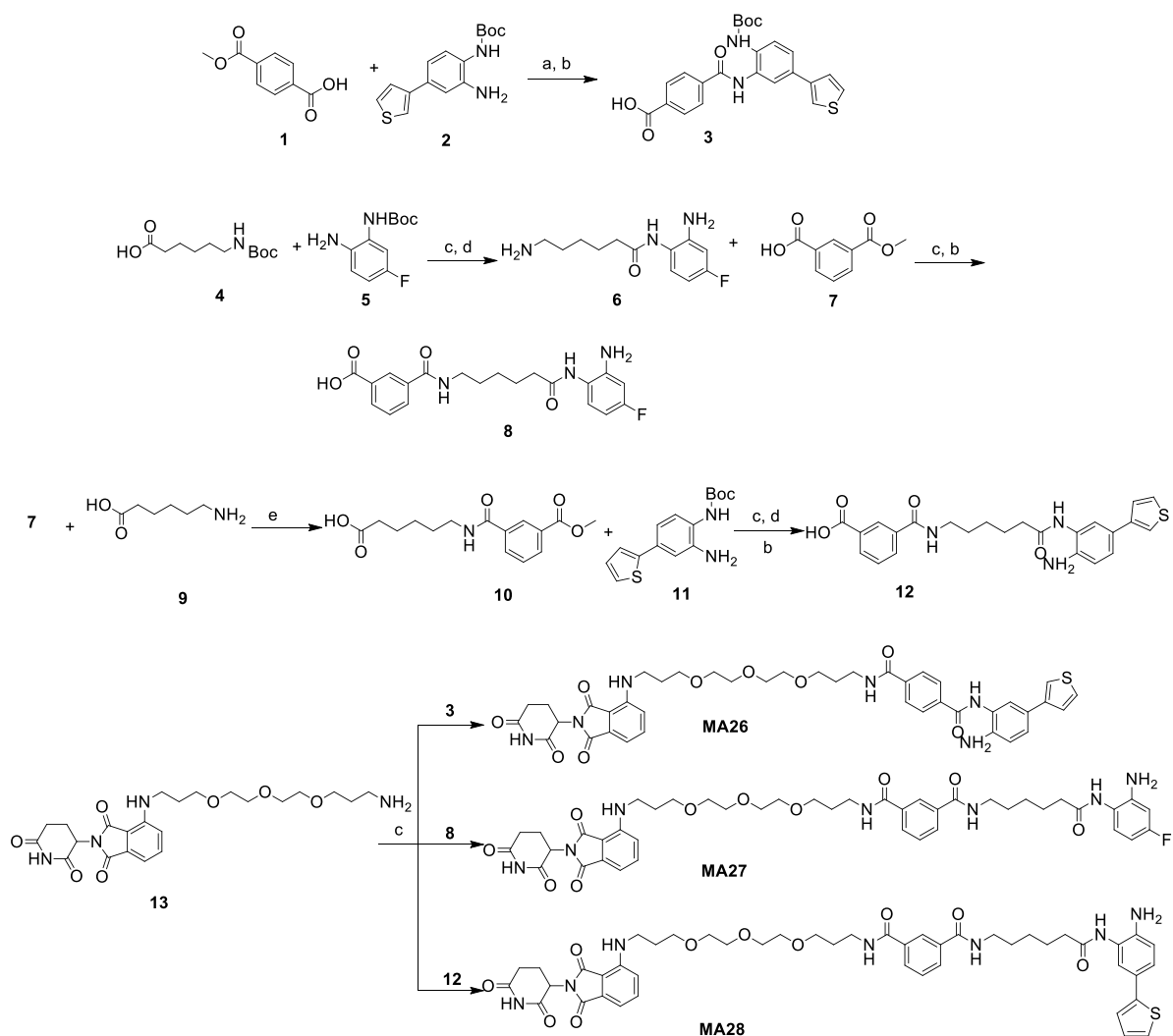
Figure 13: Synthetic scheme for preparation of compounds MA26-MA28.

Reagents and conditions: (a) (i) SOCl$_2$, 90 $^\circ$C, 1 h, (ii) DIPEA, dry THF, 0 $^\circ$C, 10 h; (b) LiOH·H$_2$O, THF, H$_2$O, RT, 6 h; (c) HATU, DIPEA, DMF, RT, 5 h; (d) TFA, DCM, RT, 30 min; (e) (i) **7**, SOCl$_2$, 90 $^\circ$C, 1 h, (ii) **9**, 1M aq. NaOH, dry THF, RT, 10 h, 1 M HCl till pH 2.
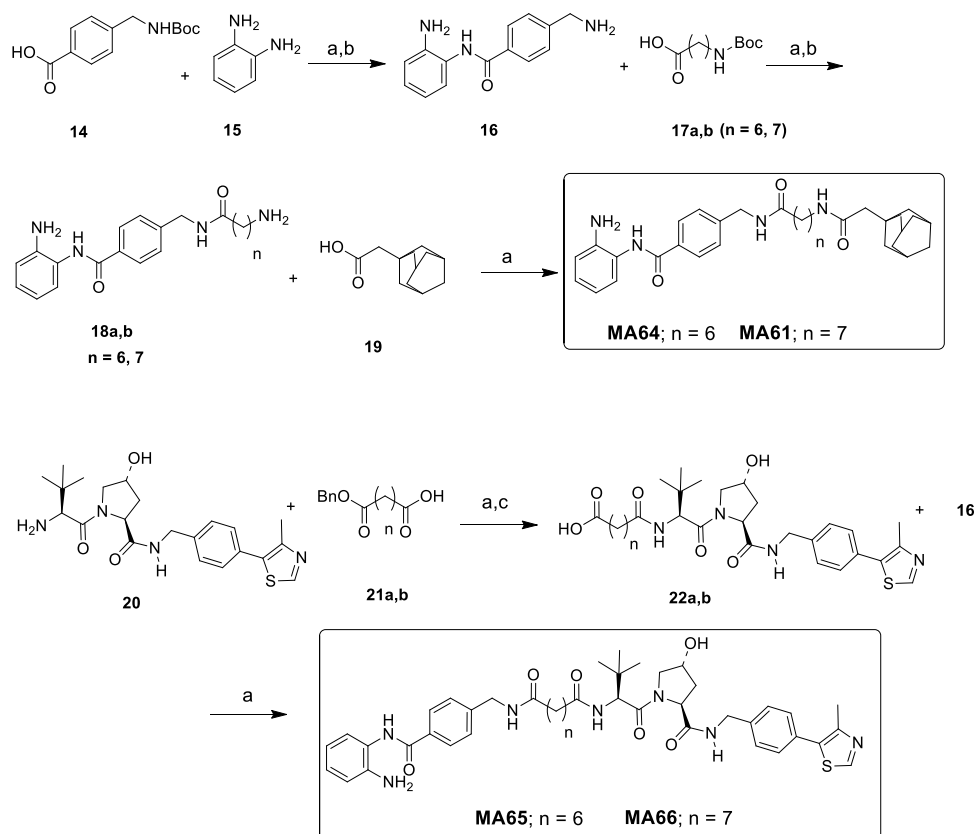
Figure 14: Synthetic scheme for preparation of compounds MA61, MA64-MA66.

Reagents and conditions: (a) HATU, DIPEA, DMF, RT, 1 h; (b) TFA, DCM, RT, 30 min; (c) LiOH·H_2O, THF, H_2O, RT, 3 h.

The SAHA-based HDAC PROTACs were synthesized using almost the same strategy as shown in **Figures 15-19**. Firstly, different E3 ligase ligands such as the VHL ligand and pomalidomide, as well as the adamantly scaffold as a hydrophobic tag, were connected to the appropriate alkyl linker functionalized with either free amino or carboxylic acid groups (**Figure 15**). The second main step involved the synthesis of the protected hydroxamic acid HDAC inhibitor part functionalized with either a free amino or carboxylic acid group for coupling with the E3 ligase ligand counterpart at the final step. Two different protecting groups for the hydroxamic acid functionality were used, namely the benzyl group in the case of intermediate **40** (**Figures 16, 17**) and the 2-tetrahydropyran (THP) group in the case of intermediate **49** (**Figure 18, 19**). The third step included the amide coupling between the two counterparts followed by the removal of the protecting groups through catalytic hydrogenation in the presence of palladium, as in the case of benzyl-protected hydroxamic acids (compounds **MA54-MA57**; **Figures 16** and **17**) or using diluted hydrochloric acid in the case of THP-protected hydroxamates (compounds **MA58** and **MA59**; **Figures 18** and **19**).

The detailed procedures for the synthesis of intermediates and final compounds are described in **Section 4.3** (**Materials and methods**).
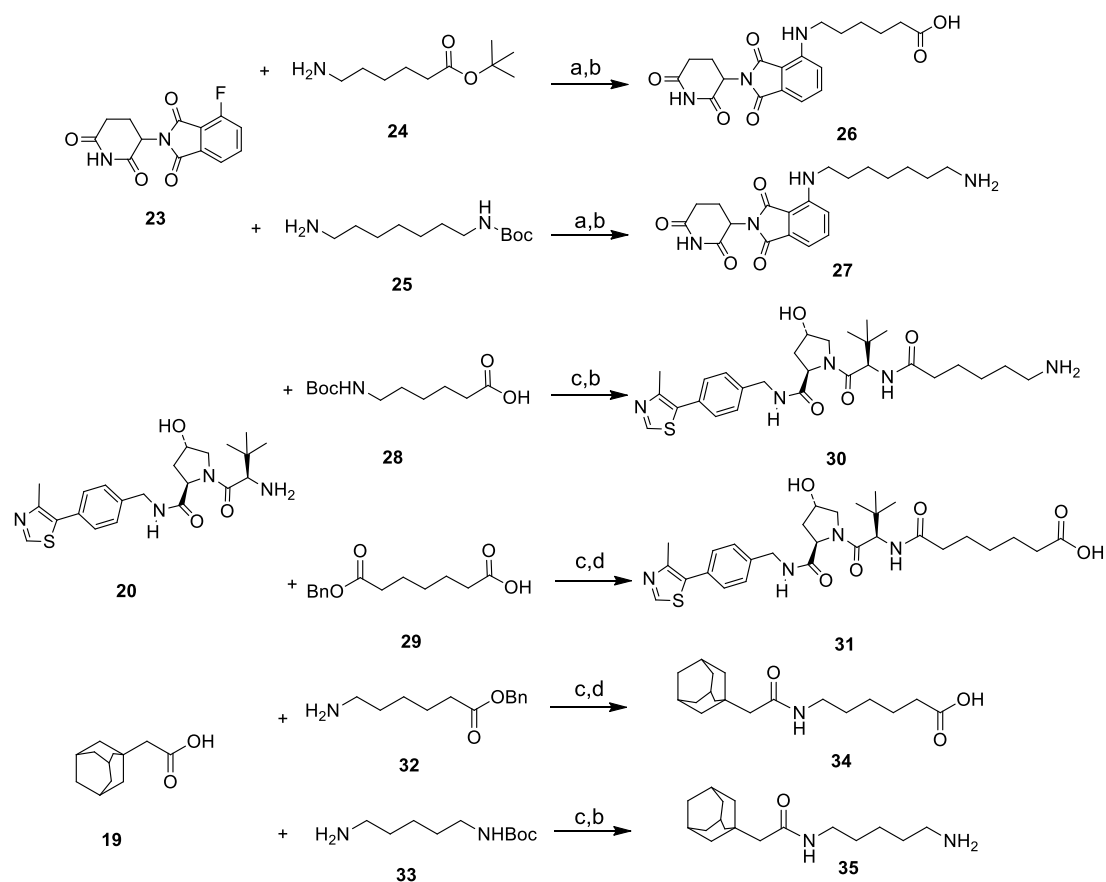
Figure 15: Synthetic scheme for preparation of linkers connected to different E3 ligase ligands or adamantly hydrophobic tag part.

Reagents and conditions: (a) DIPEA, NMP, MW, 110 °C, 2 h; (b) TFA, DCM, RT, 1-3 h; (c) HATU, DIPEA, DMF, RT, 2-3 h; (d) LiOH·H$_2$O, THF, H$_2$O, RT, 3 h.
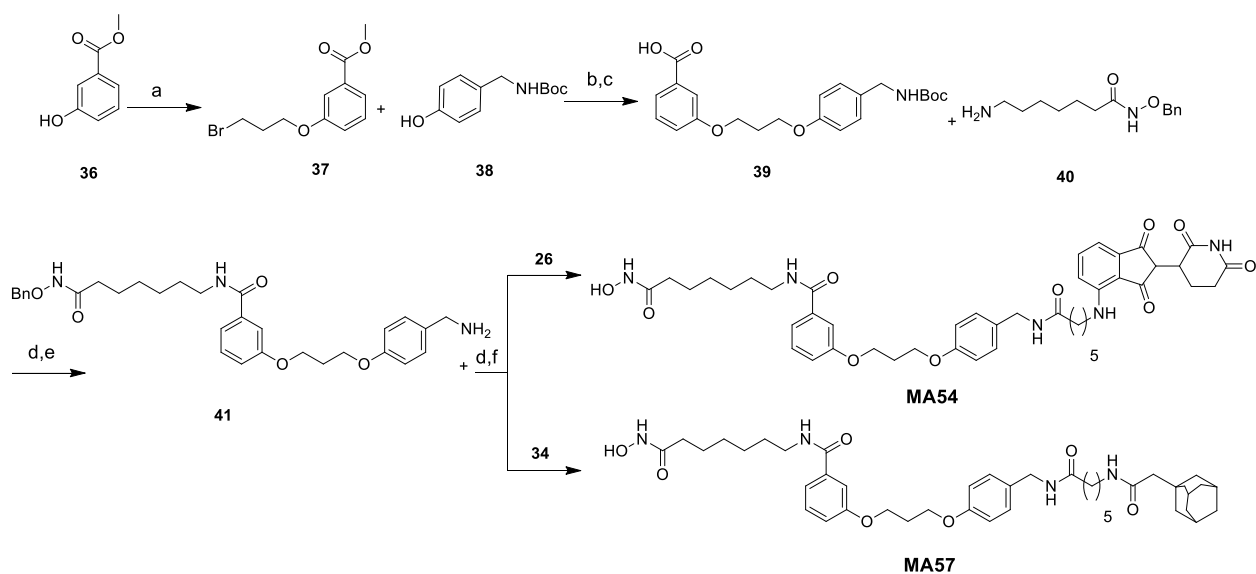
Figure 16: Synthetic scheme for preparation of compounds MA54 and MA57.

Reagents and conditions: (a) 1,3-dibromopropane, K_2CO_3, DMF, 50 °C, 16 h; (b) K_2CO_3, acetonitrile, 80 °C, 16 h; (c) LiOH·H_2O, THF, H_2O, RT, 3 h; (d) HATU, DIPEA, DMF, RT, 5 h; (e) TFA, DCM, RT, 30 min; (f) Pd/C (10%), H_2, ethyl acetate, THF, RT, 3 h.
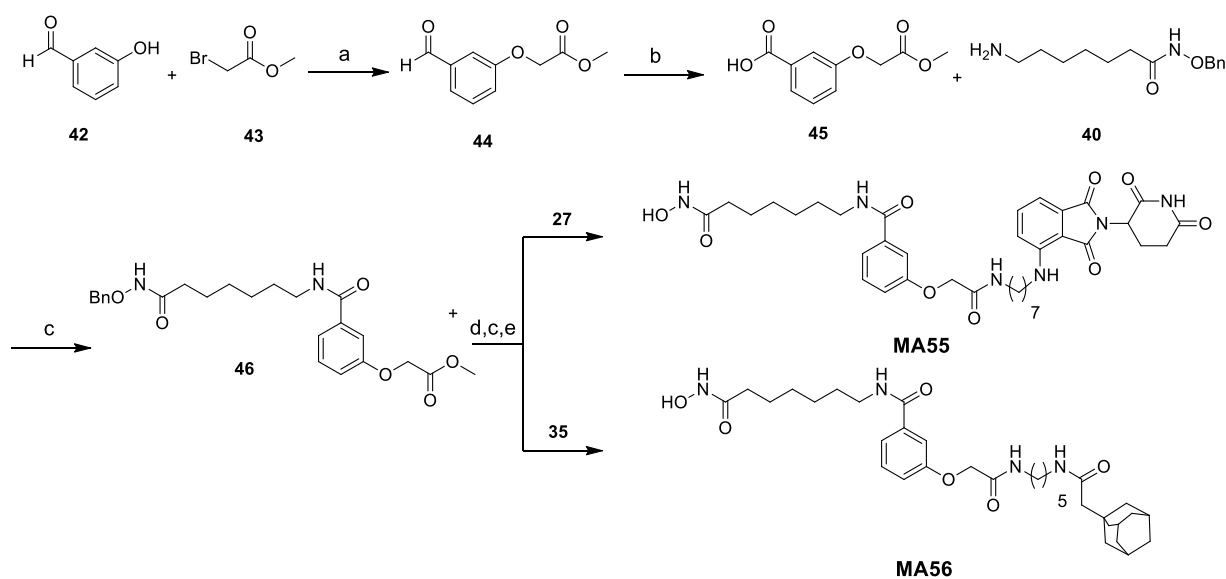
Figure 17: Synthetic scheme for preparation of compounds MA55 and MA56.

Reagents and conditions: (a) K_2CO_3, acetonitrile, 80 °C, 16 h; (b) 2-methyl-2-butene, NaH_2PO_4·$4H_2O$, $NaClO_2$, *tert*-butanol, H_2O, RT; 4 h, 1 M HCl; (c) HATU, DIPEA, DMF, RT, 5 h; (d) LiOH·H_2O, THF, H_2O, RT, 5 h; (e) Pd/C (10%), H_2, ethyl acetate, THF, RT, 3 h.
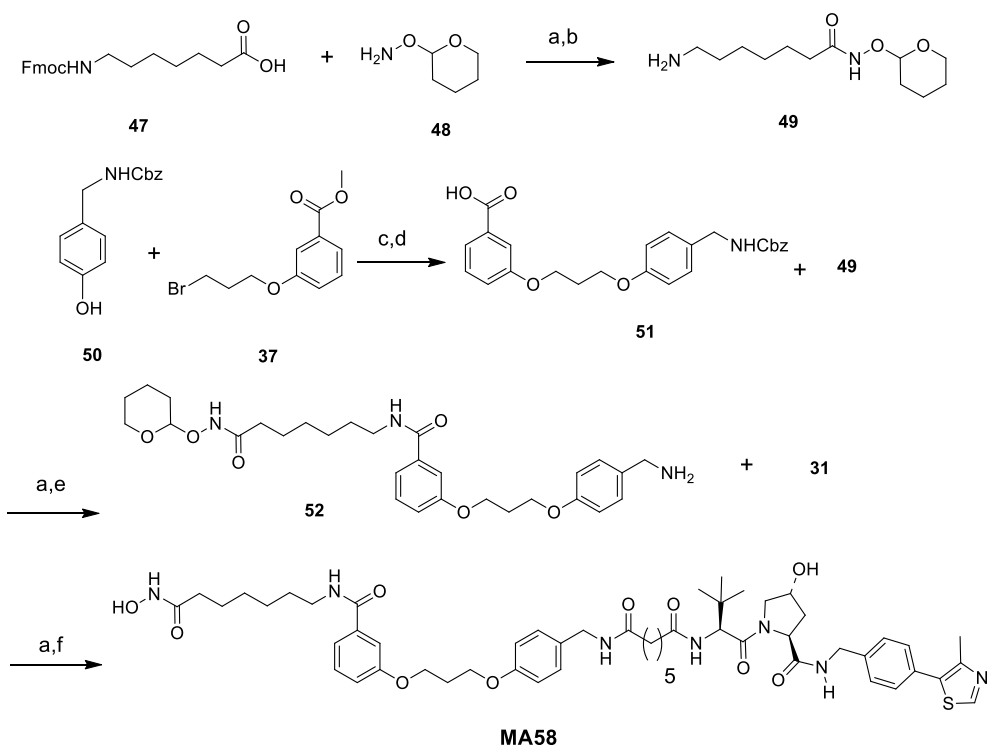
Figure 18: Synthetic scheme for preparation of compound MA58.

Reagents and conditions: (a) HATU, DIPEA, DMF, RT, 5 h; (b) piperidine, DCM, RT, 1 h; (c) K_2CO_3, acetonitrile, 80 $^\circ$C, 16 h; (d) LiOH·H_2O, THF, H_2O, RT, 5 h; (e) Pd/C (10%), H_2, ethyl acetate, MeOH, RT, 6 h; (f) 1 M HCl, THF, MeOH, RT, 2 h.
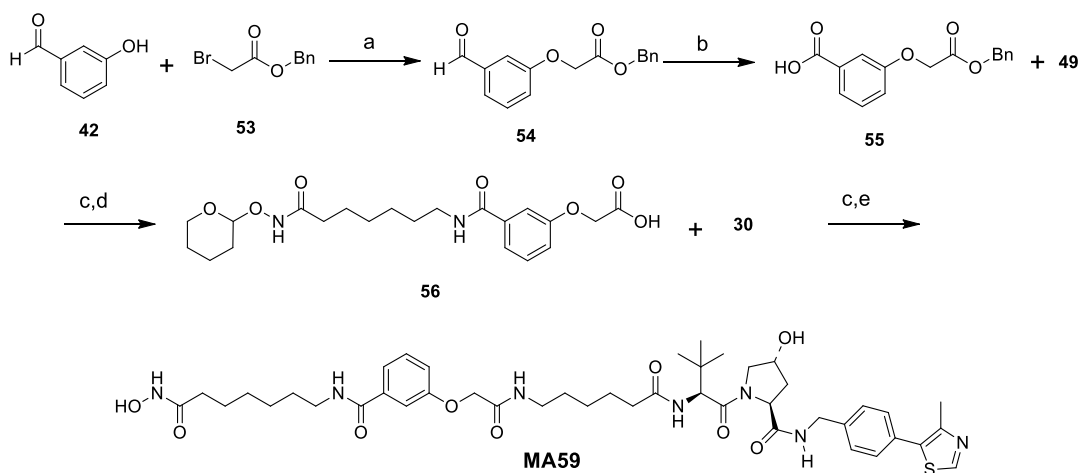
Figure 19: Synthetic scheme for preparation of compound MA59.

Reagents and conditions: (a) K_2CO_3, acetonitrile, 80 $^\circ$C, 16 h; (b) 2-methyl-2-butene, NaH_2PO_4·$4H_2O$, $NaClO_2$, *tert*-butanol, H_2O, RT; 4 h, 1 M HCl; (c) HATU, DIPEA, DMF, RT, 5 h; (d) Pd/C (10%), H_2, ethyl acetate, MeOH, RT, 4 h; (e) 1 M HCl, THF, MeOH, RT, 2h.

38

4.2. Biological Evaluation

4.2.1. In Vitro HDAC Inhibition Assay

The in vitro inhibitory activity of the 2-aminobenzamide-based PROTACs (**MA26-MA28**, **MA61**, and **MA64-MA66**) were assessed on human HDAC1-3 using a fluorogenic peptide derived from p53 (Ac-RHKK(Acetyl)-AMC) (**Table 1**) [176]. Compounds **MA26** and **MA28** bearing a thienyl substituent at the benzamide scaffold showed good inhibitory activity and high selectivity for HDAC1 and 2 over HDAC3. On the other hand, the fluoro-derivative **MA27** displayed, as expected, higher in vitro selectivity for HDAC3 over HDAC1 and 2. Meanwhile, compounds **MA61** and **MA64-MA66** displayed moderate inhibitory activity against HDAC1-3. Additionally, the SAHA-based HDAC PROTACs **MA54-MA59** were tested against HDAC1-3, 6, and 8 (**Table 2**). Generally, the SAHA-based PROTACs showed broad inhibitory activity against class I HDACs in the low submicromolar range. In addition, they exhibited very potent inhibition against HDAC6 in the nanomolar range (**Table 2**).

Table 1: In vitro activity IC$_{50}$ (μM) or (% inhibition) of the 2-aminobenzamide-based PROTACs against human HDAC1-3

Cpd. Id	Structure	HDAC1	HDAC2	HDAC3
MA26		0.17 ± 0.03	0.32 ± 0.01	>20
MA27		>20	>20	2.7 ± 0.1
MA28		0.17 ± 0.03	0.51 ± 0.03	65.0 ± 7.0
MA61		41% at 1 μM 60% at 10 μM	63% at 1 μM 89% at 10 μM	19% at 1 μM 45% at 10 μM
MA64		48% at 1 μM 71% at 10 μM	62% at 1μM 94% at 10 μM	22% at 1 μM 70% at 10 μM

MA65		59% at 1 µM 72% at 10 µM	58% at 1 µM 95% at 10 µM	16% at 1 µM 58% at 10 µM
MA66		51% at 1 µM 71% at 10 µM	57% at 1 µM 94% at 10 µM	18% at 1 µM 65% at 10 µM

Table 2: In vitro activity IC$_{50}$ (µM) or (% inhibition) of the SAHA-based PROTACs against human HDAC1-3, 6 and 8
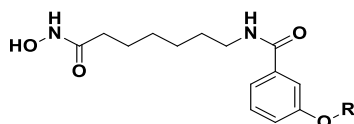
Cpd. Id	R	HDAC 1	HDAC 2	HDAC3	HDAC 6	HDAC8
MA54		0.48 ± 0.02	1.2 ± 0.1	0.38 ± 0.02	0.016 ± 0.002	46.8% at 1 µM
MA55		0.32 ± 0.02	0.67 ± 0.03	0.19 ± 0.01	0.0095± 0.0007	0.27 ± 0.031
MA56		0.26 ± 0.01	0.76 ± 0.03	0.29 ± 0.01	0.0083± 0.0006	0.29 ± 0.025
MA57		3.8 ± 0.3	11 ± 1	3.1 ± 0.2	0.089± 0.006	20.5% at 1 µM
MA58		0.31 ± 0.02	0.92 ± 0.04	0.35 ± 0.03	0.0085± 0.0005	0.998 ± 0.153
MA59		0.25 ± 0.01	0.53 ± 0.02	0.28 ± 0.02	0.0057± 0.0007	0.538 ± 0.078

4.2.2. Cellular testing

The developed compounds were tested against human pancreatic adenocarcinoma (PSN1) and colorectal carcinoma (HCT116) cell lines (**Table 3**). Compounds **MA61** and **MA64** showed moderate anti-proliferative activity against HCT116 cell line (**Table 3**). In order to evaluate the degradation capability of the synthesized PROTACs, the cellular levels of HDAC1-3 in PSN1 and HCT116 cell lines were analyzed by Western blots (**Figures 20**). In addition, the acetylation level of histone 3 Lys 9 (H3k9ac), known HDAC1/2 substrate, was determined. There was a slight increase in histone acetylation level in HCT116 cells after 6h treatment with 1µM concentration of PROTACs **MA61** and **MA64** compared to the DMSO control (**Figures 20**). Unfortunately, no degradation of HDAC1-3 isoforms was observed so far in the tested cell lines. Further phenotypic screenings of the developed PROTACs against other cancer cell lines as well as degradation assays are currently in progress.

Table 3: IC$_{50}$ values of developed degraders against PSN1 and HCT116 cell lines

Cpd. Id	PSN1 (IC$_{50}$ µM)	HCT116 (IC$_{50}$ µM)
MA55	7.1	10.1
MA61	5.6	2.2
MA64	3.8	2.9
MA65	n.d*	n.d
MA66	n.d	5.7

* n.d: not determined
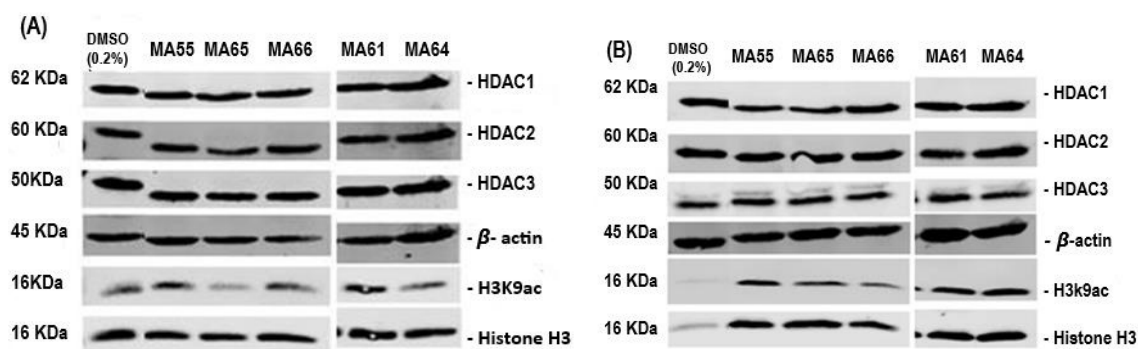
Figure 20: Western blots of HDAC1, 2, and 3 levels in different cell lines. PSN1(A) and HCT116 (B) cells were treated with 1µM of PROTACs (MA55, MA65, MA66) and hydrophobic tags (MA61 and MA64) after 6h incubation, DMSO was used as a vehicle, *β*-actin was used as loading control, the level of H3K9ac as a marker for the acetylation of Histone 3 was measured.

4.3. Materials and methods

4.3.1. General experimental information

Materials and reagents were purchased from Sigma-Aldrich Co., Ltd. (Darmstadt, Germany) and abcr GmbH (Karlsruhe, Germany). All solvents were analytically pure and dried before use. Thin-layer chromatography was carried out on aluminum sheets coated with silica gel 60 F254 (Merck, Darmstadt, Germany). For medium-pressure chromatography (MPLC), silica gel 60 (0.036-0.200 mm) was used. Purity was measured by UV absorbance at 254 nm. The elution system used for HPLC consists of MeOH, H_2O, and 0.05% trifluoroacetic acid. The HPLC consisted of a LiChrosorb® RP-18 (5 µm) 100-4.6 Merck column (Merck, Darmstadt, Germany), two LC-10AD pumps, a SPD-M10A VP PDA detector, and a SIL-HT autosampler, all from the manufacturer Shimadzu (Kyoto, Japan). The absorption spectra were recorded with a Shimadzu SPD-M10A diode array detector spectrophotometer (Kyoto, Japan). For the preparative HPLC, a LiChrosorb® RP-18 (7 µm) 250-25 Merck (Merck, Darmstadt, Germany) column was used. The applied mobile phase was a gradient with increasing polarity composed of acetonitrile/water and 0.1% formic acid. Mass spectrometry analyses were performed with a Finnigan MAT710C (Thermo Separation Products, San Jose, CA, USA) for the ESI MS spectra and with a LTQ (linear ion trap) Orbitrap XL hybrid mass spectrometer (Thermo Fisher Scientific, Bremen, Germany) for the HRMS-ESI (high-resolution mass spectrometry) spectra. For the HRMS analyses, the signal for the isotopes with the highest prevalence was given and calculated. ^{1}H NMR spectra were taken on a

Varian Inova 400 using deuterated DMSO as solvent. Chemical shifts were referenced to the residual solvent signals. The following abbreviations and formulas for solvents and reagents were used: thionyl chloride (SOCl$_2$), tetrahydrofuran (THF), *N*, *N*-diisopropylethylamine (DIPEA), hexafluorophosphate azabenzotriazole tetramethyl uronium (HATU), ethyl acetate (EtOAc), *N, N*-dimethylformamide (DMF), trifluoroacetic acid (TFA), lithium hydroxide monohydrate (LiOH.H$_2$O) dimethyl sulfoxide (DMSO), methanol (MeOH), water (H$_2$O), sodium sulphate (Na$_2$SO$_4$), dichloromethane (DCM), potassium carbonate (K$_2$CO$_3$), sodium dihydrogen phosphate tetrahydrate (NaH$_2$PO$_4$·4H$_2$O), sodium chlorite (NaClO$_2$), hydrochloric acid (HCl), fluorenylmethoxycarbonyl (Fmoc), benzyloxycarbonyl (Cbz), *tert*-butyloxycarbonyl (Boc) and tetrahydropyranyl (THP).

4.3.2. General Synthetic Methods

Method I: Amide coupling.

Method IA:

Thionyl chloride (SOCl$_2$) (3 mL) was added to the appropriate carboxylic acid (1 eq.), and the reaction mixture was heated at 90 $^\circ$C for 1 h. The mixture was evaporated under reduced pressure. The obtained residue was diluted with dry tetrahydrofuran (THF) (10 mL) and added at 0 $^\circ$C to a solution of the appropriate amine (1.1 eq.) and DIPEA (5 eq.) in dry THF (10 mL). The mixture was stirred at RT for 10 h. After completion of the reaction, water was added, and the mixture was extracted using ethyl acetate. The combined organic layer was washed with an aqueous 1 M ammonium chloride solution, followed by an aqueous 1 M sodium bicarbonate solution and brine. The combined organic extract was dried over anhydrous Na$_2$SO$_4$, and the organic layer was filtered and evaporated in vacuo to yield the crude amide, which was purified by medium pressure liquid chromatography (MPLC) using DCM: MeOH (0–1% MeOH).

Method IB:

A solution of the appropriate carboxylic acid (1 eq.), HATU (1 eq.), and DIPEA (5 eq.) in DMF (5 mL) was stirred for 10 min at RT, then the corresponding amine (1.2 eq.) was added. The reaction mixture was stirred at RT for 5 h. After completion of the reaction as indicated by TLC, water was added, and the mixture was extracted using ethyl acetate as described in the previous method. The crude amide was purified by MPLC using DCM: MeOH (1–10% MeOH).

Method II: Hydrolysis of methyl or benzyl ester. To a stirred suspension of the appropriate ester (1 eq.) in THF:H$_2$O (1:1) (10 mL), LiOH·H$_2$O (5 eq.) was added, and the mixture was stirred at RT for 3-6 h. After completion of the reaction, the pH value of the mixture was adjusted to 5. The resulting solid was filtered, washed with water to provide the corresponding carboxylic acid, which was used for the next step without further purification.

Method III: Hydrolysis of tert-butyl ester. The appropriate *tert*-butyl ester was dissolved at 0 °C in dry DCM (5 mL), then TFA (5 mL) was added. The reaction mixture was stirred at RT for 2-3 h. The solvent was evaporated to dryness to provide the corresponding carboxylic acid.

Method IV: N-Boc-deprotection. The appropriate *N*-Boc-protected amine derivative was dissolved at 0 °C in dry DCM (5 mL), then TFA (5 mL) was added. The reaction mixture was stirred at RT for 30-60 min. The solvent was evaporated to dryness to provide the corresponding amine derivative as a TFA salt.

Method V: Synthesis of pomalidomide-based linkers

DIPEA (3 eq.) was added to a solution of 2-(2,6-dioxo-3-piperidinyl)-4-fluoro-1*H*-isoindole-1,3(2*H*)-dione (**23**) (1 eq.) and the appropriate amine linker (**24, 25**) (1.1 eq.) in *N*-methyl-2-pyrrolidone (3 mL). The reaction mixture was heated at 110 °C for 2 h in the microwave. The mixture was cooled to RT, then water (10 mL) was added, and the mixture was extracted with EtOAc (30 mL), washed with brine (20 mL), and dried over anhydrous Na$_2$SO$_4$. The combined organic layers were evaporated under reduced pressure and purified by MPLC using EtOAc and hexane. The obtained protected linkers were dissolved at 0 °C in dry DCM (5 mL), and then TFA (2.5 mL) was added. The reaction mixture was stirred at RT for 1 h. Volatile substances were removed under reduced pressure. The obtained residue was purified by MPLC using DCM and MeOH (1-4% MeOH) to obtain the corresponding pomalidomide-based linkers (**26, 27**).

Method VI: Alkylation reaction

To a suspension of the appropriate phenolic derivative (1 eq.) and K$_2$CO$_3$ (3 eq.) in acetonitrile (30 mL), the appropriate alkyl halide (1-3 eq.) was added, and the mixture was heated at 80 °C for 16 h. The mixture was cooled to RT, filtered, and washed with acetonitrile. The filtrate was evaporated under reduced pressure, then water (10 mL) was added, and the mixture was extracted with EtOAc (30 mL), washed with brine (20 mL), and dried over

anhydrous Na_2SO_4. The combined organic layers were evaporated under reduced pressure and purified by MPLC using EtOAc and hexane.

Method VII: Deprotection of tetrahydropyranyl (THP)-protected hydroxamic acids

To a solution of the THP-protected product (1 eq.) in THF (5 mL) with a few drops of MeOH and 15 drops of 1 M hydrochloric acid were added, and the reaction mixture was stirred at RT until the TLC showed completion of the reaction. The solvent was then evaporated under vacuum, and the crude product was purified by preparative HPLC.

Method VIII: Deprotection of benzyl (Bn)-protected hydroxamic acids, benzyl ester and Cbz-protected amines

To a stirred solution of the appropriate Bn or Cbz protected intermediate (1 eq.) in a mixture of ethyl acetate and THF mixture (1:1), a catalytic amount of Pd/C (10%) was added. The reaction mixture was put under vacuum, followed by a hydrogen atmosphere. The mixture was stirred at RT until the completion of the reaction. The mixture was then filtered through celite, and the solvent was evaporated to give the crude residue, which was purified by MPLC using DCM and MeOH (3-10% MeOH).

Method IX: Oxidation of aldehyde to the corresponding carboxylic acid

To a solution of the appropriate aldehyde derivative (1 eq.) in a mixture of *tert*-butanol:water (4:1), successively 2-methyl-2-butene (4.4 eq.), sodium dihydrogen phosphate tetrahydrate ($NaH_2PO_4 \cdot 4H_2O$) (1 eq.), and sodium chlorite ($NaClO_2$) (3.3 eq.) were added at 0 $^\circ$C, then the reaction was allowed to warm to RT and stirred for 4 h. The *tert*-butanol was evaporated, then water (10 mL) was added, and the pH was adjusted to 4 using 1 M HCl. The obtained solid was filtered, washed with water, and dried under vacuum to give the corresponding carboxylic acid.

Method X: Deprotection of Fmoc-protected amine

The Fmoc-protected amine was dissolved in 20% piperidine in DCM (30 mL), and the reaction was stirred for 1 h. The reaction was evaporated under reduced pressure, redissolved in DCM, and evaporated three times. The obtained residue was purified by MPLC using DCM and MeOH to get the corresponding free amine.

4.3.3. Characterization data of key intermediates and final compounds.

Intermediates **2, 5, 11** [177], **13** [174], **20** [175], **23** [178], and **40** [179] were synthesized according to the previously reported procedures. The compounds were confirmed with ^{1}HNMR and mass spectroscopy.

4-((2-((*tert*-Butoxycarbonyl)amino)-5-(thiophen-3-yl)phenyl)carbamoyl)benzoic acid (3)
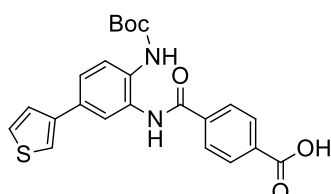
Intermediate **3** was synthesized by the coupling 4-(methoxycarbonyl)benzoic acid (**1**) and *tert*-butyl (2-amino-4-(thiophen-3-yl)phenyl)carbamate (**2**) using $SOCl_2$ according to **method IA**, followed by methyl ester hydrolysis according to **method II**. Yield: 45% over 2 steps. ^{1}H NMR (400 MHz, DMSO-d_6) δ 10.04 (s, 1H), 8.73 (s, 1H), 8.10 – 8.01 (m, 4H), 7.84 (d, *J* = 1.8 Hz, 1H), 7.80 (dd, *J* = 2.9, 1.3 Hz, 1H), 7.65 – 7.60 (m, 2H), 7.58 – 7.53 (m, 1H), 7.50 (dd, *J* = 5.1, 1.3 Hz, 1H), 1.44 (s, 9H). MS m/z: 461.17 $[M+Na]^+$.

6-Amino-*N*-(2-amino-4-fluorophenyl)hexanamide (6)
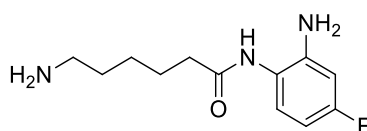
Intermediate **6** was prepared through the amide coupling of the commercially available 6-(Boc-amino)hexanoic acid (**4**) and the boc-protected aniline derivative **5** according to **method IB**, followed by boc-deprotection according to **method IV**. Yield: 41% over 2 steps. ^{1}H NMR (400 MHz, DMSO-d_6) δ 8.99 (s, 1H), 7.07 (dd, *J* = 8.7, 6.4 Hz, 1H), 6.46 (dd, *J* = 11.2, 2.9 Hz, 1H), 6.28 (td, *J* = 8.5, 2.9 Hz, 1H), 5.10 (s, 2H), 2.55 (t, *J* = 6.8 Hz, 2H), 2.27 (t, *J* = 7.4 Hz, 2H), 1.61 – 1.50 (m, 2H), 1.44 – 1.24 (m, 4H). MS m/z: 240.26 $[M+H]^+$.

3-((6-((2-Amino-4-fluorophenyl)amino)-6-oxohexyl)carbamoyl)benzoic acid (8)
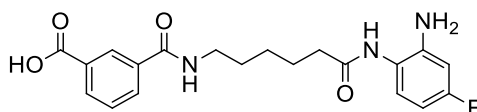
Intermediate **8** was prepared through the amide coupling of intermediate **6** and 3-(methoxycarbonyl)benzoic acid (**7**) according to **method IB,** followed by methyl ester

hydrolysis according to *method II*. Yield: 38% over 2 steps. ^{1}H NMR (400 MHz, DMSO-d$_6$) δ 12.31 (s, br, 3H), 9.35 (s, 1H), 8.72 (t, *J* = 5.5 Hz, 1H), 8.40 (t, *J* = 1.5 Hz, 1H), 8.12 – 7.98 (m, 2H) 7.55 (t, *J* = 7.8 Hz, 1H), 7.13 (dd, *J* = 8.7, 6.4 Hz, 1H), 6.52 (dd, *J* = 11.1, 2.9 Hz, 1H), 6.29 (td, *J* = 8.5, 2.9 Hz, 1H), 3.27 – 3.21 (m, 2H), 2.33 (t, *J* = 7.4 Hz, 2H), 1.66 – 1.47 (m, 4H), 1.40 – 1.27 (m, 2H). MS m/z: 386.37 [M-H]$^-$.

6-(3-(Methoxycarbonyl)benzamido)hexanoic acid (10)
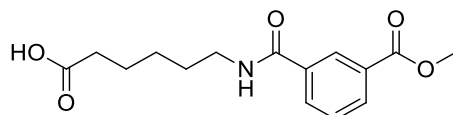
The acid chloride derivative of intermediate **7** was prepared according to *method IA*, then it was diluted in dry THF, and added at 0 °C to a solution of 6-aminohexanoic acid (**9**) in 1 M aq. solution of NaOH. The reaction mixture was stirred at RT for 10 h. The pH was adjusted to 2 using 1 M HCl. The product was purified by MPLC using DCM: MeOH to obtain intermediate **10**. Yield: 50%. ^{1}H NMR (400 MHz, DMSO-d$_6$) δ 12.06 (s, 1H), 8.64 (t, *J* = 5.3 Hz, 1H), 8.41 (s, 1H), 8.08 (t, *J* = 7.3 Hz, 2H), 7.64 – 7.54 (m, 1H), 3.87 (s, 3H), 3.24 (dd, *J* = 12.9, 6.8 Hz, 2H), 2.19 (t, *J* = 7.3 Hz, 2H), 1.59 – 1.43 (m, 4H), 1.37 – 1.24 (m, 2H). MS m/z: 292.28 [M-H]$^-$.

3-((6-((2-Amino-5-(thiophen-2-yl)phenyl)amino)-6-oxohexyl)carbamoyl)benzoic acid(12)
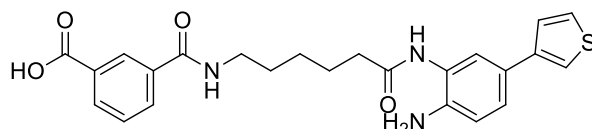
Intermediate **12** was prepared through the amide coupling reaction between intermediate **10** and **11** according to *method IB*, followed by boc-deprotection according to *method IV* and finally ester hydrolysis following *method II*. Yield: 35% over 3 steps. ^{1}H NMR (400 MHz, DMSO-d$_6$) δ 9.25 (s, 1H), 8.65 (t, *J* = 5.5 Hz, 1H), 8.43 – 8.37 (m, 1H), 8.08 – 8.01 (m, 2H), 7.62 – 7.52 (m, 1H), 7.50 (d, *J* = 1.9 Hz, 1H), 7.34 (dd, *J* = 5.1, 0.9 Hz, 1H), 7.26 – 7.15 (m, 2H), 7.02 (dd, *J* = 5.0, 3.6 Hz, 1H), 6.79 (d, *J* = 8.3 Hz, 1H), 3.31 – 3.22 (m, 2H), 2.35 (t, *J* = 7.5 Hz, 2H), 1.70 – 1.51 (m, 4H), 1.42 – 1.32 (m, 2H). MS m/z: 450.26 [M-H]$^-$.

N^1-(2-Amino-5-(thiophen-3-yl)phenyl)-*N*^{4}-(3-(2-(2-(3-((2-(2,6-dioxopiperidin-3-yl)-1,3-dioxoisoindolin-4-yl)amino)propoxy)ethoxy)ethoxy)propyl)terephthalamide (MA26)
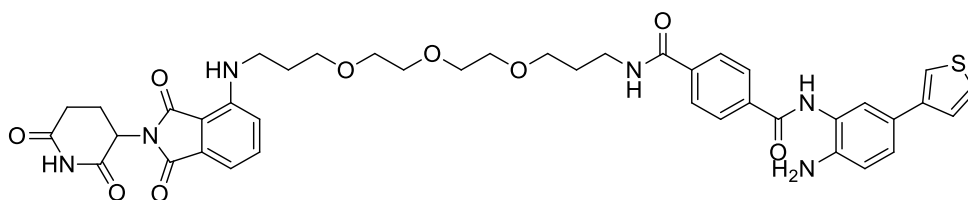
Intermediate **3** and **13** underwent an amide coupling reaction according to **method IB**, followed by Boc deprotection according to **method IV** to obtain the final compound **MA26** as yellow solid (yield: 35% over 2 steps). ^{1}H NMR (400 MHz, DMSO-d$_6$) δ 11.06 (s, 1H), 9.82 (s, 1H), 8.55 (t, J = 5.5 Hz, 1H), 8.06 (d, J = 8.2 Hz, 2H), 7.94 (d, J = 8.4 Hz, 2H), 7.60 – 7.48 (m, 4H), 7.40 (dt, J = 9.4, 4.7 Hz, 1H), 7.36 (dd, J = 8.3, 2.1 Hz, 1H), 7.08 (d, J = 8.6 Hz, 1H), 7.00 (d, J = 7.0 Hz, 1H), 6.81 (d, J = 8.3 Hz, 1H), 6.64 (t, J = 5.9 Hz, 1H), 5.03 (dd, J = 12.7, 5.5 Hz, 3H), 3.59 – 3.40 (m, 12H), 3.40 – 3.30 (m, 4H), 2.86 (ddd, J = 17.4, 14.1, 5.4 Hz, 1H), 2.62 – 2.50 (m, 2H), 2.07 – 1.96 (m, 1H), 1.85 – 1.70 (m, 4H). HRMS m/z: 819.279 [M + Na]$^+$; calculated C$_{41}$H$_{44}$N$_6$O$_9$SNa$^+$: 819.2788; HPLC: rt 10.23 min (purity 97.81%).

N^1-(6-((2-Amino-4-fluorophenyl)amino)-6-oxohexyl)-N^3-(3-(2-(2-(3-((2-(2,6-dioxopiperidin-3-yl)-1,3-dioxoisoindolin-4-yl)amino)propoxy)ethoxy)ethoxy)propyl)iso-phthalamide (MA27)
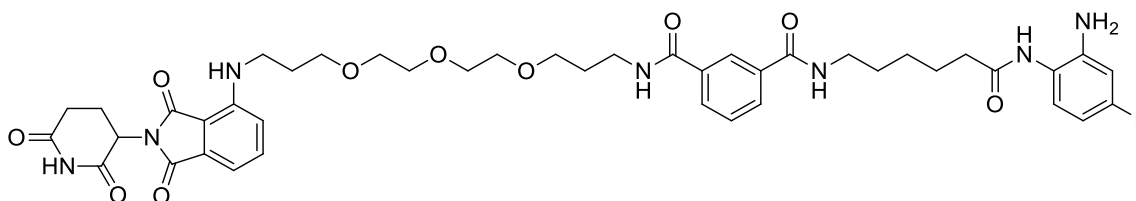
Intermediate **8** and **13** underwent an amide coupling reaction according to **method IB** to obtain the final compound **MA27** as yellow solid (yield: 50%).^{1}H NMR (400 MHz, DMSO-d$_6$) δ 11.05 (s, 1H), 8.98 (s, 1H), 8.51 (dt, J = 11.1, 5.6 Hz, 2H), 8.26 (s, 1H), 7.96 – 7.88 (m, 2H), 7.62 – 7.45 (m, 2H), 7.11 – 6.95 (m, 3H), 6.64 (t, J = 5.9 Hz, 1H), 6.46 (dd, J = 11.2, 2.9 Hz, 1H), 6.26 (td, J = 8.5, 2.9 Hz, 1H), 5.09 (s, 2H), 5.02 (dd, J = 12.8, 5.4 Hz, 1H), 3.60 – 3.40 (m, 11H), 3.39 – 3.29 (m, 4H), 3.27 – 3.20 (m, 2H), 2.86 (ddd, J = 17.4, 14.1, 5.5 Hz, 1H), 2.62 – 2.49 (m, 3H), 2.29 (t, J = 7.4 Hz, 2H), 2.07 – 1.92 (m, 1H), 1.85 – 1.69 (m, 4H), 1.58 (dq, J = 21.6, 7.4 Hz, 4H), 1.34 (dt, J = 9.7, 7.0 Hz, 2H). HRMS m/z: 884.3395 [M + K]$^+$; calculated C$_{43}$H$_{52}$N$_7$O$_{10}$FK$^+$: 884.3397; HPLC: rt 9.81 min (purity 96.01%).

N^1-(6-((2-Amino-5-(thiophen-2-yl)phenyl)amino)-6-oxohexyl)-N^3-(3-(2-(2-(3-((2-(2,6-dioxopiperidin-3-yl)-1,3-dioxoisoindolin-4-yl)amino)propoxy)ethoxy)ethoxy)propyl)-isophthalamide (MA28)
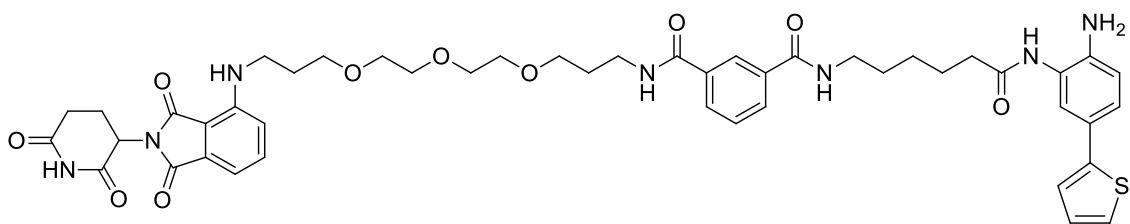
Intermediate **12** and **13** underwent an amide coupling reaction according to *method IB* to obtain the final compound **MA28** as yellow solid (yield: 30% after purification with preparative HPLC). ^{1}H NMR (400 MHz, DMSO-d6) δ 11.05 (s, 1H), 8.56 – 8.45 (m, 2H), 8.28 – 8.22 (m, 1H), 7.92 (t, *J* = 7.3 Hz, 2H), 7.60 – 7.37 (m, 5H), 7.22 – 7.13 (m, 1H), 7.14 – 6.91 (m, 4H), 6.72 (d, *J* = 8.3 Hz, 1H), 6.63 (t, *J* = 5.7 Hz, 1H), 5.14 – 4.90 (m, 3H), 3.58 – 3.38 (m, 12H), 3.38 – 3.32 (m, 4H), 2.92 – 2.77 (m, 2H), 2.62 – 2.49 (m, 2H), 2.41 – 2.27 (m, 2H), 2.10 – 1.93 (m, 2H), 1.88 – 1.68 (m, 4H), 1.68 – 1.44 (m, 4H), 1.45 – 1.29 (m, 2H). HRMS *m/z*: 932.363 [M + Na]$^+$; calculated $C_{47}H_{55}N_7O_{10}SNa^+$: 932.3629; HPLC: rt 10.38 min (purity 98.91%).

4-(Aminomethyl)-*N*-(2-aminophenyl)benzamide (16)
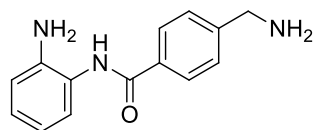
Intermediate **16** was synthesized by reacting the carboxylic acid intermediate **14** and *o*-phenylenediamine (**15**) according to *method IB*, followed by boc-deprotection according to *method IV*. ^{1}H NMR (400 MHz, DMSO-d6) δ 9.59 (s, 1H), 7.91 (d, *J* = 8.2 Hz, 2H), 7.44 (d, *J* = 8.3 Hz, 2H), 7.16 (dd, *J* = 7.8, 1.0 Hz, 1H), 6.95 (td, *J* = 8.0, 1.5 Hz, 1H), 6.77 (dd, *J* = 8.0, 1.4 Hz, 1H), 6.59 (td, *J* = 7.7, 1.4 Hz, 1H), 4.86 (s, 2H), 3.77 (s, 2H), 1.81 (s, 2H).

General procedure for the synthesis of intermediate 18a,b

The appropriate *N*-Boc-protected amino acid derivative **17a** or **17b** was reacted with intermediate **16** through an amide coupling according to *method IB*, followed by boc-deprotection according to *method IV* (Yield: 35 - 39% over 2 steps).

4-((7-Aminoheptanamido)methyl)-*N*-(2-aminophenyl)benzamide (18a)

49
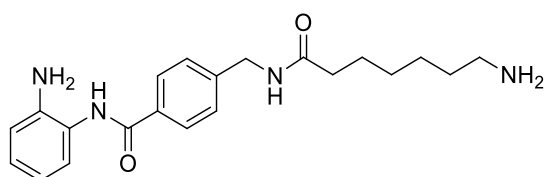
¹H NMR (400 MHz, DMSO-d₆) δ 9.59 (s, 1H), 8.35 (t, *J* = 5.9 Hz, 1H), 7.91 (d, *J* = 8.2 Hz, 2H), 7.34 (d, *J* = 8.2 Hz, 2H), 7.15 (d, *J* = 6.9 Hz, 1H), 7.00 – 6.91 (m, 1H), 6.76 (dd, *J* = 8.0, 1.3 Hz, 1H), 6.58 (td, *J* = 7.7, 1.4 Hz, 1H), 4.86 (s, 2H), 4.31 (d, *J* = 6.0 Hz, 2H), 2.54 – 2.50 (m, 2H, overlapped with DMSO), 2.14 (t, *J* = 7.4 Hz, 2H), 1.51 (dd, *J* = 14.0, 7.3 Hz, 2H), 1.37 – 1.17 (m, 8H). MS m/z: 369.42 [M+H]⁺.

4-((8-Aminooctanamido)methyl)-*N*-(2-aminophenyl)benzamide (18b)
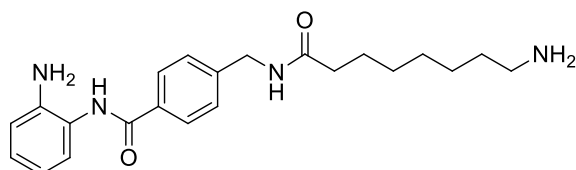
¹H NMR (400 MHz, DMSO-d₆) δ 9.59 (s, 1H), 8.36 (t, *J* = 5.6 Hz, 1H), 7.91 (d, *J* = 7.8 Hz, 2H), 7.34 (d, *J* = 8.0 Hz, 2H), 7.15 (d, *J* = 7.8 Hz, 1H), 6.95 (t, *J* = 7.1 Hz, 1H), 6.77 (d, *J* = 7.9 Hz, 1H), 6.58 (t, *J* = 7.4 Hz, 1H), 4.86 (s, 2H), 4.31 (d, *J* = 5.8 Hz, 2H), 2.91 – 2.80 (m, 2H), 2.14 (t, *J* = 7.3 Hz, 2H), 1.52 (s, 2H), 1.38 – 1.07 (m, 10H).

General procedure for the synthesis of compounds MA61 and MA64

The appropriate inhibitor-containing amine linker **18a** or **18b** was reacted with 1-adamantaneacetic acid (**19**) through the amide coupling according to ***method IB*** to afford the final compounds **MA64** and **MA61**, respectively as white solid (Yield: 37 - 40%).

4-((7-(2-(Adamantan-1-yl)acetamido)heptanamido)methyl)-*N*-(2-aminophenyl)benzamide (MA64)
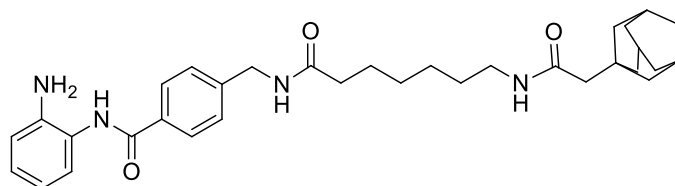
¹H NMR (400 MHz, DMSO-d₆) δ 9.59 (s, 1H), 8.35 (t, *J* = 5.9 Hz, 1H), 7.91 (d, *J* = 8.2 Hz, 2H), 7.60 (t, *J* = 5.5 Hz, 1H), 7.34 (d, *J* = 8.3 Hz, 2H), 7.15 (d, *J* = 7.4 Hz, 1H), 6.99 – 6.91 (m, 1H), 6.77 (dd, *J* = 8.0, 1.3 Hz, 1H), 6.58 (td, *J* = 7.7, 1.3 Hz, 1H), 4.86 (s, 2H), 4.31 (d, *J* = 5.9 Hz, 2H), 2.99 (dd, *J* = 12.6, 6.7 Hz, 2H), 2.14 (dd, *J* = 9.6, 5.2 Hz, 2H), 1.88 (s, 3H), 1.78 (s, 2H), 1.68 – 1.44 (m, 14H), 1.41 – 1.31 (m, 2H), 1.25 (s, 4H). HRMS *m/z*: 567.330 [M + Na]⁺; calculated C₃₃H₄₄N₄O₃Na⁺: 567.3311; HPLC: rt 10.42 min (purity 98.02%).

4-((8-(2-(Adamantan-1-yl)acetamido)octanamido)methyl)-*N*-(2-aminophenyl)benzamide (MA61)
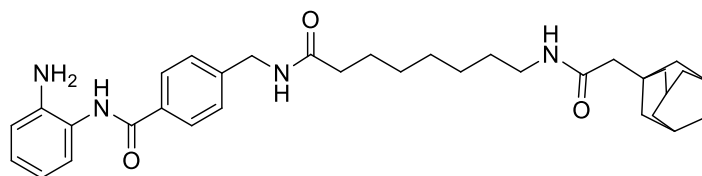
^{1}H NMR (400 MHz, DMSO-d$_6$) δ 9.69 (s, 1H), 8.35 (t, *J* = 6.0 Hz, 1H), 7.92 (d, *J* = 8.1 Hz, 2H), 7.60 (t, *J* = 5.5 Hz, 1H), 7.34 (d, *J* = 8.1 Hz, 2H), 7.18 (d, *J* = 7.4 Hz, 1H), 7.04 – 6.96 (m, 1H), 6.84 (d, *J* = 8.1 Hz, 1H), 6.68 (t, *J* = 7.3 Hz, 1H), 4.31 (d, *J* = 5.8 Hz, 2H), 2.99 (dd, *J* = 12.7, 6.5 Hz, 2H), 2.13 (t, *J* = 7.4 Hz, 2H), 1.88 (s, 2H), 1.81 – 1.71 (m, 3H), 1.68 – 1.42 (m, 14H), 1.41 – 1.30 (m, 2H), 1.24 (s, 6H). HRMS *m/z*: 559.365 [M + H]$^+$; calculated C$_{34}$H$_{47}$N$_4$O$_3{}^+$: 559.3648; HPLC: rt 14.04 min (purity 99.02%).

General procedure for the synthesis of intermediate 22a,b

The VHL ligand amine **20** was reacted with the mono-benzyl ester protected dicarboxylic acid **21a** or **21b** according to ***method IB***, followed by ester hydrolysis according to ***method II*** to afford intermediates **22a** and **22b**, respectively (Yield: 37 - 40% over 2 steps).

8-((((*S*)-1-((2*S*,4*R*)-4-Hydroxy-2-((4-(4-methylthiazol-5-yl)benzyl)carbamoyl)pyrrolidin-1-yl)-3,3-dimethyl-1-oxobutan-2-yl)amino)-8-oxooctanoic acid (22a)
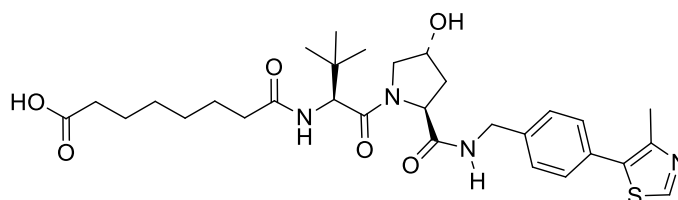
^{1}H NMR (400 MHz, DMSO-d$_6$) δ 8.97 (s, 1H), 8.52 (t, *J* = 6.0 Hz, 1H), 7.81 (d, *J* = 9.4 Hz, 1H), 7.44 – 7.26 (m, 4H), 4.52 (d, *J* = 9.4 Hz, 1H), 4.49 – 4.45 (m, 1H), 4.42 (dd, *J* = 14.7, 7.0 Hz, 2H), 4.31 (d, *J* = 21.7 Hz, 1H), 4.20 (dd, *J* = 15.9, 5.5 Hz, 1H), 3.65 (dt, *J* = 16.6, 8.2 Hz, 2H, overlapped with DMSO H$_2$O), 2.43 (s, 3H), 2.29 – 1.83 (m, 6H), 1.53 – 1.36 (m, 4H), 1.28 – 1.20 (m, 4H), 0.91 (s, 9H). MS m/z: 585.39 [M-H]$^-$.

9-((((*S*)-1-((2*S*,4*R*)-4-Hydroxy-2-((4-(4-methylthiazol-5-yl)benzyl)carbamoyl)pyrrolidin-1-yl)-3,3-dimethyl-1-oxobutan-2-yl)amino)-9-oxononanoic acid (22b)
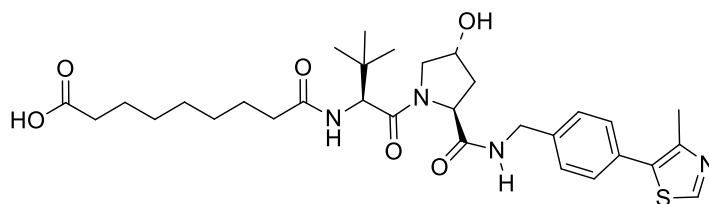
^{1}H NMR (400 MHz, DMSO-d$_6$) δ 11.92 (s, 1H), 8.96 (s, 1H), 8.52 (t, J = 6.0 Hz, 1H), 7.80 (d, J = 9.3 Hz, 1H), 7.38 (dt, J = 6.3, 5.3 Hz, 2H), 7.32 – 7.27 (m, 2H), 5.16 – 5.06 (m, 2H), 4.55 – 4.37 (m, 2H), 4.34 (s, 1H), 4.25 – 4.16 (m, 1H), 3.68 – 3.58 (m, 2H), 2.43 (s, 3H), 2.29 – 1.98 (m, 4H), 1.89 (ddd, J = 14.8, 8.5, 4.7 Hz, 1H), 1.48 (t, J = 16.0 Hz, 4H), 1.25 (d, J = 16.4 Hz, 7H), 0.91 (s, 9H). MS m/z: 599.44 [M-H]$^-$.

General procedure for synthesis of compounds MA65 and MA66

The appropriate inhibitor-containing carboxylic acid linker **22a** or **22b** was reacted with intermediate **16** through according to **_method IB_** to obtain the final compounds **MA65** and **MA66**, respectively as white solid (Yield: 35 - 38%).

N^1-(4-((2-Aminophenyl)carbamoyl)benzyl)-N^8-((S)-1-((2S,4R)-4-hydroxy-2-((4-(4-methyl -thiazol-5-yl)benzyl)carbamoyl)pyrrolidin-1-yl)-3,3-dimethyl-1-oxobutan-2-yl)octane- diamide (MA65)
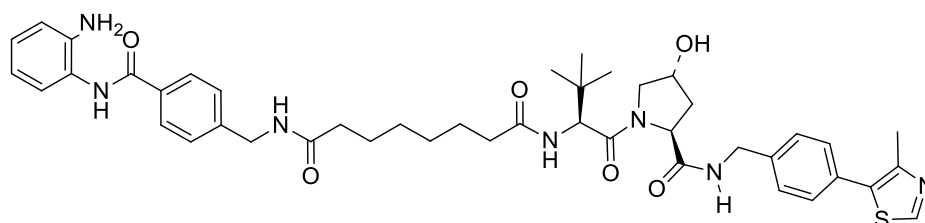
^{1}H NMR (400 MHz, DMSO-d$_6$) δ 9.59 (s, 1H), 8.96 (s, 1H), 8.53 (t, J = 6.0 Hz, 1H), 8.34 (t, J = 6.0 Hz, 1H), 7.91 (d, J = 8.2 Hz, 2H), 7.81 (d, J = 9.4 Hz, 1H), 7.44 – 7.29 (m, 6H), 7.15 (d, J = 6.9 Hz, 1H), 6.99 – 6.91 (m, 1H), 6.77 (dd, J = 8.0, 1.3 Hz, 1H), 6.63 – 6.54 (m, 1H), 5.10 (d, J = 3.6 Hz, 1H), 4.86 (s, 2H), 4.53 (d, J = 9.4 Hz, 1H), 4.45 – 4.37 (m, 2H), 4.31 (d, J = 6.0 Hz, 2H), 4.20 (dd, J = 15.8, 5.5 Hz, 1H), 3.68 – 3.57 (m, 2H), 2.43 (s, 3H), 2.28 – 2.19 (m, 1H), 2.16 – 2.10 (m, 2H), 2.04 – 1.95 (m, 1H), 1.89 (ddd, J = 12.9, 8.6, 4.6 Hz, 1H), 1.56 – 1.41 (m, 4H), 1.24 (t, J = 6.0 Hz, 6H), 0.91 (s, 9H). HRMS _m/z_: 810.4014 [M + H]$^+$; calculated C$_{44}$H$_{56}$N$_7$O$_6$S$^+$: 810.4013; HPLC: rt 12.71 min (purity 96.27%).

N^1-(4-((2-Aminophenyl)carbamoyl)benzyl)-N^9-((S)-1-((2S,4R)-4-hydroxy-2-((4-(4-methyl-thiazol-5-yl)benzyl)carbamoyl)pyrrolidin-1-yl)-3,3-dimethyl-1-oxobutan-2-yl)nonane-diamide (MA66)
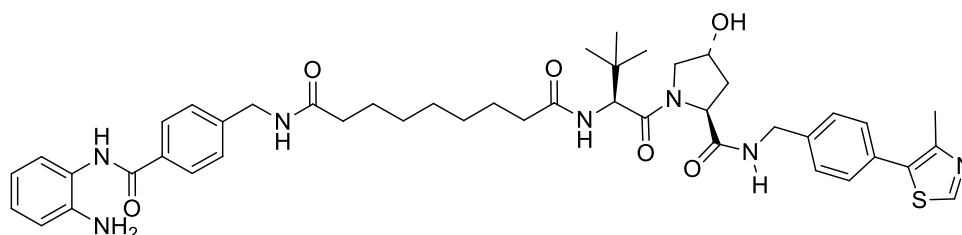
^{1}H NMR (400 MHz, DMSO-d$_6$) δ 9.59 (s, 1H), 8.96 (s, 1H), 8.53 (t, J = 6.0 Hz, 1H), 8.35 (t, J = 5.9 Hz, 1H), 7.91 (d, J = 8.0 Hz, 2H), 7.81 (d, J = 9.3 Hz, 1H), 7.49 – 7.30 (m, 6H), 7.15 (d, J = 7.6 Hz, 1H), 6.95 (t, J = 7.6 Hz, 1H), 6.77 (d, J = 8.0 Hz, 1H), 6.58 (t, J = 7.5 Hz, 1H), 5.09 (d, J = 3.5 Hz, 1H), 4.86 (s, 2H), 4.52 (t, J = 8.7 Hz, 1H), 4.45 – 4.36 (m, 2H), 4.31 (d, J = 5.9 Hz, 2H), 4.20 (dd, J = 15.9, 5.4 Hz, 1H), 3.67 – 3.60 (m, 2H), 2.43 (s, 3H), 2.29 – 2.19 (m, 1H), 2.16 – 2.08 (m, 2H), 2.07 – 2.03 (m, 1H), 1.89 (ddd, J = 12.8, 8.5, 4.5 Hz, 1H), 1.53 – 1.40 (m, 4H), 1.24 (s, br, 8H), 0.91 (s, 9H). HRMS m/z: 846.3984 [M + Na]$^+$; calculated C$_{45}$H$_{57}$N$_7$O$_6$SNa$^+$: 846.3989; HPLC: rt 12.62 min (purity 95.04%).

6-((2-(2,6-Dioxopiperidin-3-yl)-1,3-dioxoisoindolin-4-yl)amino)hexanoic acid (26)
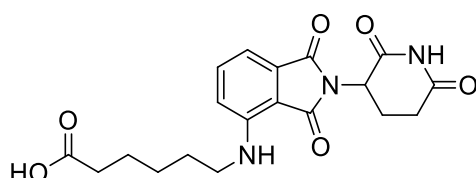
Intermediate **26** was synthesized by reacting the 4-fluorothalidomide (**23**) with *tert*-butyl 6-aminohexanoate (**24**) according to *method V*, followed by ester hydrolysis following *method III*. (Yellow solid yield: 40% over 2 steps). ^{1}H NMR (400 MHz, DMSO-d$_6$) δ 11.99 (s, br, 1H), 11.06 (s, 1H), 7.56 (dd, J = 8.6, 7.1 Hz, 1H), 7.07 (d, J = 8.6 Hz, 1H), 7.00 (d, J = 6.9 Hz, 1H), 6.51 (s, 1H), 5.03 (dd, J = 12.8, 5.4 Hz, 1H), 3.27 (t, J = 6.7 Hz, 2H), 2.91 – 2.79 (m, 1H), 2.53 (ddd, J = 9.9, 6.1, 1.7 Hz, 2H), 2.20 (t, J = 7.3 Hz, 2H), 2.07 – 1.95 (m, 1H), 1.61 – 1.48 (m, 4H), 1.39 – 1.28 (m, 2H).

6-(((S)-1-((2S,4R)-4-Hydroxy-2-((4-(4-methylthiazol-5-yl)benzyl)carbamoyl)pyrrolidin-1-yl)-3,3-dimethyl-1-oxobutan-2-yl)amino)-6-oxohexan-1-aminium 2,2,2-trifluoroacetate (30)
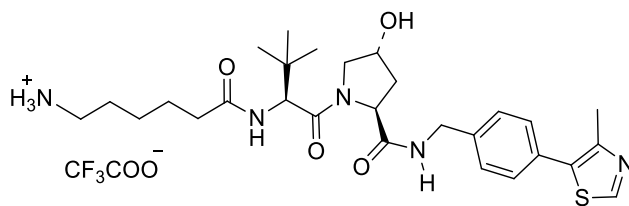
Intermediate **30** was synthesized by reacting the VHL ligand amine **20** with the *N*-Boc protected 6-aminohexanoic acid (**28**) according to **method IB,** followed by boc-deprotection according to **method IV**. (Yield: 55% over 2 steps). ^{1}H NMR (400 MHz, DMSO-d$_6$) δ 8.98 (s, 1H), 8.53 (t, *J* = 6.0 Hz, 1H), 7.84 (d, *J* = 9.3 Hz, 1H), 7.63 (s, 3H), 7.44 – 7.33 (m, 4H), 4.53 (d, *J* = 9.4 Hz, 1H), 4.47 – 4.37 (m, 2H), 4.34 (s, 1H), 4.20 (dd, *J* = 15.9, 5.4 Hz, 2H), 3.69 – 3.57 (m, 2H), 2.80 – 2.69 (m, 2H), 2.44 (s, 3H), 2.29 – 2.20 (m, 1H), 2.17 – 2.07 (m, 1H), 2.07 – 1.97 (m, 1H), 1.89 (ddd, *J* = 13.0, 8.7, 4.6 Hz, 1H), 1.56 – 1.41 (m, 4H), 1.32 – 1.19 (m, 2H), 0.91 (s, 9H). MS m/z: 544.31 [M+H]$^+$.

7-(((S)-1-((2S,4R)-4-Hydroxy-2-((4-(4-methylthiazol-5-yl)benzyl)carbamoyl)pyrrolidin-1-yl)-3,3-dimethyl-1-oxobutan-2-yl)amino)-7-oxoheptanoic acid (31)
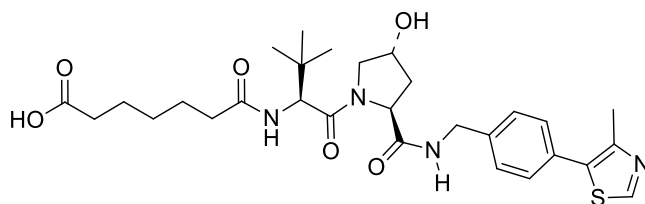
Intermediate **31** was prepared using the same protocol as described for intermediate **22a,b**. ^{1}H NMR (400 MHz, DMSO-d$_6$) δ 11.99 (s, 1H), 8.98 (s, 1H), 8.57 (t, *J* = 6.0 Hz, 1H), 7.82 (d, *J* = 9.3 Hz, 1H), 7.43 – 7.33 (m, 4H), 4.52 (d, *J* = 9.4 Hz, 1H), 4.41 (dd, *J* = 14.8, 7.0 Hz, 2H), 4.33 (s, 1H), 4.20 (dd, *J* = 15.9, 5.5 Hz, 1H), 3.67 – 3.62 (m, 2H), 2.43 (s, 3H), 2.28 – 2.19 (m, 1H), 2.18 – 2.12 (m, 2H), 2.10 (dd, *J* = 10.2, 3.9 Hz, 1H), 2.06 – 1.98 (m, 1H), 1.91 – 1.83 (m, 1H), 1.76 – 1.71 (m, 1H), 1.53 – 1.39 (m, 4H), 1.27 – 1.18 (m, 2H), 0.96 – 0.86 (m, 9H). MS m/z: 571.81 [M-H]$^-$.

6-(2-(Adamantan-1-yl)acetamido)hexanoic acid (34)
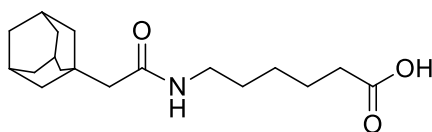
Intermediate **34** was prepared through the amide coupling reaction between 1-adamantaneacetic acid (**19**) and intermediate **32** according to **method IB**, followed by ester

hydrolysis using **method VIII** (Yield: 66%). [^1]H NMR (400 MHz, CDCl$_3$) δ 5.91 (s, 1H), 3.32 – 3.21 (m, 2H), 2.42 – 2.32 (m, 2H), 1.99 – 1.90 (m, 5H), 1.76 – 1.58 (m, 14H), 1.54 (dd, *J* = 14.6, 7.4 Hz, 2H), 1.45 – 1.35 (m, 2H). MS m/z: 330.78 [M+Na]$^+$.

5-(2-(Adamantan-1-yl)acetamido)pentan-1-aminium 2,2,2-trifluoroacetate (35)
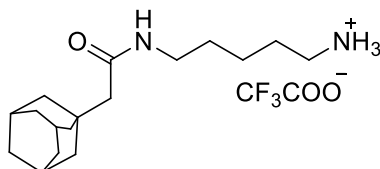
Intermediate **35** was prepared through the amide coupling reaction between 1-adamantaneacetic acid (**19**) and *N*-boc-1,5-diamino-pentane (**33**) according to **method IB**, followed by boc-deprotection using **method IV** (Yield: 60% over 2 steps). [^1]H NMR (400 MHz, CDCl$_3$) δ 7.94 (s, 1H), 6.56 – 6.62 (m, 3H), 3.21 (t, *J* = 10.7 Hz, 2H), 2.88 – 3.03 (m, 2H), 2.84 (s, 1H), 1.89 – 2.03 (m, 5H), 1.32 – 1.80 (m, 17H). MS m/z: 279.26 [M+H]$^+$.

Methyl 3-(3-bromopropoxy)benzoate (37)
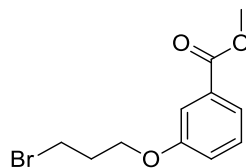
Intermediate **37** was prepared through the alkylation of intermediate **36** using 1,3-dibromopropane following **method VI**. [^1]H NMR (400 MHz, DMSO-d$_6$) δ 7.56 – 7.51 (m, 1H), 7.46 – 7.39 (m, 2H), 7.23 (ddd, *J* = 8.2, 2.7, 1.0 Hz, 1H), 4.12 (t, *J* = 6.0 Hz, 2H), 3.83 (s, 3H), 3.66 (t, *J* = 6.6 Hz, 2H), 2.24 (p, *J* = 6.3 Hz, 2H).

3-(3-(4-(((*tert*-Butoxycarbonyl)amino)methyl)phenoxy)propoxy)benzoic acid (39)
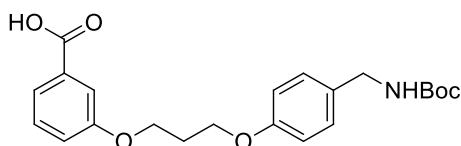
Intermediate **39** was synthesized through the alkylation reacting between intermediate **37** and **38** following **method VI**. (Yield: 40%). [^1]H NMR (400 MHz, DMSO-d$_6$) δ 7.49 – 7.40 (m, 2H), 7.27 (t, *J* = 5.9 Hz, 1H), 7.23 – 7.06 (m, 3H), 6.91 – 6.83 (m, 3H), 4.13 – 4.05 (m, 4H), 4.02 (d, *J* = 6.1 Hz, 2H), 2.14 (p, *J* = 6.3 Hz, 1H), 1.36 (s, 9H). MS m/z: 424.22 [M+Na]$^+$.

3-(3-(4-(Aminomethyl)phenoxy)propoxy)-*N*-(7-((benzyloxy)amino)-7-oxoheptyl)-benzamide (41)

Intermediate **41** was prepared through the amide coupling reaction between intermediates **39** and **40** according to *method IB*, followed by boc-deprotection using *method IV* (Yield: 51% over 2 steps). ^{1}H NMR (500 MHz, DMSO-d$_6$) δ 10.92 (s, 1H), 8.40 (t, *J* = 5.5 Hz, 1H), 8.04 (s, 3H), 7.46 – 7.26 (m, 9H), 7.08 (dd, *J* = 8.1, 1.7 Hz, 1H), 7.00 (d, *J* = 8.7 Hz, 2H), 4.76 (s, 2H), 4.16 (dd, *J* = 13.3, 6.3 Hz, 4H), 3.98 – 3.92 (m, 2H), 3.22 (dd, *J* = 12.9, 6.8 Hz, 2H), 2.18 (p, *J* = 6.2 Hz, 2H), 1.94 (t, *J* = 7.2 Hz, 2H), 1.56 – 1.40 (m, 4H), 1.34 – 1.18 (m, 4H). MS m/z: 534.67 [M+H]$^+$.

General procedure for the synthesis of compounds MA54 and MA57

The benzyl protected hydroxamic acid derivative **41** was reacted with the appropriate linker **26** or **34** through amide coupling according to *method IB*, followed by benzyl deprotection using *method VIII* to afford the final compounds **MA54** and **MA57,** respectively (Yield: 40 - 45%).

3-(3-(4-((6-((2-(2,6-Dioxopiperidin-3-yl)-1,3-dioxoisoindolin-4-yl)amino)hexanamido)-methyl)phenoxy)propoxy)-*N*-(7-(hydroxyamino)-7-oxoheptyl)benzamide (MA54)
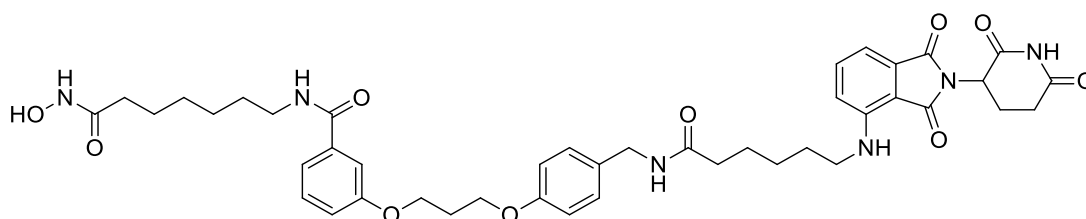
Yellow solid, ^{1}H NMR (400 MHz, DMSO-d$_6$) δ 11.06 (s, 1H), 10.30 (s, 1H), 8.70 – 8.54 (m, 1H), 8.44 – 8.34 (m, 1H), 8.18 (t, *J* = 5.7 Hz, 1H), 7.56 (dd, *J* = 8.4, 7.2 Hz, 1H), 7.41 – 7.29 (m, 3H), 7.13 (d, *J* = 8.7 Hz, 2H), 7.07 (d, *J* = 8.6 Hz, 2H), 7.00 (d, *J* = 6.9 Hz, 1H), 6.87 (d, *J* = 8.7 Hz, 2H), 6.50 (t, *J* = 5.9 Hz, 1H), 5.03 (dd, *J* = 12.9, 5.5 Hz, 1H), 4.22 – 4.03 (m, , 6H), 3.23 – 3.15 (m, 3H), 2.92 – 2.79 (m, 1H), 2.60 – 2.52 (m, 2H), 2.15 – 2.05 (m, 4H), 2.06 – 1.95 (m, 2H), 1.92 (t, *J* = 7.4 Hz, 2H), 1.63 – 1.51 (m, 4H), 1.51 – 1.39 (m, 4H), 1.35 – 1.19

(m, 6H). HRMS *m/z*: 835.3648 $[M + Na]^+$; calculated $C_{43}H_{52}N_6O_{10}Na^+$: 835.3643; HPLC: rt 10.17 min (purity 100.0%).

3-(3-(4-((6-(2-(Adamantan-1-yl)acetamido)hexanamido)methyl)phenoxy)propoxy)-*N*-(7-(hydroxyamino)-7-oxoheptyl)benzamide (MA57)
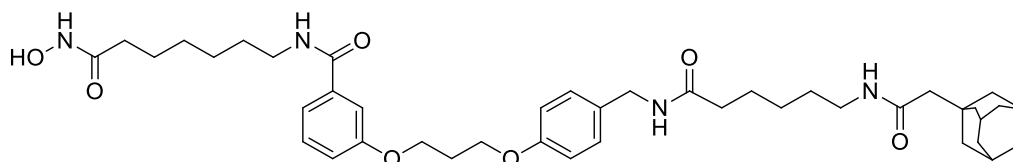
White solid, ^{1}H NMR (400 MHz, DMSO-d$_6$) δ 10.30 (s, 1H), 8.64 (s, 1H), 8.38 (dd, *J* = 9.5, 3.8 Hz, 1H), 8.17 (t, *J* = 5.8 Hz, 1H), 7.59 (t, *J* = 5.4 Hz, 1H), 7.39 (d, *J* = 7.5 Hz, 2H), 7.33 (t, *J* = 7.8 Hz, 1H), 7.13 (d, *J* = 8.6 Hz, 2H), 7.08 – 7.03 (m, 1H), 6.88 (d, *J* = 8.7 Hz, 2H), 4.21 – 4.04 (m, 6H), 3.21 (dd, *J* = 13.1, 6.7 Hz, 2H), 2.97 (dd, *J* = 12.7, 6.8 Hz, 2H), 2.19 – 2.12 (m, 2H), 2.07 (t, *J* = 7.4 Hz, 2H), 1.99 – 1.90 (m, 5H), 1.78 (s, 2H), 1.67 – 1.59 (m, 3H), 1.57 – 1.41 (m, 14H), 1.40 – 1.11 (m, 9H). HRMS *m/z*: 755.435 $[M + Na]^+$; calculated $C_{42}H_{60}N_4O_7Na^+$: 755.4359; HPLC: rt 11.40 min (purity 96.29%).

3-(2-Methoxy-2-oxoethoxy)benzoic acid (45)
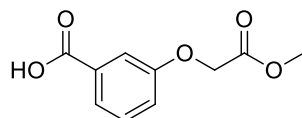
Intermediate **45** was prepared through the oxidation reaction of the benzaldehyde derivative **44** following *method IX*. Yield: 65%. ^{1}H NMR (400 MHz, DMSO-d$_6$) δ 7.57 – 7.52 (m, 1H), 7.43 – 7.35 (m, 2H), 7.18 (ddd, *J* = 8.3, 2.8, 1.0 Hz, 1H), 4.86 (s, 2H).

Methyl 2-(3-((7-((benzyloxy)amino)-7-oxoheptyl)carbamoyl)phenoxy)acetate (46)
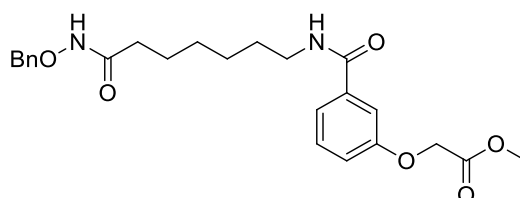
Intermediate **46** was prepared through the amide coupling reaction between intermediates **40** and **45** following *method IB*. ^{1}H NMR (400 MHz, DMSO-d$_6$) δ 10.90 (s, 1H), 8.39 (t, *J* = 5.5 Hz, 1H), 7.46 – 7.41 (m, 1H), 7.38 – 7.28 (m, 7H), 7.11 – 7.02 (m, 1H), 4.83 (s, 2H), 4.76 (s,

2H), 3.69 (s, 3H), 3.21 (dd, *J* = 13.0, 6.8 Hz, 2H), 1.93 (t, *J* = 7.3 Hz, 2H), 1.56 – 1.38 (m, 4H), 1.32 – 1.17 (m, 4H).

General procedure for the synthesis of compounds MA55 and MA56

The methyl ester **46** was hydrolyzed to the corresponding carboxylic acid according to *method II*, and the obtained acid was further reacted with the appropriate linker **27** or **35** through amide coupling according to *method IB*, followed by benzyl deprotection using *method VIII* to afford the final compounds **MA55** and **MA56,** respectively (Yield: 29-32% over 3 steps).

3-(2-((7-((2-(2,6-Dioxopiperidin-3-yl)-1,3-dioxoisoindolin-4-yl)amino)heptyl)amino)-2-oxoethoxy)-*N*-(7-(hydroxyamino)-7-oxoheptyl)benzamide (MA55)
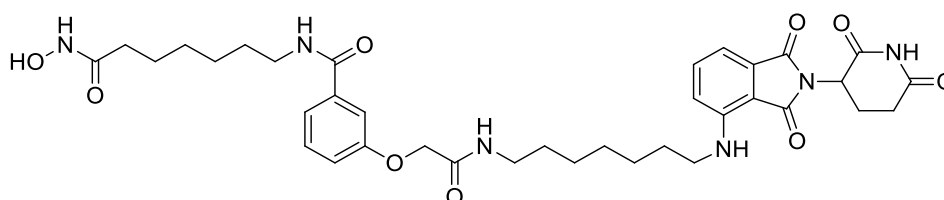
Yellow solid, ¹H NMR (400 MHz, DMSO-d₆) δ 11.06 (s, 1H), 10.30 (s, 1H), 8.62 (s, 1H), 8.38 (t, *J* = 5.5 Hz, 1H), 8.05 (t, *J* = 5.8 Hz, 1H), 7.56 (dd, *J* = 8.4, 7.2 Hz, 1H), 7.42 (dd, *J* = 8.3, 1.7 Hz, 2H), 7.34 (t, *J* = 7.9 Hz, 1H), 7.10 – 7.03 (m, 2H), 7.00 (d, *J* = 6.9 Hz, 1H), 6.50 (t, *J* = 5.9 Hz, 1H), 5.03 (dd, *J* = 12.8, 5.4 Hz, 1H), 4.49 (s, 2H), 3.28 – 3.17 (m, 4H), 3.10 (dd, *J* = 13.0, 6.7 Hz, 2H), 2.95 – 2.78 (m, 1H), 2.63 – 2.49 (m, 2H), 2.07 – 1.96 (m, 1H), 1.92 (t, *J* = 7.3 Hz, 2H), 1.58 – 1.36 (m, 8H), 1.33 – 1.13 (m, 10H). HRMS *m/z*: 729.322 [M + Na]⁺; calculated C₃₆H₄₆N₆O₉Na⁺: 729.32224; HPLC: rt 9.62 min (purity 99.85%).

3-(2-((5-(2-(Adamantan-1-yl)acetamido)pentyl)amino)-2-oxoethoxy)-*N*-(7-(hydroxyamino)-7-oxoheptyl)benzamide (MA56)
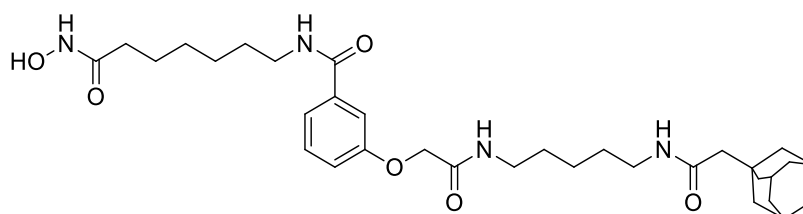
¹H NMR (400 MHz, DMSO-d₆) δ 10.30 (s, 1H), 8.62 (s, 1H), 8.39 (t, *J* = 5.5 Hz, 1H), 8.05 (t, *J* = 5.7 Hz, 1H), 7.59 (t, *J* = 5.4 Hz, 1H), 7.42 (d, *J* = 7.7 Hz, 2H), 7.35 (t, *J* = 7.9 Hz, 1H), 7.10 – 7.04 (m, 1H), 4.48 (s, 2H), 3.21 (dd, *J* = 13.1, 6.7 Hz, 2H), 3.09 (dd, *J* = 13.1, 6.7 Hz,

2H), 2.97 (dd, J = 12.7, 6.8 Hz, 2H), 1.97 – 1.84 (m, 5H), 1.77 (s, 2H), 1.62 (d, J = 11.8 Hz, 3H), 1.58 – 1.15 (m, 23H). HRMS *m/z*: 621.362 [M + Na]$^+$; calculated $C_{33}H_{50}N_4O_6Na^+$: 621.3628; HPLC: rt 9.91 min (purity 100.0%).

7-Amino-*N*-((tetrahydro-2H-pyran-2-yl)oxy)heptanamide (49)
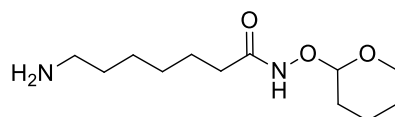
The fmoc-protected amino heptanoic acid (**47**) was reacted with the tetrahydropyran (THP) protected hydroxyl amine (**48**) according to *method IB*, followed by fmoc deprotection using *method X* to obtain intermediate **49**. (Yield: 31% over 2 steps).^{1}H NMR (400 MHz, CDCl$_3$) δ 7.02 (s, 1H), 4.93 (s, 2H), 4.02 – 3.82 (m, 2H), 2.12 (s, 2H), 1.89 – 1.73 (m, 4H), 1.71 – 1.61 (m, 4H), 1.60 – 1.52 (m, 3H), 1.49 – 1.41 (m, 2H), 1.39 – 1.28 (m, 5H). MS: 245.00 [M+H]$^+$.

3-(3-(4-(((((Benzyloxy)carbonyl)amino)methyl)phenoxy)propoxy)benzoic acid (51)
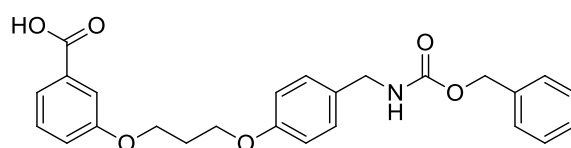
Intermediate **51** was synthesized through the alkylation reacting between intermediates **37** and **50** following *method VI*, followed by the hydrolysis of the methyl ester according to *method II*. (Yield: 45 over 2 steps %). ^{1}H NMR (400 MHz, DMSO-d$_6$) δ 7.71 (t, J = 5.9 Hz, 1H), 7.52 – 7.47 (m, 1H), 7.45 – 7.43 (m, 1H), 7.38 – 7.23 (m, 6H), 7.18 – 7.08 (m, 3H), 6.88 (d, J = 8.6 Hz, 2H), 5.01 (s, 2H), 4.15 (t, J = 6.2 Hz, 2H), 4.12 – 4.03 (m, 4H), 2.19 – 2.09 (m, 2H).

3-(3-(4-(Aminomethyl)phenoxy)propoxy)-*N*-(7-oxo-7-(((tetrahydro-2H-pyran-2-yl)oxy)amino)heptyl)benzamide (52)
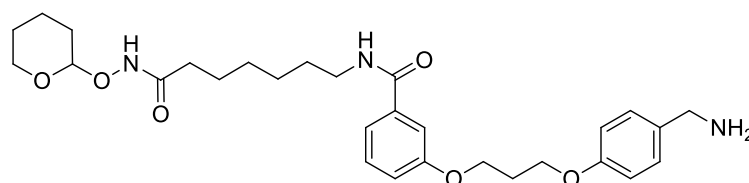
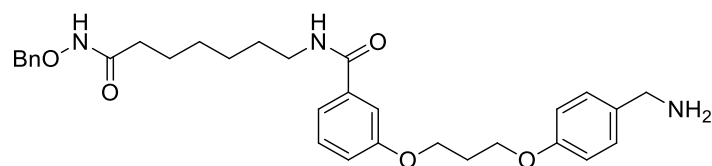Intermediate **52** was synthesized through the amide coupling reaction between intermediates **49** and **51** according to *method IB* followed by Cbz-deprotection according to *method VIII*. ^{1}H NMR (400 MHz, DMSO-d$_6$) δ 10.87 (s, 1H), 8.40 (t, J = 5.6 Hz, 1H), 7.74 (s, 2H), 7.45 – 7.29 (m, 5H), 7.14 – 7.04 (m, 1H), 6.97 (d, J = 8.7 Hz, 2H), 4.78 (s, 1H), 4.18 – 4.10 (m, 4H),

3.95 – 3.79 (m, 3H), 3.51 – 3.41 (m, 1H), 3.21 (dd, J = 13.1, 6.7 Hz, 2H), 2.23 – 2.11 (m, 2H), 1.96 (t, J = 7.3 Hz, 2H), 1.70 – 1.56 (m, 3H), 1.54 – 1.42 (m, 7H), 1.33 – 1.17 (m, 4H). MS: 528.61 [M+H]$^+$.

N1-((S)-1-((2S,4R)-4-Hydroxy-2-((4-(4-methylthiazol-5-yl)benzyl)carbamoyl)pyrrolidin-1-yl)-3,3-dimethyl-1-oxobutan-2-yl)-N^7-(4-(3-(3-((7-(hydroxyamino)-7-oxoheptyl)-carbamoyl)phenoxy)propoxy)benzyl)heptanediamide (MA58)
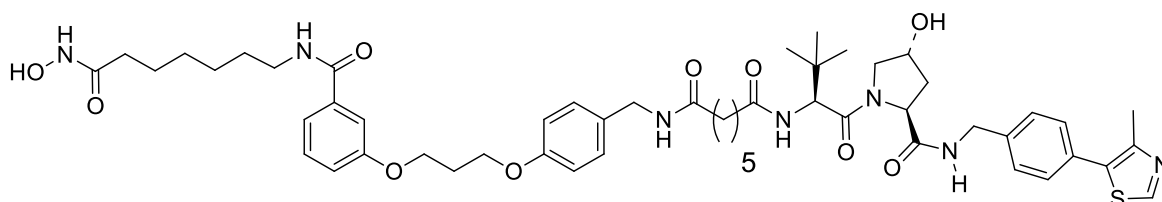
The THP-protected hydroxamic acid **52** was reacted with the VHL-carboxylic acid intermediate **31** according to ***method IB***, followed by THP-deprotection according to ***method VII*** to afford the final compound **MA58** as a white solid yield: 30% over 2 steps. ^{1}H NMR (400 MHz, DMSO-d$_6$) δ 10.30 (s, 1H), 8.96 (s, 1H), 8.61 (s, 1H), 8.53 (t, J = 6.0 Hz, 1H), 8.38 (t, J = 5.5 Hz, 1H), 8.16 (t, J = 5.8 Hz, 1H), 7.81 (d, J = 9.3 Hz, 1H), 7.49 – 7.26 (m, 7H), 7.13 (d, J = 8.7 Hz, 2H), 7.09 – 7.03 (m, 1H), 6.92 – 6.83 (m, 2H), 5.10 (s, 1H), 4.51 (t, J = 9.5 Hz, 1H), 4.48 – 4.36 (m, 2H), 4.33 (s, 1H), 4.24 – 4.17 (m, 1H), 4.16 – 4.12 (m, 3H), 4.10 (t, J = 6.2 Hz, 2H), 3.71 – 3.57 (m, 2H), 3.20 (dt, J = 14.9, 7.5 Hz, 2H), 2.43 (s, 3H), 2.29 – 1.96 (m, 8H), 1.94 – 1.83 (m, 3H), 1.59 – 1.35 (m, 8H), 1.32 – 1.12 (m, 6H), 0.92 (s, 9H). HRMS m/z: 1020.4875 [M + Na]$^+$; calculated C$_{53}$H$_{71}$N$_7$O$_{10}$SNa$^+$: 621.4881; HPLC: rt 10.60 min (purity 98.0%).

3-(2-(Benzyloxy)-2-oxoethoxy)benzoic acid (55)
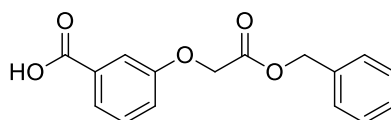
Intermediate **55** was prepared through the oxidation reaction of the benzaldehyde derivative **54** following ***method IX***. (Yield: 62%). ^{1}H NMR (400 MHz, DMSO-d$_6$) δ 7.57 – 7.53 (m, 1H), 7.44 – 7.41 (m, 1H), 7.37 – 7.31 (m, 6H), 7.17 (ddd, J = 8.2, 2.7, 0.9 Hz, 1H), 5.20 (s, 2H), 4.93 (s, 2H). MS m/z: 285.14 [M-H]$^-$.

2-(3-((7-Oxo-7-((((tetrahydro-2H-pyran-2-yl)oxy)amino)heptyl)carbamoyl)-phenoxy)-acetic acid (56)
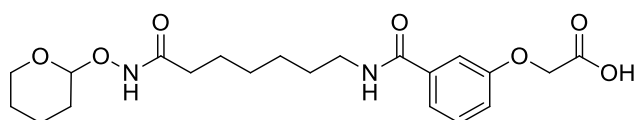
Intermediate **56** was synthesized through the amide coupling reaction between intermediates **49** and **55** according to *method IB*, followed by benzyl ester hydrolysis according to *method VIII*. (Yield: 50% over 2 steps). ^{1}H NMR (400 MHz, DMSO-d$_6$) δ 12.99 (s, 1H), 10.86 (s, 1H), 8.39 (t, *J* = 5.5 Hz, 1H), 7.42 (d, *J* = 7.8 Hz, 1H), 7.37 – 7.28 (m, 2H), 7.06 – 7.01 (m, 1H), 4.78 (s, 1H), 4.71 (s, 2H), 3.88 (dd, *J* = 18.9, 7.4 Hz, 1H), 3.51 – 3.42 (m, 1H), 3.26 – 3.17 (m, 2H), 2.02 – 1.90 (m, 2H), 1.69 – 1.54 (m, 3H), 1.47 – 1.40 (m, 7H), 1.27 – 1.20 (m, 4H). MS m/z: 421.19 [M-H]$^-$.

(2*S*,4*R*)-4-Hydroxy-1-((*S*)-2-(6-(2-(3-((7-(hydroxyamino)-7-oxoheptyl)carbamoyl)phenoxy)acetamido)hexanamido)-3,3-dimethylbutanoyl)-*N*-(4-(4-methylthiazol-5-yl)benzyl)pyrrolidine-2-carboxamide (MA59)
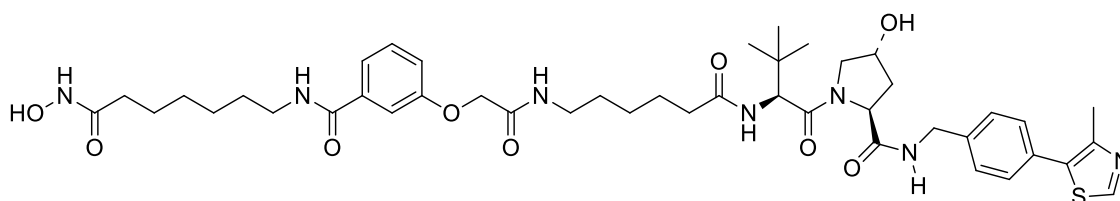
The THP-protected hydroxamic acid **56** was reacted with the VHL-linker **30** according to *method IB*, followed by THP-deprotection according to *method VII* to afford the final compound **MA59** as a white solid yield: 30% over 2 steps. ^{1}H NMR (400 MHz, DMSO-d$_6$) δ 10.30 (s, 1H), 8.96 (s, 1H), 8.62 (s, 1H), 8.53 (t, *J* = 5.9 Hz, 1H), 8.39 (t, *J* = 5.5 Hz, 1H), 8.05 (t, *J* = 5.7 Hz, 1H), 7.81 (d, *J* = 9.3 Hz, 1H), 7.49 – 7.28 (m, 7H), 7.10 – 7.04 (m, 1H), 5.10 (s, 1H), 4.52 (d, *J* = 9.4 Hz, 1H), 4.50 – 4.36 (m, 4H), 4.33 (s, 1H), 4.20 (dd, *J* = 16.0, 5.5 Hz, 1H), 3.69 – 3.58 (m, 2H), 3.21 (dd, *J* = 13.1, 6.6 Hz, 2H), 3.09 (dd, *J* = 13.1, 6.6 Hz, 2H), 2.43 (s, 3H), 2.28 – 2.17 (m, 1H), 2.14 – 2.05 (m, 1H), 2.05 – 1.97 (m, 1H), 1.96 – 1.84 (m, 3H), 1.57 – 1.35 (m, 8H), 1.32 – 1.16 (m, 6H), 0.91 (s, 9H). HRMS *m/z*: 886.414 [M + Na]$^+$; calculated C$_{44}$H$_{61}$N$_7$O$_9$SNa$^+$: 886.4149; HPLC: rt 9.12 min (purity 95.47%).

4.3.4. Experimental part of biological testing

4.3.4.1. In vitro HDAC Inhibition Assay

Recombinant human proteins HDAC1, HDAC2, and HDAC3/NCOR1 were purchased from ENZO Life Sciences AG (Lausen, CH). Recombinant human HDAC8 was produced by Romier et al. (IGBMC, Univ. Strasbourg), as described in [49]. The in vitro testing on

HDAC1-3, 6, and 8 was performed out by Matthes Zessin and Patrik Zeyen, Institute of Pharmacy, Martin-Luther-University Halle-Wittenberg, Halle, Germany as described in [177, 180]. The measurements were performed in assay buffer (50 mM Hepes, 150 mM NaCl, 5 mM MgCl$_2$, 1 mM TCEP, and 0.2 mg/mL BSA, pH 7.4 adjusted with NaOH) at 37 ˚C. All compounds at different concentrations were incubated with 10 nM HDAC1, 3 nM HDAC2, or 3 nM HDAC3 (final concentration) for at least 5 min. The reaction was first started with the addition of a fluorogenic peptide substrate (20 μM final concentration) and incubated for 30 min for HDAC2 and HDAC3 and 90 min for HDAC1. The reaction was then stopped with a solution of 1 mg/mL trypsin and 20 μM SAHA in 1 mM HCl and incubated for 1 h at 37 ˚C. The fluorescence intensity was measured with an Envision 2104 Multilabel Plate Reader (PerkinElmer, Waltham, MA, USA) with an excitation wavelength of 380 ± 8 nm and an emission wavelength of 430 ± 8 nm. The measured fluorescence intensities were normalized with uninhibited reaction as 100% and the reaction without enzyme as 0%. A nonlinear regression analysis was done to determine the IC$_{50}$ value. The enzyme inhibition of HDAC8 was determined by using a reported homogenous fluorescence assay 2 [180]. The enzyme was incubated for 90 min at 37 ˚C, with the fluorogenic substrate ZMAL (Z(Ac)Lys-AMC) in a concentration of 10.5 μM and increasing concentrations of tested compounds. Fluorescence intensity was reported at an excitation wavelength of 390 nm and an emission wavelength of 460 nm in a microtiter plate reader (BMG Polarstar).

4.3.4.2. Cellular testing

In order to determine the HDAC degradation activity of the designed degraders in PSN1 and HCT116 cancer cell lines, the following procedure was performed. PSN1 and HCT116 cell lines were seeded on cell culture dishes, which were subsequently treated by different 1 μ concentration of the degraders for a 6 h (**Figure 21**). The treated cells were harvested to get their proteins in the IP buffer, and the corresponding protein level was determined by Western blot. The data was provided by the group of Prof. Günter Schneider, Technical University of Munich, Munich, Germany.
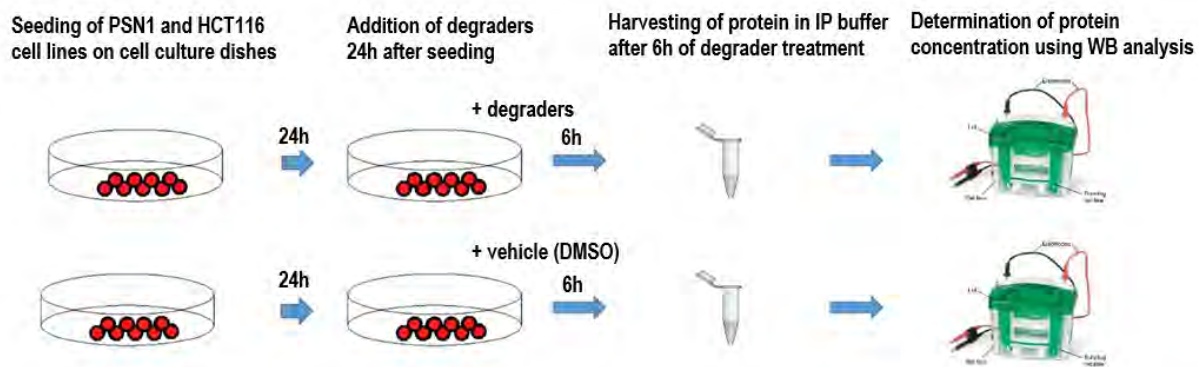
Figure 21: Cellular screening to determine the HDAC degradation potency of the synthesized degraders. The figure was provided by Prof. Günter Schneider, Technical University of Munich, Munich, Germany.

5. Discussion of the results

5.1. Identification of novel class I HDAC inhibitors and their biological evaluation against different cancer cell lines

The results obtained in studies **3.1 - 3.3** will be briefly discussed in this part.

The main objective of these studies was the design and synthesis of selective class I HDAC inhibitors and the evaluation of their biological activity against different acute myeloid leukemia and pancreatic cancer cell lines.

5.1.1. Identification of novel class I HDAC inhibitors with potential anti-leukemic activity

Due to the good class I HDAC selectivity profile of the 2-aminobenzamides exemplified by entinostat (MS-275), we selected this chemotype for further structural optimization to develop novel selective HDAC inhibitors with enhanced in vitro activity and stronger anti-leukemic effects. First, the middle phenyl ring (the linker part) of entinostat was replaced by more polar pyrimidine or pyrazine rings to improve the solubility properties of the final compounds (**Figure 22**). The capping groups are known to interact with amino acid residues at the rim of the binding channel; therefore, different aromatic and heterocyclic scaffolds were used as capping groups instead of the pyridine ring of entionstat (**Figure 22**). The carbamate connecting unit of entinostat was also replaced by a piperazine scaffold. In addition, another idea was to target the foot pocket of class I HDACs through the substitution of the 2-aminobenzamide scaffold at position 5 with bulky aromatic substituents and at position 4 with small atoms or groups to investigate the effect on individual isoform selectivity (**Figure 22**).
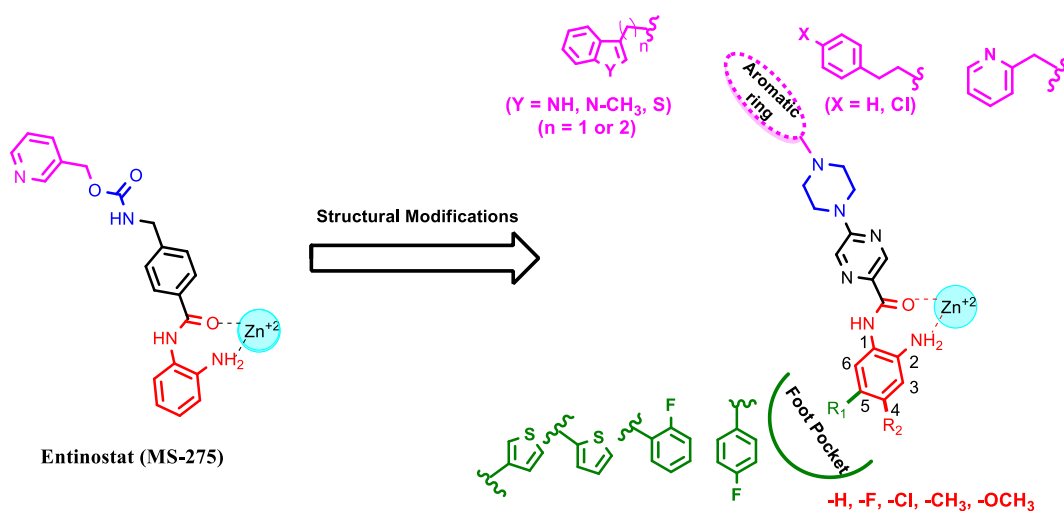
Figure 22: Design strategy and structural modifications of entinostat (MS-275) to develop novel class I HDAC inhibitors.

The newly synthesized compounds as well as some reported HDAC1-3 inhibitors were tested for their inhibitory activity against human class I HDACs (HDAC1, 2, 3, and 8). In general, the inhibitors containing pyrazine linker showed good HDAC1-3 inhibitory activity, while the replacement of the pyrazine ring with the pyrimidine moiety resulted in a significant decrease in the inhibitory activity. Moreover, it was observed that the compounds containing the 3-indolyl or *N*-methyl-3-indolyl capping groups exhibited better HDAC1-3 inhibitory activity compared with other aromatic capping groups. For instance, compound **19f** (**Figure 23**) exhibited potent inhibitory activity against HDAC1, 2, and 3 in the submicromolar range and was more potent than the reference inhibitors entinostat, mocetinostat, and tacedinaline. As expected, compounds bearing a 2-thienyl substituent at position 5 of the 2-aminobenzamide scaffold exhibited high selectivity for HDAC1 and 2 over HDAC3 as exemplified by **21a** (**Figure 23**). Interestingly, removal of the 3-indolyl capping group of compound **21a** resulted in a significant increase in the inhibitory activity for HDAC1, 2 while maintaining the selectivity over HDAC3 as exemplified by compound **29b** which showed an IC_{50} value of 70 nM against HDAC1. Docking studies were in line with the in vitro testing and could explain why the inhibitors with bulky aromatic substituents on the ZBG were not tolerated in the foot pocket of HDAC3. On the other hand, substitution of the 2-aminobenzamide at position 4 with a fluorine atom resulted in a slight increase in the HDAC3 selectivity over HDAC1 and 2, as in the case of compound **23a**.

Based on the aforementioned in vitro activity and low cellular toxicity against human embryonic kidney cells (HEK293), compounds **19f**, **21a**, and **29b** were selected for further

biological characterization against MV4-11, MOLM-13, and HEL leukemic cell lines. The cellular results demonstrated that compound **19f** was the most potent inhibitor among the tested compounds. Compound **19f** was at least 4-fold more potent than entinostat (**MS-275**) for apoptosis induction in MV4-11 and MOLM-13 cell lines (**Figure 24**). Moreover, it showed potent growth inhibitory activity against both cell lines with IC_{50} values in the submicromolar range (**Figure 24**). In addition, immunoblot analyses illustrated that compound **19f** triggered the accumulation of acetylated histone H3 in both MV4-11 and MOLM-13 cells in a dose-dependent manner and more potently than **MS-275** did (**Figure 24**).

19f

IC_{50} (HDAC1) **0.13 ± 0.01** µM
IC_{50} (HDAC2) **0.28 ± 0.01** µM
IC_{50} (HDAC3) **0.31 ± 0.01** µM
IC_{50} (HDAC8)   0% at 1 µM

21a

IC_{50} (HDAC1) **0.26 ± 0.01** µM
IC_{50} (HDAC2) 2.47 ± 0.01 µM
IC_{50} (HDAC3)   0% at 1 µM
IC_{50} (HDAC8)   0% at 1 µM

29b

IC_{50} (HDAC1) **0.07 ± 0.01** µM
IC_{50} (HDAC2) 0.26 ± 0.01 µM
IC_{50} (HDAC3) 6.1 ± 0.01 µM
IC_{50} (HDAC8)   n.d

23a

IC_{50} (HDAC1) 3.3 ± 0.2 µM
IC_{50} (HDAC2) 2.2 ± 0.2 µM
IC_{50} (HDAC3) **0.4 ± 0.01** µM
IC_{50} (HDAC8)   0% at 1 µM
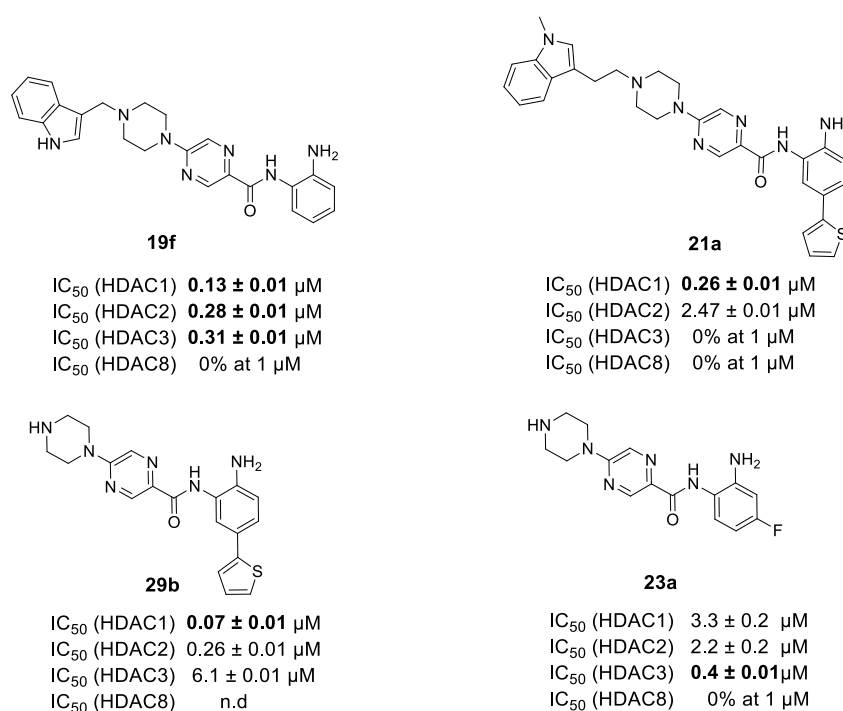
Figure 23: The most promising class I HDAC inhibitors and their inhibitory activity towards different HDAC isoforms.
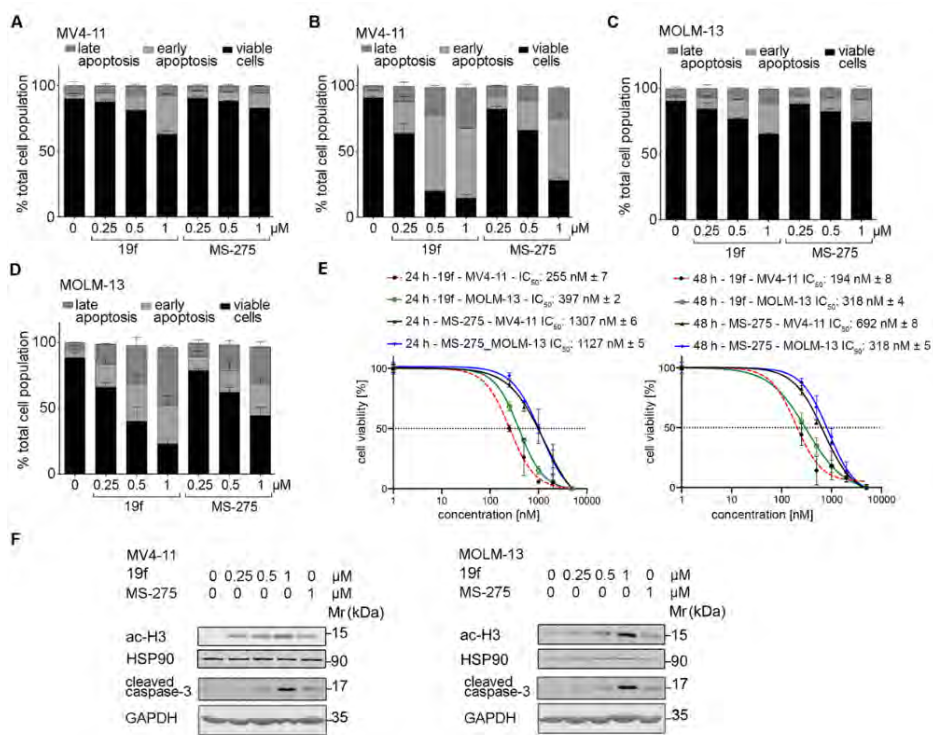
Figure 24: Pro-apoptotic effects of 19f and MS-275 in MV4-11 and MOLM-13 cells. (**A, B**) MV4-11 cells were treated with 0.25, 0.5, 1 µM 19f or MS-275 for 24 h (**A**) or 48 h (**B**) and analyzed for annexin-V/PI by flow cytometry. (**C, D**) The same experiments were conducted with MOLM-13 cells. (**E**) IC_{50} values were determined for **19f**. (**F**) Immunoblot was done with the stated antibodies and lysates of MV4-11 and MOLM-13 cells that were incubated with the HDACi for 24 h. Cells were incubated with 0.25, 0.5, 1 µM **19f**, or 1 µM MS-275.

5.1.2. Identification of novel class I HDAC inhibitors and their biological evaluation against pancreatic cancer

Based on the promising results of the HDAC inhibitors developed in the previous study, we aimed in this study to develop new analogs with an improved selectivity profile and to further explore the biological activity of the synthesized HDAC inhibitors against pancreatic cancer cell lines. Since the previously described derivatives **19f** and **29b** (**Figure 23**) displayed the most promising in vitro results, we decided to pursue further studies on these compounds. First, the *N*-methylated piperazine derivative of **29b**, compound **10** (**Figure 25**), was additionally synthesized to assess the effect of this substitution on the inhibitory potency and selectivity profile. Interestingly, this compound showed the highest inhibitory activity against

HDAC1 (IC_{50} HDAC1 = 40 nM) among all herein synthesized benzamide derivatives with improved selectivity for HDAC1 over HDAC2. As expected, it also showed no significant inhibition of HDAC3.

Compound **10** together with compounds **19f** and **29b** were additionally tested against murine pancreatic ductal adenocarcinoma (PDAC) cell lines F2612 and F5061. In this study, HDAC2 or HDAC3 were genetically knocked out from the tested cell lines, as indicated in **Figure 26**. Compounds **19f** and **29b** showed good activity with IC_{50} values in the low micromolar to submicromolar range, while the reference inhibitor entinostat (MS-275) displayed comparatively weak inhibition. On the other hand, the highly potent HDAC1 inhibitor **10** was less active with an IC_{50} value above 5 µM.

Only small changes in the IC_{50} values were observed when comparing HDAC2-proficient and deficient F2612 cells. However, when comparing the IC_{50} values of HDAC3-proficient and deficient F5061 cells, a shift towards a higher IC_{50} value was observed in the HDAC3-deficient cells suggesting that the sensitivity of the tested cell lines towards these derivatives might be driven by HDAC3.

10

IC_{50} (HDAC1) **0.04 ± 0.01** µM
IC_{50} (HDAC2) 0.79 ± 0.02 µM
IC_{50} (HDAC3)   6% at 1 µM
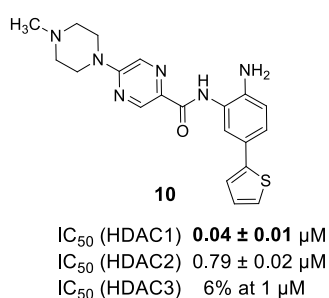
Figure 25: The chemical structure of compound 10 and its inhibitory activity against HDAC 1, 2, and 3.

Dose-response of 19f
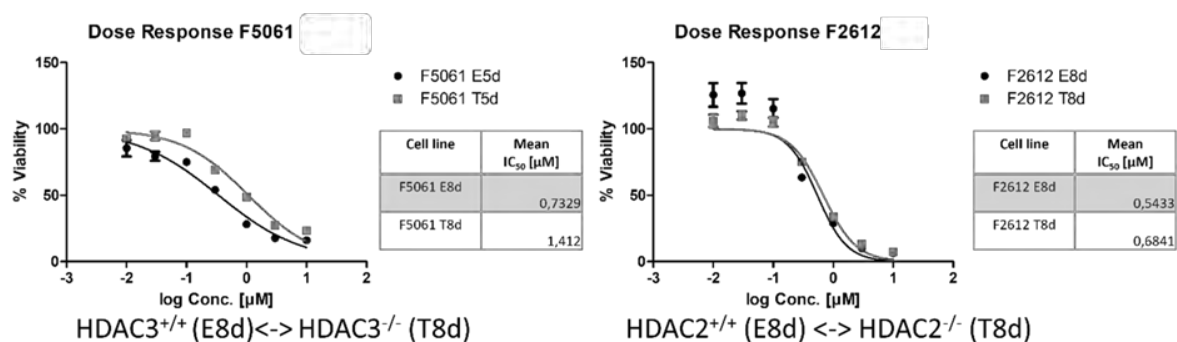
Dose-response of 29b
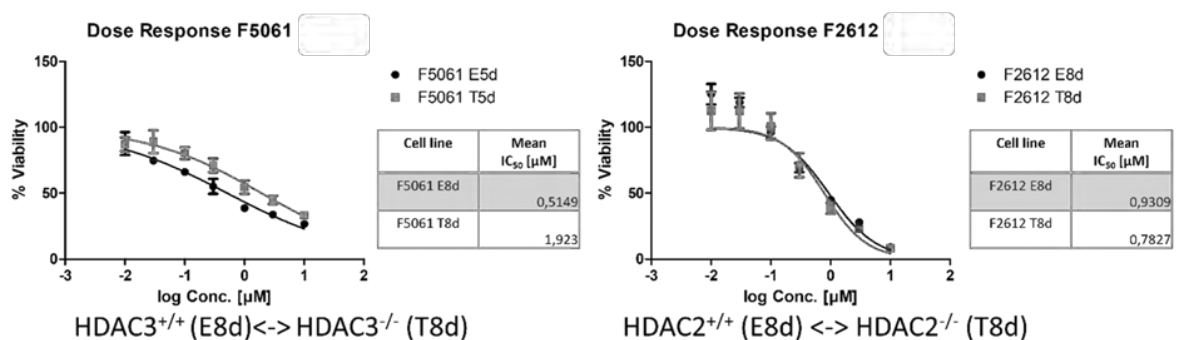
Figure 26: Dose-response curves of HDAC2-proficient/deficient F2612 and HDAC3-proficient/deficient F5061 (PDAC) cell lines treated with compounds 19f and 29b.

5.1.3. Using computational approaches to predict the selectivity profile of the developed class I HDAC inhibitors

The main focus of study **3.3** was to test whether binding free energy (BFE) calculations can be utilized to provide predictive models that can be used for the development of novel HDAC inhibitors bearing 2-aminobenzamide scaffolds. In this regard, the thirty 2-aminobenzamide derivatives that were developed in studies **3.1** and **3.2** were chosen as a training set in this study. For HDAC2, the crystal structure PDB ID: 4LY1 was selected to dock the training set as it showed the best re- and cross-docking results. In the case of HDAC1, the crystal structure (PDB ID: 4BKX) in complex with the docked original ligand from the crystal structure of HDAC2 (PDB ID: 4LY1) was used, while for HDAC3, the crystal structure PDB ID: 4A69 in complex with the docked ligand BG45 was used. The docking studies for each isoform revealed that the docking poses correspond to the observed binding modes of similar inhibitors. However, the docking scores showed a low correlation with the experimental

70

activities. Therefore, the selected docking poses were rescored by performing binding free-energy calculations using different setups. Several models were built, and three models (one best model per HDAC subtype, **Figure 27**) were selected based on the highest observed R^2 values. In addition, these models showed good results in terms of leave-one-out cross-validation and root-mean-square error (RMSE). The three selected models were further validated against an external test set of newly synthesized compounds, and the models were indeed capable of correctly classifying them into actives and inactives. Thus, the developed BFE models are cost-effective methods that can help to reduce the time required to prioritize compounds for further studies.
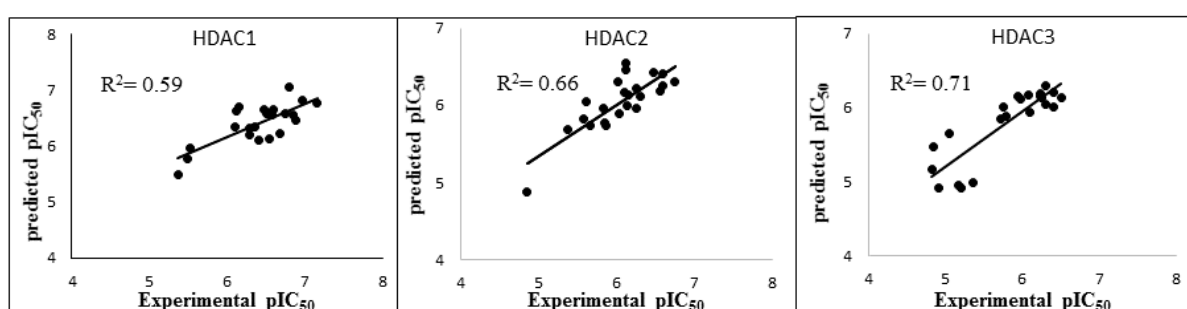
Figure 27: The correlation plots of the best binding free-energy models showing correlation between the predicted data and experimental data for each HDAC subtype.

5.2. Development of bioreductive prodrugs of class I HDAC inhibitors and their biological evaluation against acute myeloid leukemia

The results obtained in study **3.4** will be briefly discussed in this part.

The promising in vitro and cellular results of the HDAC inhibitors developed in studies **3.1** and **3.2** encouraged us to apply the prodrug concept to the developed inhibitors to enhance their targeted-tissue specificity and to develop novel candidates with improved therapeutic indices and lower toxicity profiles. In this study, a series of novel bioreducible prodrugs for class I HDAC inhibitors were designed and synthesized by masking the aminobenzamide moiety (ZBG) of different HDAC inhibitors using nitroarylmethyl moieties (**Figure 28**). As expected, the developed prodrugs showed very weak HDAC in vitro inhibitory activity compared to their parent inhibitors. The activation of the bioreducible prodrugs depends mainly on the presence of high levels of nitroreductase enzymes in hypoxic tumor cells, which catalyze the reduction of the nitro group of various nitroaromatic substrates to the

corresponding nitroso intermediate which is further reduced to the hydroxylamine derivative, followed by self-immolation and fragmentation to release the active inhibitor, as shown in **Figure 28**. Therefore, the prodrugs and the corresponding parent inhibitors were further tested against wild-type and nitroreductase (NTR) transfected-THP1 leukemic cells. The cellular testing revealed that compounds **5** and **6** (**Figure 29**) were activated by the NTR prodrug system and exhibited potent activity against NTR-THP1 leukemic cells. Interestingly, both prodrugs contain 2-nitroimidazoles as the masking group, which is in agreement with previous findings on the better activation of prodrugs containing nitro-heterocyclic masking groups [181]. Moreover, both prodrugs showed cellular effects in the range of their parent HDAC inhibitor, indicating almost full conversion. Compound **6** showed the highest cellular activity in leukemic cells (GI_{50} = 77 nM) and exhibited a moderate selectivity for NTR-THP1 cells over wild-type THP1-cells. The activation of the prodrug by NTR was also confirmed by LC-MS analysis which showed the release of the parent inhibitor after incubation of prodrug **6** with *E. coli* NTR. Compound **6**, hence, represents a promising lead structure which can be further optimized to achieve prodrugs with higher cellular potency and improved selectivity window.
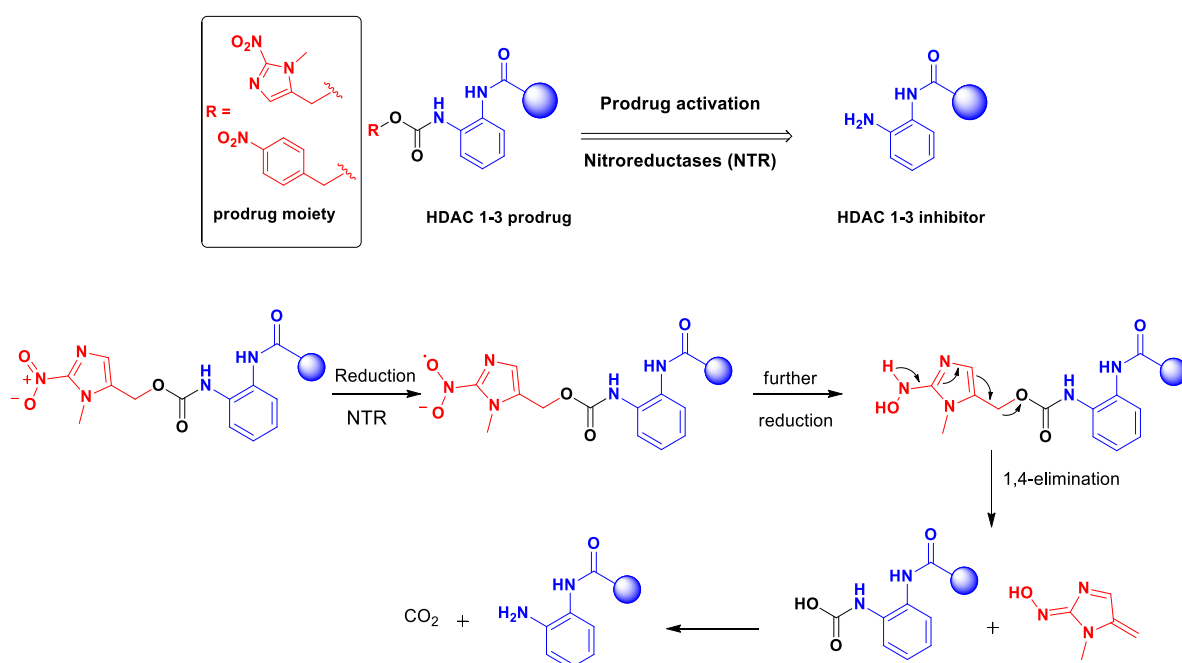
Figure 28: The rationale for the design of novel class I HDAC prodrugs based on different 2-aminobenzamides and the postulated schematic pathway of HDAC inhibitor release.

72

5

GI$_{50}$ (THP1) = 12.3 ± 0.7 µM
GI$_{50}$ (THP1-NTR) = 1.84 ± 0.4 µM
Selectivity window = 6.7

6

GI$_{50}$ (THP1) = 914 ± 357 nM
GI$_{50}$ (THP1-NTR) = 77 ± 4 nM
Selectivity window = 11.8
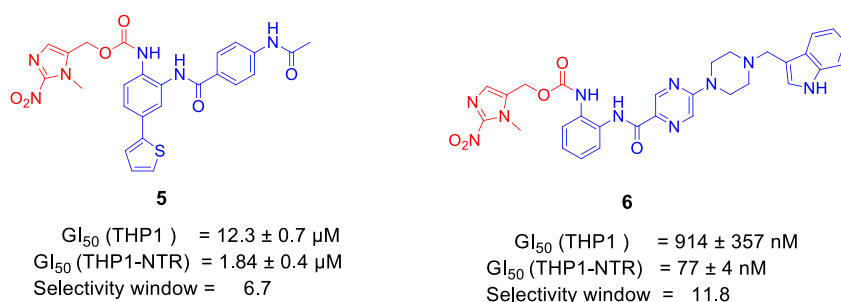
Figure 29: GI$_{50}$ values of the most active prodrugs against wild-type and transfected NTR-THP1 leukemic cells and their selectivity windows.

5.3. Design and synthesis of novel HDACs degraders

The results obtained in study **3.5**, as well as the unpublished results in **Chapter 4** will be briefly discussed in this part.

The main focus of study **3.5** was to design and synthesize selective class I HDAC degraders. In this regard, the selective HDAC3 inhibitor (**BRD3308**) was used as the POI warhead and was connected to the CRBN E3 ligase ligand (pomalidomide) using a polyethylene glycol (PEG) linker, as shown in **Figure 30**. Compound **5** was developed and tested against class I HDAC isoforms. It displayed weak inhibitory activity against HDAC1 and 2, while it showed moderate activity against HDAC3 (IC$_{50}$ = 3.4 µM) (**Figure 30**). Compound **5** was further tested against the pancreatic cancer cell line (PSN1) and the human colorectal carcinoma cell line (HCT116). The cellular levels of HDAC1-3 in the tested cells were analyzed by Western blot. Unfortunately, compound **5** did not show degradation for the targeted HDACs. Since the E3 ligase recognition motif as well as the linker composition and length can influence the formation of the ternary complex and hence, the activity of PROTACs, further structural modifications were performed as described in the unpublished results (**Chapter 4, Figure 12**) in an attempt to achieve the desired degradation activity. These modifications included using different HDAC inhibitors belonging to different classes (2-aminobenzamides, hydroxamic acid-based scaffolds). Moreover, the VHL ligand was used instead of pomalidomide. The concept of hydrophobic tag-based degradation was also applied by replacing the E3 ligase ligands with the adamantly moiety which has been frequently used for the design of hydrophobic tag-based degraders. Additionally, different linkers were used for the design of the planned degraders. The newly synthesized compounds were subjected to in vitro testing against different HDAC isoforms in addition to different cancer cell lines. Although most of

them showed good in vitro inhibitory activity against different HDAC isoforms, they showed weak to moderate cellular activity against PSN1 and HCT116 cell lines. In addition, no degradation was observed for HDAC1-3 in the tested cancer cell lines. It is worth mentioning that most of the developed SAHA-based bifunctional molecules showed potent inhibitory activity against HDAC6 in the low nanomolar range. Therefore, it is planned to perform further phenotypic screenings of the SAHA-based PROTACs against other cancer cell lines.

(A)

BRD 3308

IC$_{50}$ (HDAC1) 1.08 µM
IC$_{50}$ (HDAC2) 1.15 µM
IC$_{50}$ (HDAC3) 0.064 µM

(B)

Pomalidomide

(C)

Compound 5

IC$_{50}$ (HDAC1) 18.0 µM
IC$_{50}$ (HDAC2) 14.0 µM
IC$_{50}$ (HDAC3) 3.4 µM
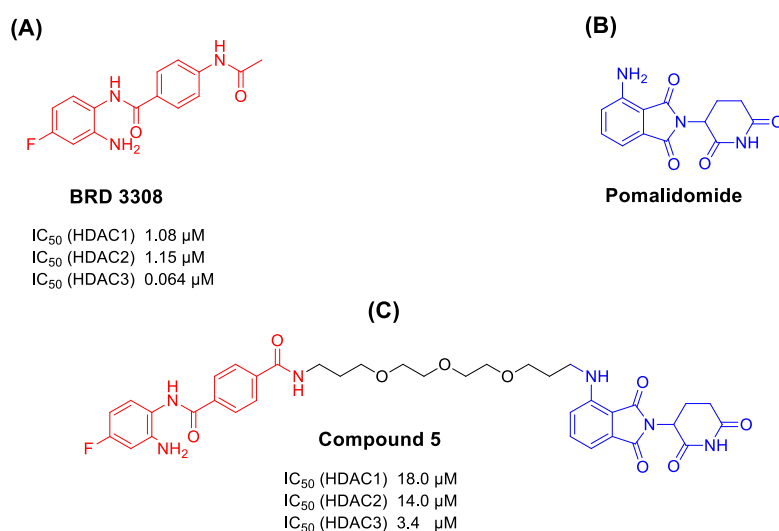
Figure 30: Design of HDAC-PROTACs. (A) Example of HDAC3 inhibitor. **(B)** Pomalidomide as an example of CRBN E3 ligase ligand. **(C)** Designed HDAC-PROTAC. IC$_{50}$ values obtained in the in vitro assay against HDAC1-3 are listed.

5.4. HDAC inhibitors as antischistosomal agents

Study **3.6** will be briefly discussed in this part.

The main objective of the review article in study **3.6** was to collect and discuss the latest advances in the development of inhibitors for *Schistosoma mansoni* histone deacetylases, with a particular focus on *sm*HDAC8 which has been recently identified as a potential therapeutic target for schistosomiasis. As previously mentioned, cancer cells and parasites are quite similar in some aspects, such as reproductive activity, high metabolic rates, and their ability to survive within the host immune system. Following that, the "piggyback" approach as an attractive strategy to repurpose the approved anticancer HDAC inhibitors as potential

antischistosomal agents has been discussed. Then, we discussed the structural similarities and differences between the crystal structures of *sm*HDAC8 and the human orthologue and accordingly, the possibility of designing HDAC8 inhibitors with improved selectivity for the parasitic HDAC8 to reduce the potential for toxicity. Several *sm*HDAC8 inhibitors have been reviewed in this study, and some of them exhibited a preference for *sm*HDAC8 over human HDAC8. The majority of the reported *sm*HDAC8 inhibitors are hydroxamates which showed potent HDAC8 inhibitory activity and some of them demonstrated phenotypic effects against different stages of the Schistosoma's life cycle (compounds **1-13**, **Figure 31**). Other *sm*HDAC8 inhibitors containing different ZBGs have been reported; however, they showed reduced *sm*HDAC8 inhibitory activity compared to the hydroxamic acid-based inhibitors.

1 (J1038)

IC$_{50}$ (smHDAC8) = 1.48 μM
IC$_{50}$ (hHDAC8) = 0.97 μM
IC$_{50}$ (hHDAC1) = 27.48 μM
IC$_{50}$ (hHDAC6) = 3.56 μM

2 (J1075)

IC$_{50}$ (smHDAC8) = 4.3 μM
IC$_{50}$ (hHDAC8) = 3.1 μM
IC$_{50}$ (hHDAC1) = 11.6 μM
IC$_{50}$ (hHDAC6) = 1.9 μM
at 50 μM = 100 % reduction of
viability and pairing (3days)

3

IC$_{50}$ (smHDAC8) = 0.44 μM
IC$_{50}$ (hHDAC8) = 0.47 μM
IC$_{50}$ (hHDAC1) = 20.2 μM
IC$_{50}$ (hHDAC6) = 8.2 μM
EC$_{50}$ (Larval stage) = 6.5 μM

4

IC$_{50}$ (smHDAC8) = 0.18 μM
IC$_{50}$ (hHDAC8) = 0.18 μM
IC$_{50}$ (hHDAC1) = 7.7 μM
IC$_{50}$ (hHDAC6) = 3.2 μM
EC$_{50}$ (Larval stage) = 11.8 μM

5 (TH31)

IC$_{50}$ (smHDAC8) = 0.47μM
IC$_{50}$ (hHDAC8) = 0.58 μM
IC$_{50}$ (hHDAC1) = 33.6 μM
IC$_{50}$ (hHDAC6) = 3.0 μM

6 (TH65)

IC$_{50}$ (smHDAC8) = 0.075 μM
IC$_{50}$ (hHDAC8) = 0.026 μM
IC$_{50}$ (hHDAC1) = 6.3 μM
IC$_{50}$ (hHDAC6) = 0.4 μM
at 20 μM = 100 % reduction of
viability (2 days), 90% of pairing
(5 days)

7

IC$_{50}$ (smHDAC8) = 0.092 μM
IC$_{50}$ (hHDAC8) = 0.14 μM
IC$_{50}$ (hHDAC1) = 2.08 μM
IC$_{50}$ (hHDAC6) = 0.6 μM

8

IC$_{50}$ (smHDAC8) = 0.27 μM
IC$_{50}$ (hHDAC8) = 0.32 μM
IC$_{50}$ (hHDAC1) = 18.51 μM
IC$_{50}$ (hHDAC6) = 0.29 μM
EC$_{50}$ (Larval stage) = 3.5 μM

9

IC$_{50}$ (smHDAC8) = 0.40 μM
IC$_{50}$ (hHDAC8) = 0.63 μM
IC$_{50}$ (hHDAC1) = 47.5% at 200 μM
IC$_{50}$ (hHDAC6) = 5.12 μM

10

IC$_{50}$ (smHDAC8) = 0.75 μM
IC$_{50}$ (hHDAC8) = 1.31 μM
IC$_{50}$ (hHDAC1) =15.3% at 200 μM
IC$_{50}$ (hHDAC6) = 7.11 μM

11

IC$_{50}$ (smHDAC8) = 1.02 μM
IC$_{50}$ (hHDAC8) = 2.11 μM
IC$_{50}$ (hHDAC1) = 3.61 μM
at 50 μM > 40 % reduction
of viability

12

IC$_{50}$ (smHDAC8) = 4.44 μM
IC$_{50}$ (hHDAC8) = 12.43 μM
IC$_{50}$ (hHDAC1) = 8.1% at 10 μM
IC$_{50}$ (hHDAC6) = 42.50 μM

13

IC$_{50}$ (smHDAC8)= 0.50 μM
IC$_{50}$ (hHDAC8) = 2.2 μM
IC$_{50}$ (hHDAC1) = 11% at 5 μM
IC$_{50}$ (hHDAC6) = - 1.5 μM at 5 μM

Figure 31: Examples of reported hydroxamic acid-based *sm*HDAC8 inhibitors. IC$_{50}$ values are cited for inhibition of the recombinant enzyme, EC$_{50}$ values refer to viability testing on schistosomula.

6. General Conclusion and Perspectives

Histone deacetylases (HDACs) constitute promising therapeutic targets for cancer and other diseases, including neurodegenerative disorders, inflammatory diseases, and human parasitic infections. This work focused mainly on HDAC1-3, members of class I HDACs which have been associated with various solid and hematological malignancies. In the present work, different medicinal chemistry approaches were applied to develop and optimize novel HDAC1-3 modulators and assess their potential as anticancer agents.

Although the active sites of HDAC1, 2, and 3 isoforms share high structural similarity, rendering the design of selective class I HDAC isoform challenging, we tried in the present work to exploit the small structural differences especially in the foot pocket region of HDAC3 compared to HDAC1 and 2 to achieve the desired HDAC isoform selectivity. In this regards, novel class I HDAC inhibitors were designed and synthesized based on different structural modifications of the general pharmacophore of previously reported HDAC inhibitors. Several compounds showed potent in vitro inhibitory activity against HDAC1, 2, and 3. Additionally, some of the developed compounds were found to have higher potencies and better HDAC-isoform selectivity profiles than the known class I HDAC inhibitors entinostat, mocetinostat, and tacedinaline. It was observed that the substitution of the 2-aminobenzamide scaffold (ZBG) with small substituents such as the fluoro atom resulted in a slight increase of HDAC3 selectivity over HDAC1 and 2. Furthermore, substitution of the 2-aminobenzamide scaffold with bulkier aryl substituents such as 2-thienyl or phenyl moieties resulted in improved selectivity for HDAC1 and 2 over HDAC3. Although some compounds showed a slight preference for HDAC1 over HDAC2, no significant selectivity between both isoforms was obtained due to their high sequence homology. An alternative approach that could be utilized to achieve the desired selectivity is the application of targeted protein degradation (TPD) concept to the most promising inhibitors in this study. Compared to conventional inhibition, TPD has a unique mechanism of action that can result in enhancing the selectivity among closely related protein [182]. Additionally, the HDAC inhibitory activity of the newly synthesized inhibitors could be measured using a cell-based assay to have an idea about the cellular HDAC inhibitory potency and selectivity of the developed compounds.

Our computational modeling studies could explain the enhanced in vitro HDAC selectivity of the developed inhibitors for HDAC1, 2 over HDAC3. Additionally, generated binding free-energy (BFE) QSAR models were found to show a good correlation with the experimentally determined inhibitory activity as well as good predictive power. The reliability and predictive accuracy of these models have already been evaluated on an external test set of newly

synthesized inhibitors. Hence, further structural optimization studies can be guided by the developed models in order to reduce the time required to prioritize compounds.

Some of the newly synthesized compounds were tested against the pancreatic ductal adenocarcinoma (PDAC) cell line, and two compounds showed good cellular activity in the submicromolar range and were more potent than the reference inhibitor entinostat. Moreover, we identified one compound that was more potent than entinostat in inducing apoptosis in a variety of acute myeloid leukemia cell lines (AML), including MV4-11 cells which also express FLT3-ITD. Since the combined pharmacological inhibition of HDACs and FLT3-ITD was shown to synergistically induce apoptosis in AML, we are planning in future work to develop novel FLT3 inhibitors and PROTACs. These will be analyzed in addition to the herein described HDAC inhibitors for their individual and combined cellular and molecular effects against AML cells. These studies might pave the way for the development of innovative and rationally designed combination therapies for the treatment of AML.

In this work we also designed and synthesized novel class I HDAC bioreductive prodrugs by masking the 2-aminobenzamide group of the developed HDAC inhibitors as well as other reported inhibitors using 4-nitrobenzyl and 2-nitroimidazolyl carbamates. As expected, the developed prodrugs showed a very weak HDAC inhibitory activity compared to their parent inhibitors. Among the synthesized compounds, two nitroimidazole-based prodrugs were best activated in the nitroreductase (NTR) transfected-THP1 leukemic cells, where they showed potent cellular activity. The activation of the prodrugs by NTR was also confirmed by LC-MS analysis which showed the release of the parent inhibitor after incubating the most active prodrug with *E. coli* NTR. The most active prodrugs showed cellular effects in the range of their parent HDAC inhibitor, indicating almost full conversion. The most promising compound in this series showed potent cellular activity against leukemic cells in the submicromolar range and exhibited a moderate selectivity for the NTR-transfected THP1 cells over the wild-type THP1 cells. In general, this study can be considered as a proof of concept that the masked-aminobenzamide derivatives could be used to design class I HDAC inhibitors-based prodrugs. However, further biological investigations are necessary to better understand why the prodrugs are still showing some cytotoxic activity against the wild-type THP1 cell line. The developed prodrugs in this study might be additionally tested against solid tumors which exhibit hypoxic conditions. The most promising prodrug in this study could be used as a good starting point for further optimization to increase potency and

enhance the selectivity profile. In this regards, other nitro-heterocyclic masking groups could be tried in future work.

Targeted protein degradation technique was applied in the current work to design degraders for class I HDACs. In total, 14 different heterobifunctional molecules were synthesized by combining several reported HDAC inhibitors with different E3 ligase ligands or the hydrophobic adamantyl moiety using different linkers. Some compounds exhibited good in vitro HDAC inhibitory activity, but with no notable degradation of the targeted HDAC isoforms in the tested cancer cells. In the current work, only the pomalidomide and the VHL ligand were utilized for the design of PROTACs. In future work, other CRBN-E3 ligands could be used instead of pomalidomide. For example, the pomalidomide moiety could be replaced by the more stable lenalidomide analogue, phenyl glutarimide derivatives, or the achiral phenyl dihydrouracil. The latter has been very recently reported to avoid the problem of racemization associated with traditional CRBN-E3 ligase ligands, which usually results in low E3-ligase binding activity and consequently the reduced potency of several PROTACs [183]. The linker design is also another important element that should be taken into consideration for future work. In the current work, only flexible alkyl linkers were used for the design of PROTACs. Recent studies have shown that flexible alkyl linkers might have undesirable physicochemical properties and poor aqueous solubility [184]. The use of more rigid linkers and incorporation of cyclic scaffolds in the design of PROTACs are alternative strategies that could be applied to improve the aqueous solubility and physicochemical properties of our PROTACs and possibly optimize their degradation potency. Triazole, piperidine, and piperazine motifs are representative examples of cyclic scaffolds that could be used in future work. Several studies have recently reported the significance of replacing the amide functionality in the alkyl linkers with the triazole motif in the design of HDAC PROTACs [105, 185, 186]. Another important aspect is the proper choice of exit vector in the E3 ligase ligand for the attachment of linkers. For example, the VHL ligand has several exit vectors other than the acetyl amide position that was used in this study [173]. Changing the attachment point of the linker might help to achieve target degradation by better enabling the ternary complex formation. Finally, the most promising HDAC1-3 inhibitors developed in the current work could be used as HDAC warheads for the development of novel class I HDAC PROTACs. Since all the previously-mentioned factors contribute to the formation of the ternary complex; they should all be systematically explored to assess their effects on the degradation of the targeted HDACs.

In the current work, we have discussed the recent advances in the design and development of inhibitors for *sm*HDAC8 which has been recently identified as a potential therapeutic target for schistosomiasis. Several hydroxamic acid-based inhibitors have exhibited a preference for *sm*HDAC8 over human HDAC8, in addition to phenotypic effects against different stages of the schistosome's life cycle. Unfortunately, several compounds with good enzymatic inhibition and selectivity profiles showed no effect on the parasite, which might be due to poor bioavailability. Additionally, little is known about the stability of HDAC inhibitors in animal models of schistosomiasis. The majority of the studies assessing the potential of HDAC inhibitors for the treatment of schistosomiasis worked with cultured schistosomes. Testing of HDAC inhibitors in animal models of schistosomiasis could provide new insights concerning the activity of HDAC inhibitors against schistosomes.

The reduced efficacy and the emergence of resistance against the conventional antimalarial treatments (artemisinin-based combination therapies) indicate the importance of providing new antimalarial agents with novel mechanisms of action that could potentially avoid or delay the rapid emergence of resistance [187]. Since several antimalarial therapies involve a combination of drugs with different mechanisms of action to enhance their therapeutic efficacy and overcome resistance, another future starting point could be the design of novel dual-targeting molecules by fusing different HDAC inhibitor motifs with Plasmodium falciparum dihydrofolate reductase (*Pf*DHFR) inhibitor scaffolds. Both *Pf*DHFR and *Pf*HDACs are considered key enzymes essential for the survival of different stages of the protozoan lifecycle and the regeneration of folic acid which is essential for DNA synthesis [188, 189]. The designed compounds will be tested against wild and mutant strains of different *Plasmodium* species. In addition, these compounds will be tested against human embryonic kidney cells (HEK293) to determine their cytotoxicity against human cells. We believe that dual inhibition of both targets in *P. falciparum* will be a novel strategy that would maximize the chance of finding new lead compounds for developing the next generation of antimalarial drugs. In addition, this strategy could provide new compounds to serve as novel leads for other parasitic diseases.

7. References

1. Delcuve, G. P.; Rastegar, M.; Davie, J. R. Epigenetic control. *J Cell Physiol* **2009**, *219* (2), 243-250. DOI: 10.1002/jcp.21678.

2. Gibney, E. R.; Nolan, C. M. Epigenetics and gene expression. *Heredity (Edinb)* **2010**, *105* (1), 4-13. DOI: 10.1038/hdy.2010.54.

3. Handy, D. E.; Castro, R.; Loscalzo, J. Epigenetic modifications: basic mechanisms and role in cardiovascular disease. *Circulation* **2011**, *123* (19), 2145-2156. DOI: 10.1161/CIRCULATIONAHA.110.956839.

4. Moore, L. D.; Le, T.; Fan, G. DNA methylation and its basic function. *Neuropsychopharmacology* **2013**, *38* (1), 23-38. DOI: 10.1038/npp.2012.112.

5. Bannister, A. J.; Kouzarides, T. Regulation of chromatin by histone modifications. *Cell Res* **2011**, *21* (3), 381-395. DOI: 10.1038/cr.2011.22.

6. Portela, A.; Esteller, M. Epigenetic modifications and human disease. *Nat Biotechnol* **2010**, *28* (10), 1057-1068. DOI: 10.1038/nbt.1685.

7. Ganesan, A.; Arimondo, P. B.; Rots, M. G.; Jeronimo, C.; Berdasco, M. The timeline of epigenetic drug discovery: from reality to dreams. *Clin Epigenetics* **2019**, *11* (1), 174. DOI: 10.1186/s13148-019-0776-0.

8. Ramazi, S.; Allahverdi, A.; Zahiri, J. Evaluation of post-translational modifications in histone proteins: A review on histone modification defects in developmental and neurological disorders. *J Biosci* **2020**, *45*, 1-29. DOI: 10.1007/s12038-020-00099-2.

9. Prajapati, H. K.; Ocampo, J.; Clark, D. J. Interplay among ATP-Dependent Chromatin Remodelers Determines Chromatin Organisation in Yeast. *Biology-Basel* **2020**, *9* (8), 190. DOI: 10.3390/biology9080190.

10. Ghoneim, M.; Fuchs, H. A.; Musselman, C. A. Histone Tail Conformations: A Fuzzy Affair with DNA. *Trends Biochem Sci* **2021**, *46* (7), 564-578. DOI: 10.1016/j.tibs.2020.12.012.

11. Grunstein, M. Histone acetylation in chromatin structure and transcription. *Nature* **1997**, *389* (6649), 349-352. DOI: 10.1038/38664.

12. Fan, J.; Krautkramer, K. A.; Feldman, J. L.; Denu, J. M. Metabolic Regulation of Histone Post-Translational Modifications. *ACS Chemical Biology* **2015**, *10* (1), 95-108. DOI: 10.1021/cb500846u.

13. Arnaudo, A. M.; Garcia, B. A. Proteomic characterization of novel histone post-translational modifications. *Epigenetics Chromatin* **2013**, *6* (1), 24. DOI: 10.1186/1756-8935-6-24.

14. Gillette, T. G.; Hill, J. A. Readers, writers, and erasers: chromatin as the whiteboard of heart disease. *Circ Res* **2015**, *116* (7), 1245-1253. DOI: 10.1161/CIRCRESAHA.116.303630.

15. Biswas, S.; Rao, C. M. Epigenetic tools (The Writers, The Readers and The Erasers) and their implications in cancer therapy. *Eur J Pharmacol* **2018**, *837*, 8-24. DOI: 10.1016/j.ejphar.2018.08.021.

16. Hubbert, C.; Guardiola, A.; Shao, R.; Kawaguchi, Y.; Ito, A.; Nixon, A.; Yoshida, M.; Wang, X. F.; Yao, T. P. HDAC6 is a microtubule-associated deacetylase. *Nature* **2002**, *417* (6887), 455-458. DOI: 10.1038/417455a.

17. Spreafico, M.; Gruszka, A. M.; Valli, D.; Mazzola, M.; Deflorian, G.; Quinte, A.; Totaro, M. G.; Battaglia, C.; Alcalay, M.; Marozzi, A.; et al. HDAC8: A Promising Therapeutic Target for Acute Myeloid Leukemia. *Front Cell Dev Biol* **2020**, *8*, 844, Original Research. DOI: 10.3389/fcell.2020.00844.

18. Haarhaus, M.; Gilham, D.; Kulikowski, E.; Magnusson, P.; Kalantar-Zadeh, K. Pharmacologic epigenetic modulators of alkaline phosphatase in chronic kidney disease. *Curr Opin Nephrol Hypertens* **2020**, *29* (1), 4-15. DOI: 10.1097/MNH.0000000000000570.

19. Kuo, M. H.; Allis, C. D. Roles of histone acetyltransferases and deacetylases in gene regulation. *Bioessays* **1998**, *20* (8), 615-626. DOI: 10.1002/(SICI)1521-1878(199808)20:8<615::AID-BIES4>3.0.CO;2-H.

20. Glozak, M. A.; Sengupta, N.; Zhang, X.; Seto, E. Acetylation and deacetylation of non-histone proteins. *Gene* **2005**, *363*, 15-23. DOI: 10.1016/j.gene.2005.09.010.

21. Sun, X. J.; Man, N.; Tan, Y.; Nimer, S. D.; Wang, L. The Role of Histone Acetyltransferases in Normal and Malignant Hematopoiesis. *Front Oncol* **2015**, *5*, 108, Review. DOI: 10.3389/fonc.2015.00108.

22. Li, G.; Tian, Y.; Zhu, W. G. The Roles of Histone Deacetylases and Their Inhibitors in Cancer Therapy. *Front Cell Dev Biol* **2020**, *8*, 576946, Review. DOI: 10.3389/fcell.2020.576946.

23. Kumar, S.; Attrish, D.; Srivastava, A.; Banerjee, J.; Tripathi, M.; Chandra, P. S.; Dixit, A. B. Non-histone substrates of histone deacetylases as potential therapeutic targets in

epilepsy. *Expert Opin Ther Targets* **2021**, *25* (1), 75-85. DOI: 10.1080/14728222.2021.1860016.

24. Ropero, S.; Esteller, M. The role of histone deacetylases (HDACs) in human cancer. *Mol Oncol* **2007**, *1* (1), 19-25. DOI: 10.1016/j.molonc.2007.01.001.

25. Verza, F. A.; Das, U.; Fachin, A. L.; Dimmock, J. R.; Marins, M. Roles of Histone Deacetylases and Inhibitors in Anticancer Therapy. *Cancers (Basel)* **2020**, *12* (6). DOI: 10.3390/cancers12061664.

26. Haberland, M.; Montgomery, R. L.; Olson, E. N. The many roles of histone deacetylases in development and physiology: implications for disease and therapy. *Nat Rev Genet* **2009**, *10* (1), 32-42. DOI: 10.1038/nrg2485.

27. Wang, P.; Wang, Z.; Liu, J. Role of HDACs in normal and malignant hematopoiesis. *Mol Cancer* **2020**, *19* (1), 5. DOI: 10.1186/s12943-019-1127-7.

28. Mahgoub, M.; Monteggia, L. M. A role for histone deacetylases in the cellular and behavioral mechanisms underlying learning and memory. *Learn Mem* **2014**, *21* (10), 564-568. DOI: 10.1101/lm.036012.114.

29. Cantley, M. D.; Haynes, D. R. Epigenetic regulation of inflammation: progressing from broad acting histone deacetylase (HDAC) inhibitors to targeting specific HDACs. *Inflammopharmacology* **2013**, *21* (4), 301-307. DOI: 10.1007/s10787-012-0166-0.

30. Ho, T. C. S.; Chan, A. H. Y.; Ganesan, A. Thirty Years of HDAC Inhibitors: 2020 Insight and Hindsight. *J Med Chem* **2020**, *63* (21), 12460-12484. DOI: 10.1021/acs.jmedchem.0c00830.

31. Hess, L.; Moos, V.; Lauber, A. A.; Reiter, W.; Schuster, M.; Hartl, N.; Lackner, D.; Boenke, T.; Koren, A.; Guzzardo, P. M.; et al. A toolbox for class I HDACs reveals isoform specific roles in gene regulation and protein acetylation. *PLoS Genet* **2022**, *18* (8), e1010376. DOI: 10.1371/journal.pgen.1010376.

32. Yang, W.-M.; Tsai, S.-C.; Wen, Y.-D.; Fejér, G.; Seto, E. Functional Domains of Histone Deacetylase-3*. *Journal of Biological Chemistry* **2002**, *277* (11), 9447-9454. DOI: https://doi.org/10.1074/jbc.M105993200.

33. Wolfson, N. A.; Pitcairn, C. A.; Fierke, C. A. HDAC8 substrates: Histones and beyond. *Biopolymers* **2013**, *99* (2), 112-126. DOI: 10.1002/bip.22135.

34. Alam, N.; Zimmerman, L.; Wolfson, N. A.; Joseph, C. G.; Fierke, C. A.; Schueler-Furman, O. Structure-Based Identification of HDAC8 Non-histone Substrates. *Structure* **2016**, *24* (3), 458-468. DOI: 10.1016/j.str.2016.02.002.

35. Delcuve, G. P.; Khan, D. H.; Davie, J. R. Roles of histone deacetylases in epigenetic regulation: emerging paradigms from studies with inhibitors. *Clin Epigenetics* **2012**, *4* (1), 5. DOI: 10.1186/1868-7083-4-5.

36. Milazzo, G.; Mercatelli, D.; Di Muzio, G.; Triboli, L.; De Rosa, P.; Perini, G.; Giorgi, F. M. Histone Deacetylases (HDACs): Evolution, Specificity, Role in Transcriptional Complexes, and Pharmacological Actionability. *Genes (Basel)* **2020**, *11* (5), 556. DOI: 10.3390/genes11050556.

37. Lakowski, B.; Roelens, I.; Jacob, S. CoREST-like complexes regulate chromatin modification and neuronal gene expression. *J Mol Neurosci* **2006**, *29* (3), 227-239. DOI: 10.1385/JMN:29:3:227.

38. Ayer, D. E. Histone deacetylases: transcriptional repression with SINers and NuRDs. *Trends Cell Biol* **1999**, *9* (5), 193-198. DOI: 10.1016/s0962-8924(99)01536-6.

39. Guenther, M. G.; Barak, O.; Lazar, M. A. The SMRT and N-CoR corepressors are activating cofactors for histone deacetylase 3. *Mol Cell Biol* **2001**, *21* (18), 6091-6101. DOI: 10.1128/MCB.21.18.6091-6101.2001.

40. Ito, A.; Kawaguchi, Y.; Lai, C. H.; Kovacs, J. J.; Higashimoto, Y.; Appella, E.; Yao, T. P. MDM2-HDAC1-mediated deacetylation of p53 is required for its degradation. *EMBO J* **2002**, *21* (22), 6236-6245. DOI: 10.1093/emboj/cdf616.

41. Martinez-Balbas, M. A.; Bauer, U. M.; Nielsen, S. J.; Brehm, A.; Kouzarides, T. Regulation of E2F1 activity by acetylation. *EMBO J* **2000**, *19* (4), 662-671. DOI: 10.1093/emboj/19.4.662.

42. Leus, N. G.; van der Wouden, P. E.; van den Bosch, T.; Hooghiemstra, W. T. R.; Ourailidou, M. E.; Kistemaker, L. E.; Bischoff, R.; Gosens, R.; Haisma, H. J.; Dekker, F. J. HDAC 3-selective inhibitor RGFP966 demonstrates anti-inflammatory properties in RAW 264.7 macrophages and mouse precision-cut lung slices by attenuating NF-kappaB p65 transcriptional activity. *Biochem Pharmacol* **2016**, *108*, 58-74. DOI: 10.1016/j.bcp.2016.03.010.

43. Millard, C. J.; Watson, P. J.; Fairall, L.; Schwabe, J. W. R. Targeting Class I Histone Deacetylases in a "Complex" Environment. *Trends Pharmacol Sci* **2017**, *38* (4), 363-377. DOI: 10.1016/j.tips.2016.12.006.

44. Somoza, J. R.; Skene, R. J.; Katz, B. A.; Mol, C.; Ho, J. D.; Jennings, A. J.; Luong, C.; Arvai, A.; Buggy, J. J.; Chi, E.; et al. Structural snapshots of human HDAC8 provide insights into the class I histone deacetylases. *Structure* **2004**, *12* (7), 1325-1334. DOI: 10.1016/j.str.2004.04.012.

45. Luo, Y.; Li, H. Structure-Based Inhibitor Discovery of Class I Histone Deacetylases (HDACs). *Int J Mol Sci* **2020**, *21* (22), 8828. DOI: 10.3390/ijms21228828.

46. Ho, T. T.; Peng, C.; Seto, E.; Lin, H. Trapoxin A Analogue as a Selective Nanomolar Inhibitor of HDAC11. *ACS Chem Biol* **2023**, *18* (4), 803-809. DOI: 10.1021/acschembio.2c00840.

47. Kutil, Z.; Mikesova, J.; Zessin, M.; Meleshin, M.; Novakova, Z.; Alquicer, G.; Kozikowski, A.; Sippl, W.; Barinka, C.; Schutkowski, M. Continuous Activity Assay for HDAC11 Enabling Reevaluation of HDAC Inhibitors. *ACS Omega* **2019**, *4* (22), 19895-19904. DOI: 10.1021/acsomega.9b02808.

48. Whitehead, L.; Dobler, M. R.; Radetich, B.; Zhu, Y.; Atadja, P. W.; Claiborne, T.; Grob, J. E.; McRiner, A.; Pancost, M. R.; Patnaik, A.; et al. Human HDAC isoform selectivity achieved via exploitation of the acetate release channel with structurally unique small molecule inhibitors. *Bioorg Med Chem* **2011**, *19* (15), 4626-4634. DOI: 10.1016/j.bmc.2011.06.030.

49. Marek, M.; Shaik, T. B.; Heimburg, T.; Chakrabarti, A.; Lancelot, J.; Ramos-Morales, E.; Da Veiga, C.; Kalinin, D.; Melesina, J.; Robaa, D.; et al. Characterization of Histone Deacetylase 8 (HDAC8) Selective Inhibition Reveals Specific Active Site Structural and Functional Determinants. *J Med Chem* **2018**, *61* (22), 10000-10016. DOI: 10.1021/acs.jmedchem.8b01087.

50. Patra, S.; Panigrahi, D. P.; Praharaj, P. P.; Bhol, C. S.; Mahapatra, K. K.; Mishra, S. R.; Behera, B. P.; Jena, M.; Bhutia, S. K. Dysregulation of histone deacetylases in carcinogenesis and tumor progression: a possible link to apoptosis and autophagy. *Cell Mol Life Sci* **2019**, *76* (17), 3263-3282. DOI: 10.1007/s00018-019-03098-1.

51. Mazzone, R.; Zwergel, C.; Artico, M.; Taurone, S.; Ralli, M.; Greco, A.; Mai, A. The emerging role of epigenetics in human autoimmune disorders. *Clin Epigenetics* **2019**, *11* (1), 34. DOI: 10.1186/s13148-019-0632-2.

52. Li, Y.; Seto, E. HDACs and HDAC Inhibitors in Cancer Development and Therapy. *Cold Spring Harb Perspect Med* **2016**, *6* (10). DOI: 10.1101/cshperspect.a026831.

53. Ishihama, K.; Yamakawa, M.; Semba, S.; Takeda, H.; Kawata, S.; Kimura, S.; Kimura, W. Expression of HDAC1 and CBP/p300 in human colorectal carcinomas. *J Clin Pathol* **2007**, *60* (11), 1205-1210. DOI: 10.1136/jcp.2005.029165.

54. Yoon, S.; Eom, G. H. HDAC and HDAC Inhibitor: From Cancer to Cardiovascular Diseases. *Chonnam Med J* **2016**, *52* (1), 1-11. DOI: 10.4068/cmj.2016.52.1.1.

55. Bassett, S. A.; Barnett, M. P. The role of dietary histone deacetylases (HDACs) inhibitors in health and disease. *Nutrients* **2014**, *6* (10), 4273-4301. DOI: 10.3390/nu6104273.

56. Oehme, I.; Deubzer, H. E.; Wegener, D.; Pickert, D.; Linke, J. P.; Hero, B.; Kopp-Schneider, A.; Westermann, F.; Ulrich, S. M.; von Deimling, A.; et al. Histone deacetylase 8 in neuroblastoma tumorigenesis. *Clin Cancer Res* **2009**, *15* (1), 91-99. DOI: 10.1158/1078-0432.CCR-08-0684.

57. Sharma, S.; Sarathlal, K. C.; Taliyan, R. Epigenetics in Neurodegenerative Diseases: The Role of Histone Deacetylases. *CNS Neurol Disord Drug Targets* **2019**, *18* (1), 11-18. DOI: 10.2174/1871527317666181004155136.

58. De Simone, A.; Milelli, A. Histone Deacetylase Inhibitors as Multitarget Ligands: New Players in Alzheimer's Disease Drug Discovery? *ChemMedChem* **2019**, *14* (11), 1067-1073. DOI: 10.1002/cmdc.201900174.

59. Das Gupta, K.; Shakespear, M. R.; Iyer, A.; Fairlie, D. P.; Sweet, M. J. Histone deacetylases in monocyte/macrophage development, activation and metabolism: refining HDAC targets for inflammatory and infectious diseases. *Clin Transl Immunology* **2016**, *5* (1), e62. DOI: 10.1038/cti.2015.46.

60. Zaikos, T. D.; Painter, M. M.; Sebastian Kettinger, N. T.; Terry, V. H.; Collins, K. L. Class 1-Selective Histone Deacetylase (HDAC) Inhibitors Enhance HIV Latency Reversal while Preserving the Activity of HDAC Isoforms Necessary for Maximal HIV Gene Expression. *J Virol* **2018**, *92* (6). DOI: 10.1128/JVI.02110-17.

61. Makkar, R.; Behl, T.; Arora, S. Role of HDAC inhibitors in diabetes mellitus. *Curr Res Transl Med* **2020**, *68* (2), 45-50. DOI: 10.1016/j.retram.2019.08.001.

62. Fioravanti, R.; Mautone, N.; Rovere, A.; Rotili, D.; Mai, A. Targeting histone acetylation/deacetylation in parasites: an update (2017-2020). *Curr Opin Chem Biol* **2020**, *57*, 65-74. DOI: 10.1016/j.cbpa.2020.05.008.

63. Hailu, G. S.; Robaa, D.; Forgione, M.; Sippl, W.; Rotili, D.; Mai, A. Lysine Deacetylase Inhibitors in Parasites: Past, Present, and Future Perspectives. *J Med Chem* **2017**, *60* (12), 4780-4804. DOI: 10.1021/acs.jmedchem.6b01595.

64. Bellucci, L.; Dalvai, M.; Kocanova, S.; Moutahir, F.; Bystricky, K. Activation of p21 by HDAC inhibitors requires acetylation of H2A.Z. *PLoS One* **2013**, *8* (1), e54102. DOI: 10.1371/journal.pone.0054102.

65. Bolden, J. E.; Shi, W.; Jankowski, K.; Kan, C. Y.; Cluse, L.; Martin, B. P.; MacKenzie, K. L.; Smyth, G. K.; Johnstone, R. W. HDAC inhibitors induce tumor-

cell-selective pro-apoptotic transcriptional responses. *Cell Death Dis* **2013**, *4* (2), e519. DOI: 10.1038/cddis.2013.9.

66. Deroanne, C. F.; Bonjean, K.; Servotte, S.; Devy, L.; Colige, A.; Clausse, N.; Blacher, S.; Verdin, E.; Foidart, J. M.; Nusgens, B. V.; et al. Histone deacetylases inhibitors as anti-angiogenic agents altering vascular endothelial growth factor signaling. *Oncogene* **2002**, *21* (3), 427-436. DOI: 10.1038/sj.onc.1205108.

67. Zhang, J.; Ng, S.; Wang, J.; Zhou, J.; Tan, S. H.; Yang, N.; Lin, Q.; Xia, D.; Shen, H. M. Histone deacetylase inhibitors induce autophagy through FOXO1-dependent pathways. *Autophagy* **2015**, *11* (4), 629-642. DOI: 10.1080/15548627.2015.1023981.

68. Chiao, M. T.; Cheng, W. Y.; Yang, Y. C.; Shen, C. C.; Ko, J. L. Suberoylanilide hydroxamic acid (SAHA) causes tumor growth slowdown and triggers autophagy in glioblastoma stem cells. *Autophagy* **2013**, *9* (10), 1509-1526. DOI: 10.4161/auto.25664.

69. Rosato, R. R.; Almenara, J. A.; Grant, S. The histone deacetylase inhibitor MS-275 promotes differentiation or apoptosis in human leukemia cells through a process regulated by generation of reactive oxygen species and induction of p21(CIP1/WAF1). *Cancer Research* **2003**, *63* (13), 3637-3645. (acccessed 5/21/2023).

70. Bieliauskas, A. V.; Pflum, M. K. Isoform-selective histone deacetylase inhibitors. *Chem Soc Rev* **2008**, *37* (7), 1402-1413. DOI: 10.1039/b703830p.

71. Melesina, J.; Simoben, C. V.; Praetorius, L.; Bulbul, E. F.; Robaa, D.; Sippl, W. Strategies To Design Selective Histone Deacetylase Inhibitors. *ChemMedChem* **2021**, *16* (9), 1336-1359. DOI: 10.1002/cmdc.202000934.

72. Finnin, M. S.; Donigian, J. R.; Cohen, A.; Richon, V. M.; Rifkind, R. A.; Marks, P. A.; Breslow, R.; Pavletich, N. P. Structures of a histone deacetylase homologue bound to the TSA and SAHA inhibitors. *Nature* **1999**, *401* (6749), 188-193. DOI: 10.1038/43710.

73. Saito, A.; Yamashita, T.; Mariko, Y.; Nosaka, Y.; Tsuchiya, K.; Ando, T.; Suzuki, T.; Tsuruo, T.; Nakanishi, O. A synthetic inhibitor of histone deacetylase, MS-27-275, with marked in vivo antitumor activity against human tumors. *Proc Natl Acad Sci U S A* **1999**, *96* (8), 4592-4597. DOI: 10.1073/pnas.96.8.4592.

74. Mwakwari, S. C.; Patil, V.; Guerrant, W.; Oyelere, A. K. Macrocyclic histone deacetylase inhibitors. *Curr Top Med Chem* **2010**, *10* (14), 1423-1440. DOI: 10.2174/156802610792232079.

75. Fass, D. M.; Shah, R.; Ghosh, B.; Hennig, K.; Norton, S.; Zhao, W. N.; Reis, S. A.; Klein, P. S.; Mazitschek, R.; Maglathlin, R. L.; et al. Effect of Inhibiting Histone Deacetylase with Short-Chain Carboxylic Acids and Their Hydroxamic Acid Analogs on Vertebrate Development and Neuronal Chromatin. *ACS Med Chem Lett* **2010**, *2* (1), 39-42. DOI: 10.1021/ml1001954.

76. Furumai, R.; Matsuyama, A.; Kobashi, N.; Lee, K. H.; Nishiyama, M.; Nakajima, H.; Tanaka, A.; Komatsu, Y.; Nishino, N.; Yoshida, M.; et al. FK228 (depsipeptide) as a natural prodrug that inhibits class I histone deacetylases. *Cancer Res* **2002**, *62* (17), 4916-4921.

77. Liu, J.; Kelly, J.; Yu, W.; Clausen, D.; Yu, Y.; Kim, H.; Duffy, J. L.; Chung, C. C.; Myers, R. W.; Carroll, S.; et al. Selective Class I HDAC Inhibitors Based on Aryl Ketone Zinc Binding Induce HIV-1 Protein for Clearance. *ACS Med Chem Lett* **2020**, *11* (7), 1476-1483. DOI: 10.1021/acsmedchemlett.0c00302.

78. Wang, Y.; Stowe, Ryan L.; Pinello, Christie E.; Tian, G.; Madoux, F.; Li, D.; Zhao, Lisa Y.; Li, J.-L.; Wang, Y.; Wang, Y.; et al. Identification of Histone Deacetylase Inhibitors with Benzoylhydrazide Scaffold that Selectively Inhibit Class I Histone Deacetylases. *Chemistry & Biology* **2015**, *22* (2), 273-284. DOI: https://doi.org/10.1016/j.chembiol.2014.12.015.

79. Sun, P.; Wang, J.; Khan, K. S.; Yang, W.; Ng, B. W.; Ilment, N.; Zessin, M.; Bulbul, E. F.; Robaa, D.; Erdmann, F.; et al. Development of Alkylated Hydrazides as Highly Potent and Selective Class I Histone Deacetylase Inhibitors with T cell Modulatory Properties. *J Med Chem* **2022**, *65* (24), 16313-16337. DOI: 10.1021/acs.jmedchem.2c01132.

80. Lobera, M.; Madauss, K. P.; Pohlhaus, D. T.; Wright, Q. G.; Trocha, M.; Schmidt, D. R.; Baloglu, E.; Trump, R. P.; Head, M. S.; Hofmann, G. A.; et al. Selective class IIa histone deacetylase inhibition via a nonchelating zinc-binding group. *Nat Chem Biol* **2013**, *9* (5), 319-325. DOI: 10.1038/nchembio.1223.

81. Duvic, M.; Talpur, R.; Ni, X.; Zhang, C.; Hazarika, P.; Kelly, C.; Chiao, J. H.; Reilly, J. F.; Ricker, J. L.; Richon, V. M.; et al. Phase 2 trial of oral vorinostat (suberoylanilide hydroxamic acid, SAHA) for refractory cutaneous T-cell lymphoma (CTCL). *Blood* **2007**, *109* (1), 31-39. DOI: 10.1182/blood-2006-06-025999 (acccessed 6/12/2023).

82. Neri, P.; Bahlis, N. J.; Lonial, S. Panobinostat for the treatment of multiple myeloma. *Expert Opin Investig Drugs* **2012**, *21* (5), 733-747. DOI: 10.1517/13543784.2012.668883.

83. Yang, L.; Xue, X. W.; Zhang, Y. H. Simple and Efficient Synthesis of Belinostat. *Synthetic Communications* **2010**, *40* (17), 2520-2524. DOI: 10.1080/00397910903277870.

84. Shimony, S.; Horowitz, N.; Ribakovsky, E.; Rozovski, U.; Avigdor, A.; Zloto, K.; Berger, T.; Avivi, I.; Perry, C.; Abadi, U.; et al. Romidepsin treatment for relapsed or refractory peripheral and cutaneous T-cell lymphoma: Real-life data from a national multicenter observational study. *Hematol Oncol* **2019**, *37* (5), 569-577. DOI: 10.1002/hon.2691.

85. Dong, M.; Ning, Z.; Newman, M. J.; Xu, J.; Dou, G.; Cao, H.; Shi, Y.; Gingras, M. A.; Lu, X.; Feng, F. Phase I study of chidamide (CS055/HBI-8000), a novel histone deacetylase inhibitor, in patients with advanced solid tumors and lymphomas. *Journal of Clinical Oncology* **2009**, *27* (15), 3529-3529. DOI: 10.1200/jco.2009.27.15_suppl.3529.

86. Suraweera, A.; O'Byrne, K. J.; Richard, D. J. Combination Therapy With Histone Deacetylase Inhibitors (HDACi) for the Treatment of Cancer: Achieving the Full Therapeutic Potential of HDACi. *Front Oncol* **2018**, *8*, 92. DOI: 10.3389/fonc.2018.00092.

87. Shah, R. R. Safety and Tolerability of Histone Deacetylase (HDAC) Inhibitors in Oncology. *Drug Saf* **2019**, *42* (2), 235-245. DOI: 10.1007/s40264-018-0773-9.

88. Shen, S.; Kozikowski, A. P. Why Hydroxamates May Not Be the Best Histone Deacetylase Inhibitors--What Some May Have Forgotten or Would Rather Forget? *ChemMedChem* **2016**, *11* (1), 15-21. DOI: 10.1002/cmdc.201500486.

89. Connolly, R. M.; Rudek, M. A.; Piekarz, R. Entinostat: a promising treatment option for patients with advanced breast cancer. *Future Oncol* **2017**, *13* (13), 1137-1148. DOI: 10.2217/fon-2016-0526.

90. Batlevi, C. L.; Kasamon, Y.; Bociek, R. G.; Lee, P.; Gore, L.; Copeland, A.; Sorensen, R.; Ordentlich, P.; Cruickshank, S.; Kunkel, L.; et al. ENGAGE- 501: phase II study of entinostat (SNDX-275) in relapsed and refractory Hodgkin lymphoma. *Haematologica* **2016**, *101* (8), 968-975. DOI: 10.3324/haematol.2016.142406.

91. Fournel, M.; Bonfils, C.; Hou, Y.; Yan, P. T.; Trachy-Bourget, M. C.; Kalita, A.; Liu, J.; Lu, A. H.; Zhou, N. Z.; Robert, M. F.; et al. MGCD0103, a novel isotype-selective

histone deacetylase inhibitor, has broad spectrum antitumor activity in vitro and in vivo. *Mol Cancer Ther* **2008**, *7* (4), 759-768. DOI: 10.1158/1535-7163.MCT-07-2026 (acccessed 5/21/2023).

92. Moradei, O. M.; Mallais, T. C.; Frechette, S.; Paquin, I.; Tessier, P. E.; Leit, S. M.; Fournel, M.; Bonfils, C.; Trachy-Bourget, M. C.; Liu, J.; et al. Novel aminophenyl benzamide-type histone deacetylase inhibitors with enhanced potency and selectivity. *J Med Chem* **2007**, *50* (23), 5543-5546. DOI: 10.1021/jm701079h.

93. Witter, D. J.; Harrington, P.; Wilson, K. J.; Chenard, M.; Fleming, J. C.; Haines, B.; Kral, A. M.; Secrist, J. P.; Miller, T. A. Optimization of biaryl Selective HDAC1&2 Inhibitors (SHI-1:2). *Bioorg Med Chem Lett* **2008**, *18* (2), 726-731. DOI: 10.1016/j.bmcl.2007.11.047.

94. Wagner, F. F.; Lundh, M.; Kaya, T.; McCarren, P.; Zhang, Y. L.; Chattopadhyay, S.; Gale, J. P.; Galbo, T.; Fisher, S. L.; Meier, B. C.; et al. An Isochemogenic Set of Inhibitors To Define the Therapeutic Potential of Histone Deacetylases in beta-Cell Protection. *ACS Chem Biol* **2016**, *11* (2), 363-374. DOI: 10.1021/acschembio.5b00640.

95. Malvaez, M.; McQuown, S. C.; Rogge, G. A.; Astarabadi, M.; Jacques, V.; Carreiro, S.; Rusche, J. R.; Wood, M. A. HDAC3-selective inhibitor enhances extinction of cocaine-seeking behavior in a persistent manner. *Proc Natl Acad Sci U S A* **2013**, *110* (7), 2647-2652. DOI: 10.1073/pnas.1213364110.

96. O'Brien Laramy, M. N.; Luthra, S.; Brown, M. F.; Bartlett, D. W. Delivering on the promise of protein degraders. *Nat Rev Drug Discov* **2023**, *22* (5), 410-427. DOI: 10.1038/s41573-023-00652-2.

97. Liu, Z.; Hu, M.; Yang, Y.; Du, C.; Zhou, H.; Liu, C.; Chen, Y.; Fan, L.; Ma, H.; Gong, Y.; et al. An overview of PROTACs: a promising drug discovery paradigm. *Mol Biomed* **2022**, *3* (1), 46. DOI: 10.1186/s43556-022-00112-0.

98. Long, M. J.; Gollapalli, D. R.; Hedstrom, L. Inhibitor mediated protein degradation. *Chem Biol* **2012**, *19* (5), 629-637. DOI: 10.1016/j.chembiol.2012.04.008.

99. Slabicki, M.; Kozicka, Z.; Petzold, G.; Li, Y. D.; Manojkumar, M.; Bunker, R. D.; Donovan, K. A.; Sievers, Q. L.; Koeppel, J.; Suchyta, D.; et al. The CDK inhibitor CR8 acts as a molecular glue degrader that depletes cyclin K. *Nature* **2020**, *585* (7824), 293-297. DOI: 10.1038/s41586-020-2374-x.

100.   Banik, S. M.; Pedram, K.; Wisnovsky, S.; Ahn, G.; Riley, N. M.; Bertozzi, C. R. Lysosome-targeting chimaeras for degradation of extracellular proteins. *Nature* **2020**, *584* (7820), 291-297. DOI: 10.1038/s41586-020-2545-9.

101.   Ji, C. H.; Kim, H. Y.; Lee, M. J.; Heo, A. J.; Park, D. Y.; Lim, S.; Shin, S.; Ganipisetti, S.; Yang, W. S.; Jung, C. A.; et al. The AUTOTAC chemical biology platform for targeted protein degradation via the autophagy-lysosome system. *Nat Commun* **2022**, *13* (1), 904. DOI: 10.1038/s41467-022-28520-4.

102.   Foley, K. P.; Ye, L.; Wang, M.; Ying, C.; Yin, W.; Zhang, L.; Ying, W. Chaperone-mediated protein degradation (CHAMP): A novel technology for tumor-targeted protein degradation. *Cancer Research* **2021**, *81* (13_Supplement), 971-971.

103.   Xie, H.; Liu, J.; Alem Glison, D. M.; Fleming, J. B. The clinical advances of proteolysis targeting chimeras in oncology. *Explor Target Antitumor Ther* **2021**, *2* (6), 511-521. DOI: 10.37349/etat.2021.00061.

104.   Fischer, F.; Alves Avelar, L. A.; Murray, L.; Kurz, T. Designing HDAC-PROTACs: lessons learned so far. *Future Med Chem* **2022**, *14* (3), 143-166. DOI: 10.4155/fmc-2021-0206.

105.   Yang, K.; Song, Y.; Xie, H.; Wu, H.; Wu, Y. T.; Leisten, E. D.; Tang, W. Development of the first small molecule histone deacetylase 6 (HDAC6) degraders. *Bioorg Med Chem Lett* **2018**, *28* (14), 2493-2497. DOI: 10.1016/j.bmcl.2018.05.057.

106.   Chotitumnavee, J.; Yamashita, Y.; Takahashi, Y.; Takada, Y.; Iida, T.; Oba, M.; Itoh, Y.; Suzuki, T. Selective degradation of histone deacetylase 8 mediated by a proteolysis targeting chimera (PROTAC). *Chem Commun (Camb)* **2022**, *58* (29), 4635-4638, 10.1039/D2CC00272H. DOI: 10.1039/d2cc00272h.

107.   Darwish, S.; Ghazy, E.; Heimburg, T.; Herp, D.; Zeyen, P.; Salem-Altintas, R.; Ridinger, J.; Robaa, D.; Schmidtkunz, K.; Erdmann, F.; et al. Design, Synthesis and Biological Characterization of Histone Deacetylase 8 (HDAC8) Proteolysis Targeting Chimeras (PROTACs) with Anti-Neuroblastoma Activity. *Int J Mol Sci* **2022**, *23* (14), 7535. DOI: 10.3390/ijms23147535.

108.   Macabuag, N.; Esmieu, W.; Breccia, P.; Jarvis, R.; Blackaby, W.; Lazari, O.; Urbonas, L.; Eznarriaga, M.; Williams, R.; Strijbosch, A.; et al. Developing HDAC4-Selective Protein Degraders To Investigate the Role of HDAC4 in Huntington's Disease Pathology. *J Med Chem* **2022**, *65* (18), 12445-12459. DOI: 10.1021/acs.jmedchem.2c01149.

109. Smalley, J. P.; Adams, G. E.; Millard, C. J.; Song, Y.; Norris, J. K. S.; Schwabe, J. W. R.; Cowley, S. M.; Hodgkinson, J. T. PROTAC-mediated degradation of class I histone deacetylase enzymes in corepressor complexes. *Chem Commun (Camb)* **2020**, *56* (32), 4476-4479, 10.1039/D0CC01485K. DOI: 10.1039/d0cc01485k.

110. Smalley, J. P.; Baker, I. M.; Pytel, W. A.; Lin, L. Y.; Bowman, K. J.; Schwabe, J. W. R.; Cowley, S. M.; Hodgkinson, J. T. Optimization of Class I Histone Deacetylase PROTACs Reveals that HDAC1/2 Degradation is Critical to Induce Apoptosis and Cell Arrest in Cancer Cells. *J Med Chem* **2022**, *65* (7), 5642-5659. DOI: 10.1021/acs.jmedchem.1c02179.

111. Cao, F.; de Weerd, S.; Chen, D.; Zwinderman, M. R. H.; van der Wouden, P. E.; Dekker, F. J. Induced protein degradation of histone deacetylases 3 (HDAC3) by proteolysis targeting chimera (PROTAC). *Eur J Med Chem* **2020**, *208*, 112800. DOI: 10.1016/j.ejmech.2020.112800.

112. Xiao, Y.; Wang, J.; Zhao, L. Y.; Chen, X.; Zheng, G.; Zhang, X.; Liao, D. Discovery of histone deacetylase 3 (HDAC3)-specific PROTACs. *Chem Commun (Camb)* **2020**, *56* (68), 9866-9869, 10.1039/D0CC03243C. DOI: 10.1039/d0cc03243c.

113. Tae, H. S.; Sundberg, T. B.; Neklesa, T. K.; Noblin, D. J.; Gustafson, J. L.; Roth, A. G.; Raina, K.; Crews, C. M. Identification of hydrophobic tags for the degradation of stabilized proteins. *Chembiochem* **2012**, *13* (4), 538-541. DOI: 10.1002/cbic.201100793.

114. Neklesa, T. K.; Crews, C. M. Chemical biology: Greasy tags for protein removal. *Nature* **2012**, *487* (7407), 308-309. DOI: 10.1038/487308a.

115. Shi, Y.; Long, M. J.; Rosenberg, M. M.; Li, S.; Kobjack, A.; Lessans, P.; Coffey, R. T.; Hedstrom, L. Boc(3)Arg-Linked Ligands Induce Degradation by Localizing Target Proteins to the 20S Proteasome. *ACS Chem Biol* **2016**, *11* (12), 3328-3337. DOI: 10.1021/acschembio.6b00656.

116. Collins, I.; Wang, H.; Caldwell, J. J.; Chopra, R. Chemical approaches to targeted protein degradation through modulation of the ubiquitin-proteasome pathway. *Biochem J* **2017**, *474* (7), 1127-1147. DOI: 10.1042/BCJ20160762.

117. Wang, Y.; Jiang, X.; Feng, F.; Liu, W.; Sun, H. Degradation of proteins by PROTACs and other strategies. *Acta Pharm Sin B* **2020**, *10* (2), 207-238. DOI: 10.1016/j.apsb.2019.08.001.

118. Xie, T.; Lim, S. M.; Westover, K. D.; Dodge, M. E.; Ercan, D.; Ficarro, S. B.; Udayakumar, D.; Gurbani, D.; Tae, H. S.; Riddle, S. M.; et al. Pharmacological

targeting of the pseudokinase Her3. *Nat Chem Biol* **2014**, *10* (12), 1006-1012. DOI: 10.1038/nchembio.1658.

119.   Ma, A.; Stratikopoulos, E.; Park, K. S.; Wei, J.; Martin, T. C.; Yang, X.; Schwarz, M.; Leshchenko, V.; Rialdi, A.; Dale, B.; et al. Discovery of a first-in-class EZH2 selective degrader. *Nat Chem Biol* **2020**, *16* (2), 214-222. DOI: 10.1038/s41589-019-0421-4.

120.   Liao, Y.; Xu, L.; Ou, S.; Edwards, H.; Luedtke, D.; Ge, Y.; Qin, Z. H(2)O(2)/Peroxynitrite-Activated Hydroxamic Acid HDAC Inhibitor Prodrugs Show Antileukemic Activities against AML Cells. *ACS Med Chem Lett* **2018**, *9* (7), 635-640. DOI: 10.1021/acsmedchemlett.8b00057.

121.   Bhagat, S. D.; Singh, U.; Mishra, R. K.; Srivastava, A. An Endogenous Reactive Oxygen Species (ROS)-Activated Histone Deacetylase Inhibitor Prodrug for Cancer Chemotherapy. *ChemMedChem* **2018**, *13* (19), 2073-2079. DOI: 10.1002/cmdc.201800367.

122.   Mistry, I. N.; Thomas, M.; Calder, E. D. D.; Conway, S. J.; Hammond, E. M. Clinical Advances of Hypoxia-Activated Prodrugs in Combination With Radiation Therapy. *Int J Radiat Oncol Biol Phys* **2017**, *98* (5), 1183-1196. DOI: 10.1016/j.ijrobp.2017.03.024.

123.   Skwarska, A.; Calder, E. D. D.; Sneddon, D.; Bolland, H.; Odyniec, M. L.; Mistry, I. N.; Martin, J.; Folkes, L. K.; Conway, S. J.; Hammond, E. M. Development and pre-clinical testing of a novel hypoxia-activated KDAC inhibitor. *Cell Chem Biol* **2021**, *28* (9), 1258-1270 e1213. DOI: 10.1016/j.chembiol.2021.04.004.

124.   Calder, E. D. D.; Skwarska, A.; Sneddon, D.; Folkes, L. K.; Mistry, I. N.; Conway, S. J.; Hammond, E. M. Hypoxia-activated pro-drugs of the KDAC inhibitor vorinostat (SAHA). *Tetrahedron* **2020**, *76* (21), 131170. DOI: 10.1016/j.tet.2020.131170.

125.   Rana, Z.; Diermeier, S.; Hanif, M.; Rosengren, R. J. Understanding Failure and Improving Treatment Using HDAC Inhibitors for Prostate Cancer. *Biomedicines* **2020**, *8* (2), 22. DOI: 10.3390/biomedicines8020022.

126.   Robey, R. W.; Chakraborty, A. R.; Basseville, A.; Luchenko, V.; Bahr, J.; Zhan, Z.; Bates, S. E. Histone deacetylase inhibitors: emerging mechanisms of resistance. *Mol Pharm* **2011**, *8* (6), 2021-2031. DOI: 10.1021/mp200329f.

127.   Lee, J.-H.; Choy, M. L.; Marks, P. A. Chapter Two - Mechanisms of Resistance to Histone Deacetylase Inhibitors. In *Advances in Cancer Research*, Grant, S. Ed.; Vol. 116; Academic Press, 2012; pp 39-86.

128. Fantin, V. R.; Richon, V. M. Mechanisms of resistance to histone deacetylase inhibitors and their therapeutic implications. *Clin Cancer Res* **2007**, *13* (24), 7237-7242. DOI: 10.1158/1078-0432.CCR-07-2114 (acccessed 6/13/2023).

129. Witta, S. E.; Dziadziuszko, R.; Yoshida, K.; Hedman, K.; Varella-Garcia, M.; Bunn, P. A., Jr.; Hirsch, F. R. ErbB-3 expression is associated with E-cadherin and their coexpression restores response to gefitinib in non-small-cell lung cancer (NSCLC). *Ann Oncol* **2009**, *20* (4), 689-695. DOI: 10.1093/annonc/mdn703.

130. Gordon, S. W.; McGuire, W. P., 3rd; Shafer, D. A.; Sterling, R. K.; Lee, H. M.; Matherly, S. C.; Roberts, J. D.; Bose, P.; Tombes, M. B.; Shrader, E. E.; et al. Phase I Study of Sorafenib and Vorinostat in Advanced Hepatocellular Carcinoma. *Am J Clin Oncol* **2019**, *42* (8), 649-654. DOI: 10.1097/COC.0000000000000567.

131. Takeuchi, S.; Hase, T.; Shimizu, S.; Ando, M.; Hata, A.; Murakami, H.; Kawakami, T.; Nagase, K.; Yoshimura, K.; Fujiwara, T.; et al. Phase I study of vorinostat with gefitinib in BIM deletion polymorphism/epidermal growth factor receptor mutation double-positive lung cancer. *Cancer Sci* **2020**, *111* (2), 561-570. DOI: 10.1111/cas.14260.

132. Pei, X. Y.; Dai, Y.; Grant, S. Synergistic induction of oxidative injury and apoptosis in human multiple myeloma cells by the proteasome inhibitor bortezomib and histone deacetylase inhibitors. *Clin Cancer Res* **2004**, *10* (11), 3839-3852. DOI: 10.1158/1078-0432.CCR-03-0561 (acccessed 6/13/2023).

133. Ocio, E. M.; Vilanova, D.; Atadja, P.; Maiso, P.; Crusoe, E.; Fernandez-Lazaro, D.; Garayoa, M.; San-Segundo, L.; Hernandez-Iglesias, T.; de Alava, E.; et al. In vitro and in vivo rationale for the triple combination of panobinostat (LBH589) and dexamethasone with either bortezomib or lenalidomide in multiple myeloma. *Haematologica* **2010**, *95* (5), 794-803. DOI: 10.3324/haematol.2009.015495.

134. Hui, K. F.; Chiang, A. K. Combination of proteasome and class I HDAC inhibitors induces apoptosis of NPC cells through an HDAC6-independent ER stress-induced mechanism. *Int J Cancer* **2014**, *135* (12), 2950-2961. DOI: 10.1002/ijc.28924.

135. Mazzone, R.; Zwergel, C.; Mai, A.; Valente, S. Epi-drugs in combination with immunotherapy: a new avenue to improve anticancer efficacy. *Clin Epigenetics* **2017**, *9* (1), 59. DOI: 10.1186/s13148-017-0358-y.

136. Woods, D. M.; Sodre, A. L.; Villagra, A.; Sarnaik, A.; Sotomayor, E. M.; Weber, J. HDAC Inhibition Upregulates PD-1 Ligands in Melanoma and Augments

Immunotherapy with PD-1 Blockade. *Cancer Immunol Res* **2015**, *3* (12), 1375-1385. DOI: 10.1158/2326-6066.CIR-15-0077-T (acccessed 6/13/2023).

137. Orillion, A.; Hashimoto, A.; Damayanti, N.; Shen, L.; Adelaiye-Ogala, R.; Arisa, S.; Chintala, S.; Ordentlich, P.; Kao, C.; Elzey, B.; et al. Entinostat Neutralizes Myeloid-Derived Suppressor Cells and Enhances the Antitumor Effect of PD-1 Inhibition in Murine Models of Lung and Renal Cell Carcinoma. *Clin Cancer Res* **2017**, *23* (17), 5187-5201. DOI: 10.1158/1078-0432.CCR-17-0741 (acccessed 6/13/2023).

138. Munster, P.; Marchion, D.; Bicaku, E.; Lacevic, M.; Kim, J.; Centeno, B.; Daud, A.; Neuger, A.; Minton, S.; Sullivan, D. Clinical and biological effects of valproic acid as a histone deacetylase inhibitor on tumor and surrogate tissues: phase I/II trial of valproic acid and epirubicin/FEC. *Clin Cancer Res* **2009**, *15* (7), 2488-2496. DOI: 10.1158/1078-0432.CCR-08-1930 (acccessed 6/13/2023).

139. Marchion, D. C.; Bicaku, E.; Turner, J. G.; Daud, A. I.; Sullivan, D. M.; Munster, P. N. Synergistic interaction between histone deacetylase and topoisomerase II inhibitors is mediated through topoisomerase IIbeta. *Clin Cancer Res* **2005**, *11* (23), 8467-8475. DOI: 10.1158/1078-0432.CCR-05-1073 (acccessed 6/13/2023).

140. Sayar, H.; Cripe, L. D.; Saliba, A. N.; Abu Zaid, M.; Konig, H.; Boswell, H. S. Combination of sorafenib, vorinostat and bortezomib for the treatment of poor-risk AML: report of two consecutive clinical trials. *Leuk Res* **2019**, *77*, 30-33. DOI: 10.1016/j.leukres.2018.12.011.

141. Saliba, A. N.; Boswell, H. S.; Cripe, L. D.; Abu Zaid, M. I.; Weisenbach, J.; Sayar, H. Final Results of Phase I/II Study of Combination of Sorafenib, Vorinostat, and Bortezomib in Acute Myeloid Leukemia with FLT3-ITD Mutation or Poor-Risk Cytogenetics. *Blood* **2017**, *130* (Supplement 1), 3897-3897. DOI: 10.1182/blood.V130.Suppl_1.3897.3897 (acccessed 6/13/2023).

142. Short, N. J.; Rytting, M. E.; Cortes, J. E. Acute myeloid leukaemia. *Lancet* **2018**, *392* (10147), 593-606. DOI: 10.1016/S0140-6736(18)31041-9.

143. Zhang, J.; Gao, X.; Yu, L. Roles of Histone Deacetylases in Acute Myeloid Leukemia With Fusion Proteins. *Front Oncol* **2021**, *11*, 741746, Review. DOI: 10.3389/fonc.2021.741746.

144. Daver, N.; Schlenk, R. F.; Russell, N. H.; Levis, M. J. Targeting FLT3 mutations in AML: review of current knowledge and evidence. *Leukemia* **2019**, *33* (2), 299-312. DOI: 10.1038/s41375-018-0357-9.

145. Wachholz, V.; Mustafa, A. M.; Zeyn, Y.; Henninger, S. J.; Beyer, M.; Dzulko, M.; Piee-Staffa, A.; Brachetti, C.; Haehnel, P. S.; Sellmer, A.; et al. Inhibitors of class I HDACs and of FLT3 combine synergistically against leukemia cells with mutant FLT3. *Arch Toxicol* **2022**, *96* (1), 177-193. DOI: 10.1007/s00204-021-03174-1.

146. Li, Y. Z.; Yu, S.; Yan, P. A.; Gong, D. Y.; Wu, F. L.; He, Z.; Yuan, Y. Y.; Zhao, A. Y.; Tang, X.; Zhang, R. Q.; et al. Crotonoside exhibits selective post-inhibition effect in AML cells via inhibition of FLT3 and HDAC3/6. *Oncotarget* **2017**, *8* (61), 103087-103099. DOI: 10.18632/oncotarget.20710.

147. Buchwald, M.; Pietschmann, K.; Muller, J. P.; Bohmer, F. D.; Heinzel, T.; Kramer, O. H. Ubiquitin conjugase UBCH8 targets active FMS-like tyrosine kinase 3 for proteasomal degradation. *Leukemia* **2010**, *24* (8), 1412-1421. DOI: 10.1038/leu.2010.114.

148. Nishioka, C.; Ikezoe, T.; Yang, J.; Takeuchi, S.; Koeffler, H. P.; Yokoyama, A. MS-275, a novel histone deacetylase inhibitor with selectivity against HDAC1, induces degradation of FLT3 via inhibition of chaperone function of heat shock protein 90 in AML cells. *Leuk Res* **2008**, *32* (9), 1382-1392. DOI: 10.1016/j.leukres.2008.02.018.

149. Ghazy, E.; Abdelsalam, M.; Robaa, D.; Pierce, R. J.; Sippl, W. Histone Deacetylase (HDAC) Inhibitors for the Treatment of Schistosomiasis. *Pharmaceuticals (Basel)* **2022**, *15* (1). DOI: 10.3390/ph15010080.

150. Coleman, B. I.; Skillman, K. M.; Jiang, R. H. Y.; Childs, L. M.; Altenhofen, L. M.; Ganter, M.; Leung, Y.; Goldowitz, I.; Kafsack, B. F. C.; Marti, M.; et al. A Plasmodium falciparum histone deacetylase regulates antigenic variation and gametocyte conversion. *Cell Host Microbe* **2014**, *16* (2), 177-186. DOI: 10.1016/j.chom.2014.06.014.

151. Andrews, K. T.; Haque, A.; Jones, M. K. HDAC inhibitors in parasitic diseases. *Immunol Cell Biol* **2012**, *90* (1), 66-77. DOI: 10.1038/icb.2011.97.

152. Darkin-Rattray, S. J.; Gurnett, A. M.; Myers, R. W.; Dulski, P. M.; Crumley, T. M.; Allocco, J. J.; Cannova, C.; Meinke, P. T.; Colletti, S. L.; Bednarek, M. A.; et al. Apicidin: a novel antiprotozoal agent that inhibits parasite histone deacetylase. *Proc Natl Acad Sci U S A* **1996**, *93* (23), 13143-13147. DOI: 10.1073/pnas.93.23.13143.

153. Andrews, K. T.; Walduck, A.; Kelso, M. J.; Fairlie, D. P.; Saul, A.; Parsons, P. G. Anti-malarial effect of histone deacetylation inhibitors and mammalian tumour cytodifferentiating agents. *Int J Parasitol* **2000**, *30* (6), 761-768. DOI: 10.1016/s0020-7519(00)00043-6.

154. Andrews, K. T.; Gupta, A. P.; Tran, T. N.; Fairlie, D. P.; Gobert, G. N.; Bozdech, Z. Comparative gene expression profiling of P. falciparum malaria parasites exposed to three different histone deacetylase inhibitors. *PLoS One* **2012**, *7* (2), e31847. DOI: 10.1371/journal.pone.0031847.

155. Patel, V.; Mazitschek, R.; Coleman, B.; Nguyen, C.; Urgaonkar, S.; Cortese, J.; Barker, R. H.; Greenberg, E.; Tang, W.; Bradner, J. E.; et al. Identification and characterization of small molecule inhibitors of a class I histone deacetylase from Plasmodium falciparum. *J Med Chem* **2009**, *52* (8), 2185-2187. DOI: 10.1021/jm801654y.

156. Patil, V.; Guerrant, W.; Chen, P. C.; Gryder, B.; Benicewicz, D. B.; Khan, S. I.; Tekwani, B. L.; Oyelere, A. K. Antimalarial and antileishmanial activities of histone deacetylase inhibitors with triazole-linked cap group. *Bioorg Med Chem* **2010**, *18* (1), 415-425. DOI: 10.1016/j.bmc.2009.10.042.

157. Zuma, A. A.; de Souza, W. Histone deacetylases as targets for antitrypanosomal drugs. *Future Sci OA* **2018**, *4* (8), FSO325. DOI: 10.4155/fsoa-2018-0037.

158. Carrillo, A. K.; Guiguemde, W. A.; Guy, R. K. Evaluation of histone deacetylase inhibitors (HDACi) as therapeutic leads for human African trypanosomiasis (HAT). *Bioorg Med Chem* **2015**, *23* (16), 5151-5155. DOI: 10.1016/j.bmc.2014.12.066.

159. Loeuillet, C.; Touquet, B.; Guichou, J. F.; Labesse, G.; Sereno, D. A Tiny Change Makes a Big Difference in the Anti-Parasitic Activities of an HDAC Inhibitor. *Int J Mol Sci* **2019**, *20* (12), 2973. DOI: 10.3390/ijms20122973.

160. Araujo-Silva, C. A.; De Souza, W.; Martins-Duarte, E. S.; Vommaro, R. C. HDAC inhibitors Tubastatin A and SAHA affect parasite cell division and are potential anti-Toxoplasma gondii chemotherapeutics. *Int J Parasitol Drugs Drug Resist* **2021**, *15*, 25-35. DOI: 10.1016/j.ijpddr.2020.12.003.

161. Sodji, Q.; Patil, V.; Jain, S.; Kornacki, J. R.; Mrksich, M.; Tekwani, B. L.; Oyelere, A. K. The antileishmanial activity of isoforms 6- and 8-selective histone deacetylase inhibitors. *Bioorg Med Chem Lett* **2014**, *24* (20), 4826-4830. DOI: 10.1016/j.bmcl.2014.08.060.

162. Gray, D. J.; Ross, A. G.; Li, Y. S.; McManus, D. P. Diagnosis and management of schistosomiasis. *BMJ* **2011**, *342*, d2651. DOI: 10.1136/bmj.d2651.

163. Domling, A.; Khoury, K. Praziquantel and schistosomiasis. *ChemMedChem* **2010**, *5* (9), 1420-1434, https://doi.org/10.1002/cmdc.201000202. DOI: 10.1002/cmdc.201000202 (acccessed 2023/06/13).

164. Doenhoff, M. J.; Kusel, J. R.; Coles, G. C.; Cioli, D. Resistance of Schistosoma mansoni to praziquantel: is there a problem? *Trans R Soc Trop Med Hyg* **2002**, *96* (5), 465-469. DOI: 10.1016/s0035-9203(02)90405-0.

165. Doenhoff, M. J.; Cioli, D.; Utzinger, J. Praziquantel: mechanisms of action, resistance and new derivatives for schistosomiasis. *Curr Opin Infect Dis* **2008**, *21* (6), 659-667. DOI: 10.1097/QCO.0b013e328318978f.

166. Doenhoff, M. J.; Pica-Mattoccia, L. Praziquantel for the treatment of schistosomiasis: its use for control in areas with endemic disease and prospects for drug resistance. *Expert Rev Anti Infect Ther* **2006**, *4* (2), 199-210. DOI: 10.1586/14787210.4.2.199.

167. Oger, F.; Dubois, F.; Caby, S.; Noel, C.; Cornette, J.; Bertin, B.; Capron, M.; Pierce, R. J. The class I histone deacetylases of the platyhelminth parasite Schistosoma mansoni. *Biochem Biophys Res Commun* **2008**, *377* (4), 1079-1084. DOI: 10.1016/j.bbrc.2008.10.090.

168. Nowak, R. P.; DeAngelo, S. L.; Buckley, D.; He, Z.; Donovan, K. A.; An, J.; Safaee, N.; Jedrychowski, M. P.; Ponthier, C. M.; Ishoey, M.; et al. Plasticity in binding confers selectivity in ligand-induced protein degradation. *Nat Chem Biol* **2018**, *14* (7), 706-714. DOI: 10.1038/s41589-018-0055-y.

169. Zorba, A.; Nguyen, C.; Xu, Y.; Starr, J.; Borzilleri, K.; Smith, J.; Zhu, H.; Farley, K. A.; Ding, W.; Schiemer, J.; et al. Delineating the role of cooperativity in the design of potent PROTACs for BTK. *Proc Natl Acad Sci U S A* **2018**, *115* (31), E7285-E7292. DOI: 10.1073/pnas.1803662115.

170. Lai, A. C.; Toure, M.; Hellerschmied, D.; Salami, J.; Jaime-Figueroa, S.; Ko, E.; Hines, J.; Crews, C. M. Modular PROTAC Design for the Degradation of Oncogenic BCR-ABL. *Angew Chem Int Ed Engl* **2016**, *55* (2), 807-810. DOI: 10.1002/anie.201507634.

171. Zoppi, V.; Hughes, S. J.; Maniaci, C.; Testa, A.; Gmaschitz, T.; Wieshofer, C.; Koegl, M.; Riching, K. M.; Daniels, D. L.; Spallarossa, A.; et al. Iterative Design and Optimization of Initially Inactive Proteolysis Targeting Chimeras (PROTACs) Identify VZ185 as a Potent, Fast, and Selective von Hippel-Lindau (VHL) Based Dual Degrader Probe of BRD9 and BRD7. *J Med Chem* **2019**, *62* (2), 699-726. DOI: 10.1021/acs.jmedchem.8b01413.

172. Smith, B. E.; Wang, S. L.; Jaime-Figueroa, S.; Harbin, A.; Wang, J.; Hamman, B. D.; Crews, C. M. Differential PROTAC substrate specificity dictated by orientation of

recruited E3 ligase. *Nat Commun* **2019**, *10* (1), 131. DOI: 10.1038/s41467-018-08027-7.

173. Krieger, J.; Sorrell, F. J.; Wegener, A. A.; Leuthner, B.; Machrouhi-Porcher, F.; Hecht, M.; Leibrock, E. M.; Muller, J. E.; Eisert, J.; Hartung, I. V.; et al. Systematic Potency and Property Assessment of VHL Ligands and Implications on PROTAC Design. *ChemMedChem* **2023**, *18* (8), e202200615. DOI: 10.1002/cmdc.202200615.

174. Abdelsalam, M.; Zessin, M.; Schmidt, M.; Schutkowski, M.; Sippl, W. N4-(2-Amino-4-fluorophenyl)-N1-(3-{2-[2-(3-{[2-(2,6-dioxo-3-piperidyl)-1,3-dioxoisoindolin-4-yl]amino}propoxy)ethoxy]ethoxy}propyl)terephthalamide. *Molbank* **2022**, *2022* (4), M1501.

175. Crew, A. P.; Raina, K.; Dong, H.; Qian, Y.; Wang, J.; Vigil, D.; Serebrenik, Y. V.; Hamman, B. D.; Morgan, A.; Ferraro, C.; et al. Identification and Characterization of Von Hippel-Lindau-Recruiting Proteolysis Targeting Chimeras (PROTACs) of TANK-Binding Kinase 1. *J Med Chem* **2018**, *61* (2), 583-598. DOI: 10.1021/acs.jmedchem.7b00635.

176. Zessin, M.; Kutil, Z.; Meleshin, M.; Novakova, Z.; Ghazy, E.; Kalbas, D.; Marek, M.; Romier, C.; Sippl, W.; Barinka, C.; et al. One-Atom Substitution Enables Direct and Continuous Monitoring of Histone Deacylase Activity. *Biochemistry* **2019**, *58* (48), 4777-4789. DOI: 10.1021/acs.biochem.9b00786.

177. Ibrahim, H. S.; Abdelsalam, M.; Zeyn, Y.; Zessin, M.; Mustafa, A. M.; Fischer, M. A.; Zeyen, P.; Sun, P.; Bulbul, E. F.; Vecchio, A.; et al. Synthesis, Molecular Docking and Biological Characterization of Pyrazine Linked 2-Aminobenzamides as New Class I Selective Histone Deacetylase (HDAC) Inhibitors with Anti-Leukemic Activity. *Int J Mol Sci* **2021**, *23* (1). DOI: 10.3390/ijms23010369.

178. Steinebach, C.; Lindner, S.; Udeshi, N. D.; Mani, D. C.; Kehm, H.; Kopff, S.; Carr, S. A.; Gutschow, M.; Kronke, J. Homo-PROTACs for the Chemical Knockdown of Cereblon. *ACS Chem Biol* **2018**, *13* (9), 2771-2782. DOI: 10.1021/acschembio.8b00693.

179. Rangasamy, L.; Ortin, I.; Zapico, J. M.; Coderch, C.; Ramos, A.; de Pascual-Teresa, B. New Dual CK2/HDAC1 Inhibitors with Nanomolar Inhibitory Activity against Both Enzymes. *ACS Med Chem Lett* **2020**, *11* (5), 713-719. DOI: 10.1021/acsmedchemlett.9b00561.

180. Heimburg, T.; Kolbinger, F. R.; Zeyen, P.; Ghazy, E.; Herp, D.; Schmidtkunz, K.; Melesina, J.; Shaik, T. B.; Erdmann, F.; Schmidt, M.; et al. Structure-Based Design

and Biological Characterization of Selective Histone Deacetylase 8 (HDAC8) Inhibitors with Anti-Neuroblastoma Activity. *J Med Chem* **2017**, *60* (24), 10188-10204. DOI: 10.1021/acs.jmedchem.7b01447.

181. Herrlinger, E. M.; Hau, M.; Redhaber, D. M.; Greve, G.; Willmann, D.; Steimle, S.; Muller, M.; Lubbert, M.; Miething, C. C.; Schule, R.; et al. Nitroreductase-Mediated Release of Inhibitors of Lysine-Specific Demethylase 1 (LSD1) from Prodrugs in Transfected Acute Myeloid Leukaemia Cells. *Chembiochem* **2020**, *21* (16), 2329-2347. DOI: 10.1002/cbic.202000138.

182. Guenette, R. G.; Yang, S. W.; Min, J.; Pei, B.; Potts, P. R. Target and tissue selectivity of PROTAC degraders. *Chem Soc Rev* **2022**, *51* (14), 5740-5756, 10.1039/D2CS00200K. DOI: 10.1039/d2cs00200k.

183. Xie, H.; Li, C.; Tang, H.; Tandon, I.; Liao, J.; Roberts, B. L.; Zhao, Y.; Tang, W. Development of Substituted Phenyl Dihydrouracil as the Novel Achiral Cereblon Ligands for Targeted Protein Degradation. *J Med Chem* **2023**, *66* (4), 2904-2917. DOI: 10.1021/acs.jmedchem.2c01941.

184. Zografou-Barredo, N. A.; Hallatt, A. J.; Goujon-Ricci, J.; Cano, C. A beginner's guide to current synthetic linker strategies towards VHL-recruiting PROTACs. *Bioorg Med Chem* **2023**, *88-89*, 117334. DOI: 10.1016/j.bmc.2023.117334.

185. Cross, J. M.; Coulson, M. E.; Smalley, J. P.; Pytel, W. A.; Ismail, O.; Trory, J. S.; Cowley, S. M.; Hodgkinson, J. T. A 'click' chemistry approach to novel entinostat (MS-275) based class I histone deacetylase proteolysis targeting chimeras. *RSC Med Chem* **2022**, *13* (12), 1634-1639, 10.1039/D2MD00199C. DOI: 10.1039/d2md00199c.

186. Yang, K.; Wu, H.; Zhang, Z.; Leisten, E. D.; Nie, X.; Liu, B.; Wen, Z.; Zhang, J.; Cunningham, M. D.; Tang, W. Development of Selective Histone Deacetylase 6 (HDAC6) Degraders Recruiting Von Hippel-Lindau (VHL) E3 Ubiquitin Ligase. *ACS Med Chem Lett* **2020**, *11* (4), 575-581. DOI: 10.1021/acsmedchemlett.0c00046.

187. Nsanzabana, C. Resistance to Artemisinin Combination Therapies (ACTs): Do Not Forget the Partner Drug! *Tropical Medicine and Infectious Disease* **2019**, *4* (1), 26.

188. Joshi, M. B.; Lin, D. T.; Chiang, P. H.; Goldman, N. D.; Fujioka, H.; Aikawa, M.; Syin, C. Molecular cloning and nuclear localization of a histone deacetylase homologue in Plasmodium falciparum. *Mol Biochem Parasitol* **1999**, *99* (1), 11-19. DOI: 10.1016/s0166-6851(98)00177-7.

189. Zhao, L.; Pi, L.; Qin, Y.; Lu, Y.; Zeng, W.; Xiang, Z.; Qin, P.; Chen, X.; Li, C.; Zhang, Y.; et al. Widespread resistance mutations to sulfadoxine-pyrimethamine in

malaria parasites imported to China from Central and Western Africa. *Int J Parasitol Drugs Drug Resist* **2020**, *12*, 1-6. DOI: 10.1016/j.ijpddr.2019.11.002.

8. Appendix
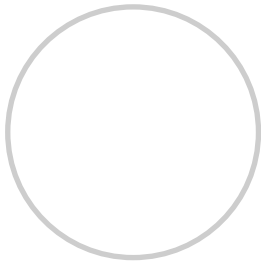
Mohamed Abdelsalam

✉ **Email:** mohamed.abdelsalam@pharmazie.uni-halle.de

in LinkedIn: linkedin.com/in/mohamed-abdelsalam-0651b71b2

WORK EXPERIENCE

[04/2022 – Current]

Wissenschaftlicher Mitarbeiter

Institute of Pharmacy, Martin-Luther-University (Halle-Wittenberg), Germany

City: Halle
Country: Germany

[05/2014 – 11/2018]

Research and teaching assistant

Pharmaceutical Chemistry Department, Faculty of Pharmacy, Alexandria University, Egypt

City: Alexandria
Country: Egypt

[08/2013 – 10/2017]

Pharmacist

"Alaraby" Community Pharmacy

EDUCATION AND TRAINING

[04/2019 – 03/2022]

Research stay in the Medicinal Chemistry group of Prof. Wolfgang Sippl

Institute of Pharmacy, Martin- Luther University, Halle (Saale) (Germany)

- Design and synthesis of novel Class-I histone deacetylase inhibitors as anticancer agents
- Development of prodrugs and PROTACs for class-I HDACs
- Design and synthesis of dual DHFR-HDAC inhibitors as anti parasitic agents
- Design, synthesis and biological evaluation of novel PROTACs for FLT3-ITD

[12/2018 – 03/2019]

German Language course

Goethe-Institute, Göttingen (Germany)

[09/2013 – 12/2016]

Master of Pharmaceutical Sciences "Pharmaceutical Chemistry"

Faculty of Pharmacy, Alexandria University, Egypt

- Design and synthesis of novel β-carboline derivatives of potential therapeutic activity

[08/2008 – 06/2013]

Bachelor of Pharmaceutical Sciences (Distinction Honor)

Faculty of Pharmacy, Alexandria University, Egypt

- Learning different basic Pharmaceutical Sciences

[08/2005 – 06/2008] **General secondary certificate with grade 96.4%**

El-Abbsia Secondary School, Alexandria, Egypt

LANGUAGE SKILLS

Mother tongue(s): Arabic

Other language(s):

English

LISTENING C1 **READING** C1 **WRITING** C1

SPOKEN PRODUCTION C1 **SPOKEN INTERACTION** C1

German

LISTENING B1 **READING** B1 **WRITING** B1

SPOKEN PRODUCTION B1 **SPOKEN INTERACTION** B1

Levels: A1 and A2: Basic user; B1 and B2: Independent user; C1 and C2: Proficient user

COMMUNICATION AND INTERPERSONAL SKILLS

Communication skills

- Good communication skills (through work with students and international colleagues)
- Networking (through collaboration with different working groups in Germany, France,...)
- Presentation skills (posters and oral presentations in conferences and group seminars)

PROJECTS

[2022 – Current]

Synthesis and pharmacology of novel inhibitors of histone deacetylases and of proteolysis targeting chimeras (PROTACs) for mutant FMS-like tyrosine kinase-3

[2022 – Current] **Development of novel dual targeting anti-malaria drug leads**

SCHOLARSHIPS

German Egyptian Research Long-term Scholarships (GERLS)

German Egyptian Research Long-term Scholarships (GERLS): scholarship of DAAD (German Academic Exchange Service) at Martin-Luther University, Halle, Germany (2019-2021)

CONFERENCES AND SEMINARS

XXVI EFMC International virtual Symposium on Medicinal Chemistry (EFMC-ISMC 2021) "Poster presentation" 2021

European School of Medicinal Chemistry, ESMEC, Italy (Urbino) "Poster presentation" 2022

List of publications

Publications which are part of the PhD thesis

1- Ibrahim HS*, **Abdelsalam M***, Zeyn Y, Zessin M, Mustafa AM, Fischer MA, Zeyen P, Sun P, Bülbül EF, Vecchio A, Erdmann F, Schmidt M, Robaa D, Barinka C, Romier C, Schutkowski M, Krämer OH, Sippl W.Synthesis, molecular docking and biological characterization of pyrazine linked 2-aminobenzamides as new class I selective histone deacetylase (HDAC) inhibitors with anti-leukemic activity. *International Journal of Molecular Sciences*, **2021**, *23*(1), 369. *shared first authorship.

2- **Abdelsalam M**, Ibrahim HS, Krauss L, Zessin M, Vecchio A, Hastreiter S, Schutkowski M, Schneider G, Sippl W. Development of Pyrazine-Anilinobenzamides as Histone Deacetylase HDAC1–3 Selective Inhibitors and Biological Testing Against Pancreas Cancer Cell Lines. In *HDAC/HAT Function Assessment and Inhibitor Development: Methods and Protocols*, **2022**, (pp. 145-155). New York, NY: Springer US.

3- Bülbül EF, Melesina J, Ibrahim HS, **Abdelsalam M**, Vecchio A, Robaa D, Zessin M, Schutkowski M, Sippl W. Docking, Binding Free Energy Calculations and In Vitro Characterization of Pyrazine Linked 2-Aminobenzamides as Novel Class I Histone Deacetylase (HDAC) Inhibitors. *Molecules*, **2022**, *27*(8), 2526.

4- **Abdelsalam M**, Zmysila M, Schmidtkunz K, Vecchio A, Hilscher S, Schutkowski M, Jung M, Jessen-Trefzer C, Sippl W. Design and synthesis of bioreductive prodrugs of class I histone deacetylase inhibitors and their biological evaluation in virally transfected acute myeloid leukemia cells. ChemRxiv, **2023**. https://doi.org/10.26434/chemrxiv-2023-hrxsl

5- **Abdelsalam M**, Zessin M, Schmidt M, Schutkowski M, Sippl W. N^4-(2-Amino-4-fluorophenyl)-N^1-(3-{2-[2-(3-{[2-(2,6-dioxo-3-piperidyl)-1,3-dioxoisoindolin-4-yl]amino}propoxy)ethoxy]ethoxy}propyl)terephthalamide. *Molbank*, **2022**(4), M1501.

6- Ghazy E*, **Abdelsalam M*,** Robaa D, Pierce RJ, Sippl W. Histone deacetylase (HDAC) inhibitors for the treatment of schistosomiasis. *Pharmaceuticals*, **2022**, *15*(1), 80. *shared first authorship.

Other publications/patents

Patent application

Identification of novel HDAC and DHFR dual-targeting inhibitors as potent antimalarials

E. Ghazy, C. Pierrot, M**. Abdelsalam**, J. Khalife, W. Sippl.

Patent application submitted May 2023

Selbstständigkeitserklärung/Declaration of Authorship

Hiermit erkläre ich, dass ich die vorliegende Dissertationsschrift selbständig und ohne fremde Hilfe angefertigt, keine anderen als die angegebenen Quellen und Hilfsmittel benutzt und die aus ihnen wörtlich oder inhaltlich entnommenen Stellen als solche kenntlich gemacht habe. Die Arbeit wurde ausschließlich der Mathematisch-Naturwissenschaftlichen Fakultät I der Martin-Luther-Universität Halle-Wittenberg vorgelegt und an keiner anderen Universität oder Hochschule weder im In- und Ausland zur Erlangung des Doktorgrades eingereicht.

I hereby declare that I am the sole author of this thesis and that I have not used any sources other than those listed in the bibliography and identified as references. I further declare that I have not submitted this thesis at any other institution in order to obtain a degree.

Halle (Saale), 16.08.2023